Title

Mechanically Sensitive Polydiacetylene Langmuir Films: Structure, Properties and Applications

Author

Finney, Tanner Joseph

Publication Date

2023

Peer reviewed|Thesis/dissertation

Mechanically Sensitive Polydiacetylene Langmuir Films: Structure, Properties and Applications

By

TANNER J. FINNEY

DISSERTATION

Submitted in partial satisfaction of the requirements for the degree of

DOCTOR OF PHILOSOPHY

in

Chemical Engineering

in the

OFFICE OF GRADUATE STUDIES

of the

UNIVERSITY OF CALIFORNIA

DAVIS

Approved:

Tonya L. Kuhl, Chair

Volkmar Heinrich

Harishankar M. Manikantan

Keishi Suga

Committee in Charge

2023

To my parents
Mark and Joni Finney
and my grandparents
Charlotte and Norris Fagerhaug
Lois and Joseph Finney

Contents

Mechanically Sensitive Polydiacetylene Langmuir Films: Structure, Properties and Applications

Abstract

Polydiacetylenes (PDAs) have attracted great interested due to their spectacular chromatic transition in response to external stimuli. In particular, application of shear stress induces a colorimetric transition from a non-fluorescent blue phase to a fluorescent red phase. This turn-on fluorescence in response to mechanical stress is sensitive to very small forces, which are typically quite difficult to measure. Described herein is the development of a fluorescent mechanical stress sensor derived from PDAs. First, techniques were developed to fabricate high quality PDA Langmuir films and tune their properties towards different regimes. Using a modified Surface Forces Apparatus (SFA), the fluorescent response of select PDA Langmuir films to mechanical stress was quantified. The PDAs studied here were measured to be sensitive to shear stress on the order of magnitude of kPa. The migration of the slime mold *Physarum polycephalum* was then examined using PDA Langmuir films. Stresses exerted by the slime mold induced the blue to red transition. The paths explored by the slime mold and a range of stresses were calculated from the fluorescent response. Finally, the structural differences between the blue and red phases PDAs were examined using Grazing Incidence X-ray Diffraction, X-ray Reflectivity and Atomic Force Microscopy.

Acknowledgments

I would like to express my deepest gratitude to Prof. Tonya Kuhl for guidance throughout my time at UC Davis. Without her constant encouragement, advice, and guidance, this dissertation would not have been possible. I would like to thank my dissertation committee members, Prof. Volkmar Heinrich, Prof. Harishankar Manikantan, and Prof. Keishi Suga for helpful discussions over the past few years, and providing insightful feedback on my dissertation. I would like to thank Prof. Adam Moulé for all of his guidance, expertise and help, usually in the form of impromptu chats in the hallway and for letting me use all the cool toys in his lab.

I'd like to thank all of my friends and colleagues in the Kuhl Lab for all the lively scientific arguments, grueling QE examinations, and rafting trips. In roughly chronological order: Dr. Amanda Dang, Dr. Deepshika Gilbile, Michael Bull, Ryan Edmonds, Evan Haning, Zhongrui Liu, Kevin Gu, Shwetha Jayachandran, John Miller, Jiayun Hou, and Debdyuti Roy. I'd also like to thank all of my dedicated undergraduate researchers, Christopher Dixon, Skye Frank, Uyioenwongo Udoh, and Quin Spooner.

I'd like to thank the following professors and their graduate students and postdocs for sharing their equipment, expertise and letting me take underutilized things from their labs: Dr. Kevin Yates and Justin Wong and Profs. Karen McDonald and Somen Nandi, Dr. Zachary Rollins and Prof. Steven George, Dr. Janis Patiño and Prof. Veronica Morales, Dr. Naomi Hamada and Prof. Marjorie Longo, Timothy Hui and Prof. William Ristenpart, Dr. Lucas Solano, Dr. Junwei Zhao, Prof. Kit Lam, Prof. Ye Chen-Izu, Meghna Jha and Prof. Adam Moule, and David Coppage, Linnea Dolph, Leah Thompson and Prof. Annaliese Franz. I'd also like to thank Prof. Roland Faller for access to HPC1.

I'd like to thank the members of the Chemical Engineering and Materials Science and Engineering Graduate Student Organization (CHMS-GSO) for letting me lord over them for two years. A particular thanks to my predecessors, Dr. Matthew McNulty and Dr. Christine Smudde and recent successors, Fox Thorpe and Hudson Shih.

I'd like to acknowledge the various NIH funding organs that funded this research. In particular, the NIH T-32 Training Program in Basic and Translational Cardiovascular Science. Within the program, I'd like to thank Prof. Nipavan Chiamvimonvat and Chandra Reid for their support and excellent learning opportunities.

I'd like to thank the Chemical Engineering Department Staff for keeping everything running, in particular Ryan Gorsiski, Grace Woods and Bill Doering.

I'd like to acknowledge and thank all of my friends and colleagues at UC Davis who are too numerous to mention here. Rather I'll say a "Shibboleth", if the phrase Cold Duck Time means anything to you, then you have my deepest thanks and gratitude. I owe you a beer, kava, or well-shaken glass of palm wine. Davis was a great place to spend a pandemic, sitting outside on a patio, denouncing the hypocrisies of our times.

Finally, I'd like to thank my family for their continuing and unending support.

CHAPTER 1

Introduction

1.1. Motivation

Quantitative cell adhesion and motility studies are vital for understanding fundamental cellular processes including spreading, growth, proliferation, migration, and organoid formation that impact normal and disease processes such as organ development during embryogenesis, wound healing, cancer progression, and neuronal development and migration. There is a need for expanding the armamentarium to evaluate the forces involved in these processes.

Existing techniques for examining the forces involved in cell adhesion, migration, and motility can broadly be placed into two categories: simple, qualitative observation and quantitative traction force microscopy (TFM) techniques. While qualitative observation can provide insight into the rates of cell migration, it is limited in what can be said about the stresses the cell applies to its surroundings and requires continuous observation. Conversely, TFM techniques are very high resolution, and can quantitatively measure cell applied stresses through the displacement of small fluorescent beads embedded within an elastic gel. TFM and related techniques, however, require significant analysis to calculate cell stresses from the strain measured, require continuous observation, are limited to a specific range of well-characterized elastic substrates, and are best suited to studying single cells.

At present, there exists a gap between qualitative culture-dish assays and quantitative measurements by TFM. The goal of this work is to contribute to closing this gap through the design and development of a new sensor of cellular locomotion based on Polydiacetylenes (PDAs). PDAs are a class of polymers renowned for their dramatic colorimetric transitions and an associated turn-on of fluorescence.

1.2. Brief Overview of Polydiacetylenes (PDAs)

Polydiacetylenes (PDA) are a class of linear polymers that exhibit chromatic transitions. Diacetylene (DA) monomers, as their name suggests have two triple bonds. Exposure to UV light induces polymerization creating a conjugated backbone of alternating double and triple bonds, the so-called ene-yne motif. This occurs via the 1,4 addition of each monomer to the polymer chain. PDAs undergo topochemical polymerization, in which the topography of the system must meet specific geometric and packing requirements for polymerization to take place. Initial polymerization creates a polymer that appears visibly blue, often referred to as the blue phase. Further exposure to light, (*photochromism*), heat, (*thermochromism*), mechanical stress, (*mechanochromism*), solvents, (*solvatochromism*),or changes in pH, (*halochromism*), depending on the particular PDA, can induce a transition to a polymer that appears visibly red, the so-called red phase. The red phase is strongly fluorescent, while the blue phase is negligibly fluorescent. The mechanism of this chromatic, blue to red, transition is still debated and not fully understood. A number of mechanisms have been proposed, but there is disagreement between different fields on the correct terminology, electronic, and molecular states that elicit the blue-to-red behavior.

The mechanism can be broadly described as a two-step process. (1) Initial polymerization of monomers to the blue phase leaves strain in the polymer backbone. To wit, steric effects and other intermolecular interactions from the side groups of the polymer prevent the polymer backbone from adopting its preferred conformation. (2) These interactions are overcome when the polymer is exposed to some external stimuli, allowing the backbone to "relax", to red-phase PDA.

While PDAs exist in many material forms with a wide variety of side groups, of primary interest here are PDAs made from diacetylene (DA) surfactants, for instance, 10, 12-pentacosadiynoic acid (PCDA). PCDA and similar DA molecules can be deposited using a Langmuir-Blodgett trough. When compressed they form a nominally 3-layer film or trilayer that can be polymerized. The trilayers are several nm thick and can be transferred to a solid support – making a sensing platform. The molecular interactions, which confer strain in the blue phase, can be modified by the DA molecular structure and/or concentration of divalent cations in the subphase to tune the force

required to transition from blue-to-red as well as the sensitivity to other perturbations such as temperature, pH, or further exposure to UV light after initial polymerization.

1.3. Dissertation Structure

Chapter 2 is a survey and review of the key properties of PDAs. PDAs derived from fatty acids are the primary focus as they are the most widely used for sensing, however other important PDAs are also reviewed. Monomer functionalization, synthesis methods and design considerations are discussed. The electronic, optical and structural characteristics of the PDA backbone with a particular focus on exploiting these properties to design sensors is reviewed. Finally, morphological characteristics and control of PDA Langmuir films, vesicles and other self assembled systems are discussed. All figures presented in Chapter 2 have been obtained with permission from their respective publishers.

Chapter 3 details our investigations into making and depositing PDA Langmuir films. The objective of this work was to develop techniques and methodology to produce a wide range of PDA films that could be sensitive to mechanical stress. In particular, modifying the chain length and introducing metal cations into the subphase of the Langmuir trough were found to strongly govern the properties of PDAs.

Chapter 4 employs the PDA films developed in chapter 3 as mechanical stress sensors. The goal was to formulate a quantitative description of PDA mechanochromism and demonstrate their viability with a model class of micro-organisms. The mechanical response of PDA films was quantified using a combined Surface Forces Apparatus (SFA) and fluorescent microscope. PDA films were then demonstrated as mechanical stress sensors using the slime mold *Physarum polycephalum*. Slime mold migration across the film induced the blue to red transition enabling a passive, fluorescent readout of migration patterns and the forces associated with them.

Chapter 5 examined the molecular structure of PDA films made using the techniques developed in chapter 3. The goal of this work was to contribute to a better understanding of the structure of the blue and red phases. In particular, development of high quality sensors rests upon a strong understanding of the underlying mechanism and hence structures of the film in different phases. Grazing incidence X-ray diffraction (GIXD), x-ray reflectivity (XRR) and atomic force microscopy

(AFM) were used to develop a structural model of the blue and red phases. It was observed that the blue phase is composed of aligned planar molecules with a straight polymer backbone. The red phase was observed to be non-planar. Two potential structures were proposed, a twisted model and a kinked model. The feasibility of these models were evaluated using Density Functional Theory (DFT) calculations to compare the model's UV-vis spectra to experimental measurements.

Langmuir film synthesis, surface forces apparatus and slime mold experimental procedures are detailed in Appendix A. X-ray characterization techniques are described in Appendix B

CHAPTER 2

A Tutorial Review of Polydiacetylene Langmuir Films & Vesicles

Summary, Scope and Purpose

A version of this chapter is being developed for a review paper. Very likely significant differences will exist between the version presented here and the final published one.

There are many reviews on the applications of PDAs as sensors. While informative, most reviews ignore the process of actually making PDA films and vesicles, and focus largely on clever applications and technology demonstrations. This review aims to fill that gap by describing some considerations in synthesizing vesicles and Langmuir films from fatty acid PDAs. A brief history and description of diacetylene synthesis procedures will be discussed, followed by a description of the polymerization mechanism and the electronic and optical properties of the polymer backbone. Finally, the morphology of thin films, vesicles and other self assembled systems will be reviewed.

Abstract

Polydiacetylenes are a class of linear conjugated polymers that exhibit remarkable chromatic transitions, e.g. blue to red when exposed to external stimuli. These chromatic transitions have attracted great interest for use as inexpensive, passive sensors. This review details key properties of polydiacetylenes: synthesis, polymerization kinetics, optical and electronic properties, and common morphologies. A particular focus is on fatty-acid diacetylenes, which self-assemble into films, vesicles, and other nanostructures and exhibit remarkable chromatic transitions in response to external stimuli.

2.1. Introduction

Polydiacetylenes (PDAs) are known today for their brilliant chromatic transitions in response to stimuli. This ranges extensively from heat: *thermochromism*, light: *photochromism*, mechanical stress:

mechanochromism, solvents: *solvatochromism* and specific molecules: *affinochromism/biochromism*. For PDAs synthesized from colorless fatty acid diacetylene monomers (DA), the initial polymerized state is the "blue phase". The blue phase appears non-fluorescent, and is visibly blue. Application of any one of the aforementioned stimuli (light, heat mechanical stress etc.) can induce a transition from the blue phase to the red phase. PDA in the red phase appears visibly red and much more fluorescent. The phases can be directly observed by a wide variety of techniques including by naked eye, UV-vis, Raman, and FTIR spectroscopy, and fluorescent microscopy/spectroscopy.

Prior to the explosion of interest in their use as sensors, PDAs were widely studied for their polymerization behavior, optical properties, and applications as a model system for studying a wide variety of phenomena in polymer science and quantum chemistry. Diacetylene (DA) monomers are defined by their two adjacent triple bonds. Packing these monomers together and exposing the system to UV light induces polymerization. The resulting polymer backbone consists of an alternating double bond, triple bond (ene-yne) motif. Unsurprisingly, diacetylenes are not the end of this trend, with triacetylenes, etc., and their polymers also attracting interest [1]. Depending on the choice of monomer, crystals of PDA appear in a wide variety of colors. Of particular interest here is PDAs made from fatty acids, which exhibit the well-known blue and red phases.

Fatty acids and surfactants have several attractive qualities for building PDA sensors. First, the topochemical constraint (section 2.4) means that growth of polymers is not driven by diffusion of monomers to a reactive polymer end, but rather is governed by closely packed and properly arranged molecules. Given properly designed monomers, the amphiphilic nature of fatty acids drives self-assembly, providing a convenient source of ordered monomers. Furthermore, there exists a vast wealth of literature and established knowledge about surfactants self-assembling into different morphologies ranging from nano-scale to macro-scale systems. Vesicles and Langmuir films, among several other self-assembled systems have been found to be amenable to polymerization [2]. The sensing modality is derived from the meta-stable nature of the blue phase. Initial polymerization leaves the PDA backbone in a "strained" geometry dictated by side chain interactions (hydrogen bonding, van der Waals forces, etc.). Application of external stimuli drives the system to the red

phase. With careful tuning and functionalization, this blue to red transition is then exploited as the sensing mechanism.

PDA synthesis was first described by Wegner in 1969 and detailed in a series of articles [3–6] Subsequent synthesis of fatty acid diacetylenes by Tieke et al. enabled the formation of Langmuir films and vesicles that exhibited chromatic transitions [7–10]. The educational and potential sensing applications of PDAs were recognized early on by Patel and Yang, with interesting observations and demonstrations of thermochromism and mechanochromism [11]. Self-assembled PDAs attracted great interest as sensors after demonstration of their sensitivity and properties by Charych et al. [12–14]. Since then, research into using PDAs as sensors has expanded and has been the subject of many extensive reviews (section 2.9).

Key properties and early characterization was surveyed in 1985 by Bloor and Chance [15], and Cantow et al. [16]. The spectral and nonlinear optical properties of PDAs were the subject of a book by Chemla, D.S. and Zyss, J. [17–19]. An extensive review of fatty acid diacetylenes, their properties and morphology up to 1985 was done by Tieke [10]. Polymerizing lipid-like diacetylenes in vesicles and films were reviewed by Ringsdorf et al. [20].

Rather than focus exclusively on sensing applications, this review will survey the properties of diacetylene monomers (section 2.2), the polymerization mechanism and kinetics (section 2.4), optical and electronic properties (section 2.5), the morphology and properties of fatty acid PDAs in Langmuir films and vesicles, with a brief survey other self assembled systems (sections 2.3, 2.6, 2.7, 2.8 respectively). An extensive list of reviews covering the sensing applications of PDAs is in section 2.9.

2.2. Common Diacetylenes

This section details the structure and properties of commonly encountered diacetylene monomers, in particular, fatty acid diacetylenes. The first diacetylenes synthesized by Wegner had toluenesulfonate (tosylate) side groups [3–6]. Urethane substituted PDAs introduced by Patel have been used extensively to examine the optical properties and electronic structure of PDAs [21]. Much of the fundamental characterization work was based on these two systems. Details of their structure

are described in section 2.11.1. Most commonly encountered today, and commercially available, are fatty acid diacetylenes with a carboxylic head group and long alkyl tail. Additionally, many two-tailed lipid-like diacetylenes have been synthesized, though they often lack the brilliant chromatic transitions of fatty acid DAs. Many other diacetylenes have been used historically, or have niche applications, the properties of these other DAs have been summarized in the following reports [15, 16, 18, 22, 23].

2.2.1. Fatty Acid Diacetylenes. Most of the commercially available diacetylenes today consist of long chain fatty acids with the diacetylene motif embedded somewhere within the alkyl tail. The positioning of the diacetylene motif strongly governs the polymerization behavior, chromatic transitions and morphology of the subsequent polymer. Much of the early work on fatty acid diacetylenes was extensively reviewed by Tieke [10]. A range of fatty acid diacetylenes exist, with 10,12-pentacosadiynoic acid (PCDA, C25) and 10,12-tricosadiynoic acid (TCDA, C23) being the most common. Nomenclature for fatty acid diacetylenes is not well standardized. Early literature often referred to fatty acid DAs as m/n acids, with m generally referring to the number of carbons between the terminal methyl group and diacetylene motif, and n referring to the number of CH_2 between the carboxylic acid head group and the diacetylene motif. Later on a wide range of initialisms, acronyms and abbreviations have been employed to describe fatty acid diacetylenes, some commonly used nomenclature is described in Table 2.1.

Figure 2.1 represents the most common naming scheme for PCDA. Synthesis is described in brief in Schott and Wegner [18] ,Tieke [10] and in detail by Tieke et al. [7] and more recently by Villarreal et al. [24], among others [9, 25–27]. Fatty acid diacetylene monomers have been extensively used to make thin films, vesicles, and other nano-assemblies, both as model polymerized membranes and as versatile sensors of heat, biomolecules, solvents, and mechanical stress. Fatty acids bearing diacetylene moieties are also found naturally; for instance, 9,11-octadecadiynoic acid is found in the seeds of *Heisteria silvanii* [28]. 10, 12-Tricosadiynoic acid (TCDA, C23) has also been found to play a role in the inhibition of enzymes related to hepatic mitochondrial dysfunction in rats [29].

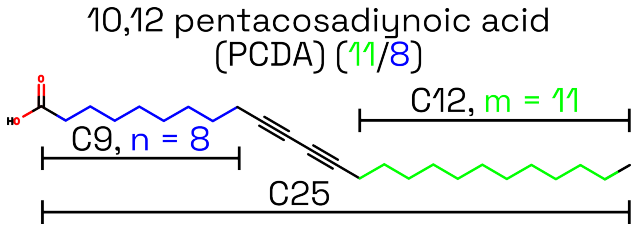

FIGURE 2.1. 10,12-pentacosadiynoic acid (PCDA), also referred to as C25 or 11/8 Acid

2.2.2. Lipid-Like Diacetylenes. A great variety of lipid-like diacetylenes have also been synthesized [20, 30–35]. The most common is the commercially available 1,2-bis(10,12-tricosadiynoyl)-sn-glycero-3-phosphocholine, or 23:2 diyne PC, Figure 2.2. These lipid-like DAs readily form vesicles and Langmuir films and have been studied as vehicles for stable model liposomes, black lipid membranes, for drug delivery, and as monolayers [20, 36].

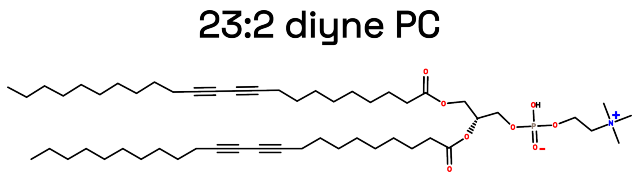

FIGURE 2.2. 1,2-bis(10,12-tricosadiynoyl)-sn-glycero-3-phosphocholine (23:2 diyne PC)

2.2.3. Storage Considerations and Purification. Fatty acid diacetylenes often appear quite reactive at room temperature and can appear to polymerize over time if left out on the benchtop. This may be driven either from thermally induced polymerization, or by self-sensitization of small amounts of PDA polymer to visible light and heat, as discussed in section 2.4.1.4. At a minimum, all diacetylene monomers should be stored in a freezer and exposed minimally to all light. Because of the ease of polymerization, most commercially purchased diacetylene powders appear visibly blue and contain polymerized material. This polymer contamination can interfere with forming defect free films, but it is straightforward to purify.

Several approaches are commonly used. The most effective is to use flash silica gel chromatography. Most PDA polymers longer than a few oligomers are insoluble in common organic solvents, hence only monomers are eluted [37, 38]. This has the added advantage of removing any other contaminants

potentially present. Chloroform (Rf = 0.22), dichloromethane, and 25%/75% ethyl acetate/hexanes (Rf = 0.23) are effective mobile phases. Ideal storage conditions are dark, cold ($< -20°C$) and in an inert atmosphere (argon) [39, 40]. Even with good storage, DA powders will slowly polymerize to some degree and may appear slightly blue after 6-months to one year.

Other methods to purify DA powders are to dissolve the monomers in chloroform or another suitable solvent and filter with a PTFE syringe filter [41]. They are however expensive and can only filter small quantities before becoming clogged, and some small oligomers may still pass through the filter. Purification through recrystallization from petroleum ether [42], and through centrifugation at 16000g for 30 minutes have also been reported [43].

2.2.4. Fatty Acid Diacetylene Functionalization. An advantage of fatty acid diacetylenes is their carboxylic acid head group, which is readily modifiable. As elaborated on in other reviews [2, 44, 45], this has enables self assembled PDA systems to be chromatic and colorimetric sensors to a wide variety of stimuli. Many functional groups can directly replace the carboxylic head group, conferring unique properties to the PDA assembly, ranging from improving hydrogen bonding to enable more stable PDA monolayers [38, 46], to coupling with small peptide or amino acid sequences to detect bacteria, or other biomolecules [47]. Several synthesis routes can be used, generally with high yield and straightforward workups. The first is to use carbodiimide coupling agents such as EDC (1-Ethyl-3-(3-dimethylaminopropyl)carbodiimide), DCC (N,N'-Dicyclohexylcarbodiimide) or DIC (N,N'-Diisopropylcarbodiimide) in combination with NHS (N-Hydroxysuccinimide), or HOBt (Hydroxybenzotriazole). A typical reaction scheme is as follows [35, 45, 48, 49]. 1 equivalent PCDA (or another fatty acid DA) is dissolved in dichloromethane (or chloroform) along 1.1 equivalents of EDC and NHS. This reaction is then stirred at room temperature for several hours, after which solvent is removed *in vacuo*. The crude product is then worked up by dissolving in ethyl acetate, and washing with water, optionally with saturated $NaHCO_3$ and saturated NaCl, and then dried over anhydrous $MgSO_4$. The ethyl acetate is then removed *in vacuo*. The resulting NHS-PCDA is a white powder that can be stored at -20°C away from light and used at a later date. NHS-PCDA is quite reactive, and will readibly polymerize when exposed to visible light. This method is widely used and very effective for coupling to primary amines. EDC/HOBt coupling agents in N,N

dimethylformamide (DMF) are also effective if the desired product is less soluble in moderately polar organic solvents. NHS-PCDA and the functional molecule (1.1 equivalents) are then dissolved in a suitable organic solvent and stirred overnight. For a product soluble in ethyl acetate (or chloroform), purification, or the workup, is straightforward and similar to the NHS-PCDA workup. The crude product is then generally purified using silica gel chromatography.

Alternatively, acyl chlorides are effective for coupling diacetylene monomers to other functional groups, with the most widely used being oxalyl chloride [38, 50]. The resulting acid chloride can require a more sophisticated setup, as oxalyl chloride is water reactive and must be carried out under anhydrous conditions. Furthermore, oxalyl chloride is significantly more toxic than carbodiimide coupling agents. A typical reaction scheme follows standard acid-chloride synthesis. First, PCDA is dissolved in dichloromethane, and oxalyl chloride (1.1 equivalents) is added drop-wise to a flame dried, inert atmosphere (argon) reaction vessel with stir bar. After bubbling and off-gassing subsides, a catalytic amount of DMF is added to the reaction vessel (∼1 drop from a glass syringe). After 1 hour of stirring, the solvent is removed and evaporated to dryness. The resulting acid chloride (Cl-PCDA) is highly water reactive and should be kept in an inert atmosphere and used quickly. From here, the acid chloride is dissolved in tetrahydrofuran (THF) (or another suitable solvent) along with the target molecule (often a primary amine) (∼1.1 equivalents). Depending on the specific chemistry, triethylamine (TEA) is added to buffer out HCl produced from the acid chloride. This reaction is stirred overnight and then solvent is removed. The workup for these reactions is highly dependent on the specific reagents, but generally: the crude residuals are dissolved in ethyl acetate, washed with water, saturated base, and saturated brine, and then dried and concentrated *in vacuo*. The product is then purified using silica gel chromatography in a suitable solvent.

2.3. General Properties of Fatty Acid Diacetylenes

While a plethora of PDAs populate the published literature, the most active area of PDA research investigates the properties of polymers made from fatty acid diacetylenes, such as PCDA and TCDA. These diacetylenes as described in section 2.2 can form Langmuir films, vesicles and other self-assembled systems. This section will discuss common features observed in these self-assembled

systems, such as their chromatic response and reversibility (or lack thereof). An in-depth review of the research on surfactant and fatty acid diacetylenes up to 1985 was done by Tieke [10].

2.3.1. Measuring the Colorimetric Response to Stimuli. The well-known colors of PDAs arise from extensive conjugation of the polymer backbone. In PDAs made from fatty acids, initial exposure to UV light produces blue phase polymer, with prolonged exposure, or application of some external stimulus, the film undergoes a chromatic shift to the red phase, Figure 2.3A. The red phase is fluorescent, whereas the blue phase is negligibly fluorescent. This chromatic shift is the primary modality through which PDAs are used as sensors. The blue to red transition can be monitored through a wide range of techniques such as visible spectroscopy, fluorescence spectroscopy and microscopy, and Raman spectroscopy. At the macro scale, taking color images of PDAs and decomposing them into their individual R,G,B components enables the phase behavior of PDAs to be estimated [51–54]. The optical properties are discussed in detail in section 2.5.

2.3.1.1. *Visible Spectrophotometry.* Shifts in the visible spectra of PDA are widely used. As a stimulus is applied, the blue to red transition and degree of transition can directly be observed from the shifting of the peaks from blue wavelengths to red wavelengths, (Figure 2.3B). Charych et al. were among the first to quantify this as the "colorimetric response", or CR [12, 55]. CR is essentially the normalized ratio between the primary blue and red peak before, (f_0) and after, (f_1) some stimuli has been applied, equations 2.1 - 2.3.

$$f_0 = \frac{I_{0,blue,max}}{I_{0,red,max} + I_{0,blue,max}} \tag{2.1}$$

$$f_1 = \frac{I_{1,blue,max}}{I_{1red,max} + I_{1,blue,max}} \tag{2.2}$$

$$CR = \frac{f_0 - f_1}{f_0} \tag{2.3}$$

Where $I_{j,blue,max}$ and $I_{j,red,max}$ are the absorbance intensities at the primary blue and red peaks, typically around 640 nm and 540 nm respectively.

A more involved approach described by Lifshitz et al. [56] to track both the polymerization and blue to red transition is to decompose and fit the individual peaks in the absorbance spectra, integrate

those peaks and then compare the relative area of the blue and red peaks. If a first order reaction is assumed, then the kinetics may be modeled using a series of coupled differential equations (equations 2.4-2.8) [56].

$$\text{Monomer } (M) \rightarrow \text{Blue Phase } (B) \rightarrow \text{Red Phase } (R) \tag{2.4}$$

$$\text{Polymer } (P) = B + R \tag{2.5}$$

$$\frac{dM}{dx} = -k_1 M \tag{2.6}$$

$$\frac{dB}{dx} = k_1 M - k_2 B \tag{2.7}$$

$$\frac{dR}{dx} = k_2 B \tag{2.8}$$

2.3.1.2. *Fluorescence Spectroscopy and Microscopy.* Fluorescence spectroscopy and microscopy are powerful tools to examine the blue to red transition, as only the red phase is fluorescent, providing an additional avenue for validating UV-vis and other spectroscopic observations. For fluorescence spectroscopy, typically an excitation wavelength around 485 nm is used, with emission captured for wavelengths longer than $\sim$ 500 nm. For microscopy, the PDA emission spectra is quite broad and many "red" filter cubes can be utilized, such as Texas Red, mCherry or any with excitation wavelengths ranging from 520-580 nm and emission wavelengths greater than 590 nm [37, 57]. Figure 2.3C shows the increase in fluorescent intensity as a function of increasing UV light exposure.

A "Fluorescent Colorimetric Response", or FCR may be employed if fluorescence spectrophotometry being used, equation 2.9 [58, 59].

$$FCR = \frac{I_1 - I_0}{I_{max}} \tag{2.9}$$

Where I_0, I_1 are the fluorescent intensities at the peak fluorescence wavelength, typically around 640 nm before and after application of an external stimulus, with I_{max} being a maximally red phase PDA reference sample.

Similarly, Bubeck et al. monitored polymerization and the blue-to-red transition using absorbance and fluorescence spectroscopy and then simply integrated the total area under the spectra to measure the total polymer content [60]. Fluorescence microscopy can also be used to examine the phase behavior of PDAs. While not as quantitative, the fluorescence of a film often appears binary, and can be exploited as such, Juhasz et al. has shown that fluorescence intensity increases with applied mechanical stress using simultaneous atomic force microscopy and fluorescent microscopy [61]. Fluorescence microscopy further enables the morphology and phase to be examined simultaneously [37, 62]. As discussed in detail in section 2.6, fluorescent polarized light microscopy can reveal the orientation and size of polymer domains, and the amount of red phase within a polymer domain.

2.3.2. Two-tailed and Lipid PDAs. While diacetylenes with two tails such as Diyne-PC do polymerize and exhibit color, they lack the striking blue to red chromatic transitions that are the hallmark of fatty acid derived PDAs. Rather, they often appear orange or red [10, 63]. Hence, while they have many applications in forming polymerized vesicles and drug delivery and may be mixed in with fatty acid PDAs like TCDA or PCDA, they are not the focus of this review [20, 30, 34, 64–68]. Formation of vesicles and characterization is covered in section 2.7.

2.3.3. Tuning the Blue to Red Transition. The polymerization kinetics and chromatic transitions in PDA films can be tuned and controlled based the conditions under which the PDA assembly was formed. These will be discussed for particular examples in the following sections, but there are some general considerations.

2.3.3.1. *Position of the DA Moiety.* The alkyl chain length and position of the DA moiety within the alkyl chain of the fatty acid strongly determines degree of polymerization and the blue to red transition. The relationship between the distance between the DA moiety and the terminal methyl group, m in Figure 2.1 and chromatic transitions relatively straightforward and intuitive. Increasing the alkyl chain length leads to an increase in van der Waals attractions between neighboring chains, stabilizing the blue phase, and increasing the stimulus required to undergo the blue to red transition [37, 55, 69, 70]

Correlations between the polymerization behavior, stimuli responsiveness, and length of the CH_2 spacer between the head group and DA moiety, n in Figure 2.1, have proven difficult to develop.

For instance, it has been observed that 5,7 docsadiynoic acid (DCDA) (13/4) is more sensitive to temperature changes [55, 71], mechanical stress [61], and (when functionalized) cholera toxin [72] than PCDA (11/8). Conversely, Khanantong et al. observed that decreasing n increasing the melting temperature of the DA and the thermal transition temperature [70]. Locating the DA motif very close to the head group, for instance, with $n = 0$, may produce very stable DA Langmuir monolayers but with limited polymerization ability, with the close proximity of the DA motif to the head group inhibiting topochemical requirements [69, 73].

2.3.3.2. *Metal Cations.* The properties of fatty acid DA assemblies can also be tuned by introducing metal cations. The addition of Cd^{2+} to improve the stability of Langmuir films is well established [74, 75]. Likewise, much of the early work on PDA Langmuir films examined monolayers stabilized by Cd^{2+} cations. PDAs formed with Zn^{2+} have been observed to exhibit reversible blue to red transitions when heated, and strongly favor the blue phase [37, 76–78]. Cu^{2+} cations have been observed to strongly favor the red phase [79]. Other cations such as Mg^{2+}, or Ba^{2+} have only a modest effect on the properties of PDAs [80]. Interactions between cations and the carboxylic acid head groups have been probed with Fourier Transform Infrared Spectroscopy (FTIR). Zn^{2+} were observed to exhibit strong bridging bidentate interactions (binding between two neighboring fatty acids). Cu^{2+} cations likewise exhibited bridging bidendate interactions, and differences in their observed behavior, while not fully elucidated, have been attributed to different coordination types [76, 80]. Cd^{2+} cations likely exhibit a monodentate binding between on carboxylic acid and one cation, and other cations like Ba^{2+} appear to exhibit mostly ionic or hydrogen bonding interactions. The stronger interactions observed with cations like Zn^{2+} over Ba^{2+} or Mg^{2+} has been attributed to strong electronegativity and binding affinities [79]. Unlike divalent cations, Monovalent cations such as Na^{+} generally have a limited effect on the chromatic properties of PDAs though Li^{+} have been reported to improve the stability of Langmuir monolayers [43, 81].

2.3.3.3. *Reversibility.* The blue to red transition of un-modified fatty acid PDAs is generally not reversible. Represented schematically in 2.4, application of external stimuli induces the blue to red transition and the system stays red after removal of the stimuli. Several strategies have been successfully employed to engender reversibility in PDAs. The overall goal is to make the blue phase more favorable. This is accomplished by adding additional electrostatic interactions through

metal cations, or modifying the carboxylic head group to have enhanced hydrogen bonding with adjacent molecules. In either case, individual molecules must still be packed sufficiently to sustain topochemical polymerization (section 2.4).

Metal cations are straightforward to introduce, with Zn^{2+} and ZnO nanoparticles demonstrating remarkable reversibility [56, 77]. Alternatively, replacing the carboxylic acid head group with a different functional group with greater hydrogen bonding has also been employed. For instance, Ahn et al. functionalized PCDA with Aminobenzoic acid. The resulting PCDA-mBZA (among others), exhibited reversibility in response to changes in temperature and pH [50, 82]. Similarly, glutamate functionalized DA and esterified PCDAs also exhibited low temperature reversibility [83, 84]. Carter et al. observed that during deposition of red phase PDA (NCDA, (15,8)) Langmuir-Blodgett multi-layers, some red phase PDA transitions back to the blue phase as subsequent multi-layers are built up. It appears that building the multilayer structure, imposes strain on the polymer backbones that forces a conversion from the preferred red phase back to (higher energy) the blue phase [19]. This suggests that transitions even in pure PDAs may be reversible to some degree, however, the underlying mechanism for reversible chromatic transitions remains under-explored.

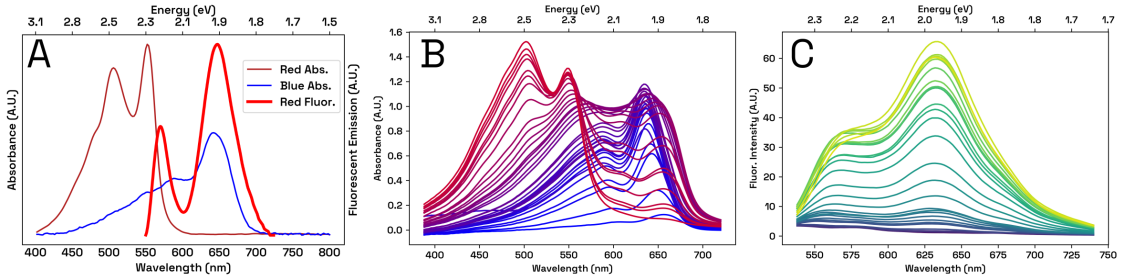

FIGURE 2.3. (A) Absorbance and Fluorescent Emission Spectra for Langmuir films and Vesicles made from polymerized fatty acid diacetylenes (PCDA). (B) Evolution of absorbance and (C) fluorescence emission spectra from PDA (PCDA) vesicles with prolonged exposure to UV light. Data adapted from [10, 37, 56, 60]

.

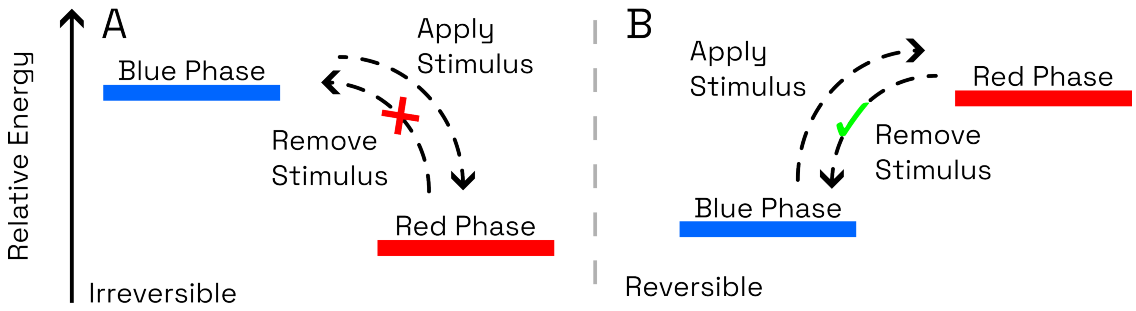

FIGURE 2.4. Schematic of hypothesized energy differences between PDA phases when (A) irreversible, and (B) reversible. In the irreversible case, after removal of external stimulus (UV, heat, etc) the polymer remains in the red phase. Conversely, if the system is reversible, the blue phase is lower in energy than the red phase and the system returns to the blue phase after cessation of stimulus. Figure adapted data and ideas the following references [50, 85, 86].

2.4. Polymerization of Diacetylenes

Polydiacetylenes follow what is known as topochemical polymerization. That is, for polymerization to occur, the "topography" of the packed monomers must be within geometrical and spacing requirements. Broadly, the polymerization process has been described as the 1,4 addition of monomers to a radicalized monomer. As described by Bässler, repulsive forces between the 1,4 carbons in adjacent monomers must be overcome, and rotation of the monomer assembly must occur before polymer bonds can form [87]. This energy barrier necessitates exposure of a packed monomer assembly to high energy UV light, x-rays [88] or γ rays. UV-C light is particularly well-suited to inducing polymerization as the DA monomer absorbs strongly at $\sim$ 256 and 242 nm, thus initiating the polymerization process [10, 30]. While much of our understanding of the polymerization behavior was developed using other diacetylene monomers such as TS-6, TS-12 and n-BCMU (see section 2.11.1), the polymerization mechanism described here is the same for PDAs derived from fatty acids [10, 15, 16, 18, 89].

The polymerization of diacetylenes has been extensively studied and attracted great interest as a well controlled system to study not only PDAs as a unique system, but also general phenomena in polymerization kinetics. Several features of PDA lend it well to the study of these phenomena: solid state, 1-D linear orientation and relative lack of disorder. This combined with high resolution

techniques such as NMR (nuclear magnetic resonance), electron spin resonance (ESR), x-ray and electron diffraction and low temperature spectroscopy have enabled observation of the reaction intermediates and the development of a detailed mechanism. Polymerization is also subject to environmental effects, most notably, the presence of oxygen when exposing the diacetylene assembly to UV light. Oxygen radicals have been posited to reduce polymer film uniformity and create more defects and cracks in self-assembled thin films [40, 90].

2.4.1. Topochemical Polymerization.

2.4.1.1. *Packing Requirements.* PDAs polymerize via a solid state reaction that has specific packing requirements which must be met for polymerization to occur. Schematically this polymerization is shown in Figure 2.5. In general the diacetylene moiety from two adjacent molecules must be located within $\sim$ 4 Å of each other, with the spacing between neighboring molecules being less than approximately 4.9-5.2 Å [87, 89, 91, 92]. As the DA assembly undergoes polymerization, there is rotation around the center of each diacetylene center to produce the polymer chain. As no diffusion, or phase transition is required, this polymerization process can produce large defect free single crystals.

2.4.1.2. *Initiation, and propagation.* UV-C (254 nm) light is most commonly used to initiate and propagate polymerization, with γ and x-rays also being effective for polymerization. Longer wavelengths of light such as UV-A, visible light and IR lasers have also been reported to induce polymerization, however in general are less efficient [23, 41, 87, 93]. Exposure of light (UV or otherwise) to packed monomers produces excited, radical monomers. At low temperatures ($<$10 K), the reaction slow significantly and intermediates can be observed. As described by Sixl [91], these photo-initiated radical monomers then form either di-radical (DR) butatriene structures or asymmetric carbene radicals (AC). A schematic of this polymerization process and nomenclature is shown in Figure 2.6. DR molecules possess alternating double-single bonds, with radical electrons at both ends of the polymer chain. This chain can continue to propagate through continued addition of an adjacent monomer and photon. Excited monomers may combine to form an asymmetric, single radical carbene with an alternating double-triple bond structure (AC). This structure propagates only from one end of the chain. The di-radical structure may irreversibly convert to the asymmetric radical (AC) structure (thus terminating one end of the chain), while the other end of the chain

continued to propagate. During the initial stages of polymerization, the DR butatriene structure was observed to be more stable, but as the chain length increases (n>5-7), the AC structure becomes more favored and a cross-over to this structure generally occurs. This process continues until it runs out of topochemically packed monomers, or photons, at which point the polymerization process terminates and a stable polymer is formed [91].

2.4.1.3. *Termination.* The structure of the terminal groups of stable PDA chains are not well established. Several end groups have been proposed, but there is little experimental evidence for any of them. Two structures have been proposed, a pseudo-cyclopropene moiety proposed by Hersel et al., Figure 2.7A and a structure with an additional triple bond before the adjacent terminal monomer, Figure 2.7B [91]. In either case, it was generally thought that once a chain terminates, restarting polymerization was not possible [6, 94–96].

2.4.1.4. *Restarting Polymerization.* With the proposed end groups as shown in Figure 2.7, restarting of the polymer chain is not thought to occur, however, there have been reports of the polymerization process "restarting" and propagating with longer wavelengths of UV light (UV-A) and visible light [10, 60], with Tieke remarking that monomer DA crystals appear blue when exposed to sunlight through a glass window. The process generally occurs through polymerization of a monomeric DA assembly to UV-C light. After initial polymerization, the partially polymerized chains are now significantly more reactive and will continue to polymerize if exposed to longer wavelengths of light (UVA and visible). This "self-sensitization" process, through which polymer chains become sensitive and reactive to longer wavelengths of light is not fully elucidated. Bubeck et al. suggest that the charge carries are created in the polymer backbone by exposure to visible light. As the PDA backbone is highly conjugated, these charge carriers move along the chain and migrate to the polymer chain ends, reactivating them. The radicalized chain ends will then enable the continued addition of adjacent monomers [60]. This mechanism is representation schematically in Figure 2.8. PDAs are not only self-sensitized by longer wavelengths of light, but have also been observed to polymerize when visible light absorbing dyes are added into the diacetylene assembly. The mechanism of this energy transfer is not fully elucidated, see Bubeck et al., Fouassier et al., Bara et al. [97–99] for details. Further self-sensitization behavior in self-assembled monolayers and crystals have been reported [99–101].

2.4.2. How Long are PDA chains? While the mechanism of polymerization is well described, the chain length of PDAs is not as well characterized. With few exceptions, PDAs are not soluble in any common solvents, eliminating the ability to utilize SEC/GPC (size exclusion chromatography/gel permeation chromatography) to examine their molecular weights. This includes polymers composed of fatty acids such as PCDA and TCDA. Polymers made from 3-BCMU and TS-12 are soluble in many organic solvents, and their molecular weights have been characterized [102, 103]. The molecular weight distribution for different polymerization stages of TS-12 is shown in Figure 2.9. From this it can be seen that small chains form at the initial stages of polymerization, and as polymerization proceeds, only long chain polymers are observed. From these molecular weight studies, Wenz and Wegner [102] and Enkelmann [96], concluded that short chains forming early on remain short even as polymerization proceeds, indicating that polymerization does not restart after the chain is formed. Chain propagation behavior was observed strongly dependent on temperature, with longer chains forming at lower temperatures and shorter chains forming at higher temperature [96, 102]. Using Nuclear Reaction Analysis, Spagnoli et al. developed a method for estimating polymer content in PDAs. Langmuir films of PCDA were observed not to polymerize fully, with a polymerization maxing out at 50-60% [104]. Similarly, in studies of PDAs formed as monolayers on highly oriented pyrolytic graphite (HOPG), PDA polymerization has been directly driven by using the tip of a scanning tunneling microscope, via a similar mechanism [105–107], with the conversion and degree of polymerization characterized via the fluorescent response of the polymerized monolayer [108, 109].

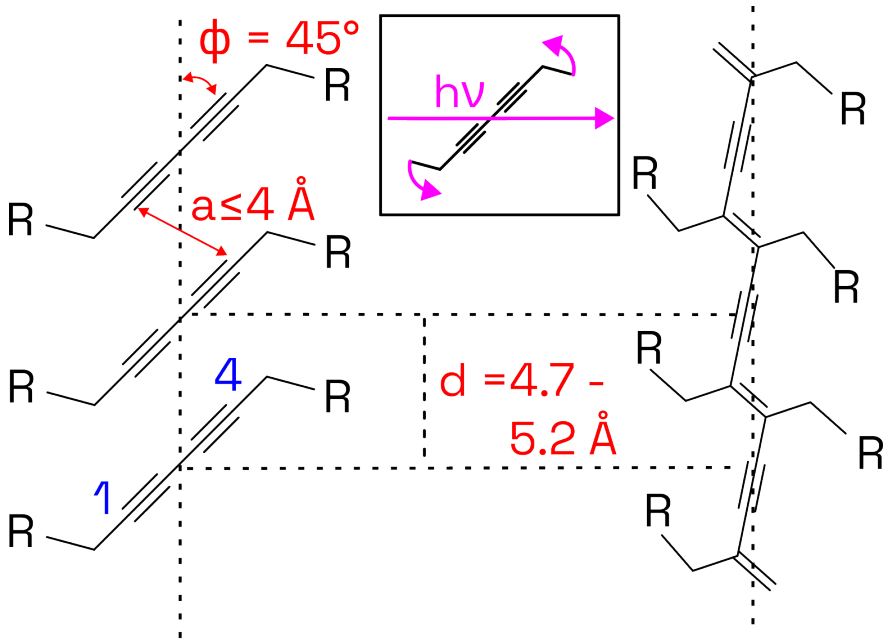

FIGURE 2.5. Spacing and packing requirements for topochemical polymerization of diacetylenes in the solid phase. The "1" carbon (noted in blue) must be less than 4 Å from the adjacent "4" carbon on another chain. The photo-initiated polymerization process necessitates a rotation in the monomer triple bond moeity to form a linear PDA chain. Figure is adapted from Wegner, Menzel et al. [6, 87, 92, 96].

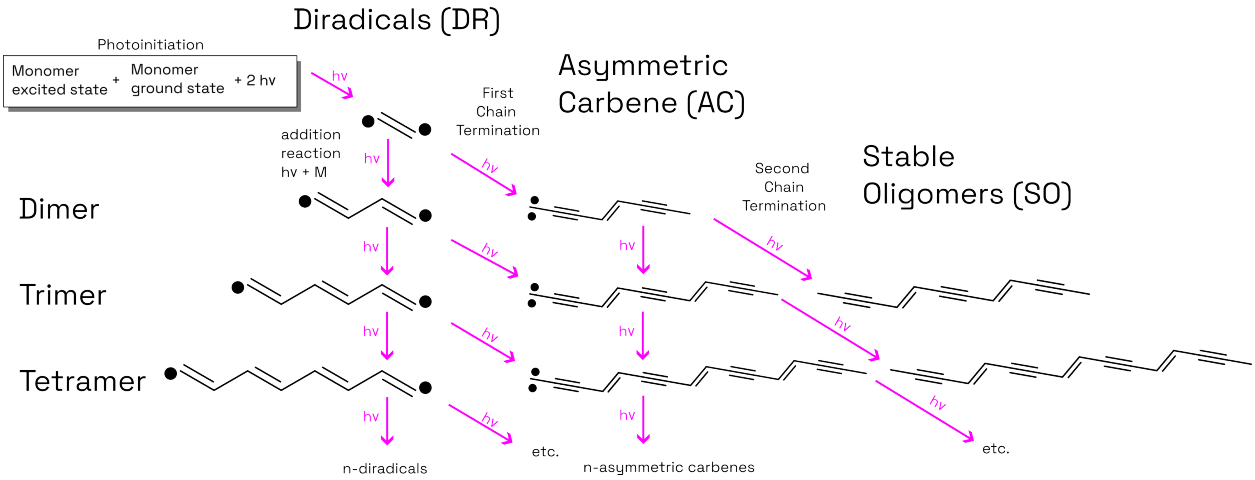

FIGURE 2.6. Simplified schematic representation of the photopolymerization of diacetylenes at low temperatures, adapted from Sixl[91]. A photon-excited monomer combines with a ground state monomer to form a diradical butatriene (three repeating triple bonds) structure (DR). The polymerization process proceeds from both ends with the addition of 1 monomer and 1 photon. If one end of the DR terminates, the asymmetric carbene structure forms, with propagation continuing from one end. The second chain then terminates forming a stable oligomer (SO). This process in examined in greater detail in the following references [15, 91].

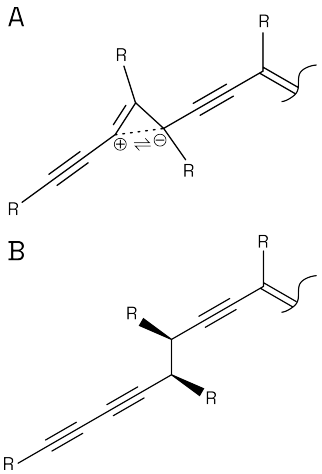

FIGURE 2.7. Schematic representation of the two proposed end groups. (A) As proposed by Hersel et al., a stabilized radical in a psuedo-cyclopropene configuration and (B) monomer inserted directly at the end of the polymer chain [91, 94].

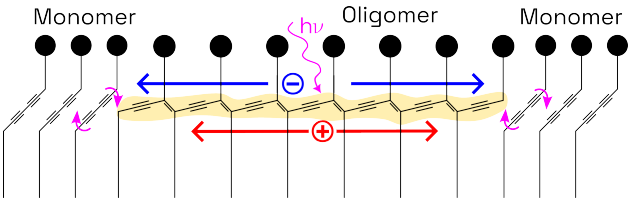

FIGURE 2.8. Schematic of a potential self-sensitization process in PDAs. The oligomer is initially polymerized with UVC light. Subsequent exposure of the partially polymerized PDA assembly to visible light can restart polymerization and grow the polymer chain. Magenta line represents visible/UVA light exciting the polymer backbone (yellow), creating charge carriers that migrate to the end-groups, restarting polymerization (red and blue arrows and charges). Figure adapted from [60].

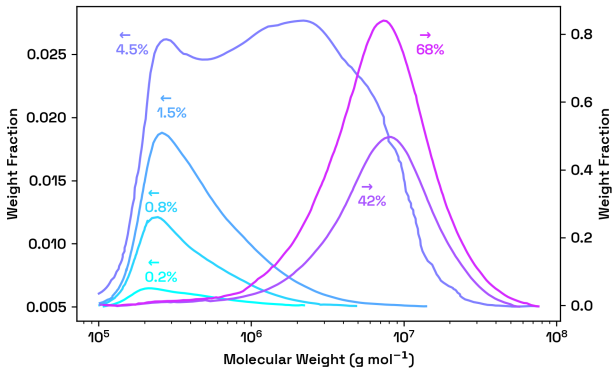

FIGURE 2.9. Molecular weight distribution of PDAs made from 12-TS. Conversions less than 4.5% follow the left y-axis, and higher conversitions follow the right y-axis. In high conversion experiments, the short chain PDAs are still observed, but the relative ratio differs by several orders of magnitude. Figure adapted from Enkelmann, Wenz and Wegner [96, 102, 110].

2.5. Optical and Electronic Properties of Polydiacetylenes

The highly conjugated polymer backbone, consisting of an alternating double bond, triple bound structure, Figure 2.5, confers a range of fascinating optical and electronic properties. Extensive conjugation engenders delocalization of π electrons along the polymer backbone. This highly conjugated system is responsible for the remarkable optical and electronic properties including strong absorbance and fluorescence in the visible range [18, 111], conduction [112–115], third order non-linear susceptibility, and third harmonic generation [18, 19, 116–124]. The ene-yne structure is resonant with a butatriene structure. While this structure may be preferred for very short chains

(see Figure 2.6), for longer chains, it has been discounted through detailed calculations [125], x-ray crystallography and nuclear magnetic resonance spectroscopy [19, 87, 126, 127].

The mechanism of optical absorption in PDAs is broadly described by a π to π^* transition within the conjugated polymer backbone. The side chains of most DA monomers are chosen not to exhibit any absorption in the visible range as to not interfere with the absorbance of the backbone [112]. For fatty acid diacetylenes formed as Langmuir films and vesicles, initial photopolymerization produces blue phase polymer, which upon the application of further stimulus such as heat or light undergoes the blue to red transition and produces a red phase polymer. Structural studies and ab initio calculations have found that the transition from blue to red is not necessarily a transition from order to disorder (or vice versa), but rather a shift in the backbone conformation from a linear, planar, backbone to have some degree of twisting, zigzag, or other non-planar geometry [42, 127, 128].

2.5.1. Ground State Geometry of the PDA Backbone. The backbone of PDAs is centrosymmetric, exhibiting $C2_h$ symmetry [18, 129]. Molecules with a centrosymmetric point groups possess a center of inversion and a horizontal mirror plane. Reflections across the mirror plane are either symmetric A, or antisymmetric B. Operations across the inversion center are labeled as g (gerade, even) or u (ungerade, odd). The ground state of PDAs, S_0, is assigned $1A_g$, and the first optically allowed one photon transition is label as $1B_u$, followed by $2A_g$. All wavefunctions are therefore labeled as A_g (even), or B_u odd. Of interest to understanding the many unique optical properties of PDAs are the two-photon $2A_g$ state, the one-photon $1B_u$ excited state, and the mA_g charge transfer state. These states are responsible for many of the observed nonlinear optical properties of red and blue phase PDAs [18, 112, 129, 130]. The relative energetic position of the $1B_u$ and $2A_g$ states determines whether fluorescence emission is allowed from the different phases of PDAs [129]. Figure 2.10 schematically shows the different states in blue and red phase PDA. In the case of blue PDA chains, the lowest lying excited state has A_g symmetry and thus the transition is optically forbidden. Fluorescence is allowed in the red phase as the $1B_u$ state lies below the A_g state [112, 129, 131].

2.5.2. The Blue Phase. Blue phase PDAs often have two peaks in the absorption spectra, Figure 2.11. For fatty acid DAs, such as PCDA, the primary absorption peak is located at ~ 640nm,

with a prominent vibrational peak present usually around 550 nm. Low temperature spectroscopy and Raman scattering has found that these vibrational lines originate from stretching of the double and triple bonds [112]. The planar geometry of the PDA backbone renders the lowest lying excited state to have A_g symmetry. As the ground state also has A_g symmetry, one-photon transitions are dipole forbidden; absorbed photons non-radiatively transit back to the ground state and the blue phase is non-fluorescent, Figure 2.13 [129].

This behavior is observed in PDAs formed from both DA fatty acids and bulk n-BCMU crystals. However, for isolated chains at low temperature (4K), weak fluorescence from the blue chain can be observed [112, 132, 133]. Blue phase fluorescence is extremely weak however, with a fluorescence quantum yield of less than 10^{-5} [133]. Quantum yield is defined here as the ratio of the total number of photons emitted compared to the total number of absorbed photons [134, 135] Figure 2.11 highlights several Blue PDA systems. Blue phase fatty acid DAs and Blue n-BCMU have been widely studied, both bulk n-BCMU polymer and isolated blue chains have been examined in depth and are the subject of several reviews and books detailing their electronic properties and structure [18, 112]. Two-photon spectroscopy has extensively employed to explore the electronic states of n-BCMU and fatty acid PDAs [18, 19, 118, 119, 122].

2.5.3. The Red Phase. Prolonged radiation, or application of external stimuli induces a transition from the blue phase to the red phase. The red phase exhibits a blue shift of the absorption spectra to two new peaks, a primary excitation peak at ∼550 nm and a series of vibrational peaks at ∼500 nm and shorter wavelengths, Figure 2.12. Unlike the blue phase, the red phase is much more fluorescent. The quantum yield of red phase PDAs is significantly higher, with a yield of 0.30 measured for an isolated 3-BCMU chain [134]. Unlike in the blue phase, the $1A_g \rightarrow 1B_u$ transition is optically allowed and hence the red phase is fluorescent. The origin of the shift in electronic structure, and the entire blue to red transition is not fully elucidated and is under active investigation. However, spectroscopic and structural studies suggest that red chains are non-planar. This shift from linear to either a twisted, zigzag, or worm-like geometry alters the electronic structure of the backbone, shifting accessible excited states. Recent simulations by Choi et al., suggest twisting of the polymer side groups may influence the electronic strcutre of the polymer backbone [85].

Additionally, it has been observed that the excitation of a red PDA chain is spatially coherent over tens of microns, perhaps limited only by the chain length of the molecule [136]. Figure 2.13 shows two potential structures of the red phase as compared to the blue phase.

2.5.4. The Blue to Red Transition. The nature of the blue to red transition remains to be fully elucidated. However, extensive study has established a sketch of the factors involved. Early on it was hypothesized that the origin of red and blue spectra arose from different resonant structures of the PDA backbone. With the blue phase represented by the ene-yne and the red phase represented as with a resonant butatriene structure, that is, three triple bonds in sequence. However, crystallographic [87], C13 NMR [19, 126] and theoretical studies [125] have ruled out the butatrienic structure as a realistic depiction of this transition. Rather, initial polymerization yields the blue phase, a polymer with properties governed by the conformation of, and strain imposed by the side groups.

Van der Waals attractions from side groups such as alkyl chains, and hydrogen bonding between carboxylic and urethane groups all impose strain on the backbone. Hence, the extended backbone forms in a strained conformation, matching the topochemical requirements, while also matching the geometry of the constituent monomers [127, 137]. Application of external stimuli (such as heat, mechanical stress, etc.) overcomes this strained "metastable" conformation, and the polymer backbone can "relax" into the energetically favored red phase. Structural aspects of the blue to red transition in PDA Langmuir films are discussed in section 2.6.4.

The term "conjugation length" has been frequently invoked to describe the differences in electronic structure of blue and red phase PDAs. Generally "conjugation length" refers to the number of polymer repeat units that would exhibit the same absorption spectrum as the measured polymer. However, this term is not rigorously defined, and would indicate the that the blue to red transition is an order-disorder transition. Both perfectly ordered blue and red chains have been observed, and hence the difference in chromatic phases is most likley due to different geometries of the backbone [128].

It has been further observed that the blue and red phases of PDA are remarkably similar to h- and j-aggregates, which describe the packing and orientation of dye molecules and the resulting effect on

their optical transitions [138–141]. These observed similarities provide further conceptual evidence that the differences in blue and red forms also arise from the orientation and packing of the side chains and backbone [112, 142].

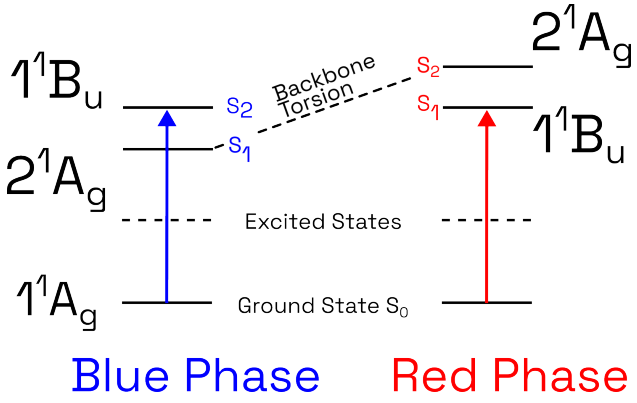

FIGURE 2.10. Simplified diagram of the electronic states in blue and red phase PDA. Ground state of PDA has A_g symmetry. In blue phase PDA the nearest accessible excited state, $2A_g$ has the same symmetry and radiative transitions are forbidden by selection rules for single photon transitions. It is thought that torsion of the polymer backbone alters the electronic structure of the polymer backbone. This twisting decreases alters electron delocalization and the B_u state becomes accessible. $A_g \rightarrow B_u$ transitions are allowed and red phase PDA is fluorescent. Figure Adapted from [116, 129, 143–146]

.

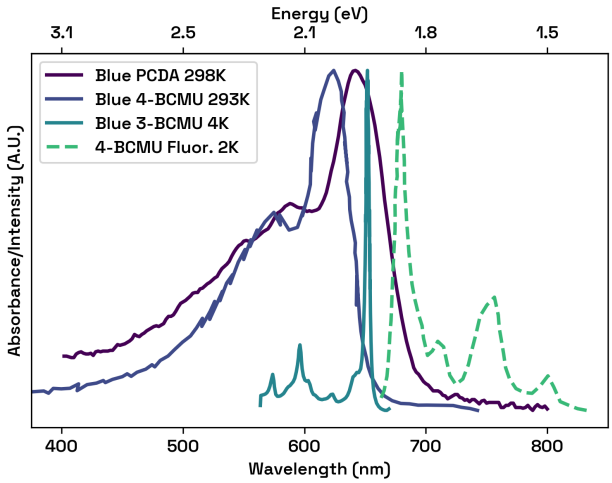

FIGURE 2.11. Absorbance/Emission Spectra of Blue Phase Polydiacetylenes composed of different DA monomers. Blue Phase PCDA is from a PCDA Langmuir film at the air-water interface at 298K. Blue 4-BCMU at 293K is from a bulk polymer crystal from Spagnoli et al. [147]. Blue 3-BCMU at 4K is from an isolated chain Pandya et al. [143]. Fluorescent emission from 4-BCMU isolated chain at 2K Schott [112]. The Stokes shift for BCMU chains is negligible.

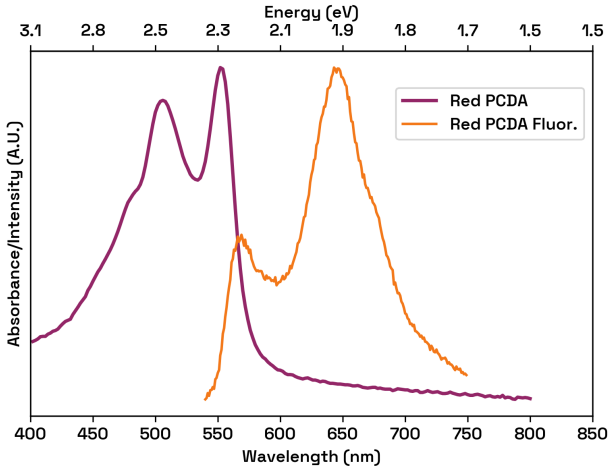

FIGURE 2.12. Absorbance/Emission Spectra of a red phase PDA trilayer Langmuir film made from PCDA. The emission spectra was captured with an excitation wavelength of 485 nm.

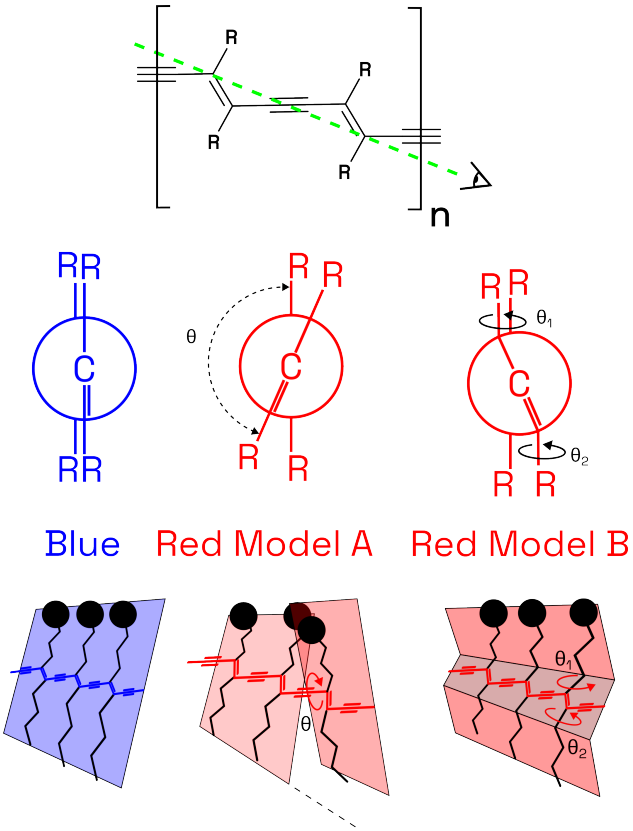

FIGURE 2.13. Newman and 3-D projections of Polydiacetylene backbone in the blue phase (linear) and two non-planar models of the red phase. Model A shows an exaggerated twisted backbone [15, 96, 143, 148], model B shows twisting of the side chains leads to a nonplanar backbone [85]. Theoretical and experiment work shows that a change in backbone torsion, noted as θ is sufficient to blue-shift the absorbance spectra. Figure adapted from [85, 143, 148].

2.6. Morphology of Fatty Acid Polydiacetylenes: Langmuir Films

PDAs made from long chain fatty acids, phospholipids and other surfactants can be deposited on a Langmuir-Blodgett (LB) trough and can form stable mono- and trilayer films. Langmuir-Blodgett and related techniques are widely used for the formation of molecularly thin films with an immense literature dating back almost 90 years. General LB theory and techniques can be found in the following references [74, 75, 149–153]. This section will primarily focus on Langmuir films (LF) formed from fatty acid diacetylenes, with these concepts generally extending to all Langmuir film forming DAs.

2.6.1. Monomer and Solvent Choice. Typical DA LF monomers are, water insoluble, long chain fatty acids such as PCDA, TCDA or NCDA. Lipid-like DAs such as 23:2 Diyne PC and derivatives of these are also widely used. In general, the DA surfactant is dissolved in a water-immiscible solvent with high vapor pressure. This solution is then deposited at the air water interface drop-wise. The solvent then evaporates, leaving the residual DA surfactant or lipid at the air water interface. Chloroform is the most commonly used solvent for depositing surfactant monomers onto the air-water interface. Typically, concentrations ranging from 0.3 to 1 $\mathrm{mg\,mL^{-1}}$ are used. Once dissolved, the DA monomers are stable for short periods (up to 1 week) of time, but may slowly polymerize at room temperature, and if exposed to light.

Solvent choice can have a remarkable effect on the DA spreading properties and resulting PDA films. Several solvents and solvent mixtures have been employed, with chloroform, benzene, and mixtures of chloroform:methanol, benzene:chloroform and ethanol:hexane being the most widely used. Benzene (and by extension, other cyclic solvents) seems to be associated with formation of larger PDA domains as observed by Tieke [10], Yamada and Shimoyama [40]. This is likely due to the slower evaporation process of benzene as compared to chloroform. Longer chain DA such as NCDA tend to be less soluble in benzene and require addition of a small amount of methanol (or other more polar solvent). Sasaki et al. likewise, utilized a 50% benzene:chloroform mixture to produce high quality LFs [38]. Chloroform can be used to produce high quality LF, however the domain size may be smaller [10, 154, 155]. Gourier et al. examined the effect of a number of different solvents on the behavior of DA Langmuir films, observing that n-hexane with the minimum amount of ethanol to dissolve the DA monomer (typically about 10%), greatly increases the stability and collapse pressure of the DA monolayer formed at the air-water interface [155]. These results are indicated in Figure 2.14III, curves A, B.

2.6.2. Compression and Collapse. Once the DA monomers are deposited at the air-water interface, they are compressed to form a film. Due to the high melting temperatures of most fatty acid DAs (PCDA has a T_m of ≈65°C), compression of the film leads directly to the formation of a condensed or solid phase monolayer. DA monomers on a pure water subphase generally form relatively unstable monolayers that collapse at relatively low surface pressures (often between 5

and 15 $mN\,m^{-1}$), see Figure 2.14I,II. The limiting area per monomer in a DA monolayer film is approximately 24-25 $Å^2$. Stable (though perhaps somewhat heterogeneous) monolayers of fatty acid diacetylenes may be produced through raising the pH, and/or adding $CdCl_2$ (or other divalent metal cations) to the subphase, with further options summarized by Gourier et al. [39, 154, 155]. The position of the diacetylene motif within the alkyl tail also plays a role in the stability of the film, with the DA motif positioned close to the head group (16/0) greatly stabilizes the monolayer film, described by Tieke [10]. Functionalizing the carboxylic acid headgroup to enhance hydrogen bonding also enables stable monolayers to be reliably formed, for example, N-(2-ethanol)-10,12-pentacosadiynamide (PCEA) forms a stable monolayer film [38]. Isotherms of some stable monolayer DA films are shown in Figure 2.14II.

Continued compression of a Langmuir monolaye results in a collapse, forming mulitlayers. This collapse is generally described as either a "constant area collapse" or a "constant pressure collapse" [156]. In a constant-area collapse, as compression continues, the surface pressure increasing significantly, peaks and rapidly decreases without a significant change in area. The resulting collapsed state is a mixture of monolayer, trilayers and thicker multi-layers [157–160]. Conversely, in a constant pressure collapse, the isotherm shows continued decrease in trough area without increasing in surface pressure, this is most commonly seen in phospholipids and biological surfactants [156]. In both cases, material can also be lost into the subphase.

A mechanism proposed by Ries and Swift for the collapsed state of fatty acid Langmuir films has been adapted and discussed in the context of diacetylene Langmuir films [154, 156, 162]. Isotherms of diacetylene fatty acids show that the collapse behavior is complex: often a small peak is observed, indicating a constant area collapse, however the pressure post collapse often remains high, indicative of a constant pressure collapse, see Figure 2.14III. Furthermore, the resulting collapsed state forms a somewhat heterogeneous trilayer film as seen by the pressure area isotherms, Figure 2.14I, and atomic force microscopy, Figure 2.17.

A schematic of the proposed mechanism is represented in Figure 2.15. Compression beyond the collapse pressure of the film leads to weakening (Figure 2.15A), folding (B), bending (C) and then finally collapse onto the existing monolayer (Ries mechanism) [157, 161, 163]. The plateaued region

following collapse is often described as monolayer-trilayer coexistence. Continued compression leads to the formation of a stable trilayer. Several mechanisms of trilayer growth have been proposed and are shown in Figure 2.15D,E. In Figure 2.15D growth of the trilayer occurs through the growth of a bilayer and sliding on top of the underlying monolayer. This growth continues until the trilayer structure covers all areas of the air-water interface [162–164]. A second mechanism shown in Figure 2.15E by Gourier et al. proposes that growth of the trilayer propagates through exclusion of molecules at the edge of a nucleated trilayer "island" [154]. The stability of the monolayer and collapse behavior has been observed to be strongly governed by spreading solvent choice, subphase pH and temperature, and compression speed, with some examples shown in Figure 2.14III [154].

The collapsed state of Langmuir films has been investigated using a number of surface sensitive techniques including Brewster angle microscopy (BAM) [165], X-ray reflecitivity (XRR) [155], and polarizion modulation infrared reflection absorption spectroscopy (PMIRRAS), among others. Details of the methodology, refinement of the Ries mechanism and theory can be found in the following references [151, 154–156, 158–172].

Initially, the presence of a trilayer was reasoned through surface pressure stabilizing at an area per molecule of ∼8 $Å^2$, which corresponds to a three molecule thick film with an area per molecule (∼24-25 $Å^2$). As subsequently show by AFM imaginging of deposited films, the trilayer film is not uniform with regions on monolayer, bilayer and multilayers also forming, Figure 2.17 [38, 57, 79]. Further compression of this trilayer may lead to further multilayer and even fiber-like structure formation [173].

2.6.3. Deposition Techniques. Diacetylene Langmuir films are sometimes amenable to typical Langmuir-Blodgett (LB) and Langmuir-Schaefer (LS) deposition techniques [74, 75, 151, 152]. Much of the initial work on PDA Langmuir films focused on multilayers built up via monolayer LB deposition [10]. The collapsed trilayer, both as a monomer film and when polymerized is significantly stiffer, and generally the transfer ratio of the LB technique is quite poor [37, 38]. Several other techniques have been developed to improve film transfer. PDA trilayers are readily amenable to traditional Langmuir-Schaefer (LS) deposition. Furthermore, an LS-like "stamping" technique is also effective. A sufficiently hydrophobic substrate is gently pressed against the film at the air-water

interface. The substrate is then removed, and blown dry with a stream of nitrogen [62]. Another effective method is an angled Langmuir-Blodgett technique, in which the substrate is angled to $\sim 45°$ from normal, and then raised, to deposit the film. A horizontal deposition technique may also yield very high film transfer. The substrates are submerged in the trough subphase, the film is formed and then the subphase is drained until the film lands on the substrate [38]. All deposition techniques may introduce cracks, gaps and other defects in the film. Furthermore, aggressive deposition of blue phase polymer films may induce the film to undergo the blue to red transition from mechanical stress applied to the film during deposition.

2.6.4. Structure of PDA Langmuir films. Exposing a diacetylene Langmuir film to UV light will induce polymerization. Films formed on a pure water subphase generally appear blue initially, with prolonged exposure to UV light inducing the blue to red transition. The structure of PDA Langmuir films has been characterized with a number of molecular scale techniques including electron diffraction, x-ray reflectivity, grazing incidence x-ray diffraction, and atomic force microscopy. These techniques have enabled direct observation of the structure of the film as it polymerizes and undergoes the blue to red transition.

2.6.4.1. *Electron Diffraction.* Some of the earliest atomistic characterization utilized electron diffraction to determine the lateral spacing of the diacetylene surfactants and small angle x-ray scattering (SAXS) to examine the structure of PDA multilayers. Tieke and Lieser studied Cd-PDA multilayers, and observed a unit cell with parameters of a = 4.86 Å, b = 7.4 Å. where "a" is defined as the direction of polymerization as it aligns with the spacing requirements for topochemical polymerization [69]. SAXS showed that the polymer layers were tilted perhaps as much as 50° to 60° from normal. They also suggested that the presence of blue and red phase PDA is a consequence of steric interactions and rearrangement of the carboxylic and alkyl side chains [69, 174, 175]. Similarly, Kuriyama et al. measured unit cell parameters of a = 4.9 Å and b = 8.4 Å, with $\gamma = 88°$ for the blue phase, and a = 4.9 Å, b = 8.2 Å, and $\gamma = 90°$ for the red phase. They suggestsed that the shift in packing between the blue and red phase was due to a transition from a planar orientation of the polymer backbone to some sort of non-planar structure [142, 176]. Day and Lando measured similar unit cell parameters from TCDA films formed on a Li^+ subphase [81]. The films were observed to

exhibit a tilt of 57°. The highly tilted nature of the monomer and polymer films was observed to be a consequence of the topochemical polymerization requirements (see section 2.4).

2.6.4.2. *X-ray Reflectivity.* The out-of-plane structure of PDA films has been examined at the air-water interface using x-ray reflectivity. Göbel et al. examined "Bronco" (dimethyl-bis-(2-hexacosa-10,12-diinoyl)-oxaethyl-ammonium bromide), a two tailed positively charged diacetylene surfactant at different temperatures [177]. At room temperature, they observed that the monolayer was titled approximately 32° from normal. Polymerization via UV-light induces a shift in tilt to 23° degrees. At lower temperatures, they observed that the tilted monomer films underwent a dramatic shift to a nearly vertical orientation during polymerization. Further electron and x-ray diffraction measurements suggest that the resulting polymer exhibits some degree of handedness [177]. Gourier et al. also studied PCDA monolayers using x-ray reflectivity and observed the molecules to be highly tilted. To produce stable monolayers, a basic suphase was used and this inhibited polymerization of the films, limiting the translatability of this work to polymerized films [155].

2.6.4.3. *Grazing Incidence X-ray Diffraction (GIXD).* GIXD is a powerful tool for examining the in-plane and vertical structure of solid phase Langmuir films. Gourier et al., and Lifshitz et al. examined the structure of PDA (PCDA) monolayers, and trilayers respectively using GIXD [137, 155]. While the chromatic behavior of the PDA films was not commented on by Gourier et al., García-Espejo et al. suggested that the films studied by Gourier et al. were likely red phase, with parameters of a = 5.05 Å, b = 4.81 Å and $\gamma = 122°$ when described as a distorted hexagonal unit cell [178]. Lifshitz et al. measured the evolution of the structure of diacetylene films while being polymerized and transformed from blue to red by the measuring x-rays. The films were modeled as two layers, the carboxyl terminated chain and the methyl terminated chain, joined by the polymer backbone. Their indexing and modeling scheme assigned the monomer and blue phase to be in a hexagonal, or centered rectangular structure. With the monomer having unit cell parameters a = 5.27 Å, b = 9.13 Å, $\gamma = 90°$. Polymerization to the blue phase shifted the structure to an oblique unit cell, with parameters: $a = 4.9$ Å, $b = 9.73$ Å, $\gamma = 85°$. Their modeling suggested that the methyl terminated tail was highly tilted, 40°, with the carboxyl terminated structure being vertical in the monomer phase and slightly tilted (18°) in the blue phase. The red phase was also indexed to an oblique unit cell, a = 4.9 Å, b = 7.82 Å, $\gamma = 84°$, with complete vertical alignment of the

carboxyl and methyl terminated chains. This shift from tilted to vertical is similar to atomic force microscopy measurements as discussed next. The shrinking of the unit cell also leads a smaller area per molecule (APM) consistent with optical microscopy, AFM and pressure-area isotherm measurements [38, 137]. Using XRD on PDA multilayers, Fischetti et al. measured a tilt of 35° and 0° for the blue and red phase respectively [179].

2.6.5. Morphology of PDA Langmuir films. PDA Langmuir films are highly ordered, with linear polymer strands all aligned within a single domain. These domains range from sub µm to millimeter in size depending on the conditions under which the film was formed. The domains of PDA Langmuir films have been investigated using polarized light microscopy, Brewster angle microscopy (BAM) [165, 180–182] and atomic force microscopy [38, 57, 183–186]. The linear backbones of PDAs give rise to linearly dichroic domains that are readily observable by a set of cross-polarizers [37, 38, 187]. Aligning the polarizers with the polymer backbone enables the structure and direction of the polymer backbone to be deduced. Several structures of PDA domains have been observed including mosaic blocks and several spherulitic structures. The mosaic block structure can be seen in Figure 2.16A,C. Spherulitic structures, Figure 2.16B have been observed with the polymer backbones radiating in a spiral pattern (as shown here), but also circumferentially [188]. Tieke and Weiss examined the morphology of multi-layers of cadmium salt PCDA films [187]. Films using benzene as a spreading solvent formed of domains as large "mosaic-block" 100 × 500 µm. They also suggest that domains formed at essentially zero surface pressure, compression of the trough then packed these domains closely together, creating hole free films. Individual layers in a multilayer film built from LB deposition were observed to not be in registry with each other [187]. This is in contrast to compressing a monolayer film to a collapsed trilayer state. In a collapsed trilayer, the individual layers were observed to be aligned with each other [38]. Day and Lando observed spontaneous formation of spherultic structures in Li-PDA films with the backbones aligned radially, spirally or circumferentially [188]. Building on a technique proposed by Day and Lando, Yamada and Shimoyama grew large (mm) scale domains and observed both left and right-handed spirals, Figure 2.16B [40, 189, 190]. Furthermore, Grunfeld and Pitt utilized electric fields to grow mm scale domains [39].

While the underlying mechanism for the diversity of domain sizes and structures is not fully understood, there are parameters than can enable the size and morphology to be tuned. As discussed previously, the spreading solvent can enhance domain size, with aromatic solvents such as benzene enabling growth of large domains. While defect and crack free domains are readily formed on other solvents, such as chloroform, Gourier et al. hinted that reactive radicals from chloroform may break or damage the diacetylene motif [155]. Diacetylene monomer choice also affects domain size. Increasing the monomer tail length leads to smaller domains [37]. Subphase composition, and in particular the presence of metal cations can also dramatically decrease the domain size. Domain size in Langmuir films formed on Cu^{2+} and Zn^{2+} subphases is often below the resolution limit of optical microscopy [37, 78, 79]. Furthermore, in deposited Langmuir films, the substrate may also affect the kinetics of polymerization. Britt et al. and Lifshitz et al. observed that deposited Langmuir films deposited prior to polymerization polymerize less fully and require more stimuli than those polymerized directly at the air-water interface [56, 191].

The nanoscale morphology of PDA Langmuir films has been further observed by AFM [38, 57, 183–186, 192]. Blue and red phases of PCDA polymer films were measured to be of 7.4 ± 0.8 nm and 9.0 ± 0.9 nm thick respectively [38]. From the height difference, they inferred that the blue phase was more tilted than the red phase, $\sim 39°$, as compared to $\sim 20°$ [38, 57]. Likewise, Lio et al. in a study of thermochromism in PDA Langmuir films, observed the thickness of a red PDA film increases by approximately 15% compared to the blue phase. High resolution scans of PDA Langmuir films reveal the linear polymer backbones, Figure 2.17A. Cracks and other defects were found to occur along domain edges, and were generally ascribed to be defects arising from deposition onto a solid substrate. Higher resolution scans reveal a high degree of orientation along the polymer backbone, with less order observed between polymer strands, Figure 2.17B,C. The structure and morphology can be significantly altered however by introduction of metal cations. Figure 2.17D shows a PDA film formed on a subphase of Zn^{2+} cations [79]. Compared to Figure 2.17A, the domains are significantly smaller and less ordered [37, 79]. The linear backbones and orientation into block-like domains can be further probed with friction force microscopy. Carpick et al. observed that the friction force is significantly lower when sliding parallel to the polymer backbone as compared perpendicular to

the domain orientation. This enabled mapping of domains based on the friction of the individual domains [193].

2.6.6. Applications of PDA LF. Langmuir films have been widely employed as model systems to examine the sensing capabilities of PDAs as detailed in numerous reviews (see section 2.9), with thermochromism [86, 183], mechanochromism [57, 61, 62], and bio-/affino-chromism [12] being among their many applications. The highly orientated backbone has enabled PDA films to act as templates to grow crystals and other nanoparticles [194–196]. Beyond sensing, the unique optical properties of PDA Langmuir films have been proposed for use for developing x-ray resists, optical waveguides, and incorporation into semiconductor devices [10, 17, 39].

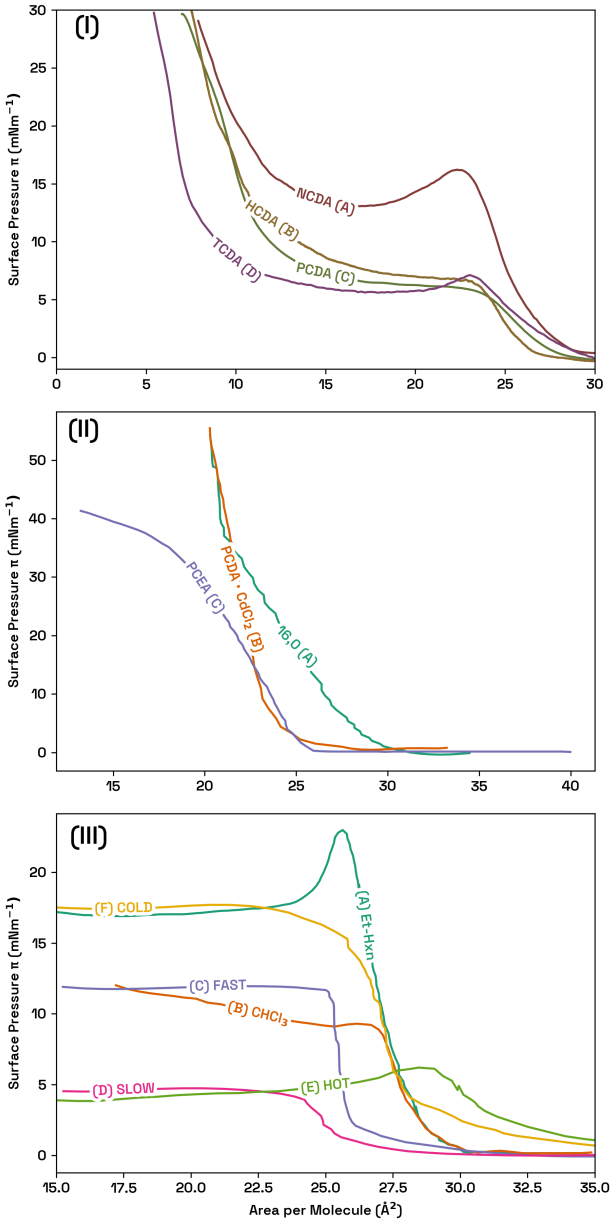

FIGURE 2.14. (I) Isotherms of diacetylenes with increasing alkyl tail length (n) and fixed m = 8 (Figure 2.1): (A) NCDA (15/8), (B) HCDA (13/8), (C) PCDA (11/8), (C) TCDA (9/8) Figure adapted from [37]. (II) Select isotherms of diacetylene films stable as monomers at high surface pressures: (A) PCEA (N-(2-ethanol)-10,12 pentacosadiynamide (11/8)), (B) PCDA on 1 mM $CdCl_2$ and (C) 2,4 heneicosadiynoic acid (16/0) on DI water and $CdCl_2$, figure adapted from [10, 38]. (III) Effect of temperature, spreading solvent, and compression speed on the collapse behavior of PCDA: (A,B) Spreading Solvent: 1:9 ethanol:hexane, chloroform, (C,D) Compression Speed 5.6, 0.056 $cm^2\,s^{-1}$, (E,F) T = 28.4, 5.9 °C, figure adapted from [154]

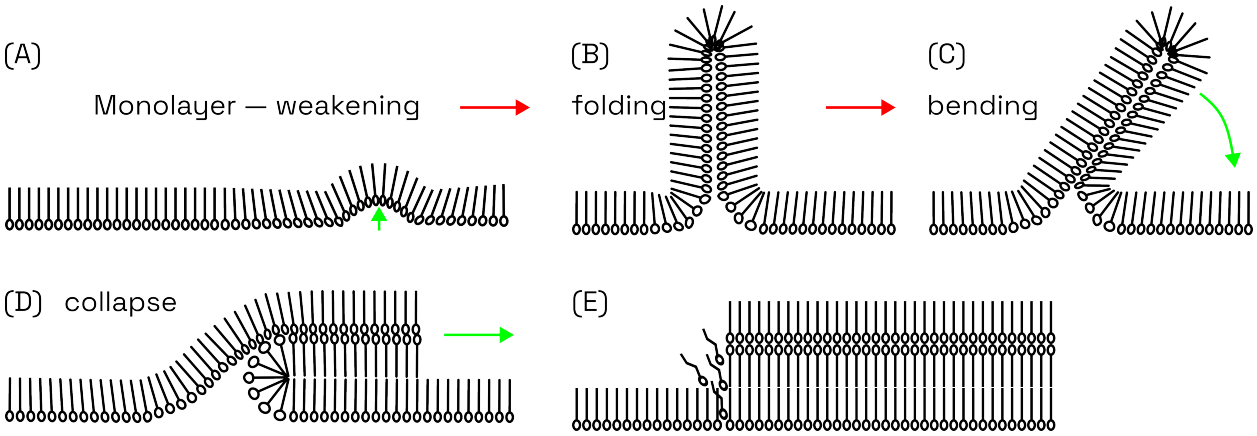

FIGURE 2.15. Proposed monolayer collapse and trilayer formation mechanisms. (A) Compression of a monolayer film leads to buckling (green arrow). (B) Buckling site begins to fold up. (C) monolayer fold collapses on top of the monolayer. (D) Trilayer growth mechanism 1: Continued compression through sliding between collapsed bilayer and monolayer, propagation direction of the trilayer is shown by the green arrow. (E) Trilayer growth mechanism 2: growth via the edge of the initially collapsed site. Figure adapted from [154, 156, 157, 161, 162, 164, 166].

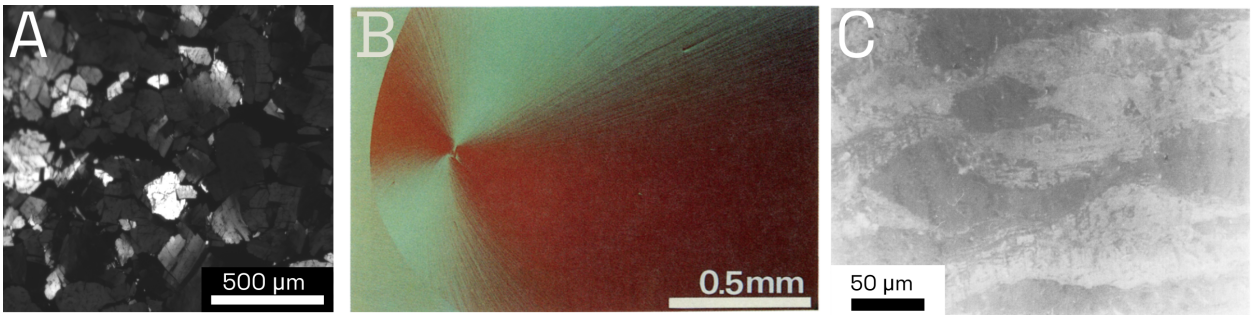

FIGURE 2.16. (A) Polarized fluorescent micrograph of a red-phase PDA (PCDA) trilayer at the air water interface with mosaic block geometry. Black and darkened regions are domains oriented in off-aligned directions from the orientation of the polarizer, from [37] (B) Polarized light micrograph of a large polymerized PCDA domain with spherulitic geometry, a left-handed spiral can be observed, from [190]. (C) Polarized light micrograph of PDA (PCDA) with monolayer with a subphase containing Cd^{2+} after annealing to 55°C and subsequent polymerization, from [187].

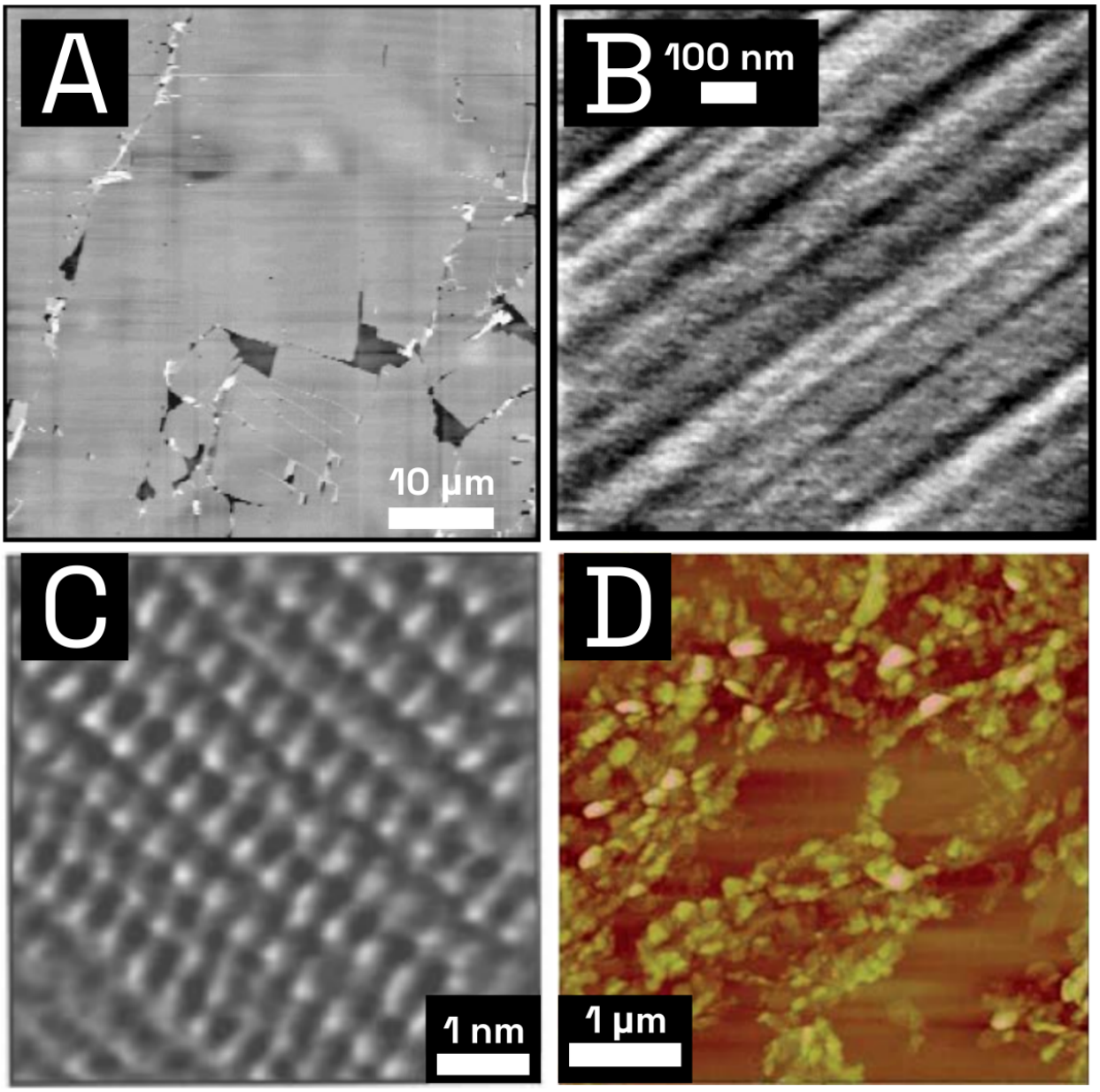

FIGURE 2.17. AFM topography of select PDA films. (A) Blue phase PCDA deposited using a horizontal aspiration method, from [38]. (B) High resolution blue phase PCDA deposited using a horizontal aspiration method, the linear strand morphology can be osberved, from [38]. (C) High resolution blue phase PCDA (with 5% silaic acid PCDA) deposited using a variant of the Langmuir-Schaeffer technique, the backbone direction can clearly be seen, from [183]. (D) PCDA formed on a subphase of 5 mM $ZnCl_2$, the linear strand morphology appear significantly disrupted, from [78].

2.7. Morphology of Fatty Acid Polydiacetylenes: PDA Vesicles

Hydrating fatty acid and lipid-like diacetylenes in an aqueous buffer leads to organization into vesicles. The self-assembled structure of these vesicles is somewhat variable and sometimes can only loosely be defined as a vesicle; they may also be referred to as liposomes, nano-aggregates or particles. Since the synthesis of fatty acid diacetylenes by Tieke et al., PDA vesicles have been extensively documented as sensors and models of membranes due to their brilliant colorimetric transitions, (see Figure 2.19), simplicity of synthesis, stability in aqueous buffers, and ease of functionalization.

Early interest was in developing stable models of bio-membranes via the polymerization of fatty acid and phospholipid diacetylenes [20, 30, 33, 34, 63, 67, 197–199]. Following the sensing demonstration of PDAs to detecting influenza virus by Charych and co-workers, research exploiting vesicles as sensors and drug delivery vehicles has exploded with numerous reviews detailed in section 2.9 [12–14, 35, 49, 55, 72, 183]. Figure 2.20A shows an electron micrograph image of polymerized vesicles formed from two tailed lipids, from [33]. This section will focus on several straightforward methods for fabricating vesicles, heuristics and methods for characterization.

2.7.1. Vesicle Assembly. DA monomers at room temperature are solid and are marginally soluble in aqueous solutions. To facilitate the formation of vesicles, DA monomers must be held above their respective melting temperature. The high melting temperature of most fatty acid DAs is the primary challenge that must be overcome for vesicles to form. Vesicles may be composed of pure fatty acid DAs, two tailed DAs, mixed with a variety of phosopholipids, and other surfactants. Several approaches to PDA vesicle formation have been developed. The first is the classic "thin film hydration" or "Bangham method" [20, 55, 72, 200, 201]. In this method, diacetylenes and other lipids are dissolved in a small amount of chloroform in a vial. Depending on the composition, a small amount of methanol (less than 10%) may also be added to facilitate complete dissolution. While rotating the vial, chloroform is then slowly evaporated using a dry stream of an inert gas, such as N_2, to form a thin film. Alternatively, rotary evaporation may be employed. The film is then fully dried under vacuum to completely remove the solvent (typically for two hours or overnight), DI water or a suitable aqueous buffer is then added. The suspension must be heated to above T_m to melt the diacetylenes. The solution is then probe tip sonicated for several minutes. The resulting

translucent vesicle suspension in then cooled to 4°C overnight to facilitate topochemical alignment of the DA monomers; enabling polymerization. Electron micrographs of vesicles formed this way can be seen in Figure 2.20A,B,C.

The film hydration method is limited by the volume of vesicles that can be produced at one time, and can produce somewhat heterogeneous assemblies, often due to the challenges of maintaining the DA monomers above T_m. The solvent injection technique is an effective alternative. The process involves dissolving the diacetylene monomers in a small amount of a water miscible organic solvent such as ethanol, N,N-dimethylformamide (DMF), or dimethylsulfoxide (DMSO). These solvents facilitate the incorporation of DAs in the aqueous phase. The DA solution is then added to a volume of water and stirred or bath sonicated at an elevated temperature until transparent. The resulting vesicle solution is then stored at 4°C to facilitate topochemical arrangement of the DA monomers. The methodology and properties of solvent injection PDAs have been detailed by Tjandra et al. and Tang et al. [80, 202, 203]. Electron and fluorescent micrographs of vesicles formed via solvent injection can be seen in Figure 2.20D, and Figure 2.21A respectively.

Regardless of method, some diacetylene vesicles will aggregate over time. This aggregation may be reduced via filtration at an elevated temperature, typically above 40 °C, before storage at 4°C. Effective approaches include passing the sonicated solution through a syringe filter (0.45 µm or 0.2 µm), or, using a vesicle extruder system and passing the sonicated solution through a polycarbonate membrane several times. DA vesicles are generally stable when stored at 4°C for short periods of time in the unpolymerized monomer state, but will eventually precipitate out of solution. The stability and properties of pure and mixed PDA vesicles has been reviewed extensively in the following literature [2, 35, 45, 52, 204, 205].

Giant vesicles may also be formed from mixed diacetylene phospholipid solutions. Compared to sonication, which produces vesicles that are roughly 100 nm in size (see next section), giant vesicles are as large as 2 µm in diameter. Pevzner et al. details a method to form giant vesicles from L-α-phosphatidylcholine (Egg PC), Dimyristoylphosphatidylcholine (DMPC) and diacetylene monomers [206]. Adapted from the method developed by Moscho et al., DAs and phospholipids are first dissolved in a chloroform:ethanol mixture and added to a round bottom flask with DI

water added along the rim of the flask. The organic solvent is then rapidly evaporated in a rotary evaporator set to 65 °C, 40 mbar and 40 RPM, leaving an "opalescent" vesicle solution. This solution is then stored overnight at 4°C, after which it can be polymerized via UV light. SEM, phase contrast, and fluorescent micrographs of giant PDA-lipid vesicles can be seen in Figure 2.21B,C,D.

A further method for fabricating PDA vesicles using a microfluidic chip has been detailed by Kim et al. [208]. In addition to fatty acid, and lipid-like diacetylenes, bolaamphiphilic diacetylenes such as 10,12-docosadiynedioic acid (Figure 2.18) may also form self assembled systems, though they often appear as ribbons rather than vesicle-like structures [209–212]. They have also been utilization to form gelators [213]. Finally, under specific conditions, functionalized diacetylene monomers may form micelles [214] and other nanostructures, with nanocomposites being the most common and reviewed in section 2.8.

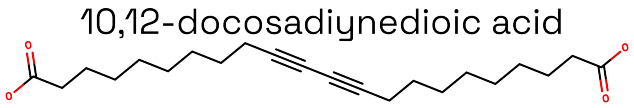

FIGURE 2.18. A bolaamphiphilic diacetylene: 10,12-docosadiynedioic acid

2.7.2. Vesicle Characterization. The spectral and optical characteristics of PDA vesicles can be measured using the techniques described in section 2.3. Fluorescence and UV-vis spectroscopy are the most common to determine the chromatic behavior of vesicles and thereby phase. Several techniques can be used to characterize the morphology of vesicles. First, the size of the vesicles can be measured by dynamic light scattering, DLS, which correlates scattered monochroamtic light to the hydrated Stokes radius of suspended particles. DLS is fast, noninvasive and nondestructive, enabling rapid characterization of vesicles and other PDA nano-assemblies. DLS is limited in that it is highly sensitive to contaminants such as dust, aggregation, and is less amenable to very broad particle size distributions. The particle size distribution of PDAs is generally reported to be centered around 100 nm. Different vesicle formation techniques and diacetylenes produce vesicles that can be larger or smaller, or with a broader particle size distribution. The distribution of particle sizes formed via solvent injection methods was examined by Tjandra et al. [202], and via thin film hydration and microfluidic devices by Kim et al. [208]. Frequently coupled with DLS are measurements of zeta (ζ) potential. ζ-potential is a measure of the charge at the slip plane of the

electric double layer that forms around a charged particle [215, 216]. Vesicles made from fatty acid DAs in DI water are generally negatively charged, with ζ-potentials typically in the range of -20 to -40 mV [217–219].

Scanning Electron Microscopy (SEM) and Transmission Electron Microscopy (TEM) have supplemented DLS measurements in characterizing PDA vesicles size and morphology. General protocols, staining and fixing procedures can be found in the following references [220, 221]. Figure 2.20 and 2.21B shows several PDA assemblies as measured by SEM and TEM. Most vesicles are spherical, but may also be aggregate, or be elongated depending on the choice of diacetylene and formation conditions.

Size information usually is difficult to obtain from light microscopy as the average size of PDA vesicles is below the diffraction limit of light. However, even small (≈ 100 nm) red phase vesicles can be detected with fluorescent microscopy as bright dots with a high magnification objective, Figure 2.21A. The morphology and structure of Giant PDA vesicles can readily be observed by either phase contrast or fluorescent microscopy, Figure 2.21C,D. The morphology is notably different compared to typical giant uniliamelar vesicles in that PDA vesicles appear "fuzzy", with multiple folded structures, compared to the uniform, smooth, spherical morpohology of GUVs. Additionally, the layer spacing and morphology has been probed by small angle x-ray scattering (SAXS) and X-ray diffraction [202, 222].

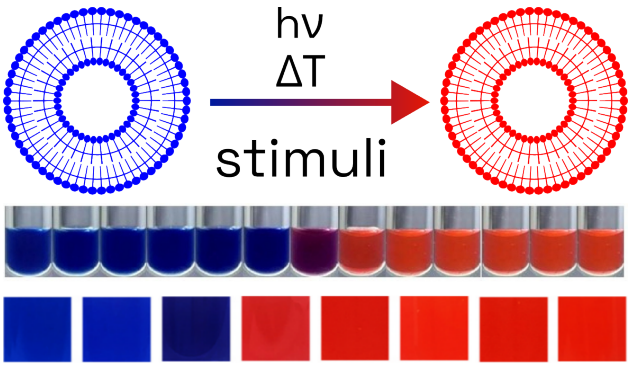

FIGURE 2.19. Schematic of the blue to red transition in PDA vesicles due to application of temperature, UV light, organic solvents or mechanical stress. Figure adapted from [70, 202].

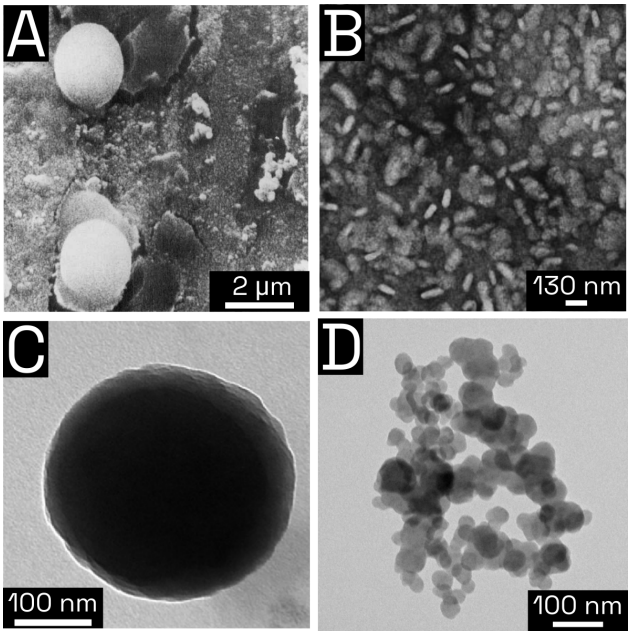

FIGURE 2.20. Electronic microscope images of PDA vesicles. (A) SEM image of polymerized liposome formed from two tailed diacetylene, from Hub et al. [33]. (B) TEM image of PDA vesicles formed via sonication of 10% silaic acid and 90% ethanol amine functionalized PDA (PCEA), from Okada et al. [55]. (C) TEM image of polymerized TCDA vesicle formed via film hydration and sonication, adpated from Pattanatornchai et al. [223]. (D) TEM image of polymerized PCDA vesicles formed via solvent injection, from Tjandra et al. [202].

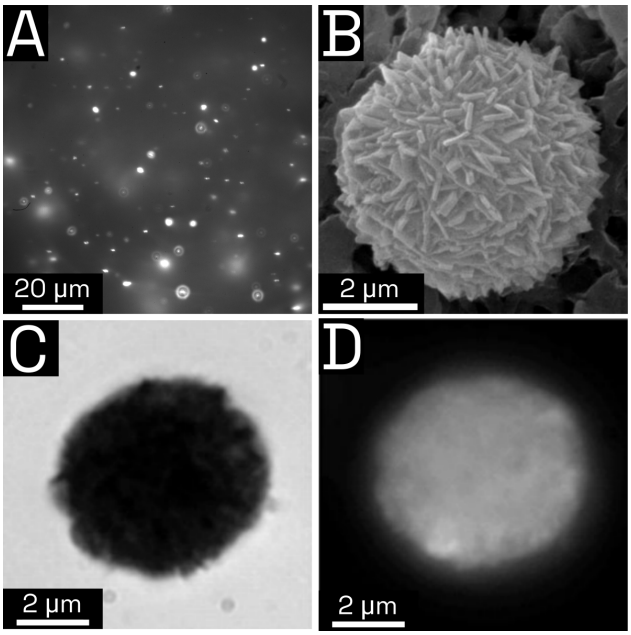

FIGURE 2.21. (A) Fluorescent micrograph of TCDA vesicles formed via solvent injection following [202, 203]. (B) SEM image of giant PDA-DMPC vesicle. (C) phase contrast micrograph of giant PDA-DMPC vesicle. (D) Fluorescent micrograph of giant PDA-DMPC vesicle. B,C,D adapted from Pevzner et al. [206].

2.8. Other PDA self-assembled systems

In addition of Langmuir films and vesicles, other self-assembled systems of PDAs have been demonstrated including interalacted mulitayers, nanotubes, thiol terminated monolayers on gold, nanocomposites and PDA films formed on highly oriented pyrolitic graphite (HOPG).

2.8.1. PDAs on HOPG (Striped PDAs). Fatty acid diacetylenes (and their derivatives) will form flat-lying monolayers when deposited HOPG, Figure 2.22A,B. This contrasts with Langmuir films, where the DA molecules are "standing-up" at the air water interface. This can be achieved through depositing a dissolved droplet of a diacetylene monomer onto HOPG and evaporation of the solvent [224–226], through a modified Langmuir-Blodgett [224, 227, 228], or through a modification of the Langmuir-Schaefer technique in which Langmuir monolayer of standing-up DA monomers at the air-water interface are converted a flat-lying state on an HOPG substrate [229]. These flat-lying monolayers, often referred to as striped PDAs (sPDA) are highly oriented and enable for remarkable control over surface morphology and pattering [24, 36, 106, 109, 115, 230–234]. sPDAs on HOPG

notably lack the color and fluorescence that are hallmarks of other PDA systems. This is due to the absorbance and fluorescence quenching of HOPG [108]. However, when these sPDAs are transferred to PDMS or polyacrylimide hydrogels, the characteristic fluorescence of PDA can be observed [109, 234, 235]. Furthermore, it was observed that the intensity of the fluorescence may correlate with degree of polymerization in these systems.

2.8.2. Polydiacetylene Monolayers on Gold Surfaces. Another interesting self-assembled system is that of thiol terminated diacetylenes, Figure 2.22C. These spontaneously form self-assembled monolayers when deposited onto a gold surface [236, 237]. Exposure to UV light creates a surface bound polymerized monolayer. Surface plasmon absorption from the gold surface quenches the characteristic absorbance and fluorescence of PDAs [238]. However, Raman spectroscopy can still be utilized to characterize the polymerization process and morphology. These thiolated PDAs have contributed to the understanding of the frictional properties of diacetylene monolayers [239], the effect of diacetylene position within a monomer alkyl tail on the polymerization kinetics [92, 240, 241], and electronic properties [242], as discussed in section 2.4.

2.8.3. Composites. Several types of PDA composites have been reported, including intercalated multi-layers [53, 243–245], and "nano-composites". Similar to PDA vesicles, these "nano-composites" consist of a nanoparticle core decorated with a PDA shell, often using silica or a metal oxide nanoparticle [246, 247], Figure 2.22D,E. These nano-assemblies often exhibit unique properties, for example, TiO_2-PDA nanoparticles were observed to polymerize when exposed to visible light [248]. ZnO-PDA systems have been observed to exhibit strong thermochromic reversibility, and are extensively tunable to bind to different chemical analytes [77, 246, 249–252].

2.8.4. Black Lipid Membranes. A mostly unrealized application of PDAs potentially lies in the formation of black lipid membranes (BLMs). Black lipid membranes are a model membrane system, ideal for studying membrane electrophysiology and protein behavior. A significant challenge exists in producing robust, stable, long-lived BLMs. Several attempts have been made to employ polymerizable lipids to enhance stability, including using PDAs. BLMs can be formed from single tailed diacetylene, however the polymerizable moieties are too far away from each other in the liquid state [10, 30, 253]. However, a two tailed diacetylene bearing a methacryloylic head group

was polymerizable, but the stability of the polymerized bilayer was not significantly different from unpolymerized BLMs [30]. Further investigations to produce more stable polymerized diacetyelene BLMs have been challenged by ensuring the topochemical requirements are met, and remain under-investigated [254, 255].

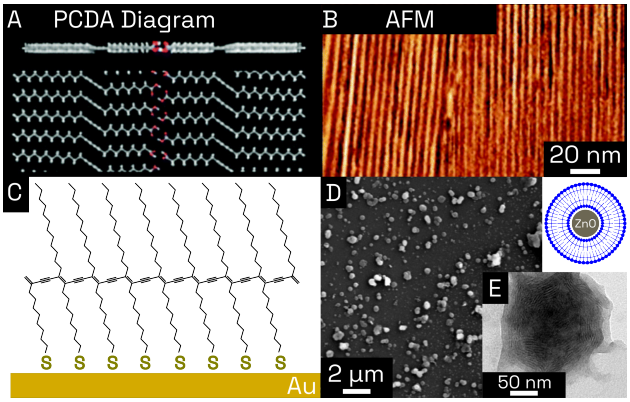

FIGURE 2.22. Survey of a few different self-assembled PDA systems. (A) schematic of flat lying PDA monolayer on HOPG. (B) AFM phase image of flat lying PDA monolayer, from [36]. (C) Schematic of a polymerized self-assembled monolayer of thiol terminated diacetyelenes on a gold surface, adapted from [239]. (D) SEM image of PDA-ZnO Nanocomposite (E) TEM image of PDA-ZnO nanocomposite and schematic of PDA-ZnO assembly, adapted from [251, 256].

2.9. A Non-exhaustive Review of PDA Sensor Review Papers

Polydiacetylenes have been utilized as sensors of many stimuli such as heat *thermochromsim*, light *photochromism*, pH *halochromism*, solvents *solvatochromism*, metal ions *ionochromism*, mechanical stress *mechanochromism*, biomolcules and organisms *affinochromism/biochromism*. The sensing literature is vast and dates back now over 20 years. It would be impossible to succinctly describe all the different devices, sensors and morphologies developed in that time frame. Rather, this section is an extensive list of reviews describing various subfields and disciplines within the broad PDA sensing community. The reviews described here generally focus extensively on applications rather than the underlying mechanisms. The early work on utilizing PDA vesicles as biosensors was summarized by Okada et al. [55]. Mechanochromism and developments up to 2004 were reviewed by Carpick et al. [127]. PDA nanowires were reviewed by Zhou et al. [257]. Further progress in bio-sensing and fabrication of PDA vesicles and other assemblies were reviewed in 2007 by A. Reppy and A. Pindzola

[2]. Ahn and Kim surveyed different approaches to utilizing PDAs as fluorescent sensors [258]. Alternate morphologies and general PDA sensors up to 2009 were reviewed by Yoon et al. [205], and Sun et al. [259]. PDA biosensors as applied to food and food spoilage were examined in 2010 in detail by Pires et al. [260] and Jang et al. [261]. Yarimaga et al. summarized the applications of PDAs to electronic devices, biosensors, volatile organic compound sensing, and printing [262]. Advances in PDA biological and chemical sensors up to 2012 were reviewed by Chen et al. [44], Lee et al. [263], and Huo et al.[264]. A general review of PDA sensors and progress up to 2013 was done by Jelinek and Ritenberg [265]. A review focused on biomolecule, peptide, lipid and antibody functionalized PDAs was done by Cho and Jung [47]. PDA functionalization, and applications were reviewed in 2018 by Wen et al. [45]. PDAs and their applications to targeting viruses were reviewed by Qian and Städler [266]. PDA vesicle sensors for sensing microorganisms were reviewed by Lebègue et al.[267]. Tunable parameters such as DA tail length, head group and mixing with other lipids were reviewed by Weston et al. in 2020 [204]. Fang et al. and Hao and Zhu reviewed a range of biomedical applications for PDA based sensors [268, 269]. Using PDAs detect and quantify volatile organic compounds was reviewed by Tjandra et al. [270]. Approaches to increasing the resolution of PDA biosensors through modifying the DA monomer, and intercalating with other lipids was reviewed by Kim et al. [52], with a further biosensor review done in 2020 by Huang et al.[271]. A recent general review of PDA properties and their applications was done by Hall et al. [272]. Mechanochromism and mechanically sensitive PDAs was reviewed recently (2022) by Das et al. [273].

2.10. Conclusions

This review has surveyed some key concepts to synthesizing and characterizing poldiacetylene surfactants. Properties and characteristics of monomers, the polymerization mechanism, optical and electronic properties, and the specific behavior of self-assembled PDA were reviewed. PDAs have been extensively studied since their original discovery by Wegner and co-workers. Initially, as a model conjugated polymer system, and subsequently for their application as stimuli responsive materials, capable of sensing a wide range of external stimuli. Despite extensive research into these

polymers, the field is still rapidly evolving with new observations and applications being continuously discovered, re-discovered, and created.

2.11. Supporting Information

2.11.1. Historically Important Diacetylenes.

2.11.1.1. *Toluene sulfonate diacetylenes: TS-6 and TS-12.* The first diacetylenes synthesized by Wegner had toluenesulfonate (tosylate) groups bound to the triple bond motif (Figure 1). Much of the literature examining polymerization kinetics from both UV and thermal polymerization utilized hexadiyne-1,6-diol-bis-p-toluene sulfonate (TS-6). TS-6 is susceptible to both thermal and UV-light polymerization. Synthesis details are described in detail in [5, 18]. A closely related compound is dodeca-5,7-diyn-1,12-ylene di-p-toluenesulfonate (TS-12) [102, 110]. Unlike many other polydiacetylenes, TS-12 polymers are soluble in a wide variety of common organic solvents, enabling molecular weight determinations as a function of degree of polymerization as surveyed in section 2.4.2 [96, 102, 110]

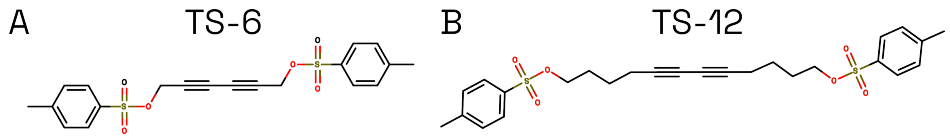

FIGURE 2.23. TS-6 (hexadiyne-1,6-diol-bis-p-toluene sulfonate) and TS-12 (dodeca-5,7-diyn-1,12-ylene di-p-toluenesulfonate)

2.11.1.2. *n-BCMU: urethane substituted diacaetylenes.* 5, 7-dodecadiyne-1, 12-bis{[(3-butoxycarbonyl)methyl]ure and 5, 7-dodecadiyne-1, 12-bis{[(4-butoxycarbonyl)methyl]urethane}, 3-BCMU, and 4-BCMU (Figure 2.24) respectively have been extensively used to examine the optical properties and polymerization processes of PDAs [18, 112]. PDAs formed from n-BCMU monomers have significant advantages for examining the blue and red transitions in PDAs. (1) They are thermally unreactive at room temperature, (2) Strong hydrogen bonding between side groups places adjacent monomers within the topochemical reaction requirements, enabling efficient polymerization with UV-light. (3) Polymers formed from n-BCMU are soluble in many organic solvents, and so their molecular weights may be measured using GPC/SEC. (4) Both blue and red phases polymers can be formed and can be

isolated to study single chains. Synthesis details for n-BCMUs are described in detail in Patel, and Se et al. [21, 274].

FIGURE 2.24. 3-BCMU (5, 7-dodecadiyne-1, 12-bis{[(3-butoxycarbonyl)methyl]urethane})

TABLE 2.1. List of common diacetylenes and their abbreviations

Abbreviation	Name	Synthesis Reference
TS-6† / PTS	hexadiyne-1,6-diol-bis-p-toluene sulfonate	[6, 18]
TS-12† / PTS-12	dodeca-5,7-diyn-1,12-ylene di-p-toluenesulfonate	[110]
3-BCMU*	5, 7-dodecadiyne-1, 12-bis{[(3-butoxycarbonyl)methyl]urethane}	[21, 274]
4-BCMU*	5, 7-dodecadiyne-1, 12-bis{[(4-butoxycarbonyl)methyl]urethane}	[21]
TCDA / 9/8 acid	10,12 tricosadiynoic acid	[8, 10]
PCDA / 11/8 acid	10,12-pentacosadiynoic acid	
HCDA / 13/8 acid	10,12-heptacosadiynoic acid	
NCDA / 15/8 acid	10,12-noncosadiynoic acid	
23:2 Diyne PC	1,2-bis(10,12-tricosadiynoyl)-sn-glycero-3-phosphocholine	[20]

† may be referred to as TS-n, for general properties of toluene sulfonate PDAs

* may be referred to as n-BCMU for general properties of urethane substituted PDAs

References

[1] Joseph W. Lauher, Frank W. Fowler, and Nancy S. Goroff. Single-Crystal-to-Single-Crystal Topochemical Polymerizations by Design. *Accounts of Chemical Research*, 41(9):1215–1229, September 2008. ISSN 0001-4842. doi: 10.1021/ar8001427.

[2] Mary A. Reppy and Bradford A. Pindzola. Biosensing with polydiacetylene materials: Structures, optical properties and applications. *Chemical Communications*, 0(42):4317–4338, 2007. doi: 10.1039/B703691D.

[3] Gerhard Wegner. Topochemische Reaktionen von Monomeren mit konjugierten Dreifachbindungen / Tochemical Reactions of Monomers with conjugated triple Bonds: I. Mitt.:

Polymerisation von Derivaten des 2.4-Hexadiin-1.6-diols im kristallinen Zustand. *Zeitschrift für Naturforschung B*, 24(7):824–832, July 1969. ISSN 1865-7117. doi: 10.1515/znb-1969-0708.

[4] Von G. Wegner. Topochemische reaktionen von monomeren mit konjugierten dreifachbindungen. II. Mitt.: Eine topochemische farb- und vernetzungsreaktion bei polymeren mit konjugierten acetylengruppen im grundbaustein. *Die Makromolekulare Chemie*, 134(1):219–229, 1970. ISSN 0025-116X. doi: 10.1002/macp.1970.021340119.

[5] Gerhard Wegner. Topochemical reactions of monomers with conjugated triple-bonds. IV. Polymerization of bis-(p-toluene sulfonate) of 2.4-hexadiin-1.6-diol. *Die Makromolekulare Chemie*, 145(1):85–94, 1971. ISSN 0025-116X. doi: 10.1002/macp.1971.021450107.

[6] G. Wegner. Topochemical polymerization of monomers with conjugated triple bonds. *Die Makromolekulare Chemie*, 154(1):35–48, 1972. ISSN 0025-116X. doi: 10.1002/macp.1972.021540103.

[7] B. Tieke, G. Wegner, D. Naegele, and H. Ringsdorf. Polymerization of Tricosa-10,12-diynoic Acid in Multilayers. *Angewandte Chemie International Edition in English*, 15(12):764–765, 1976. ISSN 1521-3773. doi: 10.1002/anie.197607641.

[8] B. Tieke, H. J. Graf, G. Wegner, B. Naegele, H. Ringsdorf, A. Banerjie, D. Day, and J. B. Lando. Polymerization of mono- and multilayer forming diacetylenes. *Colloid and Polymer Science*, 255(6):521–531, June 1977. ISSN 0303-402X, 1435-1536. doi: 10.1007/BF01549738.

[9] B. Tieke, G. Lieser, and G. Wegner. Polymerization of diacetylenes in multilayers. *Journal of Polymer Science: Polymer Chemistry Edition*, 17(6):1631–1644, 1979. ISSN 1542-9369. doi: 10.1002/pol.1979.170170607.

[10] Bernd Tieke. Polymerization of butadiene and butadiyne (diacetylene) derivatives in layer structures. In Henri Benoit, Hans-Joachim Cantow, Gino Dall'Asta, Karel Dušek, John D. Ferry, Hiroshi Fujita, Manfred Gordon, Gisela Henrici-Olivé, Günter Heublin, Hartwig Höcker, Hans-Henning Kausch, Joseph P. Kennedy, Anthony Ledwith, Seizo Okamura, Salvador Olivé, Charles G. Overberger, Helmut Ringsdorf, Takeo Saegusa, Günther Victor Schulz, William P. Slichter, and John K. Stille, editors, *Analysis/Reactions/Morphology*, volume 71, pages 79–151. Springer Berlin Heidelberg, Berlin, Heidelberg, 1985. ISBN 978-3-540-15482-2 978-3-540-39435-8. doi: 10.1007/3-540-15482-5_8.

[11] Gordhan N. Patel and Nan-Loh Yang. Polydiacetylenes: An ideal color system for teaching polymer science. *Journal of Chemical Education*, 60(3):181, March 1983. ISSN 0021-9584, 1938-1328. doi: 10.1021/ed060p181.

[12] Deborah H. Charych, Jon O. Nagy, Wayne Spevak, and Mark D. Bednarski. Direct Colorimetric Detection of a Receptor-Ligand Interaction by a Polymerized Bilayer Assembly. *Science*, 261 (5121):585–588, July 1993. doi: 10.1126/science.8342021.

[13] Deborah Charych, Quan Cheng, Anke Reichert, Geoffrey Kuziemko, Mark Stroh, Jon O. Nagy, Wayne Spevak, and Raymond C. Stevens. A 'litmus test' for molecular recognition using artificial membranes. *Chemistry & Biology*, 3(2):113–120, February 1996. ISSN 10745521. doi: 10.1016/S1074-5521(96)90287-2.

[14] Anke Reichert, Jon O. Nagy, Wayne Spevak, and Deborah Charych. Polydiacetylene Liposomes Functionalized with Sialic Acid Bind and Colorimetrically Detect Influenza Virus. *Journal of the American Chemical Society*, 117(2):829–830, January 1995. ISSN 0002-7863. doi: 10.1021/ja00107a032.

[15] D. Bloor and R. R. Chance. *Polydiacetylenes: Synthesis, Structure and Electronic Properties*. Springer Science & Business Media, 1985. ISBN 978-94-017-2713-6.

[16] Hans-Joachim Cantow, Hans-Joachim Cantow, Gino Dall'Asta, Karel Dušsek, John D. Ferry, Hiroshi Fujita, Manfred Gordon, Gisela Henrici-Olivé, G. Heublein, H. Höcker, Joseph P. Kennedy, Werner Kern, Seizo Okamura, Salvador Olivé, Charles G. Overberger, Takeo Saegusa, Günter Victor Schulz, William P. Slichter, and John K. Stille, editors. *Polydiacetylenes*, volume 63 of *Advances in Polymer Science*. Springer, Berlin, Heidelberg, 1984. ISBN 978-3-540-13414-5 978-3-540-38951-4. doi: 10.1007/BFb0017649.

[17] Chemla, D.S. and Zyss, J. *Nonlinear Optical Properties of Organic Molecules and Crystals*, volume 2. 1987. ISBN 978-0-12-170612-8.

[18] M. Schott and G. Wegner. Chapter III-1 - Basic Structural and Electronic Properties of Polydiacetylenes. In D. S. Chemla and J. Zyss, editors, *Nonlinear Optical Properties of Organic Molecules and Crystals*, pages 3–49. Academic Press, January 1987. ISBN 978-0-12-170612-8. doi: 10.1016/B978-0-12-170612-8.50003-1.

[19] G. M. Carter, Y. J. Chen, M. F. Rubner, D. J. Sandman, M. K. Thakur, and S. K. Tripathy. Chapter III-3 - Degenerate Third-Order Nonlinear Optical Susceptibility of Polydiacetylenes. In D. S. Chemla and J. Zyss, editors, *Nonlinear Optical Properties of Organic Molecules and Crystals*, pages 85–120. Academic Press, January 1987. ISBN 978-0-12-170612-8. doi: 10.1016/B978-0-12-170612-8.50005-5.

[20] Helmut Ringsdorf, Bernhard Schlarb, and Joachim Venzmer. Molecular Architecture and Function of Polymeric Oriented Systems: Models for the Study of Organization, Surface Recognition, and Dynamics of Biomembranes. *Angewandte Chemie International Edition in English*, 27(1):113–158, 1988. ISSN 1521-3773. doi: 10.1002/anie.198801131.

[21] G Patel. Soluble Polydiacetylenes. I. Synthesis And Properties. In *American Chemical Society, Polymer Preprints, Division of Polymer Chemistry*, volume 176, page 6, Miami Beach Fl, 1978. ACS Publications.

[22] Abhijit Sarkar, Shuji Okada, Hiroshi Matsuzawa, Hiro Matsuda, and Hachiro Nakanishi. Novel polydiacetylenes for optical materials: Beyond the conventional polydiacetylenes. *Journal of Materials Chemistry*, 10(4):819–828, January 2000. ISSN 1364-5501. doi: 10.1039/A907438D.

[23] J. B. Lando, D. Day, and V. Enkelmann. Molecular mechanisms in the formation of polydiacetylenes in the solid state. *Journal of Polymer Science: Polymer Symposia*, 65(1):73–78, 1978. ISSN 1936-0959. doi: 10.1002/polc.5070650109.

[24] Terry A. Villarreal, Shane R. Russell, Jae Jin Bang, Justin K. Patterson, and Shelley A. Claridge. Modulating Wettability of Layered Materials by Controlling Ligand Polar Headgroup Dynamics. *Journal of the American Chemical Society*, 139(34):11973–11979, August 2017. ISSN 0002-7863. doi: 10.1021/jacs.7b05930.

[25] Mark D. Mowery and Christine E. Evans. The synthesis of conjugated diacetylene monomers for the fabrication of polymerized monolayer assemblies. *Tetrahedron Letters*, 38(1):11–14, January 1997. ISSN 0040-4039. doi: 10.1016/S0040-4039(96)02262-9.

[26] David Day and Helmut Ringsdorf. Polymerization of diacetylene carbonic acid monolayers at the gas-water interface. *Journal of Polymer Science: Polymer Letters Edition*, 16(5):205–210, 1978. ISSN 1543-0472. doi: 10.1002/pol.1978.130160501.

[27] Maaike van den Heuvel, Dennis W. P. M. Löwik, and Jan C. M. van Hest. Effect of the Diacetylene Position on the Chromatic Properties of Polydiacetylenes from Self-Assembled Peptide Amphiphiles. *Biomacromolecules*, 11(6):1676–1683, June 2010. ISSN 1525-7797, 1526-4602. doi: 10.1021/bm100376q.

[28] Volker Spitzer, Werner Tomberg, Rudolf Hartmann, and Reiner Aichholz. Analysis of the seed oil of Heisteria silvanii (Olacaceae)—A rich source of a novel C18 acetylenic fatty acid. *Lipids*, 32(11):1189–1200, 1997. ISSN 1558-9307. doi: 10.1007/s11745-997-0153-6.

[29] Jia Zeng, Senwen Deng, Yiping Wang, Ping Li, Lian Tang, and Yefeng Pang. Specific Inhibition of Acyl-CoA Oxidase-1 by an Acetylenic Acid Improves Hepatic Lipid and Reactive Oxygen Species (ROS) Metabolism in Rats Fed a High Fat Diet. *The Journal of Biological Chemistry*, 292(9):3800–3809, March 2017. ISSN 1083-351X. doi: 10.1074/jbc.M116.763532.

[30] Hubert Bader, Klaus Dorn, Bernd Hupfer, and Helmut Ringsdorf. Polymeric monolayers and liposomes as models for biomembranes. In Hans-Joachim Cantow, Gino Dall'Asta, Karel Dušek, John D. Ferry, Hiroshi Fujita, Manfred Gordon, Gisela Henrici-Olivé, G. Heublein, H. Höcker, Hans-Henning Kausch, Joseph P. Kennedy, Werner Kern, Seizo Okamura, Salvador Olivé, Charles G. Overberger, Takeo Saegusa, Günter Victor Schulz, William P. Slichter, John K. Stille, and M. Gordon, editors, *Polymer Membranes*, volume 64, pages 1–62. Springer Berlin Heidelberg, Berlin, Heidelberg, 1985. ISBN 978-3-540-13483-1 978-3-540-38960-6. doi: 10.1007/3-540-13483-2_1.

[31] D. Day, H. H. Hub, and H. Ringsdorf. Polymerization of Mono- and Bi-functional Diacetylene Derivatives in Monolayers at the Gas–Water Interface. *Israel Journal of Chemistry*, 18(3-4): 325–329, 1979. ISSN 1869-5868. doi: 10.1002/ijch.197900050.

[32] Leo Gros, Helmut Ringsdorf, and Hans Schupp. Polymeric Antitumor Agents on a Molecular and on a Cellular Level? *Angewandte Chemie International Edition in English*, 20(4):305–325, 1981. ISSN 1521-3773. doi: 10.1002/anie.198103051.

[33] H. H. Hub, B. Hupfer, H. Koch, and H. Ringsdorf. Polymerization of Lipid and Lysolipid Like Diacetylenes in Monolayers and Liposomes. *Journal of Macromolecular Science: Part A - Chemistry*, 15(5):701–715, April 1981. ISSN 0022-233X. doi: 10.1080/00222338108056762.

[34] Hans-Henning Hub, Bernd Hupfer, Horst Koch, and Helmut Ringsdorf. Polymerizable Phospholipid Analogues—New Stable Biomembrane and Cell Models. *Angewandte Chemie International Edition in English*, 19(11):938–940, 1980. ISSN 1521-3773. doi: 10.1002/anie.198009381.

[35] Wayne Spevak, Jon O. Nagy, and Deborah H. Charych. Molecular assemblies of functionalized polydiacetylenes. *Advanced Materials*, 7(1):85–89, 1995. ISSN 1521-4095. doi: 10.1002/adma.19950070120.

[36] S. A. Claridge. Standing, lying, and sitting: Translating building principles of the cell membrane to synthetic 2D material interfaces. *Chemical Communications*, 54(50):6681–6691, June 2018. ISSN 1364-548X. doi: 10.1039/C8CC02596G.

[37] Tanner J Finney, Sanjai J Parikh, Amir Berman, Darryl Y Sasaki, and Tonya L Kuhl. Characterizing and Tuning the Properties of Polydiacetylene Films for Sensing Applications. *Langmuir*, page 12, November 2021. doi: 10.1021/acs.langmuir.1c02004.

[38] Darryl Y. Sasaki, Robert W. Carpick, and Alan R. Burns. High Molecular Orientation in Mono- and Trilayer Polydiacetylene Films Imaged by Atomic Force Microscopy. *Journal of Colloid and Interface Science*, 229(2):490–496, September 2000. ISSN 0021-9797. doi: 10.1006/jcis.2000.7043.

[39] F. Grunfeld and C. W. Pitt. Diacetylene Langmuir-Blodgett layers for integrated optics. *Thin Solid Films*, 99(1):249–255, January 1983. ISSN 0040-6090. doi: 10.1016/0040-6090(83)90388-7.

[40] Susumu Yamada and Yuhei Shimoyama. Morphological Variation of the Monolayer Surface of Diacetylene during Polymerization at Air-Water Interface. *Japanese Journal of Applied Physics*, 36(Part 1, No. 8):5242–5248, August 1997. ISSN 0021-4922, 1347-4065. doi: 10.1143/JJAP.36.5242.

[41] Olga Shusterman, Amir Berman, Yuval Golan, Baruch Horovitz, and Leila Zeiri. Two-Photon Polymerization of Polydiacetylene. *The Journal of Physical Chemistry B*, 113(5):1273–1276, February 2009. ISSN 1520-6106. doi: 10.1021/jp806546u.

[42] Qun Huo, K. C. Russell, and Roger M. Leblanc. Chromatic Studies of a Polymerizable Diacetylene Hydrogen Bonding Self-Assembly: A "Self-Folding" Process To Explain the Chromatic Changes of Polydiacetylenes. *Langmuir*, 15(11):3972–3980, May 1999. ISSN

0743-7463, 1520-5827. doi: 10.1021/la990025f.

[43] S. R. Sheth and D. E. Leckband. Direct Force Measurements of Polymerization-Dependent Changes in the Properties of Diacetylene Films. *Langmuir*, 13(21):5652–5662, October 1997. ISSN 0743-7463. doi: 10.1021/la962107z.

[44] Xiaoqiang Chen, Guodong Zhou, Xiaojun Peng, and Juyoung Yoon. Biosensors and chemosensors based on the optical responses of polydiacetylenes. *Chemical Society Reviews*, 41(13): 4610–4630, June 2012. ISSN 1460-4744. doi: 10.1039/C2CS35055F.

[45] Jessica T. Wen, Jenna M. Roper, and Hideaki Tsutsui. Polydiacetylene Supramolecules: Synthesis, Characterization, and Emerging Applications. *Industrial & Engineering Chemistry Research*, 57(28):9037–9053, July 2018. ISSN 0888-5885. doi: 10.1021/acs.iecr.8b00848.

[46] Masazo Niwa, Syunsuke Shibahara, and Nobuyuki Higashi. Diacetylenic monolayers containing a boronic acid moiety form a chemically and thermally stable poly(diacetylene) film on water. *Journal of Materials Chemistry*, 10(12):2647–2651, 2000. doi: 10.1039/B004371K.

[47] Eunae Cho and Seunho Jung. Biomolecule-Functionalized Smart Polydiacetylene for Biomedical and Environmental Sensing. *Molecules*, 23(1):107, January 2018. ISSN 1420-3049. doi: 10.3390/molecules23010107.

[48] Yan-lei Su, Jin-ru Li, and Long Jiang. Chromatic immunoassay based on polydiacetylene vesicles. *Colloids and Surfaces B: Biointerfaces*, 38(1):29–33, October 2004. ISSN 0927-7765. doi: 10.1016/j.colsurfb.2004.08.010.

[49] Troy E. Wilson, Wayne Spevak, Deborah H. Charych, and Mark D. Bednarski. Enzymic Modification and X-ray Photoelectron Spectroscopy Analysis of a Functionalized Polydiacetylene Thin Film. *Langmuir*, 10(5):1512–1516, May 1994. ISSN 0743-7463, 1520-5827. doi: 10.1021/la00017a031.

[50] Dong June Ahn, Eun-Hyuk Chae, Gil Sun Lee, Hee-Yong Shim, Tae-Eun Chang, Kwang-Duk Ahn, and Jong-Man Kim. Colorimetric Reversibility of Polydiacetylene Supramolecules Having Enhanced Hydrogen-Bonding under Thermal and pH Stimuli. *Journal of the American Chemical Society*, 125(30):8976–8977, July 2003. ISSN 0002-7863. doi: 10.1021/ja0299001.

[51] Roman Volinsky, Mark Kliger, Tania Sheynis, Sofiya Kolusheva, and Raz Jelinek. Glass-supported lipid/polydiacetylene films for colour sensing of membrane-active compounds.

Biosensors and Bioelectronics, 22(12):3247–3251, June 2007. ISSN 0956-5663. doi: 10.1016/j.bios.2006.12.024.

[52] Changheon Kim, Changgi Hong, and Kangwon Lee. Structures and strategies for enhanced sensitivity of polydiacetylene(PDA) based biosensor platforms. *Biosensors and Bioelectronics*, 181:113120, June 2021. ISSN 0956-5663. doi: 10.1016/j.bios.2021.113120.

[53] Yuya Oaki, Yukiko Ishijima, and Hiroaki Imai. Emergence of temperature-dependent and reversible color-changing properties by the stabilization of layered polydiacetylene through intercalation. *Polymer Journal*, 50(4):319–326, April 2018. ISSN 1349-0540. doi: 10.1038/s41428-017-0018-2.

[54] Machi Takeuchi, Hiroaki Imai, and Yuya Oaki. Effects of the intercalation rate on the layered crystal structures and stimuli-responsive color-change properties of polydiacetylene. *Journal of Materials Chemistry C*, 5(32):8250–8255, 2017. doi: 10.1039/C7TC02218B.

[55] Sheldon Okada, Susan Peng, Wayne Spevak, and Deborah Charych. Color and Chromism of Polydiacetylene Vesicles. *Accounts of Chemical Research*, 31(5):229–239, May 1998. ISSN 0001-4842, 1520-4898. doi: 10.1021/ar970063v.

[56] Yevgeniy Lifshitz, Alexander Upcher, Olga Shusterman, Baruch Horovitz, Amir Berman, and Yuval Golan. Phase transition kinetics in Langmuir and spin-coated polydiacetylene films. *Phys. Chem. Chem. Phys.*, 12(3):713–722, 2010. ISSN 1463-9076, 1463-9084. doi: 10.1039/B915527A.

[57] R. W. Carpick, D. Y. Sasaki, and A. R. Burns. First Observation of Mechanochromism at the Nanometer Scale. *Langmuir*, 16(3):1270–1278, February 2000. ISSN 0743-7463. doi: 10.1021/la990706a.

[58] Or Raifman, Sofiya Kolusheva, Maria J. Comin, Noemi Kedei, Nancy E. Lewin, Peter M. Blumberg, Victor E. Marquez, and Raz Jelinek. Membrane anchoring of diacylglycerol lactones substituted with rigid hydrophobic acyl domains correlates with biological activities. *The FEBS Journal*, 277(1):233–243, 2010. ISSN 1742-4658. doi: 10.1111/j.1742-4658.2009.07477.x.

[59] Reut Israeli, Sofiya Kolusheva, Pablo Mateos-Gil, Electra Gizeli, and Raz Jelinek. Chromatic Dendrimer/Polydiacetylene Nanoparticles. *ACS Applied Polymer Materials*, 3(6):2931–2937, June 2021. doi: 10.1021/acsapm.1c00053.

[60] C. Bubeck, B. Tieke, and G. Wegner. Selfsensitization of the Photopolymerization of Diacetylenes Studied in Multilayers. *Berichte der Bunsengesellschaft für physikalische Chemie*, 86(6):495–498, 1982. ISSN 0005-9021. doi: 10.1002/bbpc.19820860604.

[61] Levente Juhasz, Roberto D. Ortuso, and Kaori Sugihara. Quantitative and Anisotropic Mechanochromism of Polydiacetylene at Nanoscale. *Nano Lett.*, 21(1):543–549, January 2021. ISSN 1530-6984. doi: 10.1021/acs.nanolett.0c04027.

[62] Tanner J. Finney, Skye L. Frank, Michael R. Bull, Robert D. Guy, and Tonya L. Kuhl. Tracking Mechanical Stress and Cell Migration with Inexpensive Polymer Thin-Film Sensors. *Advanced Materials Interfaces*, n/a(n/a):2201808, November 2022. ISSN 2196-7350. doi: 10.1002/admi.202201808.

[63] Bernd Hupfer, Helmut Ringsdorf, and Hans Schupp. Liposomes from polymerizable phospholipids. *Chemistry and Physics of Lipids*, 33(4):355–374, November 1983. ISSN 0009-3084. doi: 10.1016/0009-3084(83)90028-2.

[64] Encarnacion Lopez, David F. O'Brien, and Thomas H. Whitesides. Structural effects on the photopolymerization of bilayer membranes. *Journal of the American Chemical Society*, 104 (1):305–307, January 1982. ISSN 0002-7863, 1520-5126. doi: 10.1021/ja00365a064.

[65] Amichai Yavlovich, Alok Singh, Sergey Tarasov, Jacek Capala, Robert Blumenthal, and Anu Puri. Design of liposomes containing photopolymerizable phospholipids for triggered release of contents. *Journal of Thermal Analysis and Calorimetry*, 98(1):97, July 2009. ISSN 1572-8943. doi: 10.1007/s10973-009-0228-8.

[66] Yukihiro Okamoto, Yusuke Kishi, Keishi Suga, and Hiroshi Umakoshi. Induction of Chiral Recognition with Lipid Nanodomains Produced by Polymerization. *Biomacromolecules*, 18(4): 1180–1188, April 2017. ISSN 1525-7797. doi: 10.1021/acs.biomac.6b01859.

[67] D. S. Johnston, S. Sanghera, M. Pons, and D. Chapman. Phospholipid polymers–synthesis and spectral characteristics. *Biochimica Et Biophysica Acta*, 602(1):57–69, October 1980. ISSN 0006-3002. doi: 10.1016/0005-2736(80)90289-8.

[68] Kenta Okuno, Daisuke Saeki, and Hideto Matsuyama. Phase separation behavior of binary mixture of photopolymerizable diacetylene and unsaturated phospholipids in liposomes. *Biochimica et Biophysica Acta (BBA) - Biomembranes*, 1862(9):183377, September 2020. ISSN

0005-2736. doi: 10.1016/j.bbamem.2020.183377.

[69] Bernd Tieke and Günter Lieser. Influences of the structure of long-chain diynoic acids on their polymerization properties in Langmuir—Blodgett multilayers. *Journal of Colloid and Interface Science*, 88(2):471–486, August 1982. ISSN 0021-9797. doi: 10.1016/0021-9797(82)90276-4.

[70] Chanita Khanantong, Nipaphat Charoenthai, Tinnakorn Phuangkaew, Filip Kielar, Nisanart Traiphol, and Rakchart Traiphol. Phase transition, structure and color-transition behaviors of monocarboxylic diacetylene and polydiacetylene assemblies: The opposite effects of alkyl chain length. *Colloids and Surfaces A: Physicochemical and Engineering Aspects*, 553:337–348, September 2018. ISSN 0927-7757. doi: 10.1016/j.colsurfa.2018.05.081.

[71] Alice A. Deckert, Jennifer C. Horne, Barry Valentine, Lisa Kiernan, and Lara Fallon. Effects of Molecular Area on the Polymerization and Thermochromism of Langmuir-Blodgett Films of Cd2+ Salts of 5,7-Diacetylenes Studied Using UV-Visible Spectroscopy. *Langmuir*, 11(2): 643–649, February 1995. ISSN 0743-7463, 1520-5827. doi: 10.1021/la00002a048.

[72] John J. Pan and Deborah Charych. Molecular Recognition and Colorimetric Detection of Cholera Toxin by Poly(diacetylene) Liposomes Incorporating Gm1 Ganglioside. *Langmuir*, 13 (6):1365–1367, March 1997. ISSN 0743-7463. doi: 10.1021/la9602675.

[73] Zhanfang Ma and Juan Ren. Fabrication of stable polydiacetylene vesicles with 2,4-akyl-diacetylenic acid. *Colloids and Surfaces A: Physicochemical and Engineering Aspects*, 303(3): 179–183, August 2007. ISSN 0927-7757. doi: 10.1016/j.colsurfa.2007.03.038.

[74] George L. Gaines. *Insoluble Monolayers at Liquid-gas Interfaces*. Interscience Publishers, 1966. ISBN 978-0-608-10303-7.

[75] G.G. Roberts. An applied science perspective of Langmuir-Blodgett films. *Advances in Physics*, 34(4):475–512, January 1985. ISSN 0001-8732. doi: 10.1080/00018738500101801.

[76] Xin Huang, Siguang Jiang, and Minghua Liu. Metal Ion Modulated Organization and Function of the Langmuir-Blodgett Films of Amphiphilic Diacetylene: Photopolymerization, Thermochromism, and Supramolecular Chirality. *The Journal of Physical Chemistry B*, 109 (1):114–119, January 2005. ISSN 1520-6106. doi: 10.1021/jp046500m.

[77] Nisanart Traiphol, Amornsak Chanakul, Anothai Kamphan, and Rakchart Traiphol. Role of Zn2+ ion on the formation of reversible thermochromic polydiacetylene/zinc oxide

nanocomposites. *Thin Solid Films*, 622:122–129, January 2017. ISSN 0040-6090. doi: 10.1016/j.tsf.2016.12.037.

[78] Yevgeniy Lifshitz, Alexander Upcher, Anatoly Kovalev, Dmitry Wainstein, Alexander Rashkovsky, Leila Zeiri, Yuval Golan, and Amir Berman. Zinc modified polydiacetylene Langmuir films. *Soft Matter*, 7(19):9069–9077, September 2011. ISSN 1744-6848. doi: 10.1039/C1SM05904A.

[79] Alexander Upcher, Yevgeniy Lifshitz, Leila Zeiri, Yuval Golan, and Amir Berman. Effect of metal cations on polydiacetylene Langmuir films. *Langmuir: the ACS journal of surfaces and colloids*, 28(9):4248–4258, March 2012. ISSN 1520-5827. doi: 10.1021/la204735t.

[80] Si Wu, Libin Pan, Youju Huang, Ni Yang, and Qijin Zhang. Co-assemblies of polydiacetylenes and metal ions for solvent sensing. *Soft Matter*, 14(33):6929–6937, 2018. doi: 10.1039/C8SM01282B.

[81] David Day and J. B. Lando. Structure Determination of a Poly(diacetylene) Monolayer. *Macromolecules*, 13(6):1483–1487, November 1980. ISSN 0024-9297. doi: 10.1021/ma60078a024.

[82] Ulrich Jonas, Koonj Shah, Sophie Norvez, and Deborah H. Charych. Reversible Color Switching and Unusual Solution Polymerization of Hydrazide-Modified Diacetylene Lipids. *Journal of the American Chemical Society*, 121(19):4580–4588, May 1999. ISSN 0002-7863. doi: 10.1021/ja984190d.

[83] Wenjie Dong, Renzhe Zhang, and Guanhua Lin. Molecular-level design of excellent reversible thermochromic polydiacetylene materials with the simultaneous enhancement of multiple performances. *Materials Chemistry Frontiers*, 5(18):7041–7050, September 2021. ISSN 2052-1537. doi: 10.1039/D1QM00721A.

[84] In Sung Park, Hye Jin Park, Woomin Jeong, Jihye Nam, Youngjong Kang, Kayeong Shin, Hoeil Chung, and Jong-Man Kim. Low Temperature Thermochromic Polydiacetylenes: Design, Colorimetric Properties, and Nanofiber Formation. *Macromolecules*, 49(4):1270–1278, February 2016. ISSN 0024-9297. doi: 10.1021/acs.macromol.5b02683.

[85] Yeol Kyo Choi, Sang Yup Lee, and Dong June Ahn. Hyperconjugation-induced chromism in linear responsive polymers. *Journal of Materials Chemistry C*, 7(42):13130–13138, October 2019. ISSN 2050-7534. doi: 10.1039/C9TC03204E.

[86] R. W. Carpick, T. M. Mayer, D. Y. Sasaki, and A. R. Burns. Spectroscopic Ellipsometry and Fluorescence Study of Thermochromism in an Ultrathin Poly(diacetylene) Film: Reversibility and Transition Kinetics. *Langmuir*, 16(10):4639–4647, May 2000. ISSN 0743-7463, 1520-5827. doi: 10.1021/la991580k.

[87] H. Bässler. Photopolymerization of diacetylenes. In Hans-Joachim Cantow, editor, *Polydiacetylenes*, Advances in Polymer Science, pages 1–48, Berlin, Heidelberg, 1984. Springer. ISBN 978-3-540-38951-4. doi: 10.1007/BFb0017650.

[88] Mark G. Kuzyk, John E. Sohn, and Anthony F. Garito. A model for x-ray-induced solid-state polymerization. *Journal of Polymer Science Part B: Polymer Physics*, 26(2):277–287, 1988. ISSN 1099-0488. doi: 10.1002/polb.1988.090260206.

[89] David Bloor. Topochemical Polymerization: Diynes. In *Comprehensive Polymer Science and Supplements*, pages 233–249. Elsevier, 1989. ISBN 978-0-08-096701-1. doi: 10.1016/B978-0-08-096701-1.00156-7.

[90] Daisuke Takajo and Koichi Sudoh. Impact of the Air Atmosphere on Photoinduced Chain Polymerization in Self-Assembled Monolayers of Diacetylene on Graphite. *Langmuir*, 37(19):6002–6006, May 2021. ISSN 0743-7463. doi: 10.1021/acs.langmuir.1c00616.

[91] Hans Sixl. Spectroscopy of the intermediate states of the solid state polymerization reaction in diacetylene crystals. In Hans-Joachim Cantow, editor, *Polydiacetylenes*, Advances in Polymer Science, pages 49–90, Berlin, Heidelberg, 1984. Springer. ISBN 978-3-540-38951-4. doi: 10.1007/BFb0017651.

[92] H. Menzel, S. Horstmann, M. D. Mowery, M. Cai, and C. E. Evans. Diacetylene polymerization in self-assembled monolayers: Influence of the odd/even nature of the methylene spacer. *Polymer*, 41(22):8113–8119, October 2000. ISSN 0032-3861. doi: 10.1016/S0032-3861(00)00148-8.

[93] Jintana Siriboon, Nisanart Traiphol, and Rakchart Traiphol. Diacetylene-Zinc(II)-Zinc Oxide Nanocomposites for Colorimetric Detection of Ultraviolet-A Light. *ACS Applied Nano Materials*, 5(9):13198–13207, September 2022. ISSN 2574-0970, 2574-0970. doi: 10.1021/acsanm.2c02914.

[94] W. Hersel, H. Sixl, and G. Wegner. The optical intermediates of the low-temperature photopolymerization of TSHO diacetylene crystals. *Chemical Physics Letters*, 73(2):288–293, July 1980. ISSN 0009-2614. doi: 10.1016/0009-2614(80)80374-5.

[95] Roberto Diego Ortuso. *Characterisation of Polydiacetylene for the Detection of Forces in Membranes*. PhD thesis, University of Geneva, 2019.

[96] Volker Enkelmann. Structural aspects of the topochemical polymerization of diacetylenes. In Hans-Joachim Cantow, editor, *Polydiacetylenes*, Advances in Polymer Science, pages 91–136, Berlin, Heidelberg, 1984. Springer. ISBN 978-3-540-38951-4. doi: 10.1007/BFb0017652.

[97] C. Bubeck, B. Tieke, and G. Wegner. Cyanine Dyes as Sensitizers of the Photopolymerization of Diacetylenes in Multilayers. *Berichte der Bunsengesellschaft für physikalische Chemie*, 86 (6):499–504, 1982. ISSN 0005-9021. doi: 10.1002/bbpc.19820860605.

[98] J. P. Fouassier, B. Tieke, and G. Wegner. The Photochemistry of the Polymerization of Diacetylenes in Multilayers. *Israel Journal of Chemistry*, 18(3-4):227–232, 1979. ISSN 1869-5868. doi: 10.1002/ijch.197900033.

[99] M. Bara, M. Schott, and M. Schwoerer. Self-sensitized photopolymerization of a diacetylene single crystal pTS. *Chemical Physics Letters*, 175(1):23–29, November 1990. ISSN 0009-2614. doi: 10.1016/0009-2614(90)85512-B.

[100] Elisseos Verveniotis, Yuji Okawa, Kenji Watanabe, Takashi Taniguchi, Takaaki Taniguchi, Minoru Osada, Christian Joachim, and Masakazu Aono. Self-Sensitization and Photo-Polymerization of Diacetylene Molecules Self-Assembled on a Hexagonal-Boron Nitride Nanosheet. *Polymers*, 10(2):206, February 2018. ISSN 2073-4360. doi: 10.3390/polym10020206.

[101] Falk Braunschweig and Heinz Bässler. Reaction-induced secondary photopolymerization in diacetylene—bis(toluenesulfonate) (TS). *Chemical Physics Letters*, 90(1):41–45, July 1982. ISSN 0009-2614. doi: 10.1016/0009-2614(82)83321-6.

[102] G. Wenz and G. Wegner. Kinetics of the Radiation Induced Polymerization of a Diacetylene Studied by Analysis of the Molecular Weight Distribution. *Molecular Crystals and Liquid Crystals*, 96(1):99–108, July 1983. ISSN 0026-8941. doi: 10.1080/00268948308074696.

[103] G. N. Patel and E. K. Walsh. Polydiacetylenes: Solution conformation characteristics. *Journal of Polymer Science: Polymer Letters Edition*, 17(4):203–208, 1979. ISSN 1543-0472. doi:

10.1002/pol.1979.130170405.

[104] Sylvie Spagnoli, Emrick Briand, Ian Vickridge, Jean-Louis Fave, and Michel Schott. Method for Determining the Polymer Content in Nonsoluble Polydiacetylene Films: Application to Pentacosadiynoic Acid. *Langmuir*, 33(6):1419–1426, February 2017. ISSN 0743-7463. doi: 10.1021/acs.langmuir.6b03147.

[105] Yuji Okawa and Masakazu Aono. Nanoscale control of chain polymerization. *Nature*, 409 (6821):683–684, February 2001. ISSN 1476-4687. doi: 10.1038/35055625.

[106] Yuji Okawa, Megumi Akai-Kasaya, Yuji Kuwahara, Swapan K. Mandal, and Masakazu Aono. Controlled chain polymerisation and chemical soldering for single-molecule electronics. *Nanoscale*, 4(10):3013–3028, May 2012. ISSN 2040-3372. doi: 10.1039/C2NR30245D.

[107] Lander Verstraete, Brandon E. Hirsch, John Greenwood, and Steven De Feyter. Confined polydiacetylene polymerization reactions for programmed length control. *Chemical Communications*, 53(30):4207–4210, April 2017. ISSN 1364-548X. doi: 10.1039/C7CC00885F.

[108] Anni Shi, Terry A. Villarreal, Anamika Singh, Tyler R. Hayes, Tyson C. Davis, Jacob T. Brooks, and Shelley A. Claridge. Plenty of Room at the Top: A Multi-Scale Understanding of nm-Resolution Polymer Patterning on 2D Materials. *Angewandte Chemie International Edition*, 60(48):25436–25444, 2021. ISSN 1521-3773. doi: 10.1002/anie.202110517.

[109] Tyson C. Davis, Jeremiah O. Bechtold, Anni Shi, Erin N. Lang, Anamika Singh, and Shelley A. Claridge. One Nanometer Wide Functional Patterns with a Sub-10 Nanometer Pitch Transferred to an Amorphous Elastomeric Material. *ACS Nano*, 15(1):1426–1435, January 2021. ISSN 1936-0851. doi: 10.1021/acsnano.0c08741.

[110] Gerhard Wenz and Gerhard Wegner. Molecular weight distribution and solution properties of a poly(diacetylene). *Die Makromolekulare Chemie, Rapid Communications*, 3(4):231–237, 1982. ISSN 0173-2803. doi: 10.1002/marc.1982.030030409.

[111] Zoltán G. Soos, Douglas S. Galvão, and Shahab Etemad. Fluorescence and excited-state structure of conjugated polymers. *Advanced Materials*, 6(4):280–287, 1994. ISSN 1521-4095. doi: 10.1002/adma.19940060404.

[112] Michel Schott. Optical Properties of Single Conjugated Polymer Chains (Polydiacetylenes). In *Photophysics of Molecular Materials*, chapter 3, pages 49–151. John Wiley & Sons, Ltd,

2005. ISBN 978-3-527-60732-7. doi: 10.1002/3527607323.ch3.

[113] H. Nakanishi, H. Matsuda, and M. Kato. Preparation of a Variety of Polymeric Conductors from Diacetylenes. *Molecular Crystals and Liquid Crystals*, 105(1):77–88, March 1984. ISSN 0026-8941. doi: 10.1080/00268948408071644.

[114] David R. Day and Jerome B. Lando. Conduction in polydiacetylene bilayers. *Journal of Applied Polymer Science*, 26(5):1605–1612, 1981. ISSN 1097-4628. doi: 10.1002/app.1981.070260516.

[115] M. Akai-Kasaya, K. Shimizu, Y. Watanabe, A. Saito, M. Aono, and Y. Kuwahara. Electronic Structure of a Polydiacetylene Nanowire Fabricated on Highly Ordered Pyrolytic Graphite. *Physical Review Letters*, 91(25):255501, December 2003. doi: 10.1103/PhysRevLett.91.255501.

[116] D. Mukhopadhyay and Z. G. Soos. Nonlinear optical and electroabsorption spectra of polydiacetylene crystals and films. *The Journal of Chemical Physics*, 104(4):1600–1610, January 1996. ISSN 0021-9606. doi: 10.1063/1.470748.

[117] Takayoshi Kobayashi, Masayuki Yoshizawa, Uwe Stamm, Makoto Taiji, and Masamitsu Hasegawa. Relaxation dynamics of photoexcitations in polydiacetylenes and polythiophene. *JOSA B*, 7(8):1558–1578, August 1990. ISSN 1520-8540. doi: 10.1364/JOSAB.7.001558.

[118] F. Kajzar and J. Messier. Chapter III-2 - Cubic Effects in Polydiacetylene Solutions and Films. In D. S. Chemla and J. Zyss, editors, *Nonlinear Optical Properties of Organic Molecules and Crystals*, pages 51–83. Academic Press, January 1987. ISBN 978-0-12-170612-8. doi: 10.1016/B978-0-12-170612-8.50004-3.

[119] Daniela Grando, GianPiero Banfi, Davide Comoretto, and Giovanna Dellepiane. Nonlinear optical response of a polycarbazolyldiacetylene film through femtosecond two-photon spectroscopy. *Chemical Physics Letters*, 363(5):492–497, September 2002. ISSN 0009-2614. doi: 10.1016/S0009-2614(02)01247-2.

[120] Myoungsik Cha, William Torruellas, George Stegeman, Hong Xiang Wang, Akira Takahashi, and Shaul Mukamel. Spectroscopic investigations of the nonlinear response of poly (4-BCMU) films. *Chemical Physics Letters*, 228(1):73–78, September 1994. ISSN 0009-2614. doi: 10.1016/0009-2614(94)00923-6.

[121] G. P. Banfi, V. Degiorgio, and D. Fortusini. Two-photon absorption coefficient measurements based on widely tunable femtosecond pulses from parametric generation. *Pure and Applied*

Optics: Journal of the European Optical Society Part A, 7(2):361–372, March 1998. ISSN 0963-9659. doi: 10.1088/0963-9659/7/2/026.

[122] Grzegorz M. Balkowski, Michiel Groeneveld, Hong Zhang, Cindy C. J. Hendrikx, Michael Polhuis, Han Zuilhof, and Wybren J. Buma. Femtosecond Spectroscopic Studies of the One- and Two-Photon Excited-State Dynamics of 2,2,17,17-Tetramethyloctadeca-5,9,13-trien-3,7,11,15-tetrayne: A Trimeric Oligodiacetylene. *The Journal of Physical Chemistry A*, 110 (40):11435–11439, October 2006. ISSN 1089-5639. doi: 10.1021/jp0635361.

[123] Shun-li Chen, Xue-feng Zhu, Fang-yuan Yang, Xue-cong Pan, Wei Gan, and Qun-hui Yuan. Order-Disorder transition of carboxyl terminated chains in polydiacetylenes vesicles probed by second harmonic generation and two-photon fluorescence. *Chinese Journal of Chemical Physics*, 31(3):269–276, June 2018. ISSN 1674-0068. doi: 10.1063/1674-0068/31/cjcp1712238.

[124] Gang Wang, Yanran Li, Xiayun Huang, and Daoyong Chen. Polydiacetylene and its composites with long effective conjugation lengths and tunable third-order nonlinear optical absorption. *Polymer Chemistry*, 12(22):3257–3263, June 2021. ISSN 1759-9962. doi: 10.1039/D1PY00235J.

[125] Hideki Katagiri, Yukihiro Shimoi, and Shuji Abe. A density functional study of backbone structures of polydiacetylene: Destabilization of butatriene structure. *Chemical Physics*, 306 (1):191–200, November 2004. ISSN 0301-0104. doi: 10.1016/j.chemphys.2004.07.033.

[126] Hajime Tanaka, M. A. Gomez, A. E. Tonelli, and M. Thakur. Thermochromic phase transition of a polydiacetylene, poly(ETCD), studied by high-resolution solid-state carbon-13 NMR. *Macromolecules*, 22(3):1208–1215, March 1989. ISSN 0024-9297, 1520-5835. doi: 10.1021/ma00193a036.

[127] Robert W. Carpick, Darryl Y. Sasaki, Matthew S. Marcus, M. A. Eriksson, and Alan R. Burns. Polydiacetylene films: A review of recent investigations into chromogenic transitions and nanomechanical properties. *Journal of Physics: Condensed Matter*, 16(23):R679–R697, May 2004. ISSN 0953-8984. doi: 10.1088/0953-8984/16/23/R01.

[128] Michel Schott. The Colors of Polydiacetylenes: A Commentary. *The Journal of Physical Chemistry B*, 110(32):15864–15868, August 2006. ISSN 1520-6106. doi: 10.1021/jp0638437.

[129] A. Race, W. Barford, and R. J. Bursill. Low-lying excitations of polydiacetylene. *Physical Review B*, 64(3):035208, June 2001. ISSN 0163-1829, 1095-3795. doi: 10.1103/PhysRevB.64.

035208.

[130] G. Berkovic, Y. R. Shen, and P. N. Prasad. Third harmonic generation from a monolayer film of a polydiacetylene, poly-4-BCMU. *The Journal of Chemical Physics*, 87(3):1897–1898, August 1987. ISSN 0021-9606. doi: 10.1063/1.453208.

[131] Johann Nuck. *Polydiacetylene-Peptide Interaction Mechanism in Mixed Lipid Systems*. PhD thesis, Université de Genève, 2020.

[132] B. Kraabel, M. Joffre, C. Lapersonne-Meyer, and M. Schott. Singlet exciton relaxation in isolated polydiacetylene chains studied by subpicosecond pump-probe experiments. *Physical Review B*, 58(23):15777–15788, December 1998. ISSN 0163-1829, 1095-3795. doi: 10.1103/PhysRevB.58.15777.

[133] A. Yasuda, M. Yoshizawa, and T. Kobayashi. Fluorescence spectrum of a blue-phase polydiacetylene obtained by probe saturation spectroscopy. *Chemical Physics Letters*, 209(3):281–286, July 1993. ISSN 0009-2614. doi: 10.1016/0009-2614(93)80108-2.

[134] R. Lécuiller, J. Berréhar, C. Lapersonne-Meyer, M. Schott, and J. D. Ganière. Fluorescence quantum yield and lifetime of 'red' polydiacetylene chains isolated in their crystalline monomer matrix. *Chemical Physics Letters*, 314(3):255–260, December 1999. ISSN 0009-2614. doi: 10.1016/S0009-2614(99)01137-9.

[135] R. Lécuiller, J. Berréhar, J. D. Ganière, C. Lapersonne-Meyer, P. Lavallard, and M. Schott. Fluorescence yield and lifetime of isolated polydiacetylene chains: Evidence for a one-dimensional exciton band in a conjugated polymer. *Physical Review B*, 66(12):125205, September 2002. ISSN 0163-1829, 1095-3795. doi: 10.1103/PhysRevB.66.125205.

[136] François Dubin, Romain Melet, Thierry Barisien, Roger Grousson, Laurent Legrand, Michel Schott, and Valia Voliotis. Macroscopic coherence of a single exciton state in an organic quantum wire. *Nature Physics*, 2(1):32–35, January 2006. ISSN 1745-2481. doi: 10.1038/nphys196.

[137] Yevgeniy Lifshitz, Yuval Golan, Oleg Konovalov, and Amir Berman. Structural Transitions in Polydiacetylene Langmuir Films. *Langmuir*, 25(8):4469–4477, April 2009. ISSN 0743-7463. doi: 10.1021/la8029038.

[138] Nicholas J. Hestand and Frank C. Spano. Expanded Theory of H- and J-Molecular Aggregates: The Effects of Vibronic Coupling and Intermolecular Charge Transfer. *Chemical Reviews*, 118 (15):7069–7163, August 2018. ISSN 0009-2665. doi: 10.1021/acs.chemrev.7b00581.

[139] Hajime Yamagata and Frank C. Spano. Strong Photophysical Similarities between Conjugated Polymers and J-aggregates. *The Journal of Physical Chemistry Letters*, 5(3):622–632, February 2014. doi: 10.1021/jz402450m.

[140] William Barford and Max Marcus. Perspective: Optical spectroscopy in π-conjugated polymers and how it can be used to determine multiscale polymer structures. *The Journal of Chemical Physics*, 146(13):130902, April 2017. ISSN 0021-9606. doi: 10.1063/1.4979495.

[141] Frank C. Spano and Carlos Silva. H- and J-Aggregate Behavior in Polymeric Semiconductors. *Annual Review of Physical Chemistry*, 65(1):477–500, April 2014. ISSN 0066-426X, 1545-1593. doi: 10.1146/annurev-physchem-040513-103639.

[142] Keisuke Kuriyama, Hirotsugu Kikuchi, and Tisato Kajiyama. Chromatic Phase of Polydiacetylene Langmuir-Blodgett Film. *Langmuir*, 14(5):1130–1138, March 1998. ISSN 0743-7463. doi: 10.1021/la970831r.

[143] Raj Pandya, Antonios M. Alvertis, Qifei Gu, Jooyoung Sung, Laurent Legrand, David Kréher, Thierry Barisien, Alex W. Chin, Christoph Schnedermann, and Akshay Rao. Exciton Diffusion in Highly-Ordered One Dimensional Conjugated Polymers: Effects of Back-Bone Torsion, Electronic Symmetry, Phonons and Annihilation. *The Journal of Physical Chemistry Letters*, 12(14):3669–3678, April 2021. doi: 10.1021/acs.jpclett.1c00193.

[144] Raj Pandya, Qifei Gu, Alexandre Cheminal, Richard Y. S. Chen, Edward P. Booker, Richard Soucek, Michel Schott, Laurent Legrand, Fabrice Mathevet, Neil C. Greenham, Thierry Barisien, Andrew J. Musser, Alex W. Chin, and Akshay Rao. Optical Projection and Spatial Separation of Spin-Entangled Triplet Pairs from the S1 (21 Ag–) State of Pi-Conjugated Systems. *Chem*, 6(10):2826–2851, October 2020. ISSN 2451-9294. doi: 10.1016/j.chempr.2020.09.011.

[145] P. C. M. McWilliams, G. W. Hayden, and Z. G. Soos. Theory of even-parity states and two-photon spectra of conjugated polymers. *Physical Review B*, 43(12):9777–9791, April 1991. doi: 10.1103/PhysRevB.43.9777.

[146] Bruce Hudson and Bryan Kohler. Electronic structure and spectra of finite linear polyenes. *Synthetic Metals*, 9(2):241–253, April 1984. ISSN 0379-6779. doi: 10.1016/0379-6779(84)90062-6.

[147] Sylvie Spagnoli, Jean-Louis Fave, and Michel Schott. Photopolymerization of Thin Polycrystalline Diacetylene Films and Quenching of the Precursor Excited State. *Macromolecules*, 44 (8):2613–2625, April 2011. ISSN 0024-9297, 1520-5835. doi: 10.1021/ma102968w.

[148] Jean-Sébastien Filhol, Jérôme Deschamps, Sylvain G. Dutremez, Bruno Boury, Thierry Barisien, Laurent Legrand, and Michel Schott. Polymorphs and Colors of Polydiacetylenes: A First Principles Study. *Journal of the American Chemical Society*, 131(20):6976–6988, May 2009. ISSN 0002-7863. doi: 10.1021/ja803768u.

[149] Katharine B. Blodgett and Irving Langmuir. Built-Up Films of Barium Stearate and Their Optical Properties. *Physical Review*, 51(11):964–982, June 1937. doi: 10.1103/PhysRev.51.964.

[150] Katharine B. Blodgett. Films Built by Depositing Successive Monomolecular Layers on a Solid Surface. *Journal of the American Chemical Society*, 57(6):1007–1022, June 1935. ISSN 0002-7863, 1520-5126. doi: 10.1021/ja01309a011.

[151] Osvaldo N. Jr. Oliveira, Luciano Caseli, and Katsuhiko Ariga. The Past and the Future of Langmuir and Langmuir–Blodgett Films. *Chemical Reviews*, 122(6):6459–6513, March 2022. ISSN 0009-2665. doi: 10.1021/acs.chemrev.1c00754.

[152] Katsuhiko Ariga. Don't Forget Langmuir–Blodgett Films 2020: Interfacial Nanoarchitectonics with Molecules, Materials, and Living Objects. *Langmuir*, 36(26):7158–7180, July 2020. ISSN 0743-7463. doi: 10.1021/acs.langmuir.0c01044.

[153] James Kurniawan, João Francisco Ventrici de Souza, Amanda T. Dang, Gang-yu Liu, and Tonya L. Kuhl. Preparation and Characterization of Solid-Supported Lipid Bilayers Formed by Langmuir–Blodgett Deposition: A Tutorial. *Langmuir*, 34(51):15622–15639, 12 2018-12-26. ISSN 0743-7463, 1520-5827. doi: 10.1021/acs.langmuir.8b03504.

[154] C. Gourier, C. M. Knobler, J. Daillant, and D. Chatenay. Collapse of Monolayers of 10,12-Pentacosadiyonic Acid: Kinetics and Structure. *Langmuir*, 18(24):9434–9440, November 2002. ISSN 0743-7463, 1520-5827. doi: 10.1021/la026135v.

[155] C. Gourier, M. Alba, A. Braslau, J. Daillant, M. Goldmann, C. M. Knobler, F. Rieutord, and G. Zalczer. Structure and Elastic Properties of 10-12 Pentacosadiyonic Acid Langmuir Films. *Langmuir*, 17(21):6496–6505, October 2001. ISSN 0743-7463. doi: 10.1021/la001799v.

[156] Minh Dinh Phan, Jumi Lee, and Kwanwoo Shin. Collapsed States of Langmuir Monolayers. *Journal of Oleo Science*, 65(5):385–397, 2016. ISSN 1345-8957, 1347-3352. doi: 10.5650/jos.ess15261.

[157] Herman E. Ries. Stable ridges in a collapsing monolayer. *Nature*, 281(5729):287–289, September 1979. ISSN 1476-4687. doi: 10.1038/281287a0.

[158] Sarathi Kundu. Collapse of preformed cobalt stearate film on water surface. *Colloids and Surfaces A: Physicochemical and Engineering Aspects*, 348(1):196–204, September 2009. ISSN 0927-7757. doi: 10.1016/j.colsurfa.2009.07.024.

[159] Sarathi Kundu and Dominique Langevin. Fatty acid monolayer dissociation and collapse: Effect of pH and cations. *Colloids and Surfaces A: Physicochemical and Engineering Aspects*, 325(1):81–85, July 2008. ISSN 0927-7757. doi: 10.1016/j.colsurfa.2008.04.037.

[160] S. Kundu, A. Datta, and S. Hazra. Growth of a collapsing Langmuir monolayer. *Physical Review E*, 73(5):051608, May 2006. ISSN 1539-3755, 1550-2376. doi: 10.1103/PhysRevE.73.051608.

[161] Herman E. Ries and Hewson Swift. Twisted double-layer ribbons and the mechanism for monolayer collapse. *Langmuir*, 3(5):853–855, September 1987. ISSN 0743-7463, 1520-5827. doi: 10.1021/la00077a048.

[162] Craig McFate, Douglas Ward, and John Olmsted. Organized collapse of fatty acid monolayers. *Langmuir*, 9(4):1036–1039, April 1993. ISSN 0743-7463, 1520-5827. doi: 10.1021/la00028a026.

[163] E. S. Nikomarov. A slow collapse of a monolayer spread on an aqueous surface. *Langmuir*, 6 (2):410–414, February 1990. ISSN 0743-7463, 1520-5827. doi: 10.1021/la00092a021.

[164] Jose Luis Fidalgo Rodriguez, Luciano Caseli, Raul Torres Rodrigues, Jose Miñones Conde, and Patrycja Dynarowicz-Latka. Phase transition beyond the monolayer collapse – The case of stearic acid spread at the air/water interface. *Colloids and Surfaces A: Physicochemical and Engineering Aspects*, 623:126781, August 2021. ISSN 0927-7757. doi: 10.1016/j.colsurfa.2021.126781.

[165] R. Volinsky, F. Gaboriaud, A. Berman, and R. Jelinek. Morphology and Organization of Phospholipid/Diacetylene Langmuir Films Studied by Brewster Angle Microscopy and Fluorescence Microscopy. *The Journal of Physical Chemistry B*, 106(36):9231–9236, September 2002. ISSN 1520-6106. doi: 10.1021/jp020393j.

[166] Thiago Eichi Goto and Luciano Caseli. Understanding the Collapse Mechanism in Langmuir Monolayers through Polarization Modulation-Infrared Reflection Absorption Spectroscopy. *Langmuir*, 29(29):9063–9071, July 2013. ISSN 0743-7463. doi: 10.1021/la402044c.

[167] Ka Yee C. Lee. Collapse Mechanisms of Langmuir Monolayers. *Annual Review of Physical Chemistry*, 59(1):771–791, May 2008. ISSN 0066-426X, 1545-1593. doi: 10.1146/annurev.physchem.58.032806.104619.

[168] S. Kundu, A. Datta, and S. Hazra. Effect of Metal Ions on Monolayer Collapses. *Langmuir*, 21(13):5894–5900, June 2005. ISSN 0743-7463. doi: 10.1021/la0505770.

[169] Christophe Ybert, Weixing Lu, Gunter Möller, and Charles M. Knobler. Collapse of a Monolayer by Three Mechanisms. *The Journal of Physical Chemistry B*, 106(8):2004–2008, February 2002. ISSN 1520-6106. doi: 10.1021/jp013173z.

[170] A. Angelova, D. Vollhardt, and R. Ionov. 2D-3D Transformations of Amphiphilic Monolayers Influenced by Intermolecular Interactions: A Brewster Angle Microscopy Study. *The Journal of Physical Chemistry*, 100(25):10710–10720, January 1996. ISSN 0022-3654, 1541-5740. doi: 10.1021/jp960417k.

[171] S. T Milner, J. F Joanny, and P Pincus. Buckling of Langmuir Monolayers. *Europhysics Letters (EPL)*, 9(5):495–500, July 1989. ISSN 0295-5075, 1286-4854. doi: 10.1209/0295-5075/9/5/015.

[172] Bernard Sims and George Zografi. Time-dependent behavior of insoluble monomolecular films: Fatty acids and some derivatives. *Journal of Colloid and Interface Science*, 41(1):35–46, October 1972. ISSN 0021-9797. doi: 10.1016/0021-9797(72)90083-5.

[173] David R. Day and Jerome B. Lando. Formation and characterization of polydiacetylene monolayer fibers. *Journal of Polymer Science: Polymer Physics Edition*, 19(1):165–172, 1981. ISSN 1542-9385. doi: 10.1002/pol.1981.180190114.

[174] Bernd Tieke, Volker Enkelmann, Harald Kapp, Günter Lieser, and Gerhard Wegner. Topochemical Reactions in Langmuir-Blodgett Multilayers. *Journal of Macromolecular Science: Part A*

- *Chemistry*, 15(5):1045–1058, April 1981. ISSN 0022-233X. doi: 10.1080/00222338108056782.

[175] Günter Lieser, Bernd Tieke, and Gerhard Wegner. Structure, phase transitions and polymerizability of multilayers of some diacetylene monocarboxylic acids. *Thin Solid Films*, 68(1): 77–90, May 1980. ISSN 0040-6090. doi: 10.1016/0040-6090(80)90138-8.

[176] Keisuke Kuriyama, Hirotsugu Kikuchi, and Tisato Kajiyama. Chromatic Phase and Molecular Packings of Polydiacetylene Langmuir-Blodgett Films. *Chemistry Letters*, 24(12):1071–1072, December 1995. ISSN 0366-7022. doi: 10.1246/cl.1995.1071.

[177] H. D Göbel, K Kjaer, J Als-Nielsen, and H Möhwald. Reorientation of aliphatic tails during the photopolymerization of a diacetylenic lipid. *Thin Solid Films*, 179(1):41–52, November 1989. ISSN 0040-6090. doi: 10.1016/0040-6090(89)90163-6.

[178] Gonzalo García-Espejo, Marta Pérez-Morales, Michel Goldmann, María T. Martín-Romero, Juan J. Giner-Casares, and Luis Camacho. Organization and structure of mixed Langmuir films composed of polydiacetylene and hemicyanine. *Journal of Colloid and Interface Science*, 508:583–590, December 2017. ISSN 0021-9797. doi: 10.1016/j.jcis.2017.08.069.

[179] Robert F. Fischetti, Mark Filipkowski, Anthony F. Garito, and J. Kent Blasie. Profile structures of ultrathin periodic and nonperiodic multilayer films containing a disubstituted diacetylene by high-resolution x-ray diffraction. *Physical Review B*, 37(9):4714–4726, March 1988. doi: 10.1103/PhysRevB.37.4714.

[180] Shaopeng Wang, Richard Lunn, Marie Pierre Krafft, and Roger M. Leblanc. One and a Half Layers? Mixed Langmuir Monolayer of 10,12-Pentacosadiynoic Acid and a Semifluorinated Tetracosane. *Langmuir*, 16(6):2882–2886, March 2000. ISSN 0743-7463. doi: 10.1021/la991137+.

[181] Shaopeng Wang, Johnny Ramirez, Yongsheng Chen, Peng G. Wang, and Roger M. Leblanc. Surface Chemistry, Topography, and Spectroscopy of a Mixed Monolayer of 10,12-Pentacosadiynoic Acid and Its Mannoside Derivative at the Air-Water Interface. *Langmuir*, 15(17):5623–5629, August 1999. ISSN 0743-7463. doi: 10.1021/la990206h.

[182] F. Gaboriaud, R. Golan, R. Volinsky, A. Berman, and R. Jelinek. Organization and Structural Properties of Langmuir Films Composed of Conjugated Polydiacetylene and Phospholipids. *Langmuir*, 17(12):3651–3657, June 2001. ISSN 0743-7463. doi: 10.1021/la0012790.

[183] Anna Lio, Anke Reichert, Dong June Ahn, Jon O. Nagy, Miquel Salmeron, and Deborah H. Charych. Molecular Imaging of Thermochromic Carbohydrate-Modified Polydiacetylene Thin Films. *Langmuir*, 13(24):6524–6532, November 1997. ISSN 0743-7463. doi: 10.1021/la970406y.

[184] Hemasiri Vithana, David Johnson, Raymond Shih, and J. Adin Mann. Characterization of 12-8-diacetylene Langmuir-Blodgett films by scanning-force microscopy. *Physical Review E*, 51 (1):454–461, January 1995. ISSN 1063-651X, 1095-3787. doi: 10.1103/PhysRevE.51.454.

[185] O. Marti, H. O. Ribi, B. Drake, T. R. Albrecht, C. F. Quate, and P. K. Hansma. Atomic Force Microscopy of an Organic Monolayer. *Science, New Series*, 239(4835):50–52, 1988.

[186] Barbara M. Goettgens, Ralf W. Tillmann, Manfred Radmacher, and Hermann E. Gaub. Molecular order in polymerizable Langmuir-Blodgett films probed by microfluorescence and scanning force microscopy. *Langmuir*, 8(7):1768–1774, July 1992. ISSN 0743-7463, 1520-5827. doi: 10.1021/la00043a014.

[187] Bernd Tieke and Karin Weiss. The morphology of Langmuir—Blodgett multilayers of amphiphilic diacetylenes: Effects of the preparation conditions and the role of additives. *Journal of Colloid and Interface Science*, 101(1):129–148, September 1984. ISSN 0021-9797. doi: 10.1016/0021-9797(84)90014-6.

[188] David Day and J. B. Lando. Morphology of Crystalline Diacetylene Monolayers Polymerized at the Gas-Water Interface. *Macromolecules*, 13(6):1478–1483, November 1980. ISSN 0024-9297, 1520-5835. doi: 10.1021/ma60078a023.

[189] Susumu Yamada, Eiji Hatta, and Kōichi Mukasa. Preparation of Oriented Large Domains of Diacetylene Monolayer at the Air-Water Interface. *Japanese Journal of Applied Physics*, 33 (Part 1, No. 6A):3528–3530, June 1994. ISSN 0021-4922, 1347-4065. doi: 10.1143/JJAP.33.3528.

[190] Susumu Yamada and Yuhei Shimoyama. Molecular Orientation and Growth Direction of Polydiacetylene Single-Crystal Monolayer at Air-Water Interface. *Japanese Journal of Applied Physics*, 35(Part 1, No. 8):4480–4485, August 1996. ISSN 0021-4922, 1347-4065. doi: 10.1143/JJAP.35.4480.

[191] D. W. Britt, U. G. Hofmann, D. Möbius, and S. W. Hell. Influence of Substrate Properties on the Topochemical Polymerization of Diacetylene Monolayers. *Langmuir*, 17(12):3757–3765, June 2001. ISSN 0743-7463. doi: 10.1021/la001240v.

[192] Hiroaki Tachibana, Yasushi Yamanaka, Hideki Sakai, Masahiko Abe, and Mutsuyoshi Matsumoto. In Situ AFM Study on the Morphological Change of the Langmuir-Blodgett Film of Cadmium 10,12-Pentacosadiynoate during Polymerization. *Langmuir*, 16(6):2975–2977, March 2000. ISSN 0743-7463. doi: 10.1021/la990883b.

[193] R.W. Carpick, D.Y. Sasaki, and A.R. Burns. Large friction anisotropy of a polydiacetylene monolayer. *Tribology Letters*, 7(2):79–85, September 1999. ISSN 1573-2711. doi: 10.1023/A:1019113218650.

[194] Amir Berman and Deborah Charych. Uniaxial Alignment of Cadmium Sulfide on Polymerized Films: Electron Microscopy and Diffraction Study. *Advanced Materials*, 11(4):296–300, 1999. ISSN 1521-4095. doi: 10.1002/(SICI)1521-4095(199903)11:4⟨296::AID-ADMA296⟩3.0.CO;2-F.

[195] Nataly Belman, Yuval Golan, and Amir Berman. Nanocrystalline Ag2S on Polydiacetylene Langmuir Films. *Crystal Growth & Design*, 5(2):439–443, March 2005. ISSN 1528-7483. doi: 10.1021/cg049752l.

[196] Alexander Upcher, Vladimir Ezersky, Amir Berman, and Yuval Golan. Twinning and Phase Control in Template-Directed ZnS and (Cd,Zn)S Nanocrystals. *Crystal Growth & Design*, 13 (5):2149–2160, May 2013. ISSN 1528-7483. doi: 10.1021/cg4002384.

[197] D. F. O'Brien, T. H. Whitesides, and R. T. Klingbiel. The photopolymerization of lipid-diacetylenes in bimolecular-layer membranes. *Journal of Polymer Science: Polymer Letters Edition*, 19(3):95–101, 1981. ISSN 1543-0472. doi: 10.1002/pol.1981.130190302.

[198] Miquel Pons, David Samuel Johnston, and Dennis Chapman. A study of the spectra of diacetylenic phospholipid polymers in solvents and dispersions. *Journal of Polymer Science: Polymer Chemistry Edition*, 20(2):513–520, 1982. ISSN 1542-9369. doi: 10.1002/pol.1982.170200224.

[199] H. Ringsdorf and H. Schupp. Polymerization of Substituted Butadienes at the Gas-Water Interface. *Journal of Macromolecular Science: Part A - Chemistry*, 15(5):1015–1026, April 1981. ISSN 0022-233X. doi: 10.1080/00222338108056780.

[200] A. D. Bangham, M. M. Standish, and J. C. Watkins. Diffusion of univalent ions across the lamellae of swollen phospholipids. *Journal of Molecular Biology*, 13(1):238–IN27, August 1965. ISSN 0022-2836. doi: 10.1016/S0022-2836(65)80093-6.

[201] Keishi Suga, Yoko Otsuka, Kengo Yoshida, and Hiroshi Umakoshi. Smart Preparation of Polydiacetylene Hydrogel Based on Self-Assembly of Tricosadiynoic Acid and 1-Oleoylglycerol (Monoolein). *Journal of Chemical Engineering of Japan*, 52(3):311–316, 2019. doi: 10.1252/jcej.18we095.

[202] Angie Davina Tjandra, Max Weston, Junwei Tang, Rhiannon P. Kuchel, and Rona Chandrawati. Solvent injection for polydiacetylene particle synthesis – Effects of varying solvent, injection rate, monomers and needle size on polydiacetylene properties. *Colloids and Surfaces A: Physicochemical and Engineering Aspects*, 619:126497, June 2021. ISSN 0927-7757. doi: 10.1016/j.colsurfa.2021.126497.

[203] Junwei Tang, Max Weston, Rhiannon P. Kuchel, Fabio Lisi, Kang Liang, and Rona Chandrawati. Fabrication of polydiacetylene particles using a solvent injection method. *Materials Advances*, 1(6):1745–1752, September 2020. ISSN 2633-5409. doi: 10.1039/D0MA00442A.

[204] Max Weston, Angie Davina Tjandra, and Rona Chandrawati. Tuning chromatic response, sensitivity, and specificity of polydiacetylene-based sensors. *Polymer Chemistry*, 11(2):166–183, January 2020. ISSN 1759-9962. doi: 10.1039/C9PY00949C.

[205] Bora Yoon, Sumi Lee, and Jong-Man Kim. Recent conceptual and technological advances in polydiacetylene-based supramolecular chemosensors. *Chemical Society Reviews*, 38(7):1958–1968, 2009. doi: 10.1039/B819539K.

[206] A. Pevzner, S. Kolusheva, Z. Orynbayeva, and R. Jelinek. Giant Chromatic Lipid/Polydiacetylene Vesicles for Detection and Visualization of Membrane Interactions. *Advanced Functional Materials*, 18(2):242–247, 2008. ISSN 1616-3028. doi: 10.1002/adfm.200700726.

[207] A Moscho, O Orwar, D T Chiu, B P Modi, and R N Zare. Rapid preparation of giant unilamellar vesicles. *Proceedings of the National Academy of Sciences*, 93(21):11443–11447, October 1996. doi: 10.1073/pnas.93.21.11443.

[208] Gangjune Kim, Simon Song, Jung Lee, and Jong-Man Kim. Size-Controlled Fabrication of Supramolecular Vesicles for the Construction of Conjugated Polymer Sensors with Enhanced Optical Properties. *Langmuir*, 26(23):17840–17842, December 2010. ISSN 0743-7463. doi: 10.1021/la103920p.

[209] Jie Song, Justin S. Cisar, and Carolyn R. Bertozzi. Functional Self-Assembling Bolaamphiphilic Polydiacetylenes as Colorimetric Sensor Scaffolds. *Journal of the American Chemical Society*, 126(27):8459–8465, July 2004. ISSN 0002-7863. doi: 10.1021/ja039825+.

[210] Jie Song, Quan Cheng, Susanne Kopta, and Raymond C. Stevens. Modulating Artificial Membrane Morphology: pH-Induced Chromatic Transition and Nanostructural Transformation of a Bolaamphiphilic Conjugated Polymer from Blue Helical Ribbons to Red Nanofibers. *Journal of the American Chemical Society*, 123(14):3205–3213, April 2001. ISSN 0002-7863. doi: 10.1021/ja0035046.

[211] Jie Song, Quan Cheng, and Raymond C. Stevens. Morphological manipulation of bolaamphiphilic polydiacetylene assemblies by controlled lipid doping. *Chemistry and Physics of Lipids*, 114(2):203–214, February 2002. ISSN 0009-3084. doi: 10.1016/S0009-3084(02)00007-5.

[212] Simon J. Kew and Elizabeth A. H. Hall. Structural effect of polymerisation and dehydration on bolaamphiphilic polydiacetylene assemblies. *Journal of Materials Chemistry*, 16(21):2039–2047, May 2006. ISSN 1364-5501. doi: 10.1039/B600931J.

[213] Ken'ichi Aoki, Nobuyuki Tamaoki, Atsushi Seki, Kenta Narazaki, Daiki Takahashi, and Kousuke Horitsugu. Synthesis and Properties of Aromatic-Terminated Diacetylene Organogelators and Their Application to Photopatterning of Polydiacetylenes. *Langmuir*, 37(44):13160–13169, November 2021. ISSN 0743-7463. doi: 10.1021/acs.langmuir.1c02420.

[214] Edmond Gravel, Julien Ogier, Thomas Arnauld, Nicolas Mackiewicz, Frédéric Ducongé, and Eric Doris. Drug Delivery and Imaging with Polydiacetylene Micelles. *Chemistry – A European Journal*, 18(2):400–408, 2012. ISSN 1521-3765. doi: 10.1002/chem.201102769.

[215] Jacob N Israelachvili. *Intermolecular and Surface Forces*. Academic Press, 225 Wyman Street, Waltham, MA 02451, USA, third edition, 2011. ISBN 978-0-12-375182-9.

[216] Bruce Weiner. *Let There Be Light: Characterizing Physical Properties of Colloids, Nanoparticles, Polymers & Proteins Using Light Scattering*. Bruce B. Weiner, Port Jefferson, NY, 2019. ISBN 978-0-578-42857-4.

[217] Anthony David Nelson, Priyanka Shiveshwarkar, Butaek Lim, Gumaro Rojas, Izele Abure, Anura Shrestha, and Justyn Jaworski. Tuning the Surface Charge of Self-Assembled Polydiacetylene Vesicles to Control Aggregation and Cell Binding. *Biosensors*, 10(10):132, September

2020. ISSN 2079-6374. doi: 10.3390/bios10100132.

[218] Lielie Li, Xueqin An, and Xiaojuan Yan. Folate-polydiacetylene-liposome for tumor targeted drug delivery and fluorescent tracing. *Colloids and Surfaces B: Biointerfaces*, 134:235–239, October 2015. ISSN 0927-7765. doi: 10.1016/j.colsurfb.2015.07.008.

[219] Caixin Guo, Shaoqin Liu, Zhifei Dai, Chang Jiang, and Wenyuan Li. Polydiacetylene vesicles as a novel drug sustained-release system. *Colloids and Surfaces B: Biointerfaces*, 76(1):362–365, March 2010. ISSN 0927-7765. doi: 10.1016/j.colsurfb.2009.10.009.

[220] Ulrich Baxa. Imaging of Liposomes by Transmission Electron Microscopy. In Scott E. McNeil, editor, *Characterization of Nanoparticles Intended for Drug Delivery*, Methods in Molecular Biology, pages 73–88. Springer, New York, NY, 2018. ISBN 978-1-4939-7352-1. doi: 10.1007/978-1-4939-7352-1_8.

[221] Sagida Bibi, Randip Kaur, Malou Henriksen-Lacey, Sarah E. McNeil, Jitinder Wilkhu, Eric Lattmann, Dennis Christensen, Afzal R. Mohammed, and Yvonne Perrie. Microscopy imaging of liposomes: From coverslips to environmental SEM. *International Journal of Pharmaceutics*, 417(1):138–150, September 2011. ISSN 0378-5173. doi: 10.1016/j.ijpharm.2010.12.021.

[222] Sofiya Kolusheva, Ellen Wachtel, and Raz Jelinek. Biomimetic lipid/polymer colorimetric membranes. *Journal of Lipid Research*, 44(1):65–71, January 2003. ISSN 0022-2275. doi: 10.1194/jlr.M200136-JLR200.

[223] Thanutpon Pattanatornchai, Nipaphat Charoenthai, and Rakchart Traiphol. Influences of structural mismatch on morphology, phase transition temperature, segmental dynamics and color-transition behaviors of polydiacetylene vesicles. *Journal of Colloid and Interface Science*, 432:176–181, October 2014. ISSN 0021-9797. doi: 10.1016/j.jcis.2014.06.047.

[224] Atsushi Miura, Steven De Feyter, Mohamed M. S. Abdel-Mottaleb, André Gesquière, Petrus C. M. Grim, Georg Moessner, Michel Sieffert, Markus Klapper, Klaus Müllen, and Frans C. De Schryver. Light- and STM-Tip-Induced Formation of One-Dimensional and Two-Dimensional Organic Nanostructures. *Langmuir*, 19(16):6474–6482, August 2003. ISSN 0743-7463. doi: 10.1021/la027051p.

[225] J. P. Rabe, S. Buchholz, and L. Askadskaya. Scanning tunnelling microscopy of several alkylated molecular moieties in monolayers on graphite. *Synthetic Metals*, 54(1):339–349,

March 1993. ISSN 0379-6779. doi: 10.1016/0379-6779(93)91080-L.

[226] Petrus C. M. Grim, Steven De Feyter, André Gesquière, Peter Vanoppen, Markus Rüker, Suresh Valiyaveettil, Georg Moessner, Klaus Müllen, and Frans C. De Schryver. Submolecularly Resolved Polymerization of Diacetylene Molecules on the Graphite Surface Observed with Scanning Tunneling Microscopy. *Angewandte Chemie International Edition in English*, 36 (23):2601–2603, 1997. ISSN 1521-3773. doi: 10.1002/anie.199726011.

[227] Y. Okawa and M. Aono. Linear chain polymerization initiated by a scanning tunneling microscope tip at designated positions. *The Journal of Chemical Physics*, 115(5):2317–2322, August 2001. ISSN 0021-9606. doi: 10.1063/1.1384554.

[228] Rajiv Giridharagopal and Kevin F. Kelly. STM-Induced Desorption of Polydiacetylene Nanowires and Reordering via Molecular Cascades. *The Journal of Physical Chemistry C*, 111 (17):6161–6166, May 2007. ISSN 1932-7447. doi: 10.1021/jp070998l.

[229] Tyson C. Davis, Jae Jin Bang, Jacob T. Brooks, David G. McMillan, and Shelley A. Claridge. Hierarchically Patterned Noncovalent Functionalization of 2D Materials by Controlled Langmuir–Schaefer Conversion. *Langmuir*, 34(4):1353–1362, January 2018. ISSN 0743-7463. doi: 10.1021/acs.langmuir.7b03845.

[230] Shelley A. Claridge, Wei-Ssu Liao, John C. Thomas, Yuxi Zhao, Huan H. Cao, Sarawut Cheunkar, Andrew C. Serino, Anne M. Andrews, and Paul S. Weiss. From the bottom up: Dimensional control and characterization in molecular monolayers. *Chemical Society Reviews*, 42(7):2725–2745, 2013. doi: 10.1039/C2CS35365B.

[231] C. Guo, J. D. Xue, L. X. Cheng, R. C. Liu, S. Z. Kang, Q. D. Zeng, and M. Li. Two-dimensional self-assembly of diacetylenic acid derivatives and their light-induced polymerization on HOPG surfaces. *Physical chemistry chemical physics: PCCP*, 19(24):16213–16218, June 2017. ISSN 1463-9084. doi: 10.1039/c7cp02337e.

[232] Tyler R. Hayes, Jae Jin Bang, Tyson C. Davis, Caroline F. Peterson, David G. McMillan, and Shelley A. Claridge. Multimicrometer Noncovalent Monolayer Domains on Layered Materials through Thermally Controlled Langmuir–Schaefer Conversion for Noncovalent 2D Functionalization. *ACS Applied Materials & Interfaces*, 9(41):36409–36416, October 2017. ISSN 1944-8244. doi: 10.1021/acsami.7b11683.

[233] Ashlin G. Porter, Tianhong Ouyang, Tyler R. Hayes, John Biechele-Speziale, Shane R. Russell, and Shelley A. Claridge. 1-nm-Wide Hydrated Dipole Arrays Regulate AuNW Assembly on Striped Monolayers in Nonpolar Solvent. *Chem*, 5(8):2264–2275, August 2019. ISSN 2451-9294. doi: 10.1016/j.chempr.2019.07.002.

[234] Juan C. Arango, Laura O. Williams, Anni Shi, Anamika Singh, Emmanuel K. Nava, Racheal V. Fisher, Joseph A. Garfield, and Shelley A. Claridge. Nanostructured Surface Functionalization of Polyacrylamide Hydrogels Below the Length Scale of Hydrogel Heterogeneity. *ACS Applied Materials & Interfaces*, 14(38):43937–43945, September 2022. ISSN 1944-8244. doi: 10.1021/acsami.2c12034.

[235] Jeremiah O. Bechtold, Juan C. Arango, Anni Shi, Anamika Singh, and Shelley A. Claridge. Striped Poly(diacetylene) Monolayers Control Adsorption of Polyelectrolytes and Proteins on 2D Materials and Elastomers. *ACS Applied Nano Materials*, 4(7):7037–7046, July 2021. doi: 10.1021/acsanm.1c01063.

[236] Mark D. Mowery, Mei Cai, Henning Menzel, and Christine E. Evans. Nanometer-scale design and fabrication of polymer interfaces using polydiacetylene monolayers. *Journal of Vacuum Science & Technology A*, 17(4):2136–2141, July 1999. ISSN 0734-2101. doi: 10.1116/1.581739.

[237] Henning Menzel, Mark D. Mowery, Mei Cai, and Christine E. Evans. Fabrication of Noncovalent and Covalent Internal Scaffolding in Monolayer Assemblies Using Diacetylenes. *Macromolecules*, 32(13):4343–4350, June 1999. ISSN 0024-9297, 1520-5835. doi: 10.1021/ma981839q.

[238] Mei Cai, Mark D. Mowery, Henning Menzel, and Christine E. Evans. Fabrication of Extended Conjugation Length Polymers within Diacetylene Monolayers on Au Surfaces: Influence of UV Exposure Time. *Langmuir*, 15(4):1215–1222, February 1999. ISSN 0743-7463. doi: 10.1021/la981219i.

[239] Mark D. Mowery, Susanne Kopta, D. Frank Ogletree, Miquel Salmeron, and Christine E. Evans. Structural Manipulation of the Frictional Properties of Linear Polymers in Single Molecular Layers. *Langmuir*, 15(15):5118–5122, July 1999. ISSN 0743-7463. doi: 10.1021/la9815998.

[240] Henning Menzel, Mark D. Mowery, Mei Cai, and Christine E. Evans. The effect of spacer length on the polymerization of diacetylenes in sams on gold surfaces. *Macromolecular Symposia*, 142(1):23–31, 1999. ISSN 1521-3900. doi: 10.1002/masy.19991420105.

[241] Henning Menzel, Mark D. Mowery, Mei Cai, and Christine E. Evans. Vertical Positioning of Internal Molecular Scaffolding within a Single Molecular Layer. *The Journal of Physical Chemistry B*, 102(47):9550–9556, November 1998. ISSN 1520-6106. doi: 10.1021/jp9830023.

[242] Fanglue Wu, N. V. S. Dinesh K. Bhupathiraju, Andrew Brown, Zhuotong Liu, Charles Michael Drain, and James D. Batteas. Mechanical and Electronic Properties of Diacetylene and Polydiacetylene Self-Assembled Monolayers on Au(111). *The Journal of Physical Chemistry C*, 124(7):4081–4089, February 2020. ISSN 1932-7447. doi: 10.1021/acs.jpcc.9b09600.

[243] Hideto Terada, Hiroaki Imai, and Yuya Oaki. Visualization and Quantitative Detection of Friction Force by Self-Organized Organic Layered Composites. *Advanced Materials*, 30(27): 1801121, 2018. ISSN 1521-4095. doi: 10.1002/adma.201801121.

[244] Yukiko Ishijima, Hiroaki Imai, and Yuya Oaki. Tunable Mechano-responsive Color-Change Properties of Organic Layered Material by Intercalation. *Chem*, 3(3):509–521, September 2017. ISSN 2451-9294. doi: 10.1016/j.chempr.2017.05.013.

[245] Machi Takeuchi, Karthikeyan Gnanasekaran, Heiner Friedrich, Hiroaki Imai, Nico A. J. M. Sommerdijk, and Yuya Oaki. Tunable Stimuli-Responsive Color-Change Properties of Layered Organic Composites. *Advanced Functional Materials*, 28(45):1804906, 2018. ISSN 1616-3028. doi: 10.1002/adfm.201804906.

[246] Anitha Patlolla, James Zunino, Anatoly I. Frenkel, and Zafar Iqbal. Thermochromism in polydiacetylene-metal oxide nanocomposites. *Journal of Materials Chemistry*, 22(14): 7028–7035, 2012. doi: 10.1039/C2JM16175C.

[247] Yunfeng Lu, Yi Yang, Alan Sellinger, Mengcheng Lu, Jinman Huang, Hongyou Fan, Raid Haddad, Gabriel Lopez, Alan R. Burns, Darryl Y. Sasaki, John Shelnutt, and C. Jeffrey Brinker. Self-assembly of mesoscopically ordered chromatic polydiacetylene/silica nanocomposites. *Nature*, 410(6831):913–917, April 2001. ISSN 1476-4687. doi: 10.1038/35073544.

[248] Yanping Wang, Lian Li, Ke Yang, Lynne A. Samuelson, and Jayant Kumar. Nanocrystalline TiO2-Catalyzed Solid-State Polymerization of Diacetylene in the Visible Region. *Journal of the American Chemical Society*, 129(23):7238–7239, June 2007. ISSN 0002-7863. doi: 10.1021/ja071296c.

[249] Amornsak Chanakul, Nisanart Traiphol, and Rakchart Traiphol. Controlling the reversible thermochromism of polydiacetylene/zinc oxide nanocomposites by varying alkyl chain length. *Journal of Colloid and Interface Science*, 389(1):106–114, January 2013. ISSN 0021-9797. doi: 10.1016/j.jcis.2012.08.066.

[250] Nisanart Traiphol, Kunruethai Faisadcha, Ruttayapon Potai, and Rakchart Traiphol. Fine tuning the color-transition temperature of thermoreversible polydiacetylene/zinc oxide nanocomposites: The effect of photopolymerization time. *Journal of Colloid and Interface Science*, 439:105–111, February 2015. ISSN 0021-9797. doi: 10.1016/j.jcis.2014.10.033.

[251] Nisanart Traiphol, Nopparat Rungruangviriya, Ruttayapon Potai, and Rakchart Traiphol. Stable polydiacetylene/ZnO nanocomposites with two-steps reversible and irreversible thermochromism: The influence of strong surface anchoring. *Journal of Colloid and Interface Science*, 356(2):481–489, April 2011. ISSN 0021-9797. doi: 10.1016/j.jcis.2011.01.028.

[252] Natthanon Phonchai, Chanita Khanantong, Filip Kielar, Rakchart Traiphol, and Nisanart Traiphol. Low-Temperature Reversible Thermochromic Polydiacetylene/Zinc(II)/Zinc Oxide Nanocomposites for Colorimetric Sensing. *ACS Applied Nano Materials*, 2(7):4489–4498, July 2019. doi: 10.1021/acsanm.9b00876.

[253] Roland Benz, Werner Prass, and Helmut Ringsdorf. Black Lipid Membranes from Polymerizable Lipids. *Angewandte Chemie International Edition in English*, 21(5):368–369, 1982. ISSN 1521-3773. doi: 10.1002/anie.198203682.

[254] Susan M. Daly, Linda A. Heffernan, William R. Barger, and Devanand K. Shenoy. Photopolymerization of Mixed Monolayers and Black Lipid Membranes Containing Gramicidin A and Diacetylenic Phospholipids. *Langmuir*, 22(3):1215–1222, January 2006. ISSN 0743-7463, 1520-5827. doi: 10.1021/la052327p.

[255] Devanand K. Shenoy, William R. Barger, Alok Singh, Rekha G. Panchal, Martin Misakian, Vincent M. Stanford, and John J. Kasianowicz. Functional Reconstitution of Protein Ion Channels into Planar Polymerizable Phospholipid Membranes. *Nano Letters*, 5(6):1181–1185, June 2005. ISSN 1530-6984. doi: 10.1021/nl050481q.

[256] Amornsak Chanakul, Rakchart Traiphol, and Nisanart Traiphol. Utilization of polydiacetylene/zinc oxide nanocomposites to detect and differentiate organic bases in various media.

Journal of Industrial and Engineering Chemistry, 45:215–222, January 2017. ISSN 1226-086X. doi: 10.1016/j.jiec.2016.09.025.

[257] Weidong Zhou, Yuliang Li, and Daoben Zhu. Progress in Polydiacetylene Nanowires by Self-Assembly and SelfPolymerization. *Chemistry – An Asian Journal*, 2(2):222–229, 2007. ISSN 1861-471X. doi: 10.1002/asia.200600218.

[258] Dong June Ahn and Jong-Man Kim. Fluorogenic Polydiacetylene Supramolecules: Immobilization, Micropatterning, and Application to Label-Free Chemosensors. *Accounts of Chemical Research*, 41(7):805–816, July 2008. ISSN 0001-4842. doi: 10.1021/ar7002489.

[259] Xuemei Sun, Tao Chen, Sanqing Huang, Li Li, and Huisheng Peng. Chromatic polydiacetylene with novel sensitivity. *Chemical Society Reviews*, 39(11):4244–4257, 2010. doi: 10.1039/C001151G.

[260] Ana Clarissa dos Santos Pires, Nilda de Fátima Ferreira Soares, Luis Henrique Mendes da Silva, Nélio José de Andrade, Miriam Fontes Araujo Silveira, and Antônio Fernandes de Carvalho. Polydiacetylene as a Biosensor: Fundamentals and Applications in the Food Industry. *Food and Bioprocess Technology*, 3(2):172–181, April 2010. ISSN 1935-5149. doi: 10.1007/s11947-008-0171-x.

[261] Soojin Jang, Seong Uk Son, Junseok Kim, Hyungjun Kim, Jaewoo Lim, Seung Beom Seo, Byunghoon Kang, Taejoon Kang, Juyeon Jung, Sungbaek Seo, and Eun-Kyung Lim. Polydiacetylene-based hydrogel beads as colorimetric sensors for the detection of biogenic amines in spoiled meat. *Food Chemistry*, 403:134317, March 2023. ISSN 0308-8146. doi: 10.1016/j.foodchem.2022.134317.

[262] Oktay Yarimaga, Justyn Jaworski, Bora Yoon, and Jong-Man Kim. Polydiacetylenes: Supramolecular smart materials with a structural hierarchy for sensing, imaging and display applications. *Chemical Communications*, 48(19):2469–2485, February 2012. ISSN 1364-548X. doi: 10.1039/C2CC17441C.

[263] Songyi Lee, Ji-Yeong Kim, Xiaoqiang Chen, and Juyoung Yoon. Recent progress in stimuli-induced polydiacetylenes for sensing temperature, chemical and biological targets. *Chemical Communications*, 52(59):9178–9196, July 2016. ISSN 1364-548X. doi: 10.1039/C6CC03584A.

[264] Jingpei Huo, Qianjun Deng, Ting Fan, Guozhang He, Xiaohong Hu, Xiaxiao Hong, Hong Chen, Shihe Luo, Zhaoyang Wang, and Dongchu Chen. Advances in polydiacetylene development for the design of side chain groups in smart material applications – a mini review. *Polymer Chemistry*, 8(48):7438–7445, 2017. doi: 10.1039/C7PY01396E.

[265] Raz Jelinek and Margarita Ritenberg. Polydiacetylenes – recent molecular advances and applications. *RSC Advances*, 3(44):21192–21201, October 2013. ISSN 2046-2069. doi: 10.1039/C3RA42639D.

[266] Xiaomin Qian and Brigitte Städler. Polydiacetylene-Based Biosensors for the Detection of Viruses and Related Biomolecules. *Advanced Functional Materials*, 30(49):2004605, 2020. ISSN 1616-3028. doi: 10.1002/adfm.202004605.

[267] Estelle Lebègue, Carole Farre, Catherine Jose, Joelle Saulnier, Florence Lagarde, Yves Chevalier, Carole Chaix, and Nicole Jaffrezic-Renault. Responsive Polydiacetylene Vesicles for Biosensing Microorganisms. *Sensors*, 18(2):599, February 2018. ISSN 1424-8220. doi: 10.3390/s18020599.

[268] Fang Fang, Fanling Meng, and Liang Luo. Recent advances on polydiacetylene-based smart materials for biomedical applications. *Materials Chemistry Frontiers*, 4(4):1089–1104, April 2020. ISSN 2052-1537. doi: 10.1039/C9QM00788A.

[269] Yu-Jia Hao and Guang-Ming Zhu. Advances in Fabrication of Polydiacetylene Vesicles and Their Applications in Medical Detection. *Chinese Journal of Analytical Chemistry*, 48(2):164–173, February 2020. ISSN 1872-2040. doi: 10.1016/S1872-2040(19)61213-2.

[270] Angie Davina Tjandra, Andy-Hoai Pham, and Rona Chandrawati. Polydiacetylene-Based Sensors To Detect Volatile Organic Compounds. *Chemistry of Materials*, 34(7):2853–2876, April 2022. ISSN 0897-4756. doi: 10.1021/acs.chemmater.1c04318.

[271] Qiong Huang, Wei Wu, Kelong Ai, and Jianhua Liu. Highly Sensitive Polydiacetylene Ensembles for Biosensing and Bioimaging. *Frontiers in Chemistry*, 8, 2020. ISSN 2296-2646.

[272] Amy V. Hall, Osama M. Musa, and Jonathan W. Steed. Properties and Applications of Stimuli-Responsive Diacetylenes. *Crystal Growth & Design*, 21(6):3614–3638, June 2021. ISSN 1528-7483. doi: 10.1021/acs.cgd.1c00300.

[273] Bratati Das, Seiko Jo, Jianlu Zheng, Jiali Chen, and Kaori Sugihara. Recent Progress in Polydiacetylene Mechanochromism. *Nanoscale*, 14(5):1670–1678, 2022. doi: 10.1039/D1NR07129G.

[274] Kazunori Se, Hiroshi Ohnuma, and Tadao Kotaka. Urethane Substituted Polydiacetylene: Synthesis and Characterization of Poly[4,6-decadiyn-1,10-diol-bis(n-butoxy-carbonyl-methyl-urethane)]. *Polymer Journal*, 14(11):895–905, November 1982. ISSN 0032-3896, 1349-0540. doi: 10.1295/polymj.14.895.

CHAPTER 3

Characterizing and Tuning the Properties of Polydiacetylene Films for Sensing Applications

*Tanner J. Finney, Sanjai J. Parikh, Amir Berman, Darryl Y. Sasaki, Tonya L. Kuhl**

T. J. Finney, T. L. Kuhl

Department of Chemical Engineering, University of California, Davis, CA 95616, United States

Sanjai J. Parikh

Department of Land, Air and Water Resources, University of California, Davis, California 95616, United States

Amir Berman

Department of Biotechnology Engineering, Ben-Gurion University of the Negev, Beersheba 8410501, Israel

Darryl Y. Sasaki

Biotechnology and Bioengineering Department, Sandia National Laboratories, Livermore, California 94550, United States

Purpose, Scope, and Future Directions

A version of this chapter was published in *Langmuir* as https://pubs.acs.org/doi/10.1021/acs.langmuir.1c02004. Some small grammatical and formatting differences exist between these two versions.

The goal of this work was to establish a baseline of effective and "good" PDA Langmuir films that could then be further exploited as mechanical stress sensors. While established techniques do indeed produce PDA Langmuir films, their quality is often suspect due gross contamination from already polymerized film, and undeveloped kinetics. Here, we present techniques that make uniform

Langmuir films and provide quantitative descriptions of how to produce blue phase PDA films ideal for use as mechanical stress sensors. This also laid the groundwork for the X-ray investigations detailed in Chapter 5. In particular, techniques to produce PDA films, and how their properties can be tuned by increasing/decreasing the chain length of the monomer, and introducing metal cations are described. The underlying mechanism of cation-PDA film interactions was explored briefly by Fourier Transform Infrared Spectroscopy (FTIR).

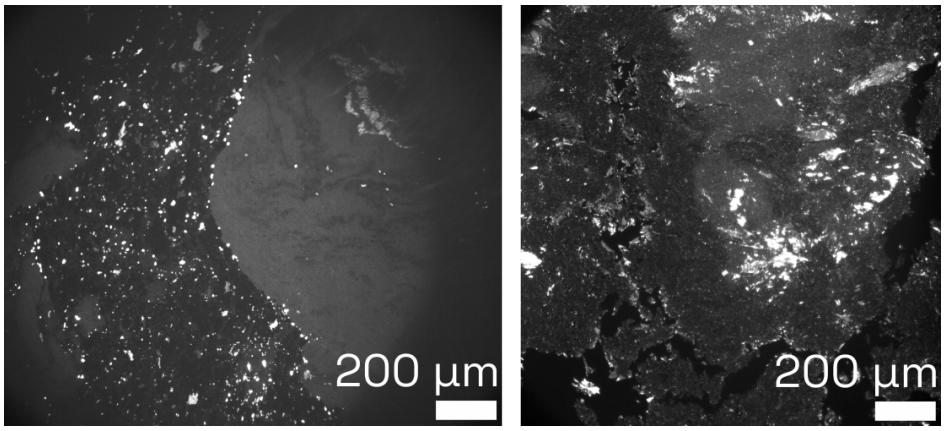

Fluorescent micrographs of PDA (PCDA) deposited onto glass slides using an angled Langmuir-Blodgett technique without prior purification. Significant heterogeneity is present within the film.

The collapse mechanism and formation of the trilayer structure and PDA domains remains under-investigated, and it would be interesting to examine the formation of these domains and multilayers with Brewster Angle Microscopy and imaging ellipsometry. The formation and organization of domains is of particular interest. Sometimes PDAs produce fascinating spirals and spherulitic domains, and other times, the exact similar PDAs may produce block-like domains. It remains unclear which conditions can reliably produce these different domain structures. While we can see in this work that these parameters are broadly a function of DA chain length, the underlying mechanism is unclear. Furthermore, the cation-film interactions and their role in changing the fluorescent properties of the films remains under-explored. We observed a significant reduction in fluorescence in films formed with Zn, Cd, and Fe cations.

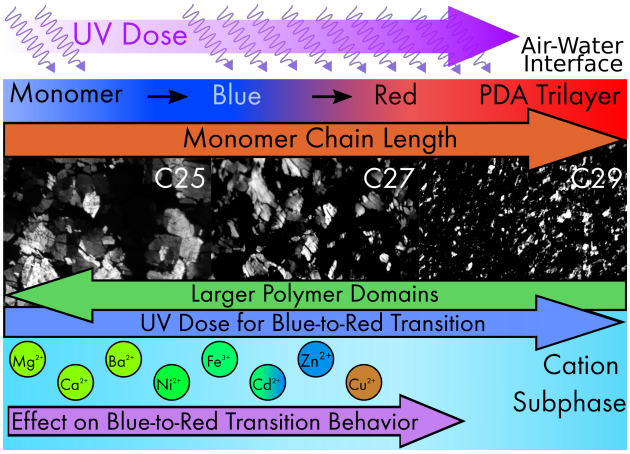

Table of contents graphic: DA Langmuir films can be driven into the blue and red phase via UV light and are readily tuned by the introduction of metal cations. Furthermore, the responsiveness can be tuned by adjusting the monomer alkyl chain length.

Abstract

Self-assembled, polymerized diacetylene (DA) nanostructures and two-dimensional films have been studied over the past two decades for sensor applications because of their straightforward visual readout. DA monomers, when exposed to UV light, polymerize to produce a visibly blue polymer. Blue phase polydiacetylenes (PDAs) when exposed to an external stimuli, such as temperature or UV light, undergo a chromatic phase transition to a fluorescent, visibly red phase. The tunability of the monomer to blue to red chromatic phase transitions by choice of diacetylene monomer in the presence of metal cations is systematically and comprehensively investigated to determine their effects on the properties of PDA Langmuir films. The Polymerization kinetics and domain morphology of the PDA films were characterized using polarized fluorescent microscopy, UV-vis-fluorescent spectroscopy, and Fourier transform infrared spectroscopy (FTIR). Increasing the monomer alkyl tail length was found to strongly increase the UV dose necessary to produce optimally blue films and fully red films. A decrease in the polymer domain size was also correlated with longer-tailed DA molecules. Metal cations have a diverse effect on the film behavior. Alkaline-earth metals such as Mg, Ca, and Ba have a negligible effect on the phase transition kinetics, but can be used to tune PDA polymer domain sizes. The Ni and Fe cations increase the UV dose to produce red phase PDA films and significantly decrease the polymer domain sizes. The Zn, Cd, and Cu ions exhibit strong directed

interactions with the PDA carboxylic acid headgroups, resulting in quenched fluorescence and a unique film morphology. FTIR analysis provides insight into the metal-PDA binding mechanisms and demonstrates that the coordination between the PDA film headgroups and the metal cations can be correlated with changes in the film morphology and kinetics. The findings from these studies will have broad utility for tuning PDA-based sensors for different applications and sensitivity ranges.

3.1. Introduction

Polydiacetylenes (PDAs) are a class of linear polymers that exhibit remarkable chromatic transitions. Proper spacing and packing of diacetylene (DA) monomers and exposure to UV light induces "topochemical" polymerization, creating a linear conjugated backbone of alternating double and triple bonds, the so-called ene-yne motif. Since their synthesis by Wegner [1], PDAs have attracted broad attention due to their potential use as sensors. PDAs formed from long-chain carboxylic acid DAs exhibit unique chromatic transitions from a visibly blue, nonfluorescent phase to a red, fluorescent phase [2, 3]. This blue-to-red chromatic transition can be exploited for use as novel colorimetric sensors, which have been summarized in several notable reviews [4–10]. The mechanism of these transitions is still not fully characterized, with both the electronic [11–15] and the structural nature of the transition still under investigation [16].

PDA Langmuir and Langmuir-Blodgett (LB) films have been widely studied. In general, Langmuir films formed from long-chain carboxylic acid DAs form stable trilayer structures [17, 18]. Both the polymerization and the blue to red transition of PDA Langmuir films follow first order kinetics [19]. Upcher et al. and Lifshitz et al. examined the effects of Ba, Cd, Cu, Zn, and Pb cations on the morphology, structure, and blue-to-red transition of PDA films. Zinc cations in particular demonstrated strong control over the behavior of PDAs, through bridging interactions between adjacent monomers and can enable chromatic reversibility [20–23]. The morphology and domains of PDA films were investigated with polarized light microscopy early on by Tieke and Weiss [24] and Day and Lando [25]. The formation of both mosaic block-like and spherulitic domains was observed. Yamada et al. expanded on this by growing and characterizing large PDA domains at the air-water interface [26–28]. AFM has been used to probe the morphology and behavior of PDA films at the

molecular level, showing that conjugated polymer backbones produce the so-called "linear strand morphology" [29, 30].

Presented here are methods and heuristics for producing, characterizing, and tuning the properties of high-quality PDA Langmuir films and for their reproducible incorporation into sensors. For use as sensors, films must have high coverage on the substrate, well-characterized blue-to-red transitions, and desired domain morphology. Effects at the air-water interface should also translate to PDA vesicles and other self-assembled nanostructures. In these studies control over the UV-dose necessary to induce the blue-to-red transition and domain size were of particular interest. As demonstrated, these properties can be tuned by metal cations in the subphase and DA monomer chain length. PDA films formed from monomers of 10,12-tricosadiynoic acid (C23, TCDA), 10,12-pentacosadiynoic acid (C25, PCDA), 10,12 heptacosadiynoic acid (C27, HCDA) and 10,12 nonacosadiynoic acid (C29, NCDA) on subphases of alkaline earth metal (Mg, Ca, Ba), Zn, Cd, Cu, Fe, and Ni cations were examined. Fluorescence microscopy and UV-Vis/fluorescent spectroscopy were used to determine the conditions for generating optimally blue films and maximally red films. Polarized fluorescence microscopy was used to examine the morphology and domains size. Fourier transform infrared spectroscopy (FTIR) enabled the interactions between metal cations and the PDA films responsible for the changes in morphological and kinetic behavior to be resolved.

3.2. Experimental Details

3.2.1. Materials. 10,12-Pentacosadiynoic acid (PCDA), 10,12-tricosadiynoic acid (TCDA), 10,12-heptacosadiynoic acid (HCDA) and 10,12-nonacosadiynoic acid (NCDA) were from TCI America and GFS Chemicals. Anhydrous zinc chloride ($ZnCl_2$) was from Honeywell Fluka. Anhydrous cadmium chloride $CdCl_2$ and barium chloride dihydrate ($BaCl_2{\cdot}2H_2O$) were from Fisher Scientific. Magnesium chloride hexahydrate ($MgCl_2{\cdot}6H_2O$) was from Acros. Anhydrous nickel (II) chloride ($NiCl_2$) was from Alfa Aesar. Calcium chloride dihydrate ($CaCl_2{\cdot}2H_2O$), iron (III) chloride hexahydrate ($FeCl_3{\cdot}6H_2O$), and copper (II) chloride dihydrate ($CuCl_2{\cdot}2H_2O$) were from Sigma Aldrich. All salts were $> 99\%$ purity and ACS grade. Chloroform (ethanol stabilized, 99.8%) was from Sigma Aldrich. Deionized, 18.2 MΩ·cm water (Barnstead NANOpure) was used for all Langmuir trough experiments.

3.2.2. Film Preparation. Purchased diacetylene (DA) powders range in appearance from bluish-gray to bright blue in color. To produce uniform, low defect films, all polymer content must be removed prior to DA deposition and film formation. Repeated syringe filtering with 0.02 μm filters is insufficient to remove all polymer content and yields heterogeneous, irreproducible films. Following Sasaki et al., a flash chromatography column was used to purify monomeric DAs [31]. Stock DA samples (60-80 mg) were dissolved in a small volume of chloroform and passed through a 10 mL silica gel (Mesh 230-400 Grade 60, Fisher Scientific) flash column (Rf = 0.22)[1]. 2-3 mL fractions were collected and analyzed with thin-layer chromatography. Fractions containing DA monomers were combined and solvent was removed under vacuum using a rotary evaporator. The rotary evaporator bath was set to $\approx 30°$C. Samples were then stored overnight under vacuum at room temperature to remove any remaining solvent. Purified, monomeric DAs were isolated as white powders. The purified samples were stored in the dark at -20°C. Under these storage conditions DA, powders were stable for at least 9 months.

Films were formed on a 300 cm^2 Langmuir-Blodgett Nima 611 trough for in-situ analysis and a Nima 611D, 600 cm^2, Langmuir-Blodgett trough for deposition. The Nima 611 was mounted under a modified Nikon MM-11 measuring microscope equipped with an epi-fluorescent light source and cross-polarizers. Fluorescent imaging utilized a Texas Red filter cube. Images were captured with an Andor Zyla 5.5 sCMOS camera. A regularly calibrated 254 nm UV pen lamp (Spectroline 110SC) was used to induce film polymerization. The UV lamp was calibrated using both a ThorLabs S120VC UV power meter and a SPER Scientific UVC Light meter with NIST certificate of calibration. UV exposure was moderated and fluorescent micrographs were taken using custom control software based on Micro-manager, and Pycromanager [32, 33].

For all experiments, a spreading solution of DA monomers was made in pure chloroform at a concentration of 0.4 mg/mL ($\sim$ 1 mM). Concentrations $>$ 0.8 mg/mL tended to lead to poor spreading of the DA monomers and yielded heterogeneous films. DA solutions in chloroform were stable for several days at room temperature, and up to one week at -20°C. Over time DAs in chloroform slowly polymerize, reducing film quality. The DA solution was deposited drop-wise and uniformly over the surface of the trough. The concentration and deposition volume was constant

[1] 25% ethyl acetate, 75 % Hexanes is also an effective solvent, Rf = 0.23

for all experiments. The trough was equilibrated for 15-20 minutes before compression to allow for solvent evaporation. Sub-phases containing cations were continuously stirred using a small integrated stir-bar in the trough. Subphase agitation did not perturb the interface or inhibit uniform film formation. The pH of the subphase in all experiments matched DI water, ≈ 5.8. The compression rate on the Nima 611 was 10 cm^2/min, and 20 cm^2/min on the Nima 611D. Films were compressed to 30 mN/m and held for several minutes. Films that were not stable at 30 mN/m were compressed to higher surface pressures shown in their respective isotherms (See Supplemental Figures S4, S7, S9, S11, S14, S18). Once compressed, the films were exposed to 254 nm light with the UV lamp mounted 1.8 cm above the trough. At this height, the lamp had an intensity of 1500 ($\pm$ 230) $\mu W/cm^2$.

Absorbance and emission spectra of the films were generated using a Perkin Elmer LAMBDA 750 UV/Vis/NIR spectrophotometer and a Varian Cary Eclipse fluorescence spectrophotometer. For these measurements, films were deposited onto thoroughly cleaned glass substrates using Langmuir-Schaefer (LS), angled Langmuir-Blodgett (LB) techniques, or a horizontal deposition method, where the trough water level was lowered until the film rested on the submerged substrates. Note: traditional, vertical, LB deposition yielded poor film transfer of both polymerized and unpolymerized films due to the stiffness of the films. Red fluorescent spectra were examined with an excitation wavelength of 488 nm and an excitation slit width of 20 nm. Transmission FTIR measurements were carried out using ZnSe windows on a Thermo Nicolet 6700 FTIR Spectrometer with a DTGS detector, co-averaging 256 scans at a $4cm^{-1}$ resolution. To generate a strong IR signal, 20 to 40 tri-layers of PDA films were built up on zinc selenide (ZnSe) crystals using the Langmuir-Schaefer deposition method.

3.2.3. Analysis Techniques.

3.2.3.1. *Fluorescent Image Analysis.* Simultaneous UV exposure and time-lapse fluorescent imagery were analyzed using ImageJ/Fiji and Scikit-Image [34–36]. Fluorescent images were binarized using the triangle thresholding method. The blue phase maximum was determined by identifying images with the least number of fluorescing regions. Initially, the film was totally non-fluorescent, and the thresholded image was noisy. As the film was continuously exposed to

UV light, the film was polymerized to the blue phase. Some of this newly polymerized blue phase undergoes the blue-to-red transition and a few small brightly fluorescing regions appear. Relative to background noise, these regions were more intense. Using in-situ fluorescence microscopy at the air-water interface, an (a) optimally blue, and (b) maximally red PDA (PCDA) film is shown in Figure 3.1.

It has been established in a variety of PDA material forms that polymerization and the blue-to-red transition follow a first order reaction kinetics [19]. Hence, an optimally blue film will show small regions of red phase PDA beginning to form. This can then be exploited by using particle counting methods, as the minimum number of fluorescing regions denotes the UV dose necessary for an optimally blue phase film. Therefore, an optimally blue phase film has been reached when the first few brightly fluorescing domains appear. A maximally red film is readily identified when the rate of fluorescing domain formation is at a minimum. Subsequently, frame number is correlated to time and thereby UV exposure dose. See supplemental figures S1, S2 for an example.

3.2.3.2. *Fluorescent Domain Analysis.* To characterize PDA film domain size, red phase films were imaged at the air-water interface with polarized fluorescent microscopy. An implementation of a local thresholding algorithm developed by Phansalkar et al. was used to identify and measure the area of individual PDA domains [37]. See supplemental for more details (Figure S3).

3.2.3.3. *Spectral Analysis.* UV-vis and IR peak detection, fitting, and deconvolution assumed Gaussian-Lorentzian line-shapes. Peak detection and fitting utilized Python and Scipy [38]. For identifying differences and notable peaks in metal ion modified IR spectra, the spectrum of the PCDA film prepared from pure water subphase was subtracted from each ion-modified spectra (supplemental figures S22, S23).

3.3. Results and Discussion

3.3.1. Pressure-Area Isotherms. Isotherms of DA Langmuir films have been extensively analyzed [17, 20]. All DA films exhibit three notable regions: (1) a monolayer that is generally unstable, (2) collapse to monolayer-trilayer coexistence beginning between 20 and 25 $Å^2$, and (3) a stable trilayer structure[18, 31, 39]. In some isotherms a sizable peak, collapse, and decrease in surface pressure was observed as the film transitions through monolayer-trilayer coexistence.

In others, surface pressure gradually increases throughout the coexistence region. It should be noted that isotherm appearance was not indicative of film quality. Evaluation of film quality at the air-water interface required polarized fluorescent microscopy. Furthermore, using DAs without purification (see materials and methods) resulted in variable, difficult to reproduce isotherms. Figure 3.2 contains representative isotherms of purified DA of increasing monomer chain length on a pure water subphase (see supplemental for complete isotherm set for cations).

3.3.2. Pure Water Films. PDA films formed from DA of increasing tail length were investigated first. It has been previously established that increasing monomer tail length increased the blue-to-red transition temperature in studies of thermochromism [40]. Figure 3.3 shows the effect of monomer chain length on the UV dose the film must be exposed to, to reach the blue phase optimum and the red phase maximum. It can be observed that increasing monomer chain length increases the UV dose required to both initiate polymerization, reach optimally blue phase PDA, and to fully transform the film to the red phase. This correlates with the higher transition temperatures of the longer DAs and an increase in van der Waals interactions between neighboring monomers that inhibit the packing rearrangements and spacing requirements for polymerization. As a result, longer DA films are less fluid and the time-scale or UV dose for polymerization and phase transition is larger. Varying the monomer chain length provides a straightforward method of directly and reproducibly tuning PDA films to different sensing regimes. For example, UV-induced blue-to-red transitions are analogous to thermochromism, with longer alkyl monomers requiring higher temperatures to induce the blue-to-red transition, compared to short-tailed monomers. Below the blue-to-red transition temperature, an optimally blue film remains non-fluorescent. We observed the transition from blue-to-red at approximately: 63-65°C for TCDA, 65-67°C for PCDA, 75-77°C for HCDA, and 80-82°C for NCDA. These transition temperatures were measured on films deposited onto glass substrates using the Langmuir-Schaefer method and were monitored using fluorescence microscopy. When heated to temperatures below the transition temperature, the films appeared slightly purple and when cooled returned to appearing fully blue.

In addition to modifying the chromatic transitions, monomer chain length was observed to have a significant effect on the size of polymer domains in the films. Figure 3.4 shows polarized fluorescent

images of PDA films formed from monomers of increasing chain length. Multiple overlapping domains are not observed, indicating that the domain orientation is coherent between each layer of the trilayer film. Most notably, average TCDA (C23) domain sizes were orders of magnitude larger than the other films with domain size going in the order of TCDA > PCDA > HCDA > NCDA. Domains of TCDA films exhibited significantly more curvature and were more continuous than the block-like domains of films formed from longer chain DAs. The domain size distribution on a pure water subphase is tabulated in Figure 3.5a. A clear shift towards smaller domains was observed as the DA monomer chain length increased. While large domains were still present, for films formed from PCDA (C25) and longer, the distribution of domains tended towards smaller and smaller domains. This is again consistent with increasing van der Waals attractions between adjacent DA monomers and increasing T_m. Stiffer systems are less prone to dynamic processes such as polymerization, leading to a decrease in domain size. This effect also manifests in the behavior of the pressure-area isotherms, Figure 2, where increasing chain length leads to an increase in the monolayer collapse pressure. Varying the monomer chain length provides one method for direct control over the polymerization kinetics and the size of polymer domains.

The behavior of films formed on pure water was also examined with UV-vis and fluorescent spectroscopy. Figure 3.6 shows the absorption and emission of blue and red phase PDA (PCDA). All PDA films formed on pure water exhibited similar absorption/emission behavior (See supplemental figure S24). The absorption and emission spectra of our films agree well with those in existing literature, with the blue phase absorbing maximally at $\sim$ 650 nm. Several other vibronic peaks were observed at shorter wavelengths. Red phase films absorb strongly at $\sim$ 550 and 510 nm. The blue phase is known to be only negligibly fluorescent. The red phase is strongly fluorescent with two peaks at $\sim$ 570 and 650 nm.

3.3.3. General Features of PDA IR spectra. Fourier transform infrared spectroscopy (FTIR) was used to investigate the behavior of both pure water and metal ion-modified PDA films. The IR spectra of PDA films and vesicles has been previously investigated by Huang et al., Ohe et al., and Wu et al. [22, 41, 42]. Fatty acid DA films exhibit several general features, regardless of headgroup coordination, corresponding to stretching and scissoring of methyl and methylene groups:

$\nu_s(CH_2)$ at 2849 cm^{-1}, $\nu_a(CH_2)$ at 2922 cm^{-1}, $\nu_a(CH_3)$ at 2955 cm^{-1}, and $\delta(CH_2)$ at 1465 cm^{-1}. (see full spectra: supplemental figures S22, S23) Hydrogen bonded carboxylates exhibit a strong band, ν(C=O), at 1694 cm^{-1}. The ν(C=O) band appears in systems that have limited directed interactions between the DA head group and cations. Coordination type between the carboxylic head group and metal ions can be determined by examining the separation, Δ, between symmetric and anti-symmetric vibrations of the carboxylate, $\Delta = \nu_a(COO) - \nu_s(COO)$. Δ has been empirically generalized to correspond to the following interactions: ionic (164 cm^{-1}) [41–43], bridging bidentate (140 - 170 cm^{-1}) [22, 42], chelating bidentate (40 - 110 cm^{-1})), monodentate (130 - 160 cm^{-1})) [22, 42–44]. A broad peak between 3200 and 3600 is often assigned as ν(OH). This can assist in discriminating between bridging bidentate and hydrogen-bonded monodentate. Importantly, FTIR spectra can be used to explain the observed differences in the morphology and kinetics between different film-ion systems. Figure 3.7 shows these key features for each film-metal system.

3.3.4. Alkaline Earth Metal Modified Films. The effects of alkaline earth cations: Mg, Ca, and Ba on PCDA films were investigated. Figure 3.8a shows the effect of these alkaline earth ions on the UV dose required to reach an optimal blue film as a function of cation concentration. For most concentrations below approximately 100 mM, the effect of these cations on the film's chromatic transitions was negligible and indistinguishable from pure water behavior. At extremely high concentrations, the UV dose to produce an optimally blue film increased modestly, but with high variability. Likewise, Figure 3.8c shows this effect on the blue-to-red transition, with the UV dose required to produce a maximally red film increasing at extreme concentrations; the mass of salt necessary for the production of these films is likely impractical for any realistic use case. Furthermore, for Ca and Ba solutions, films showed high variability on subphases with a concentration greater than 100 mM. FTIR measurements of these cation-film complexes show minimal interaction between the film and alkaline earth cations. The IR spectra of films fabricated with 1 mM Mg, Ca, and Ba cations were indistinguishable from the pure water spectra (Figure 3.7). Subtraction of these spectra from pure water yields no unique peaks. The dominating band was ν(C=O) = 1694 cm^{-1}, indicative of an undissociated, protonated carboxyl. Hence, any interactions between these films and alkaline earth cations were likely to be weak ionic screening or outer-sphere coordination, resulting in minimal effects on the film morphology or blue-to-red transition except at extremely high concentrations.

Consistent with this finding, with films formed on 1 and 10 mM Ba the thermally induced transition from blue-to-red occurred at about 67 °C, as with pure water PCDA films.

Alkaline earth ions do however have a relatively strong effect on the domain size of PDA (PCDA) films. Figure 3.5b shows the distribution of PDA domain sizes for films formed on a subphase of increasing Ca. Similar behavior was observed likewise for Ba and Mg (supplemental figure S5). At low concentrations, the behavior is similar to PCDA films formed on pure water, with a mixture of large ($> 10^2 \mu m^2$) and small ($\leq 10^1 \mu m^2$) domains. As the concentration of cations increases, small domain sizes are more strongly favored. Weak interactions between the high concentrations of metal cations and DA monomers perturb ideal packing during compression, collapse, and formation of the trilayer structure, which in turn decreases the length of aligned DA monomers, leading to smaller domains.

3.3.5. Zn Modified Films. PDA-Zn interactions have been investigated previously using FTIR, Raman and UV-vis spectroscopy [21–23]. In these studies, Zn ions were found to have directed interactions and to form coordination complexes with the films. We have observed that Zn ions had a striking effect on polymerization kinetics and film morphology due to strong bridging complexes. Zn-PDA FTIR spectra (Figure 3.7) indicate the dominating interaction was bridging bidentate, with a single Zn cation binding to two adjacent carboxylates, $\nu_a(\mathrm{COO}) = 1539\ \mathrm{cm}^{-1}$, and $\nu_s(\mathrm{COO}) = 1397\ \mathrm{cm}^{-1}$, $\Delta = 142\ \mathrm{cm}^{-1}$. The absence of $\nu(C=O)$ at $1693\ \mathrm{cm}^{-1}$ indicates strong interaction between the film and the Zn cations [22, 42]. Figure 3.9 shows the effect of increasing Zn concentration on the PDA film morphology. At low concentrations (10 μM, a), film behavior was indistinguishable from pure water as observed by fluorescent microscopy and UV-vis/fluorescent spectroscopy. Increasing concentration to 0.1 mM (b) yielded a bi-phasic system, of bright regions similar to pure water and non-fluorescent (dark), Zn bidentate governed regions.

The blue-to-red transition of the bright regions was monitored with fluorescent microscopy and deviated minimally from the behavior of PCDA films on pure water subphases (Figure 3.8b,d). As concentration increases, the methodology for calculating an optimal blue phase began to deviate due to the appearance of "Zn-governed" domains, Figure 3.8b*. These dark "Zn-governed" domains increased as the concentration of Zn increased. At 1 mM, the film was almost entirely composed of

Zn governed domains, Figure 3.9(c,d). Zn-governed films have several distinct features. These dark films could not be transformed from blue-to-red using UV light alone on any reasonable time scale. Exposure to dual 254 nm pen lamps (intensity = 3621μW/cm^2 at 1.8 cm) for upwards of three hours showed no observable transition, either visibly or spectroscopically. However, the red phase could be induced by heating, and below ~200°C was largely reversible. Above ~230°C (503 K) the film was irreversibly transformed from blue to red. This thermally induced red phase, however, was non-fluorescent as observed by both fluorescent microscopy (Figure 3.9d) and fluorescent spectroscopy. The characteristic fluorescent peaks at 560 and 650 nm were absent. The absorption spectra of both blue and red phase Zn films differ significantly from other PDA films, but are consistent with those found in literature[21]. The unusual absence of fluorescence has not been previously reported (Figure 3.10).

In addition to the change in polymerization and spectroscopic behavior, Zn cations drastically altered PDA film morphology. With typical PDA films, the domain shape, size, and orientation can be seen both with and without polarizers and can be quantitatively measured with polarized fluorescent microscopy. Zn films do not respond to polarized light and thus analysis of their domains was not possible, likely because the domain sizes were smaller than the resolution of wide-field microscopy. As the thermally induced red phase films were also non-fluorescent, the contrast between any potentially viewable domains was poor. The bridging bidentate interaction between PDA and Zn strongly governs the kinetics, morphology, and absence of fluorescent emission of Zn-PDA films.

3.3.6. Cd Modified Films. Cd modified PDA films were examined on concentrations ranging from 0.01 mM to 10 mM. On 0.1 mM Cd, there were no observable morphological or kinetic differences between Cd films and those formed on pure water. On 0.5 mM Cd, a bi-phasic regime appeared with large pure-water-like fluorescing regimes and smaller dark regimes in a maximally red film (Figure 3.11a). In regions of the Cd-PDA film that were fluorescent, there was little variation from pure-water behavior (Figure 3.8). As Cd concentration increased to 1.0 mM, the brightly fluorescing regions shrank to a number of relatively small domains, uniformly dispersed throughout the film (Figure 3.11b). Finally, at concentrations greater than 10 mM, the film appeared relatively fragmented and almost entirely non-fluorescent; (Figure 3.11c). Film heterogeneity was visible to the naked eye. At

these high concentrations, the film appears bluish-purple and similar to Zn governed films and will not readily undergo the blue-to-red transition from UV light alone. Unlike Zn-governed films, films formed on Cd exhibit greater variability and heterogeneity, with visibly un-polymerized colorless regions, red domains, and blue domains all present within a single film. This is consistent with Cd's affinity to form several different complexes with DA films. Figure 3.7 shows the FTIR spectra of PDA films formed on Cd: (1) chelating bidentate, $\Delta = \nu_a(\mathrm{COO}) - \nu_s(\mathrm{COO}) = 1534 - 1433 = 101$ cm^{-1}, and (2) H-bonded monodentate, $\Delta = \nu_a(\mathrm{COO}) - \nu_s(\mathrm{COO}) = 1534 - 1402 = 132$ cm^{-1}, $\nu(\mathrm{OH}) \approx 3400$ cm^{-1}. The appearance of these spectral bands was accordant with previous studies of Cd-PDA ion complexes [22]. Some of these interactions disrupt topochemical polymerization or the blue-to-red transition. Due to the heterogeneous morphology of Cd-PDA films, domain size was not characterized. In summary, Cd-PDA films exhibit mixed fluorescing and non-fluorescing regions (Figure 3.11, supplemental figure S10). The thermal transition temperature of Cd-modified films was likewise difficult to measure due to the heterogeneity of the films.

3.3.7. Cu Modified Films. Cu modified PDA films were evaluated from 0.1 μM to 0.1 mM. Up to 1 μM, the films behaved similar to pure water, with a clearly defined blue and red phase (Figure 3.8). From 0.01 to 0.1 mM, the morphology changed significantly and looked superficially like Zn-governed films. However, unlike Zn films, which have a strongly stabilized blue phase, the blue phase in Cu-governed films was unstable and transient. Phase analysis with fluorescent microscopy was not feasible due to the red phase being largely non-fluorescent. Visual inspection of 0.1 mM Cu films exposed to small doses of UV light, approximately a tenth of the dose necessary to produce a blue film on a pure water subphase, yielded purple-red films. Absorption and emission spectroscopy of Cu-modified films shows that at low concentrations, there was minimal deviation from pure-water PDA behavior. At concentrations of 0.1 mM and greater, fluorescence was quenched, and the blue phase was insignificant and had significant overlap with the red phase (supplemental figure S12). Similar effects have been previously observed [20, 22]. The morphology of Cu-governed films were similar to that of Zn-governed films, however, Cu films only favor the red phase. These observations were well supported by FTIR measurements. Cu modified films were dominated by bridging bidentate complexes: $\Delta = \nu_a(\mathrm{COO}) - \nu_s(\mathrm{COO}) = 1590 - 1417 = 173$ cm^{-1} interactions like Zn modified films, which exhibit similar morphology. The difference between Zn and Cu binding

interactions was examined previously by Huang et al. and Wu et al.. The difference in bridging bidentate peaks between the two cation-film complexes was attributed to differences in coordination geometry. [22, 42].

3.3.8. Ni and Fe Modified Films. Ni and Fe modified PDA films exhibited novel behavior. Rather than having a limited effect on film morphology and kinetics, like alkaline earth salts, or producing regimes of red phase with quenched fluorescence, these cations greatly increased the UV dose necessary for blue-to-red transition, while retaining pure-water subphase morphology. The effect was more pronounced in films formed on subphases containing Fe as indicated in Figure 3.8. A significant increase in UV dose to induce the blue-to-red transition was observed, without a measurable increase in UV-dose to produce optimally blue films. This effect occurred over a limited range of concentrations, however, and beyond concentrations of 0.1 mM films formation was patchy, poor, and incapable of being uniformly polymerized. This is likely due to irregular bonding between the iron cations and the film. IR spectra (Figure 3.7 of Fe-PDA films suggest interactions that are ionic, $\Delta = \nu_a(\mathrm{COO}) - \nu_s(\mathrm{COO}) = 1590 - 1430 = 165\ \mathrm{cm}^{-1}$, and chelating bidentate, $\Delta = \nu_a(\mathrm{COO}) - \nu_s(\mathrm{COO}) = 1525 - 1445 = 80\ \mathrm{cm}^{-1}$. A prominent hydrogen bonding peak is also present, $\nu(\mathrm{COO}) = 1694\ \mathrm{cm}^{-1}$. These interactions, while weak, were likely responsible for the significant change in morphology and increase in UV dose observed in the blue-to-red transition. The thermal blue-to-red temperature of Fe-PDA films at 1 μM Fe was $\approx$ 65 °C, and increased to $\approx$67-68 °C at 0.1 mM. For Fe-PDA films, with concentrations greater than 1 μM (cation to DA ratio of 1.4), the average domain size decreased to approximately 100 $\mu\mathrm{m}^2$ (Figure 3.5c). This decrease in domain size with concentration was attributable to film-ion complexing and ionic interactions disrupting the ability of the monomers to pack and form long-range patterns that fit polymerization criteria.

A similar, but less pronounced, behavior was observed with films formed on subphases containing Ni cations, with the UV dose necessary to induce the blue to red transition increasing well above the average for pure-water PDA films while retaining pure water PDA morphology (Figure 3.8). This effect was limited to concentrations on the order of 1 mM. At 10 mM, film formation was poor and no polymerizable film was observable. FTIR measurements indicate that for Ni-modified films,

the dominating effect was hydrogen bonding, $\nu(\mathrm{COO}) = 1694\ \mathrm{cm}^{-1}$, but with several smaller peaks indicative of inner-sphere-complexes. These peaks however were weak, and thus contribute to the small, but noticeable increase in UV dose necessary for the blue-to-red transition. The thermal blue-to-red temperature of Ni-PDA films was unchanged from pure water at concentrations less than 1 mM. At 1 mM, the thermal transition temperature increased modestly to ≈73 °C. Ni-PDA films exhibit similar morphological behavior to Fe-PDA films, with a decrease in domain size as concentration increased (supplemental figure S20).

3.3.9. Comparison of Counterion Effects. The interactions of Langmuir films of fatty acids and divalent cations has been extensively studied [45–49]. Due to the topochemical spacing requirements to polymerize DA fatty acids, cation-PDA interactions are relatively unique. FTIR measurements indicate that alkaline-earth cations (Mg, Ca, Ba) have limited directed interactions with the film, and primarily interact via ionic screening and hydrogen bonding. This results in a limited effect on PDA morphology and chromatic behavior. Likewise, for Ni cations, IR spectra suggest that film-cation interactions are mostly ionic screening or other outer-sphere complexes. Similar behavior is observed for Fe cations, with a more pronounced effect on film polymerization behavior. Zn, Cd, and Cu cations form complexes with the film and significantly alter polymerization, chromatic behavior, and morphology. Cd cations appear to form multiple complexes, namely chelating bidentate and monodentate complexes. The propensity to form multiple complexes is likely responsible for the observed fragmented, patchy morphology of Cd-PDA films. Cu and Zn cations form bridging bidentate complexes with the film, which creates a unique morphology that disrupts long-range domain growth and strongly alters the chromatic behavior of the film. The topochemical requirements of PDA films combined with the bridging interactions observed with Zn and Cu cations may provide further insight into more general fatty acid-cation interactions, as similar complexes may form between un-polymerizable films and divalent cations.

In studies of cation complexes, trends, such as the Irving-Williams series [50], bare and hydrated ion radius, and Electronegativity [20] can be used to correlate the observed system behavior to the physical and chemical properties of the films themselves. For PCDA, a comparison between the cation trends and observed phase transition and morphological behavior is more difficult. This is

because each cation produces unique effects that are dissimilar from each other. Mg, Ca, and Ba have minimal effects and exhibit pure-water-like behavior on film except at extreme, $>$ 100 mM, concentrations. For Ni and Fe films, the behavior is similar to pure water, but with smaller domains and higher UV doses required to produce blue and red films. At or above a concentration of 10 mM and 1 mM for Ni and Fe respectively, polymerizable films are not readily produced. For Zn, Cd, and Cu, the film enters unique regimes governed by the cations that cannot reliably be placed on a scale that readily describes one cation as having a larger "effect" than others. Broadly, the cations can be assigned to two categories, those having minimal effects, Ba, Ca, and Mg, and those that strongly modify film behavior, Zn, Cd, Cu, Fe, and Ni. It is important to reiterate however that the effects of each of these cations are unique in terms of the modifications made to the film.

Table 3.1 summarizes some of the physical and chemical properties of the cations that may be relevant to film-cation interactions. The association constants, K_a, for carboxylate-cation complexes: Fe (III) $\gg$ Cu $>$ Cd $>$ Zn $>$ Ni $>$ Ca $>$ Mg $>$ Ba, is one good predictor for PDA film behavior[20]. PDA-ion interactions with K_a greater than 0.7 (e.g. Fe, Cu, Cd, Zn, and Ni) vs. 0.4 0.5 (Mg, Ca and Ba) differentiates between strongly modified and minimally modified behavior compared to films formed on pure water. These strongly-modifying cations also are more electronegative, Ni $>$ Cu $>$ Fe (III) $>$ Cd $>$ Zn $>$ Mg $>$ Ca $>$ Ba. The solubility of the metal hydroxide K_{sp} is much lower than those of the minimal effect cations, with the trend: Ba ¿ Ca ¿ Mg ¿ Cd ¿ Ni ¿ Zn ¿ Cu ¿ Fe (III). The bare and hydrated ionic radii of the cations appear to have little-to-no correlation with the observed changes in PDA film behavior, as evident in Table 3.1.

3.3.10. Applications in Fluorescent Sensing. Polydiacetylene sensors require two criteria to be successfully employed. First, the film must be sufficiently polymerized to obtain blue phase polymer. The blue phase film should be optimized to have a low background fluorescence with a minimum of red phase PDA. Second, they must reproducibly transform from the blue-to-red phase at the desired stimulus. Insufficiently polymerized films, with too much monomer content, exhibit no fluorescent change after a stimulus has been applied. Conversely, if the film is exposed to excessive UV light during formation, the film will be partially fluorescent from red phase PDA, decreasing signal to noise. Well-calibrated UV light sources can be reliably used to polymerize films

into an ideal blue "sensing" state with different sensitivities, as demonstrated by Figures 3.3 and 3.8. The effect of metal cations and DA tail length quantified here with Langmuir films can be extended to other self-assembled PDA systems such as vesicles and self-assembled, dip-coated films.

PDA 2D Langmuir sensors, and presumably other PDA-based sensing modalities, are greatly improved by using spreading solutions composed exclusively of monomers. Commercially available diacetylenes contain already polymerized material. Dissolving stock DA powders induces solvatochromism, with large red flakes visible throughout the solution. Extensive syringe filtering yielded relatively pure DA films to the naked eye. However, inspection at the air-water interface with fluorescent microscopy showed an extensively heterogeneous film. Exposing these films to UV light yields uneven and often irreproducible film behavior that is not ideal for sensing. Passing stock DA through a silica gel column is an efficient means of purification, and proper storage as described in the experimental details can extend the quality of the purified DA.

3.3.10.1. *DA tail length.* As demonstrated, the PDA film sensitivity can be tuned by modifying film formation conditions and composition. The most straightforward method with the largest effect is to increase the length of the alkyl tail of the monomers. Longer monomer chain lengths produce films that (a) required a larger UV dose to obtain optimally blue films, and (b) a much larger UV dose to fully drive the film from the blue phase to the red phase. Decreasing the tail length resulted in a decrease in the UV dose necessary for optimal blue phase polymerization and red phase development. While the shortest chain molecule examined in this study was TCDA, C23, it is hypothesized that a further decrease in monomer alkyl tail length would further decrease the blue-to-red transition energy barrier and lead to increased sensitivity.

3.3.10.2. *Metal ion modified films.* More widely studied is the effect of metal cations on PDA films. Metal cations have a diverse array of effects on diacetylene films. These effects range from having no discernible effect on film polymerization kinetics, such as alkaline earth cations, to simply increasing the UV dose necessary for the blue-to-red transition, such as with Ni and Fe, to introducing cation governed regimes with unique properties such as Zn and Cu.

Although alkaline earth cations have a negligible effect on film polymerization and kinetic behavior, they do decrease the domain size at moderate concentrations. For instance, Ca cations decrease the

average domain size as concentration increases (Figure 3.5b). PDA domains are anisotropic, and a decrease in domain size could have applications where individual domain anisotropy is undesirable. Ni and Fe films exhibit properties similar to alkaline earth metals and pure water, in that fluorescence in the red phase is preserved. What differs is the increase in UV dose necessary to produce fully red films. This increase in UV dose is also associated with a sharp decrease in domain size. In all cases, these cations conserve the original properties of PDA films, which makes them potentially attractive due to limited changes in film morphology while allowing PDA films to be tuned to unique, higher blue-to-red threshold sensing regimes.

Cu and Cd films produce unique film-cation systems with novel properties. Cu films strongly favor the red phase, with quenched fluorescence and a lack of domain anisotropy. While previous studies have looked at the supramolecular chirality and other novel properties of Cu-modified films [22], these films are impractical for sensing purposes due to their lack of fluorescence and two-phase behavior. Cd films appear to have unique and potentially attractive properties. However, they exhibit significant heterogeneity in fluorescent and film quality. This is due to the ability of Cd ions to form different complexes with the PDA film. Some of these complexes inhibit the blue-to-red transition and quench fluorescence, and others disrupt polymerization entirely, e.g. > 10 mM $CdCl_2$ (Figure 3.11). This heterogeneity and variability make Cd-modified films less desirable for sensors.

Zn modified films have been previously investigated spectroscopically [21, 22]. Here we have investigated both the spectral, and morphological properties of Zn modified films. Notably, we have observed the presence of a bi-phasic system at moderate Zn concentrations (0.1 to 0.5 mM), with coexistence of both pure-water-like PDA domains and Zn-governed domains. This heterogeneity can be eliminated through the thorough stirring of the trough subphase or using sufficient Zn cation concentrations (greater than 1 mM) to produce fully Zn-governed films (Figure 3.9d). Zn films exhibit unique fluorescent properties, where the thermally induced red phase lacks the fluorescent emission of other PDA films. The blue-to-red phase transitions of Zn-governed films can be observed visibly, and with visible spectroscopy, but not with fluorescent microscopy or spectroscopy. Zn-governed films furthermore lack observable polymer domains. It is possible that the domains are diffraction-limited, and could be probed with friction force microscopy.

3.4. Conclusions

We have demonstrated that the blue-to-red transitions and morphology of PDA Langmuir films can be tuned based on divalent cation selection, concentration, and monomer chain length. Increasing the alkyl chain length on DA monomers yields an increase in the UV exposure dose necessary to produce an optimally blue film, a maximally red film, and a decrease in the average polymer domain size. Alkaline earth metal cations have a limited effect on film chromatic transitions and decrease the polymer domain size as concentration increases. Nickel and iron cations produce similar behavior, but more strongly favor the blue phase and decrease the domain size at much lower concentrations. Zinc cations readily form bidentate complexes to produce unique PDA film morphology, with a quenched-fluorescent red phase and strongly favored blue phase. Cadmium cations exhibit mixed behavior with greater heterogeneity and variability due to an amalgam of monodentate and bidentate complexes. These quantitative results and methods provide the ability to produce high-quality PDA films with highly tunable properties for designing improved PDA sensing platforms.

3.5. Acknowledgement

The authors thank Dr. Ed Barnard for assistance with the initial calibration of UV lamps, and Prof. Adam Moule and Meghna Jha for use of UV-vis and fluorescent spectrophotometers.

This work was partially supported by by NSF BioXFEL STC-1231306 and NIH R01 HL159993-01.

3.6. Supporting Information

Supporting information is available at https://pubs.acs.org/doi/10.1021/acs.langmuir.1c02004.

3.7. Figures

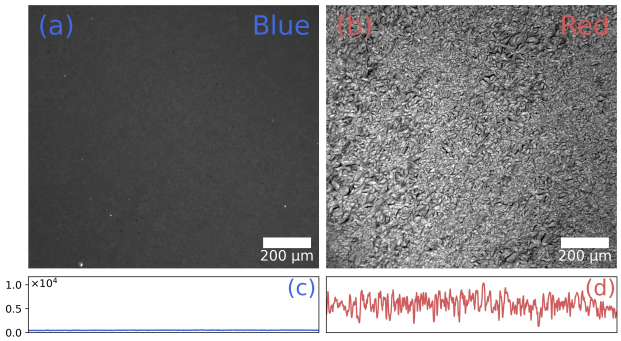

FIGURE 3.1. Fluorescent micrographs of (a) optimally blue and (b) maximally red PDA (PCDA) films at the air-water interface, scale bar is 200 μm. Intensity line profile of (c) optimally blue and (d) maximally red PDA films

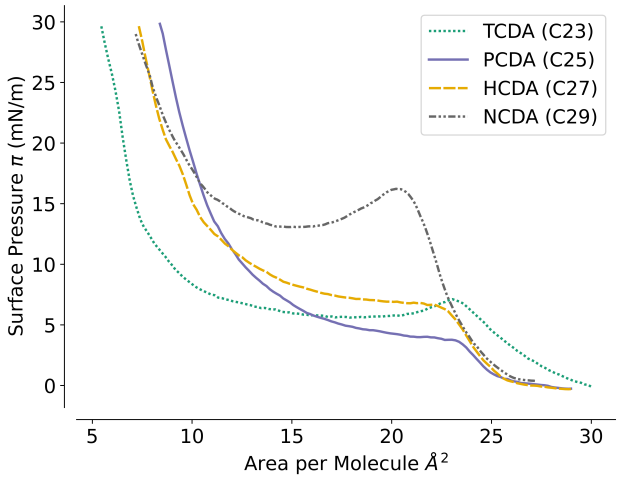

FIGURE 3.2. Representative isotherms of DA films formed on a pure water subphase

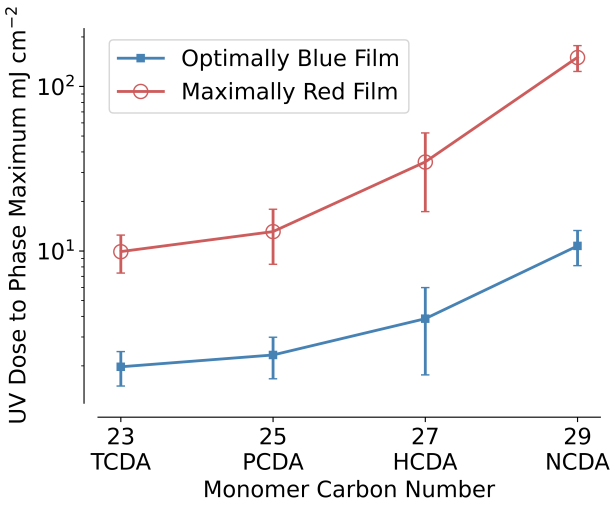

FIGURE 3.3. UV Dose required to reach the optimal blue and red phase trilayer PDA films formed from DAs of increasing tail length on a pure water subphase.

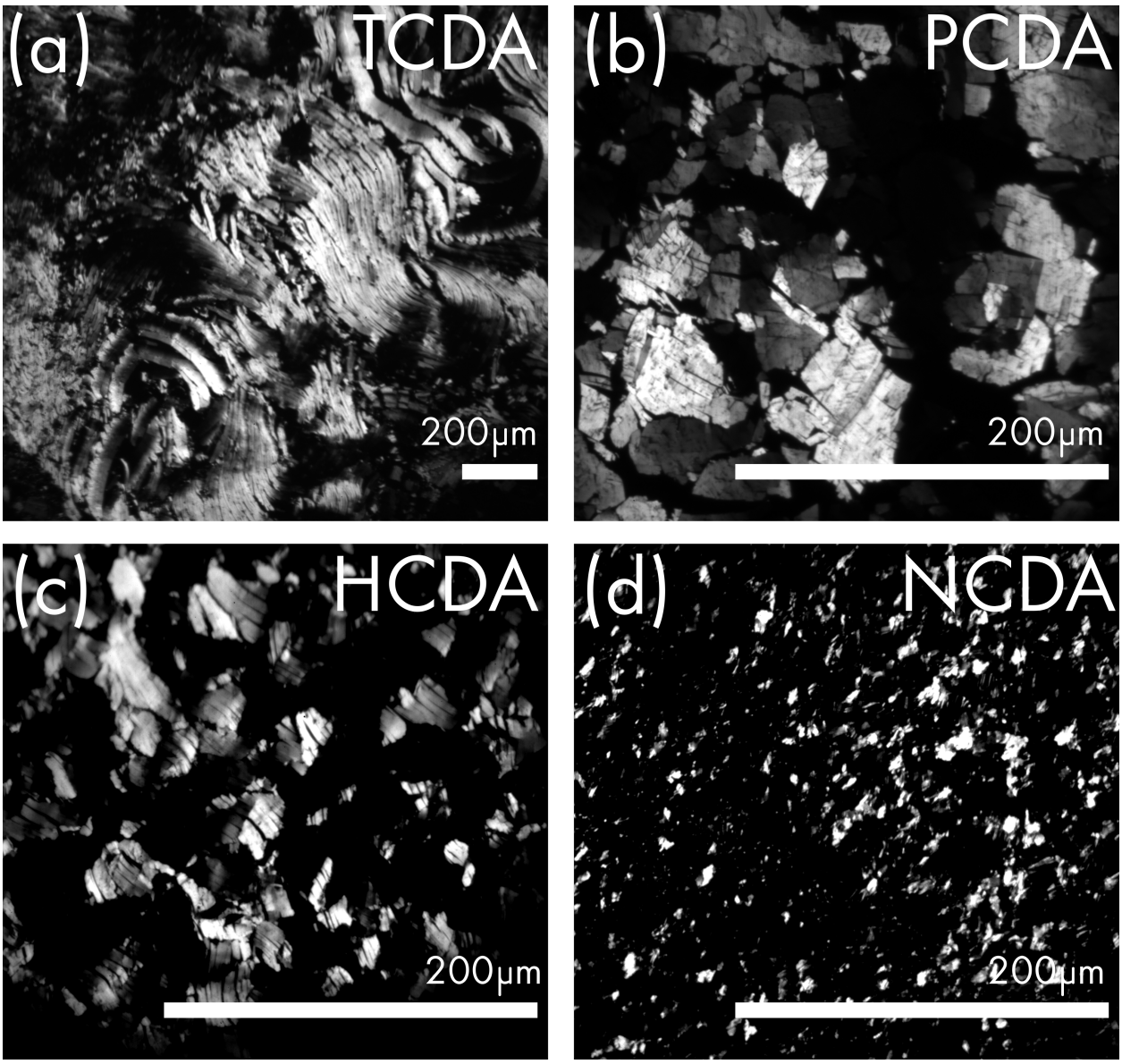

FIGURE 3.4. Polarized, fluorescent micrographs of red phase PDA films at the air water interface: (a) TCDA (b) PCDA (c) HCDA (d) NCDA.Scale bar is 200 μm.

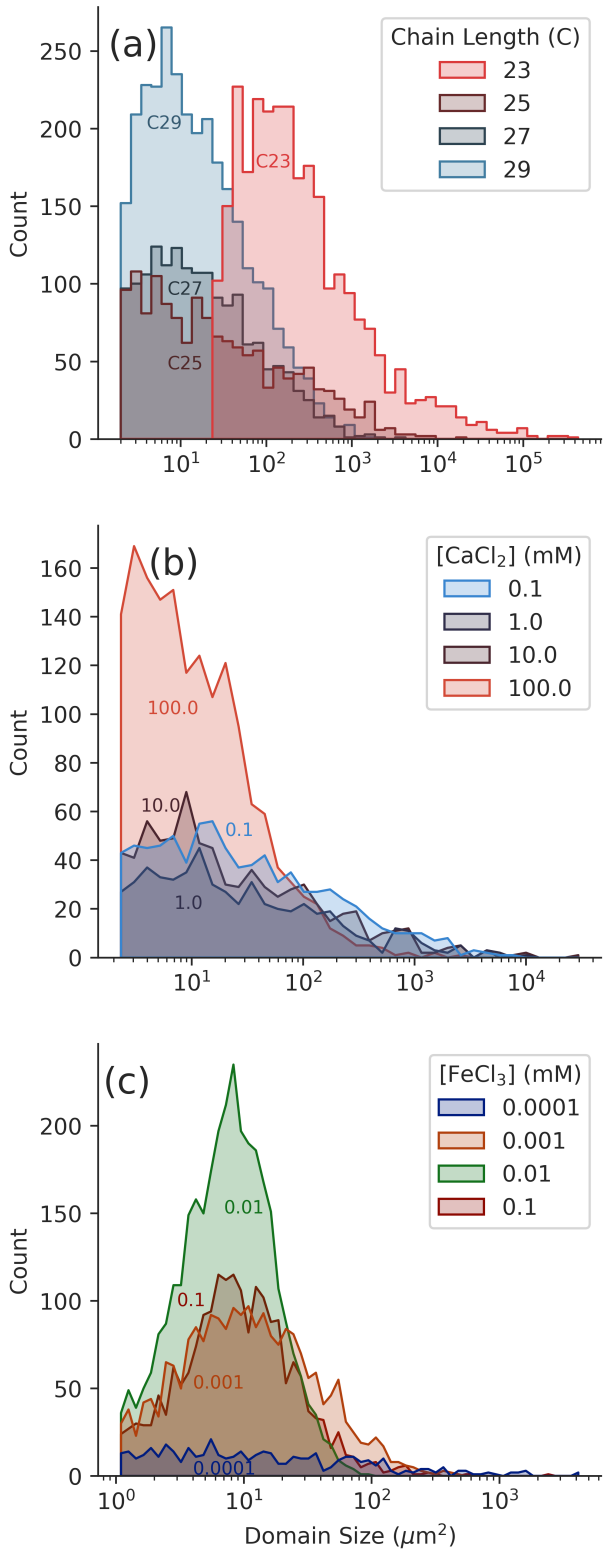

FIGURE 3.5. Distribution of domain sizes for PDA films on (a) Pure Water with different chain lengths, and with (b) $CaCl_2$, (c) $FeCl_3$ in the subphase

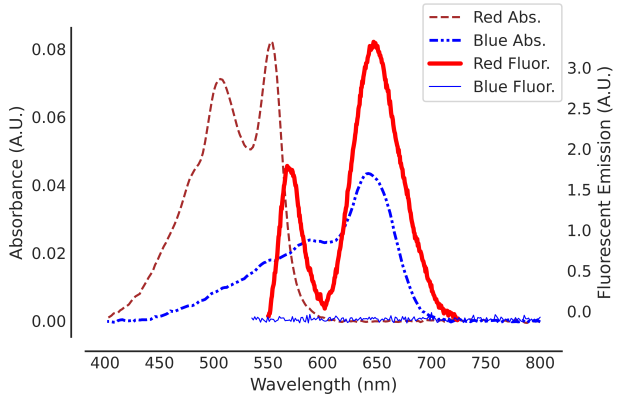

FIGURE 3.6. Absorption and Emission Spectra of PCDA formed on pure water.

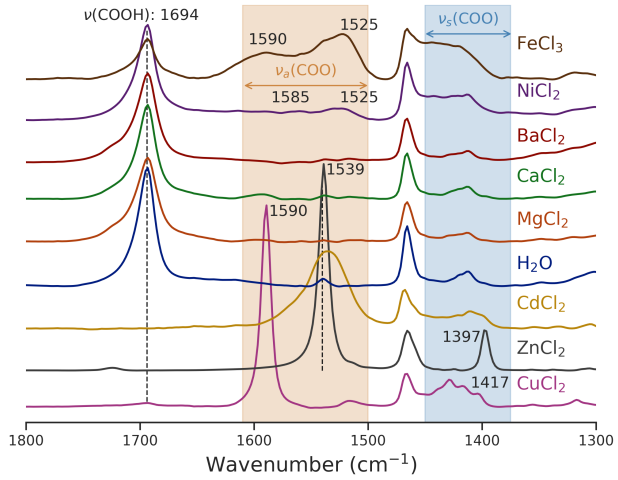

FIGURE 3.7. FTIR spectra of PCDA films formed on different subphases after polymerization and LS deposition onto ZnSe windows.

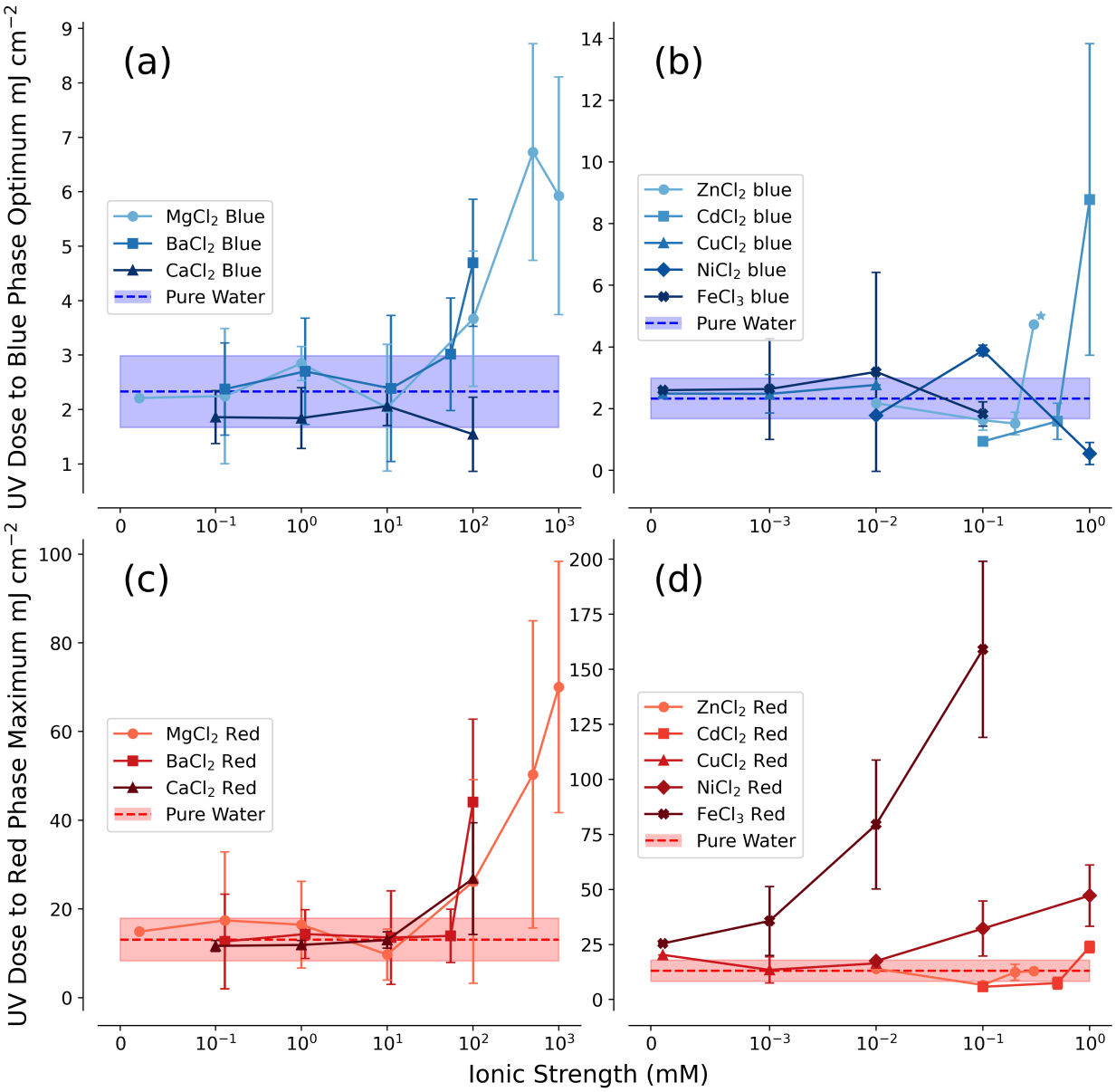

FIGURE 3.8. UV dose to reach (a,b) optimally blue and (c,d) maximally red PCDA films formed on increasing concentrations of various salt subphases. Dashed line and shaded area show behavior for pure water PCDA films with one standard deviation. The molar ratio of cation to DA monomer for a 0.1 mM subphase is ≈ 140. The "*" in (b) highlights that as zinc concentration increases the film begins to deviate from pure water behavior.

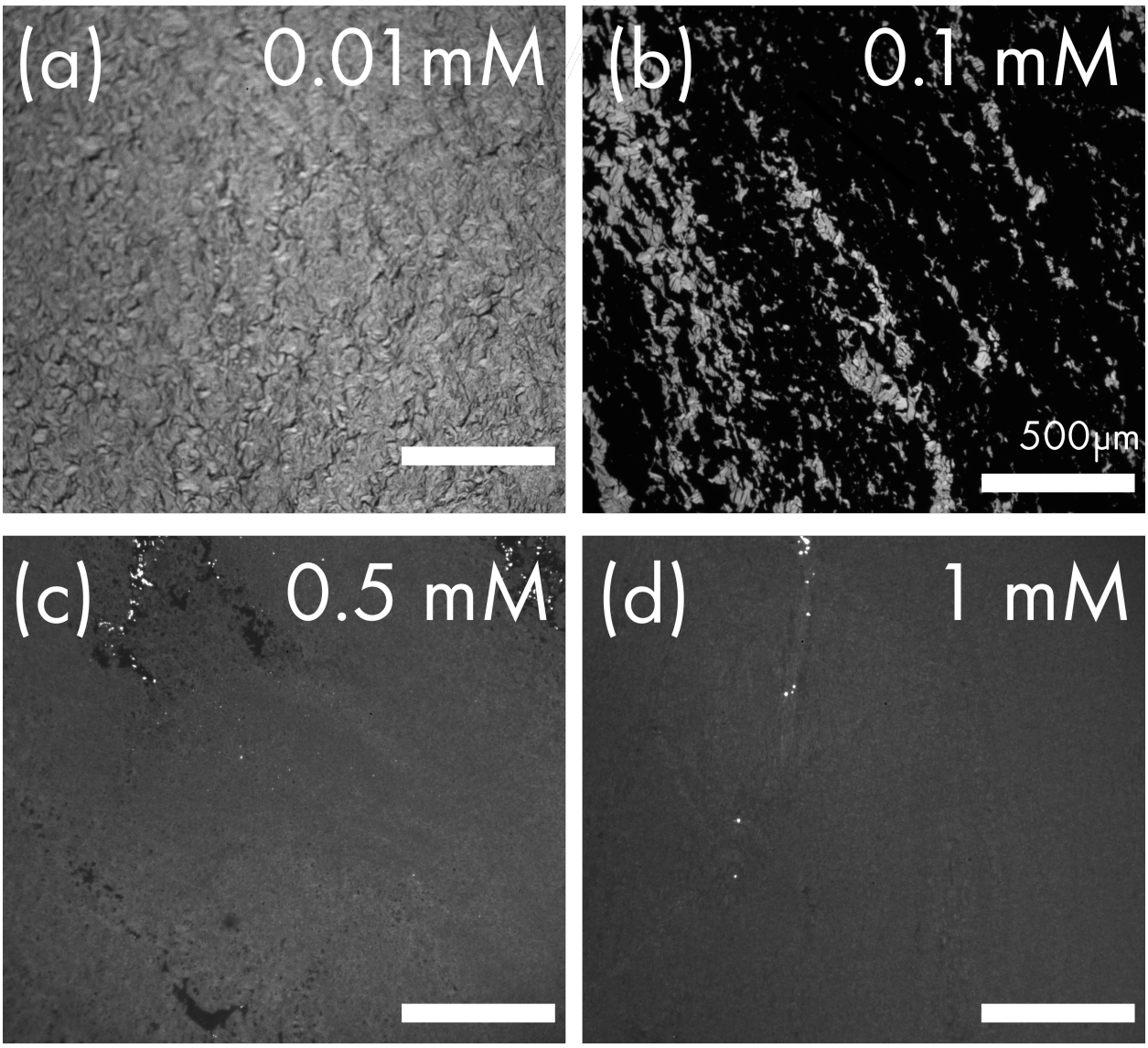

FIGURE 3.9. Fluorescent micrographs of PCDA films formed on increasing concentrations of $ZnCl_2$. (a) 0.01 mM, red-phase, fluorescent (b) 0.1 mM, red phase, mix of fluorescent and non-fluorescent (dark) film (c) 0.5 mM, red phase, non-fluorescent (d) 1 mM, red phase non-fluorescent. Scale bar is 500 μm

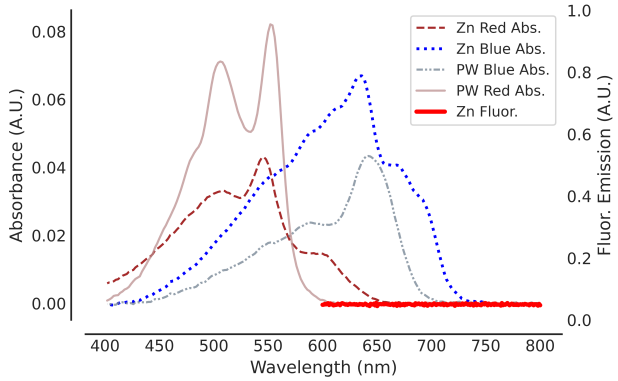

FIGURE 3.10. Absorption and Emission Spectra of PCDA films formed on 1 mM $ZnCl_2$. PW denotes spectra of PDA films taken on pure water.

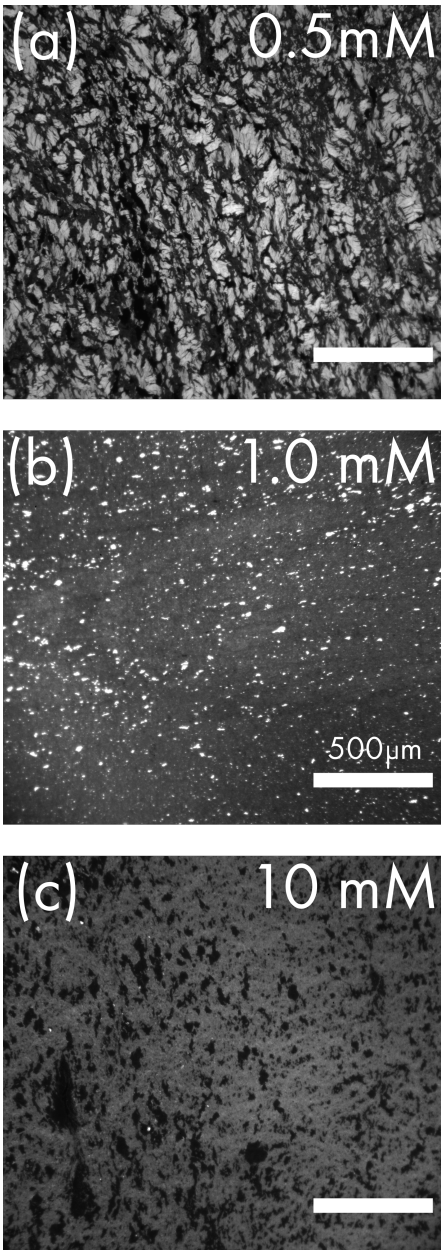

FIGURE 3.11. Fluorescent micrographs of red phase PCDA films formed on increasing concentrations of $CdCl_2$. (a) 0.5 mM red-phase, fluorescent (b) red-phase, mix of fluorescent and non-fluorescent 1.0 mM (c) 10.0 mM, non-fluorescent. Scale Bar is 500 μm.

TABLE 3.1. Potentially pertinent properties of cations in relation to PDA-cation complexes.

Metal Cation	Bare Ion Radius (Å) [51]	Hydrated Radius (Å)[51]	Association Constant (K_a) [52–54]	Electro-negativity [55]	Hydroxide Solubility (K_{sp})[a] [56]
Mg^{2+}	0.65	4.28	0.47	1.31	5.61×10^{-12}
Ca^{2+}	0.99	4.12	0.5	1	5.02×10^{-6}
Ba^{2+}	1.35	4.04	0.4	0.89	2.55×10^{-4}[b]
Fe^{3+}	0.6	4.57	8.2	1.83	2.79×10^{-39}[c]
Ni^{2+}	0.7	4.04	0.72	1.91	5.48×10^{-16}
Zn^{2+}	0.74	4.3	0.91	1.65	3.00×10^{-17}
Cd^{2+}	0.97	4.26	1.3	1.69	7.20×10^{-15}
Cu^{2+}	0.72	4.19	1.76	1.9	2.00×10^{-20}

[a] $Me(OH)_2$ unless otherwise noted.

[b] Barium Hydroxide Octahydrate

[c] Iron (III) Hydroxide

References

[1] Gerhard Wegner. Topochemische Reaktionen von Monomeren mit konjugierten Dreifachbindungen / Tochemical Reactions of Monomers with conjugated triple Bonds. *Z. Naturforsch. B*, 24 (7):824–832, July 1969. ISSN 1865-7117. doi: 10.1515/znb-1969-0708.

[2] John Olmsted and Margith Strand. Fluorescence of polymerized diacetylene bilayer films. *J. Phys. Chem.*, 87(24):4790–4792, November 1983. ISSN 0022-3654, 1541-5740. doi: 10.1021/j150642a006.

[3] Sudip Suklabaidya, Sekhar Chakraborty, Jaba Saha, Bapi Dey, Surajit Sarkar, Debajyoti Bhattacharjee, and Syed Arshad Hussain. Study of polydiacetylenes and rhodamine-800 mixed film at air–water interface and onto solid support: Trace of fluorescence resonance energy transfer (FRET). *Polym. Bull.*, 78(1):93–113, January 2021. ISSN 1436-2449. doi: 10.1007/s00289-020-03102-w.

[4] D. Bloor and R. R. Chance. *Polydiacetylenes: Synthesis, Structure and Electronic Properties*. Springer Science & Business Media, March 2013. ISBN 978-94-017-2713-6.

[5] Robert W. Carpick, Darryl Y. Sasaki, Matthew S. Marcus, M. A. Eriksson, and Alan R. Burns. Polydiacetylene films: A review of recent investigations into chromogenic transitions and nanomechanical properties. *J. Phys.: Condens. Matter*, 16(23):R679–R697, May 2004. ISSN 0953-8984. doi: 10.1088/0953-8984/16/23/R01.

[6] Mary A. Reppy and Bradford A. Pindzola. Biosensing with polydiacetylene materials: Structures, optical properties and applications. *Chem. Commun.*, 0(42):4317–4338, 2007. doi: 10.1039/B703691D.

[7] Fang Fang, Fanling Meng, and Liang Luo. Recent advances on polydiacetylene-based smart materials for biomedical applications. *Mater. Chem. Front.*, 4(4):1089–1104, April 2020. ISSN 2052-1537. doi: 10.1039/C9QM00788A.

[8] Max Weston, Angie Davina Tjandra, and Rona Chandrawati. Tuning chromatic response, sensitivity, and specificity of polydiacetylene-based sensors. *Polym. Chem.*, 11(2):166–183, January 2020. ISSN 1759-9962. doi: 10.1039/C9PY00949C.

[9] D. H. Charych, J. O. Nagy, W. Spevak, and M. D. Bednarski. Direct colorimetric detection of a receptor-ligand interaction by a polymerized bilayer assembly. *Science*, 261(5121):585–588, July 1993. ISSN 0036-8075, 1095-9203. doi: 10.1126/science.8342021.

[10] Deborah Charych, Quan Cheng, Anke Reichert, Geoffrey Kuziemko, Mark Stroh, Jon O. Nagy, Wayne Spevak, and Raymond C. Stevens. A 'litmus test' for molecular recognition using artificial membranes. *Chem. Biol*, 3(2):113–120, February 1996. ISSN 10745521. doi: 10.1016/S1074-5521(96)90287-2.

[11] Michel Schott. The Colors of Polydiacetylenes: A Commentary. *J. Phys. Chem. B*, 110(32): 15864–15868, August 2006. ISSN 1520-6106. doi: 10.1021/jp0638437.

[12] Jean-Sébastien Filhol, Jérôme Deschamps, Sylvain G. Dutremez, Bruno Boury, Thierry Barisien, Laurent Legrand, and Michel Schott. Polymorphs and Colors of Polydiacetylenes: A First Principles Study. *J. Am. Chem. Soc.*, 131(20):6976–6988, May 2009. ISSN 0002-7863. doi: 10.1021/ja803768u.

[13] Raj Pandya, Qifei Gu, Alexandre Cheminal, Richard Y. S. Chen, Edward P. Booker, Richard Soucek, Michel Schott, Laurent Legrand, Fabrice Mathevet, Neil C. Greenham, Thierry Barisien, Andrew J. Musser, Alex W. Chin, and Akshay Rao. Optical Projection and Spatial Separation of Spin-Entangled Triplet Pairs from the S1 (21 Ag–) State of Pi-Conjugated Systems. *Chem*, 6(10):2826–2851, October 2020. ISSN 2451-9294. doi: 10.1016/j.chempr.2020.09.011.

[14] Sylvie Spagnoli, Emrick Briand, Ian Vickridge, Jean-Louis Fave, and Michel Schott. Method for Determining the Polymer Content in Nonsoluble Polydiacetylene Films: Application to Pentacosadiynoic Acid. *Langmuir*, 33(6):1419–1426, February 2017. ISSN 0743-7463. doi: 10.1021/acs.langmuir.6b03147.

[15] T. Barisien, L. Legrand, G. Weiser, J. Deschamps, M. Balog, B. Boury, S. G. Dutremez, and M. Schott. Exciton spectroscopy of red polydiacetylene chains in single crystals. *Chem. Phys. Lett.*, 444(4):309–313, August 2007. ISSN 0009-2614. doi: 10.1016/j.cplett.2007.07.031.

[16] Yevgeniy Lifshitz, Yuval Golan, Oleg Konovalov, and Amir Berman. Structural Transitions in Polydiacetylene Langmuir Films. *Langmuir*, 25(8):4469–4477, April 2009. ISSN 0743-7463. doi: 10.1021/la8029038.

[17] C. Gourier, M. Alba, A. Braslau, J. Daillant, M. Goldmann, C. M. Knobler, F. Rieutord, and G. Zalczer. Structure and Elastic Properties of 10-12 Pentacosadiyonic Acid Langmuir Films. *Langmuir*, 17(21):6496–6505, October 2001. ISSN 0743-7463, 1520-5827. doi: 10.1021/la001799v.

[18] Minh Dinh Phan, Jumi Lee, and Kwanwoo Shin. Collapsed States of Langmuir Monolayers. *J. Oleo Sci.*, 65(5):385–397, 2016. ISSN 1345-8957, 1347-3352. doi: 10.5650/jos.ess15261.

[19] Yevgeniy Lifshitz, Alexander Upcher, Olga Shusterman, Baruch Horovitz, Amir Berman, and Yuval Golan. Phase transition kinetics in Langmuir and spin-coated polydiacetylene films. *Phys. Chem. Chem. Phys.*, 12(3):713–722, 2010. ISSN 1463-9076, 1463-9084. doi: 10.1039/B915527A.

[20] Alexander Upcher, Yevgeniy Lifshitz, Leila Zeiri, Yuval Golan, and Amir Berman. Effect of Metal Cations on Polydiacetylene Langmuir Films. *Langmuir*, 28(9):4248–4258, March 2012. ISSN 0743-7463. doi: 10.1021/la204735t.

[21] Yevgeniy Lifshitz, Alexander Upcher, Anatoly Kovalev, Dmitry Wainstein, Alexander Rashkovsky, Leila Zeiri, Yuval Golan, and Amir Berman. Zinc modified polydiacetylene Langmuir films. *Soft Matter*, 7(19):9069–9077, September 2011. ISSN 1744-6848. doi:

10.1039/C1SM05904A.

[22] Xin Huang, Siguang Jiang, and Minghua Liu. Metal Ion Modulated Organization and Function of the Langmuir-Blodgett Films of Amphiphilic Diacetylene: Photopolymerization, Thermochromism, and Supramolecular Chirality. *J. Phys. Chem. B*, 109(1):114–119, January 2005. ISSN 1520-6106. doi: 10.1021/jp046500m.

[23] Nisanart Traiphol, Amornsak Chanakul, Anothai Kamphan, and Rakchart Traiphol. Role of Zn2+ ion on the formation of reversible thermochromic polydiacetylene/zinc oxide nanocomposites. *Thin Solid Films*, 622:122–129, January 2017. ISSN 0040-6090. doi: 10.1016/j.tsf.2016.12.037.

[24] Bernd Tieke and Karin Weiss. The morphology of Langmuir—Blodgett multilayers of amphiphilic diacetylenes: Effects of the preparation conditions and the role of additives. *J. Colloid Interface Sci.*, 101(1):129–148, September 1984. ISSN 0021-9797. doi: 10.1016/0021-9797(84)90014-6.

[25] David Day and J. B. Lando. Morphology of Crystalline Diacetylene Monolayers Polymerized at the Gas-Water Interface. *Macromolecules*, 13(6):1478–1483, November 1980. ISSN 0024-9297, 1520-5835. doi: 10.1021/ma60078a023.

[26] Susumu Yamada, Eiji Hatta, and Kōichi Mukasa. Preparation of Oriented Large Domains of Diacetylene Monolayer at the Air-Water Interface. *Jpn. J. Appl. Phys.*, 33(Part 1, No. 6A):3528–3530, June 1994. ISSN 0021-4922, 1347-4065. doi: 10.1143/JJAP.33.3528.

[27] Susumu Yamada and Yuhei Shimoyama. Molecular Orientation and Growth Direction of Polydiacetylene Single-Crystal Monolayer at Air-Water Interface. *Jpn. J. Appl. Phys.*, 35(Part 1, No. 8):4480–4485, August 1996. ISSN 0021-4922, 1347-4065. doi: 10.1143/JJAP.35.4480.

[28] Susumu Yamada and Yuhei Shimoyama. Morphological Variation of the Monolayer Surface of Diacetylene during Polymerization at Air-Water Interface. *Jpn. J. Appl. Phys.*, 36(Part 1, No. 8):5242–5248, August 1997. ISSN 0021-4922, 1347-4065. doi: 10.1143/JJAP.36.5242.

[29] Anna Lio, Anke Reichert, Dong June Ahn, Jon O. Nagy, Miquel Salmeron, and Deborah H. Charych. Molecular Imaging of Thermochromic Carbohydrate-Modified Polydiacetylene Thin Films. *Langmuir*, 13(24):6524–6532, November 1997. ISSN 0743-7463. doi: 10.1021/la970406y.

[30] R.W. Carpick, D.Y. Sasaki, and A.R. Burns. Large friction anisotropy of a polydiacetylene monolayer. *Tribol. Lett.*, 7(2):79–85, September 1999. ISSN 1573-2711. doi: 10.1023/A:1019113218650.

[31] Darryl Y. Sasaki, Robert W. Carpick, and Alan R. Burns. High Molecular Orientation in Mono- and Trilayer Polydiacetylene Films Imaged by Atomic Force Microscopy. *J. Colloid Interface Sci.*, 229(2):490–496, September 2000. ISSN 0021-9797. doi: 10.1006/jcis.2000.7043.

[32] Arthur Edelstein, Nenad Amodaj, Karl Hoover, Ron Vale, and Nico Stuurman. Computer Control of Microscopes Using μManager. *Curr. Protoc. Mol. Biol.*, 92(1):14.20.1–14.20.17, 2010. ISSN 1934-3647. doi: 10.1002/0471142727.mb1420s92.

[33] Henry Pinkard, Nico Stuurman, Ivan E. Ivanov, Nicholas M. Anthony, Wei Ouyang, Bin Li, Bin Yang, Mark A. Tsuchida, Bryant Chhun, Grace Zhang, Ryan Mei, Michael Anderson, Douglas P. Shepherd, Ian Hunt-Isaak, Raymond L. Dunn, Wiebke Jahr, Saul Kato, Loïc A. Royer, Jay R. Thiagarajah, Kevin W. Eliceiri, Emma Lundberg, Shalin B. Mehta, and Laura Waller. Pycro-Manager: Open-source software for customized and reproducible microscope control. *Nat. Methods*, 18(3):226–228, March 2021. ISSN 1548-7105. doi: 10.1038/s41592-021-01087-6.

[34] Johannes Schindelin, Ignacio Arganda-Carreras, Erwin Frise, Verena Kaynig, Mark Longair, Tobias Pietzsch, Stephan Preibisch, Curtis Rueden, Stephan Saalfeld, Benjamin Schmid, Jean-Yves Tinevez, Daniel James White, Volker Hartenstein, Kevin Eliceiri, Pavel Tomancak, and Albert Cardona. Fiji: An open-source platform for biological-image analysis. *Nat. Methods*, 9(7):676–682, July 2012. ISSN 1548-7105. doi: 10.1038/nmeth.2019.

[35] Curtis T. Rueden, Johannes Schindelin, Mark C. Hiner, Barry E. DeZonia, Alison E. Walter, Ellen T. Arena, and Kevin W. Eliceiri. ImageJ2: ImageJ for the next generation of scientific image data. *BMC Bioinformatics*, 18(1):529, November 2017. ISSN 1471-2105. doi: 10.1186/s12859-017-1934-z.

[36] Stéfan van der Walt, Johannes L. Schönberger, Juan Nunez-Iglesias, François Boulogne, Joshua D. Warner, Neil Yager, Emmanuelle Gouillart, and Tony Yu. Scikit-image: Image processing in Python. *PeerJ*, 2:e453, June 2014. ISSN 2167-8359. doi: 10.7717/peerj.453.

[37] Neerad Phansalkar, Sumit More, Ashish Sabale, and Madhuri Joshi. Adaptive local thresholding for detection of nuclei in diversity stained cytology images. In *2011 International Conference*

on Communications and Signal Processing, pages 218–220, February 2011. doi: 10.1109/ICCSP.2011.5739305.

[38] Pauli Virtanen, Ralf Gommers, Travis E. Oliphant, Matt Haberland, Tyler Reddy, David Cournapeau, Evgeni Burovski, Pearu Peterson, Warren Weckesser, Jonathan Bright, Stéfan J. van der Walt, Matthew Brett, Joshua Wilson, K. Jarrod Millman, Nikolay Mayorov, Andrew R. J. Nelson, Eric Jones, Robert Kern, Eric Larson, C. J. Carey, İlhan Polat, Yu Feng, Eric W. Moore, Jake VanderPlas, Denis Laxalde, Josef Perktold, Robert Cimrman, Ian Henriksen, E. A. Quintero, Charles R. Harris, Anne M. Archibald, Antônio H. Ribeiro, Fabian Pedregosa, and Paul van Mulbregt. SciPy 1.0: Fundamental algorithms for scientific computing in Python. *Nat. Methods*, 17(3):261–272, March 2020. ISSN 1548-7105. doi: 10.1038/s41592-019-0686-2.

[39] C. Gourier, C. M. Knobler, J. Daillant, and D. Chatenay. Collapse of Monolayers of 10,12-Pentacosadiyonic Acid: Kinetics and Structure. *Langmuir*, 18(24):9434–9440, November 2002. ISSN 0743-7463. doi: 10.1021/la026135v.

[40] Nipaphat Charoenthai, Thanutpon Pattanatornchai, Sumrit Wacharasindhu, Mongkol Sukwattanasinitt, and Rakchart Traiphol. Roles of head group architecture and side chain length on colorimetric response of polydiacetylene vesicles to temperature, ethanol and pH. *J. Colloid Interface Sci.*, 360(2):565–573, August 2011. ISSN 0021-9797. doi: 10.1016/j.jcis.2011.04.109.

[41] C. Ohe, H. Ando, N. Sato, Y. Urai, M. Yamamoto, and K. Itoh. Carboxylate-Counterion Interactions and Changes in These Interactions during Photopolymerization of a Long-Chain Diacetylene Monocarboxylic Acid at Air-Water Interfaces: External Infrared Reflection Absorption Spectroscopic Study. *J. Phys. Chem. B*, 103(3):435–444, January 1999. ISSN 1520-6106. doi: 10.1021/jp983669p.

[42] Si Wu, Libin Pan, Youju Huang, Ni Yang, and Qijin Zhang. Co-assemblies of polydiacetylenes and metal ions for solvent sensing. *Soft Matter*, 14(33):6929–6937, 2018. doi: 10.1039/C8SM01282B.

[43] Arne Gericke and Heinrich Hühnerfuss. The effect of cations on the order of saturated fatty acid monolayers at the air-water interface as determined by infrared reflection-absorption spectrometry. *Thin Solid Films*, 245(1):74–82, June 1994. ISSN 0040-6090. doi: 10.1016/0040-6090(94)90880-X.

[44] James E. Tackett. FT-IR Characterization of Metal Acetates in Aqueous Solution. *Appl Spectrosc*, 43(3):483–489, March 1989. ISSN 0003-7028. doi: 10.1366/0003702894202931.

[45] D. K. Schwartz, R. Viswanathan, J. Garnaes, and J. A. Zasadzinski. Influence of cations, alkane chain length, and substrate on molecular order of Langmuir-Blodgett films. *J. Am. Chem. Soc.*, 115(16):7374–7380, August 1993. ISSN 0002-7863. doi: 10.1021/ja00069a040.

[46] P. B. Miranda, Q. Du, and Y. R. Shen. Interaction of water with a fatty acid Langmuir film. *Chem. Phys. Lett.*, 286(1):1–8, April 1998. ISSN 0009-2614. doi: 10.1016/S0009-2614(97)01476-0.

[47] Eric Tyrode and Robert Corkery. Charging of Carboxylic Acid Monolayers with Monovalent Ions at Low Ionic Strengths: Molecular Insight Revealed by Vibrational Sum Frequency Spectroscopy. *J. Phys. Chem. C*, 122(50):28775–28786, December 2018. ISSN 1932-7447. doi: 10.1021/acs.jpcc.8b09505.

[48] E. Le Calvez, D. Blaudez, T. Buffeteau, and B. Desbat. Effect of Cations on the Dissociation of Arachidic Acid Monolayers on Water Studied by Polarization-Modulated Infrared Reflection-Absorption Spectroscopy. *Langmuir*, 17(3):670–674, February 2001. ISSN 0743-7463, 1520-5827. doi: 10.1021/la000224v.

[49] Ellen J. Robertson, Daniel K. Beaman, and Geraldine L. Richmond. Designated Drivers: The Differing Roles of Divalent Metal Ions in Surfactant Adsorption at the Oil–Water Interface. *Langmuir*, 29(50):15511–15520, December 2013. ISSN 0743-7463. doi: 10.1021/la403665n.

[50] H. Irving and R. J. P. Williams. 637. The stability of transition-metal complexes. *J. Chem. Soc.*, (0):3192–3210, January 1953. ISSN 0368-1769. doi: 10.1039/JR9530003192.

[51] E. R. Nightingale. Phenomenological Theory of Ion Solvation. Effective Radii of Hydrated Ions. *J. Phys. Chem.*, 63(9):1381–1387, September 1959. ISSN 0022-3654. doi: 10.1021/j150579a011.

[52] John W. Bunting and Kain Men Thong. Stability constants for some 1:1 metal–carboxylate complexes. *Can. J. Chem.*, 48(11):1654–1656, June 1970. ISSN 0008-4042, 1480-3291. doi: 10.1139/v70-273.

[53] R. N. Pandey and W. MacF. Smith. Carboxylate Complexing of Iron(III). I. The Formation of Monoacetatoiron(III) in Aqueous Solution: Equilibria and Kinetics. *Can. J. Chem.*, 50(2):194–200, January 1972. ISSN 0008-4042, 1480-3291. doi: 10.1139/v72-029.

[54] Robert M. Smith and Arthur E. Martell. Critical stability constants, enthalpies and entropies for the formation of metal complexes of aminopolycarboxylic acids and carboxylic acids. *Sci. Total Environ.*, 64(1):125–147, June 1987. ISSN 0048-9697. doi: 10.1016/0048-9697(87)90127-6.

[55] Electronegativity Values on the Pauling Scale. In John R. Rumble, editor, *CRC Handbook of Chemistry and Physics*. CRC Press/Taylor & Francis, Boca Raton, FL, 102nd edition (internet version 2021) edition, 2021.

[56] Solubility Product Constants of Inorganic Salts. In John R. Rumble, editor, *CRC Handbook of Chemistry and Physics*. CRC Press/Taylor & Francis, Boca Raton, FL, 102nd edition (internet version 2021) edition, 2021.

CHAPTER 4

Tracking Mechanical Stress and Cell Migration with Inexpensive Polymer Thin-Film Sensors

*Tanner J. Finney, Skye L. Frank, Michael R. Bull, Robert D. Guy, Tonya L. Kuhl**

T. J. Finney, S. L. Frank, M. R. Bull, T. L. Kuhl

Department of Chemical Engineering, University of California, Davis, CA 95616, United States

R. D. Guy

Department of Mathematics, University of California, Davis, CA 95616, United States

Purpose, Scope and Future Directions

A version of this chapter was published in *Adv. Mater. Interfaces* as https://onlinelibrary.wiley.com/doi/10.1002/admi.202201808, some small grammatical and editing differences likely exist between the published one and the one found here.

This chapter details our investigations into PDAs as mechanical stress sensors and demonstrating their feasibility as sensors of cell-exerted stress and locomotion. In particular this work details use of a Surface Forces Apparatus (SFA) to measure the mechanical response of PDAs. The SFA is well-suited to quantifying the mechanical response of PDAs due to its high force resolution (pN) and highly controlled rate of stress application. PDA Langmuir films were then applied to measure the stress exerted via the migration of slime molds. While slime molds very likely exert more stress than the originally targeted cells (mammalian fibroblasts), it is readily conceivable that an increase in stress sensitivity is attainable through further modification and functionalization of the diacetylene monomers.

Mechanochromism is an under-explored facet of PDA sensors. As suggested by Das et al., it may even be the most fundamental mechanism of the blue to red transition. While heat, and

other binding-based sensing mechanisms are more widely studied, each adds further complexity to understanding the responsiveness of PDA sensors. *Thermochromism*, or heat induced transitions, add the complication of introducing thermal disorder as generally PDAs must be heated above the melting temperature of their substituent monomers, hence an order-disorder transition might be conflated with the blue-to-red transition. As mechanical stress does not necessarily require an increase in disorder, or any sort of binding affinity, the transition is measured directly (assuming that the force applied is actually transduced to the polymer film).

There are still many interesting questions about PDA mechanochromism that remain to be investigated. The transition has been observed to be anisotropic, and occur preferentially along the polymer backbone, however it remains unclear if the transition propagates to transform an entire domain, or if the transformation is entirely localized to where mechanical stress is applied. This question would greatly benefit from an in-depth understanding of the molecular weight of PDAs. As discussed in chapter 2, fatty acid DAs are insoluble in most organic solvents and hence typical molecular weight assessments using SEC/GPC are not feasible. It remains unclear if within a single PDA domain that may be 100s of µm in diameter if the polymer chains span the entire domain, or the domains are made of smaller chains aligned tip-to-tail. Furthermore, as we observed in chapter 5 the crystallinity of PDA trilayers at the air-water interface is much shorter than the length of the domains, with a Scherrer length often on the order of magnitude of 10s of nanometers compared to the 10s-100s of microns that are the size of PDA polymer domains. It may be that PDAs, while locally crystalline, are in a hexatic phase, and hence lose positional registry relatively rapidly. Perhaps mechanochromism propagates through the locally crystalline domain and then halts?

The force required to undergo the blue to red transition may be substrate dependent and requires further investigation. A single set of substrates were used here (glass on PDMS) for calibration. This may not necessarily be that the PDA transforms with different amounts of force depending on the substrate, but that the substrate plays a significant role in ensuring the force is actually applied to the film. Normal force induced transitions, reported here, are also not well understood. It may be that normal induced transitions were not previously observed due to the significantly higher stress requirement relative to the blue to red transition. Indeed, the most rigorous investigations

of mechanochromism have used atomic force microscopy, which isn't very good at applying large normal forces to measurable areas. At the macro-scale it is also difficult to examine normal stress induced transitions due to the difficulty of effectively transducing the applied stress to the PDA backbone. For instance, pressing down on PDA powders yields minimal macro-scale response. Indeed, the only effective macro-scale response observed was in the application of stress to two purpose built flat disks which were put into a macro-scale mechanical press with a thin PDMS layer between them and then extensively loaded.

Locomotion induced mechanochromism also has many open questions. Slime molds, while easy to culture, are not necessarily representative of mammalian cell exerted forces as they move much faster and exerted larger forces. It may be that the slime molds are at least partially transforming the PDA film due to some residual organic material left behind. The strongest evidence against this idea is that slime molds do not readily transform films even with slightly higher stress thresholds. Some unpublished experiments have involved adding drops of arginine to PDA Langmuir films. Regardless of diacetylene choice, arginine was observed to transform the films. While there might be a gradient in response as a function of stimuli threshold, the films are at least somewhat transformed by the arginine in all cases. Here, we see that the slime mold simply does not transform the film if its stress threshold is too high. We still see evidence of migration in the form of puncta (another unanswered question), but we see no evidence in the form of fluorescence. Hence, while we cannot rule out a chemical transformation of PDA caused by the slime molds, it seems unlikely given the behavior observed.

Slime molds also leave "puncta" or small holes in the PDA film. These remain underexplored. Whether they are mechanically ripped pieces of PDA that the slime mold removes as in crawls across, or they are intentionally "sampled" by the slime mold was not elucidated. The most likely explanation is that they are accidentally removed by the slime mold due to the weak adhesion of the PDA film to the substrate. Preliminary experiments examined other organisms include *C. elegans* and *Amoeba proteus*. *Amoeba* studies were stymied by poor adhesion of the *Amoebea* to the PDA film. A wide gap in focal planes was observed between *Amoeba* and the film. This indicated that *Amoeba* adhered poorly and hence did not transduce locomotion stresses to the film. It would be

interesting to revisit *Amoeba* by coating the PDA film with a bit of hydrogel (even better if it is chemically coupled to the gel).

Enhanced sensitivity to cell-exerted forces likely will arise from chemical coupling of the PDA films either directly to the cell or to a hydrogel in which the cell is migrating through. Work is already underway on engineering coupled hydrogels that chemically couple to PDA films.

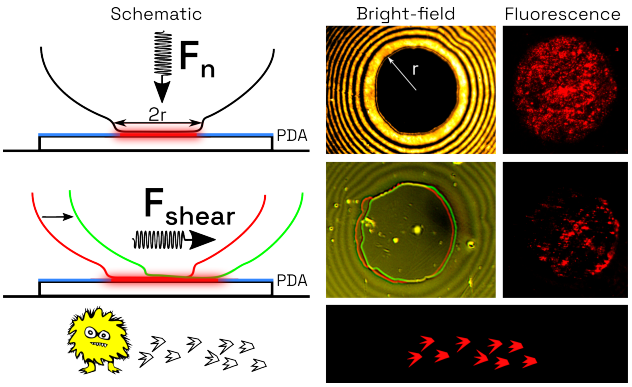

Table of contents graphic: Polydiacetylene thin films fluoresce in response to applied normal and lateral stress. The stress required is quantitative and can be tuned based on film formation conditions. PDA thin-film sensors were then applied to measure the stresses applied during *Physarum polycephalum* (slime mold) migration.

Abstract

Polydiacetylene (PDA) Langmuir films are well known for their blue to red chromatic transitions in response to a variety of stimuli, including UV light, heat, bio-molecule bindings and mechanical stress. In this work, we detail the ability to tune PDA Langmuir films to exhibit discrete chromatic transitions in response to applied mechanical stress. Normal and shear-induced transitions were quantified using the Surface Forces Apparatus and established to be binary and tunable as a function of film formation conditions. Both monomer alkyl tail length and metal cations were used to manipulate the chromatic transition force threshold to enable discrete force sensing from ∼50 to ∼500 $\mathrm{nN\,\mu m^{-2}}$ for normal loading and ∼2 to ∼40 $\mathrm{nN\,\mu m^{-2}}$ for shear-induced transitions, which are appropriate for biological cells. The utility of PDA thin-film sensors was demonstrated with the slime mold *Physarum polycephalum*. The fluorescence readout of the films enabled: the area

explored by *Physarum* to be visualized, the forces involved in locomotion to be quantified, and revealed novel puncta formation potentially associated with *Physarum* sampling its environment.

4.1. Introduction

Polydiacetylenes are a class of linear polymers that exhibit binary chromatic transitions (e.g., blue to red). PDAs can be self-assembled into Langmuir films and vesicles from various diacetylene (DA) surfactants (Supplemental S1). Exposure of the assembly to UV light induces topochemical polymerization creating a linear conjugated backbone consisting of alternating double and triple bonds [2]. This polymer is visibly blue and non-fluorescent. When exposed to external stimuli such as mechanical stress, heat or UV light, blue phase PDA can undergo a chromatic transition to a visibly red, fluorescent phase (Figure 4.1b). This chromatic transition has been described as a shift in conjugation caused by torsion of the polymer backbone but is still not fully elucidated and under active theoretical and experimental investigation [1, 3–9]. Mechanically induced blue-to-red transitions or mechanochromism in PDA Langmuir films was first described by Carpick et al. in several notable articles [10–13]. It was found that mechanochromism occurred preferentially in the direction of the polymer backbone within a given PDA domain. Subsequently, Juhasz et al. quantitatively described AFM-tip induced mechanochromism using lateral force microscopy [14] but were unable to induce transitions by applying normal force. More recent developments in other modes of mechanochromism in other material forms of PDAs were reviewed by Das et al. [1].

Of interest here is applying the unique properties of PDA mechanochromism to examine the behavior and migration of microorganisms and cells. Techniques to measure the forces involved in cell migration are often either qualitative or highly complex [15]. We demonstrate the utility and ease of use of PDA thin-film sensors using the model organism, *Physarum polycephalum*, a slime mold. *P. polycephalum* has attracted significant interest in a variety of disciplines due to its ease of culturing, cytoplasmic streaming, ameboid locomotion, and unique demonstration of "intelligence" in maze solving and other demonstrations of cognition [16–19]. In the plasmodium phase of its lifecycle, it is highly migratory and exerts measurable shear forces. The traction forces of *Physarum* microplasmodia have been examined previously using traction force microscopy (TFM) [20–23]. *Phyarsum* was observed to exert stresses on the order of magnitude of 100 Pa, with a maximum

of ~ 400 Pa. TFM enables high resolution, granular measurements of the forces exerted by cells. Conversely, the work presented here represents a passive, ensemble-level view of the forces and migration exerted by larger slime molds, based entirely on the fluorescent transitions of PDAs.

The mechanochromatic transitions of PDA Langmuir films of different compositions were precisely quantified using a modified Surface Forces Apparatus (SFA) coupled to a polarized epi-fluorescent microscope. PDA films of increasing blue to red transition threshold were fabricated and characterized with the SFA and then applied to examine the locomotion and migration of *Physarum polycephalum*. The SFA is an ideal tool for examining mechanochromism of PDA as the contact area is directly viewable and the fluorescent response to an applied force can be measured in real time. We observed that PDA films exhibited two different sensing modalities, normal stress induced transitions and shear stress induced transitions. These binary transitions occurred only when stress above the transition threshold of the film was applied. This enables applied stresses to be directly viewed through the fluorescence of the PDA film in real time or at some later time point to reveal the mechanical stress footprint. This work details the methodology to produce well-characterized PDA films with known transition properties. The PDA sensing films were then applied to the locomotion of *Physarum* revealing that the slime mold exhibits a range of forces that can be segmented and identified by using films with different mechanical stress thresholds.

4.2. Experimental Section

4.2.1. Preparation of PDA Langmuir Films. Our technique for fabricating high-quality PDA Langmuir films has been described previously [24]. 10,12-heneicosadiynoic acid (C21, ECDA) [25], 10,12-tricosadiynoic acid (C23, TCDA), 10,12-pentacosadiynoic acid (C25, PCDA), 10,12-heptacosadiynoic acid (C27, HCDA), and 10,12-nonacosadiynoic acid (C29, NCDA) were from TCI America and GFS Chemicals. Diacetylene (DA) powders were purified using flash column chromatography. The purified DAs were then dissolved in chloroform at 0.4 mg/mL and deposited dropwise onto the air-water interface of a Nima 611D Langmuir-Blodgett trough. After equilibration for 20 minutes, the trough was compressed at a rate of 20 $\mathrm{cm}^2\,\mathrm{min}^{-1}$ and exposed to 254 nm UV light for approximately 20% of the optimal blue phase UV dose once a stable trilayer film was formed. Films were then transferred to glass substrates using either an angled Langmuir-Blodgett

(LB) technique or Langmuir-Schaefer (LS) technique. Transferred films were then exposed to further UV light to maximize the blue phase prior to SFA experiments. For films formed with Zn and Fe cation subphases, the subphase was stirred continuously. Zn-PCDA films were formed with a concentration of 1 mM $ZnCl_2$ in the subphase, and Fe-PCDA films were formed with a subphase of 0.01 mM $FeCl_3$. Anhydrous zinc chloride ($ZnCl_2$) was from Honeywell Fluka and iron (III) chloride hexahydrate ($FeCl_3{\cdot}6H_2O$) was from Sigma Aldrich. See supplemental S2 for details.

4.2.2. Surface Forces Apparatus Experiments. A modified SFA Mark II was developed to carry out these experiments. The SFA was mounted underneath a polarized epi-fluorescent microscope with an Andor Zyla 5.5 sCMOS camera and Texas Red filter cube. Unlike the traditional silvered mica substrates used in typical SFA experiments, a PDA Langmuir film was directly deposited onto the cylindrically curved side of a plano-cylindrical glass lens (often referred to as an SFA disk) using the Langmuir-Schaefer technique. An identical disk was covered with a 20 µm silicone film (from Silex Ltd., Wacker Chemie). The silicone film was plasma treated to remove it from the Polyethylene terephthalate (PET) backing sheet, attached to a plastic frame, and then draped onto a UV-ozone treated SFA glass disk. The disks are then placed in specialized mounts in the SFA, one above the other with their cylindrical sides facing each other and their axes perpendicular. The contact area between the two disks is readily viewable through a window at the top of the SFA and measurable with a microscope objective. To measure normal force, the vertical movement of a calibrated spring (attached to one of the disc mounts) is tracked with an encoder. Friction forces were measured using a combined SFA friction setup composed of a bimorph driver and friction device with semiconductor strain gauges (See supplemental S3 for details) [26]. This enables precise application of sliding velocities on the order of 1-10 $\mu m\,h^{-1}$, similar to the migration rate of cells. Custom control and acquisition software was developed and utilized micro-manager and the pycro-manager interface [27–29]. This setup enabled observation of the fluorescent response to a well-defined displacement, and in subsequent experiments, measurement of the friction force associated with the fluorescent transformation of the film. Absorbance and emission spectra of the films were captured using a Perkin Elmer LAMBDA 750 UV/Vis/NIR spectrophotometer and a Varian Cary Eclipse fluorescence spectrophotometer.

4.2.3. Slime mold experiments. Cultures of *Physarum polycephalum* were purchased from Carolina Biological Supply, both as living cultures and sclerotium. *Physarum* was cultured on 2% non-nutrient agar (Sigma Aldrich) and sub-cultured every other day, fed Quaker rolled oats and stored in the dark at 24°C. For experiments with PDA films, a small, less than 1 mm radius, of the slime mold and agar was excised and deposited onto a PDA coated cover-slip. The PDA coverslip was embedded in an agar-coated Petri dish for moisture control. Slime mold migration across a PDA film was imaged with a custom polarized fluorescent microscope with an Andor Zyla 5.5 sCMOS camera. The size of the slime mold was defined as the width of the spreading plasmodium within a given area. See supplemental section S4 for more details and a schematic of experiments.

4.2.4. Statistical Analysis. Normal Force Mechanochromism: Normal force induced transitions were identified from continuous observation of applied normal force and fluorescence response of the PDA film. For each monomer with a different alkyl tail length, three samples were evaluated. Each sample provided 5-8 unique positions. The mean and standard deviation from all of these positions are reported in Figure 4.2. This analysis utilized ImageJ/Fiji and Python using numpy, uncertainties and pint.

Shear Force Mechanochromism: Shear force induced transitions were identified by the continuous acquisition of fluorescence microscopy images and response of the SFA bimoprh (See supplemental section S3 for an example of these results). For each PDA film, 3 independent SFA experiments were carried out. Within each SFA experiment, 5-7 unique positions were accessible. Friction response data was smoothed with a Savitzky-Golay filter. The distance between the sliding plateaus in the friction force were identified using a peak identification routine, which, with calibration corresponds to the friction force measured in the system (See Supplemental S3). The mean and standard deviation of these results are reported in Figure 4.4. Analysis and error propagation utilized ImageJ/Fiji and Python with numpy, pands, scipy, pint and uncertainties packages.

Slime Molds: Slime mold migration analysis was carried out by periodic imaging of migrating slime molds (See Supplemental Section S4). The size of the migrating plasmodium was measured using ImageJ/Fiji and representative samples were reported in Figures 4.6,4.7. Slime mold puncta were characterized using local image thresholding algorithms built into Fiji/ImageJ with manual

validation. The distribution of slime mold puncta are reported in Figure 4.9. The box plot shows the mean, quartiles and minimum and maximum of the measured puncta from 40 unique slime mold migration locations across all film configurations.

4.3. PDA Film Calibration

4.3.1. Normal Stress Induced Mechanochromism. The effects of normal stress on PDA mechanochromism have not been previously investigated. Atomic force microscopy studies have shown that PDA mechanochromism can be induced by lateral forces, but were unable to induce transitions by applying normal force [12, 14]. As determined in this work, the normal stress required to induce the blue-to-red transition is orders of magnitude higher than with shear stress. Using a modified SFA coupled with a fluorescent microscope we were able to simultaneously apply normal force, monitor the contact area and, fluorescent readout. For these measurements, a PDA film was deposited onto one SFA disk, and a 20 µm silicone film (a common biological model) was deposited onto the other surface. The silicone film uniformly distributed the normal force and acted as a model of an adhesive substrate, such as a cell. The experimental setup is represented schematically in Figure 4.1a. The two disks were brought into contact, loaded, and allowed to equilibrate for 10 minutes. This process was repeated at different positions with increasing load until the contact area was fully transformed from blue (non-fluorescent) to red (highly fluorescent). Figure 4.1b shows the difference in absorbance and emission spectra between the blue phase (Figure 4.1c) and mechanically transformed red phase PDA (Figure 4.1d). Initially, the film is almost entirely in the blue phase. During loading, domain edges and holes begin to fluoresce first, Figure 4.1c, followed by the bulk transformation of the film within the contact area, Figure 4.1d. Unlike shear induced transitions, normal stress induced transitions appear to transform the film without a directional dependence relative to the PDA domain orientation (aligned polymer backbone). Importantly, the transformed area does not propagate from the locally loaded area. Furthermore, normal stress mechanochromism was observed to occur from micro to macro length scales; compare Figure 4.1c,d, and insets.

This calibration method was applied to PDA films formed from DAs of increasing alkyl tail lengths ranging from ECDA, C21 to NCDA, C29. The results of these experiments are summarized in Figure 4.2. Both the normal stress to transform the bulk film as well as stress to transform the edges

and holes of the film domains follow the same trend. The difference between the bulk and edge transformation becomes more pronounced for polymer films made from DA monomers with longer alkyl tails. The UV dose required to induce the blue-to-red transition was compared to normal stress induced transitions. The dose and normal stress followed similar trends; higher doses of UV light or pressure were required to fully induce the blue-to-red transition in DA films with longer alkyl tails [24]. Interestingly, when Zn and Fe were added to the Langmuir trough subphase, the resulting PDA films were found to be unable to undergo normal stress induced transitions within the range applied by the SFA (the maximum normal stress applied in these experiments was approximately 700 $\mathrm{nN\,\mu m^{-2}}$).

When in contact with a surface, but below the critical normal stress described above, PDA films are still in the blue phase, and hence non-fluorescent. As described next, these films can be sheared to induce the blue to red transition. This enables two different sensing modes for PDA films: a normal stress sensor at relatively higher loads and a shear stress sensor at zero or lower loads.

4.3.2. Shear Stress Induced Mechanochromism. The SFA was utilized to measure shear stress induced transitions in PDA films [26]. The experimental design is represented schematically in Figure 4.3a. The PDA film was brought into contact with a thin silicone film and sheared with zero applied load at different shearing rates and displacements. The shearing velocity was targeted to be on of the order of microns per hour, as to approximate the migration of cellular locomotion [20, 30]. Films sheared with rates between 1 Hz and 100 µHz yielded similar friction forces and fluorescent response. To precisely quantify the shear force, the conditions under which shear induced transformation occurred were first mapped out with the fluorescent coupled SFA and then carefully replicated using a standard SFA configuration, which can precisely measure shear force [26, 31]. Combined with the contact area, critical shear stress was calculated. Below this critical shear stress, films can be repeatedly sheared without any measurable increase in fluorescence. An increase in DA monomer alkyl length leads to an increase in the critical shear stress required for a transformation, as indicated in Figure 4.4. The increase in mechanochromism induced by shear stress agrees well with previous observations of the effect of DA alkyl tail length on normal stress transitions, UV dose and thermal transition temperature required to induce the blue to red transition. Van der

Waals interactions and hydrogen bonding between neighboring monomers increase as alkyl tail length increases, hence we hypothesize that this increase in van der Waals attraction and hydrogen bonding increases the stimulus necessary to induce the blue-to-red transition [7, 32–34].

Shear induced mechanochromism is also anisotropic [11, 14]. PDA domains are formed from aligned polymer backbones. PDA backbones that align with the direction of shearing transform at lower shear stresses than those perpendicular or offset from the direction of sliding. The direction of PDA backbones can be observed using polarized light microscopy. Films formed from TCDA (C23) exhibit massive polymer domains, often as large as 0.1mm^2, while films formed from DAs with longer alkyl tails have domains typically between 10 and 100 μm^2 [24]. Figure 4.3b shows a transformed TCDA contact region where the entire area of contact was contained within a single domain, and the shear direction was aligned with the orientation of the domain.

Conversely, in Figure 4.3c, with small PCDA domains, only the domains aligned with the sliding direction transformed. While in Figure 4.3d, most of the very small NCDA domains were off aligned resulting in relatively small fluorescent patches within the contact area. Large domains in conjunction with polarized light microscopy provide additional avenues for improving stress sensing resolution, as the direction and magnitude of applied stresses may be measured. Conversely, using fabrication methods to obtain ultra-small domains homogenizes the sensor, as described next.

Domain size and the shear stress required for the blue-to-red transition can be strongly modified by adding metal cations during film formation, providing an independent means for tuning the characteristics of the PDA film [24, 35–38]. Our previous work characterized the effect of metal cations on UV light induced blue to red transitions [24]. Building upon this work, the mechanochromism of Fe-PCDA and Zn-PCDA were investigated. Modifying films with Fe or Zn decreases the domain size and increases the stimulus (normal stress, shear stress or UV Dose) required to transform the film (Figure 4.4).

Zn modified films exhibit additional novel behavior. Zn-PDA films lack UV photochromism: UV light polymerizes the film to the blue phase, but additional UV light is unable to transform the film to the red phase. Zn-PDA films demonstrate: strong reversible thermochromism at temperatures $< 200°\text{C}$, but the fluorescence is inhibited when thermally transformed [24, 35, 36]. When sheared,

Zn-PCDA films undergo the blue to red transition with fluorescence, Figure 4.5. We hypothesize that shearing disrupts the Zn^{2+} bridging bidentate complexes between neighboring carboxylic acid head groups [24, 35, 38], which enables it to fluorescence similar to a regular film in the absence of Zn^{2+} cations. These strong bridging interactions are responsible for reversible thermochromism and inhibited fluorescence. Hence, Zn cations create a novel sensing modality where shear stress alone can induce fluorescent mechanochromism.

4.4. Slime Mold Locomotion Induced Mechanochromism

Slime molds, particularly *Physarum polycephalum*, have been extensively studied due to their simplicity, the amoeboid-like behavior of the plasmodium, and their puzzle-solving ability [16–19, 21, 39]. Low stress threshold ECDA/C21 films were used to examine the migration and document the area explored by *Physarum* as seen in Figure 4.6a. When a slime mold is placed on a PDA film, migration by the slime mold induces the blue to red transition. Hence, the fluorescent readout indicates every location where the slime mold explored, Figure 4.6a. A complete record of *Physarum's* migration is captured on the film as the fluorescence is permanent. This is useful because slime molds move relatively slow, less than 0.5 $\mathrm{mm\,h^{-1}}$, and avoid light (negative phototaxis) [23, 40–42]. PDA films offer a simple and effective means for passive, non-invasive, long-term surveillance.

PDA films with different stress activation thresholds can distinguish some different potentially shear-applying methods of *Physarum*. Low stress threshold ECDA/C21 (2.1 ± 0.5 $\mathrm{nN\,\mu m^{-2}}$) films display a range of fluorescent intensity after slime mold migration, Figure 4.6a. Shear stresses from the spreading plasmodium and veins were the primary driver of high fluorescence in ECDA/C21 films. Diffuse fluorescence from the spreading plasmodium, bright fluorescent spots and small dark holes of removed film or "puncta" can all be seen. The brighter, more intense fluorescence observed along Figure 4.6a(i) is likely due to higher stresses exerted by the presence of large vein-like structures over a larger and more uniform region by large vein-like structures. Conversely, diffuse fluorescence is due to small local regions of stress application by the spreading plasmodium. On PCDA and NCDA films with a transition shear stress greater than 4 ± 0.2 $\mathrm{nN\,\mu m^{-2}}$, only the localized bright fluorescent spots are present as indicated in Figure 4.6b and c respectively. These

fluorescent spots were potentially from stress fibers and adhesion/anchoring of the organism to the film. Though the slime mold is somewhat autofluorescent, the fluorescence of the PDA film can be observed beneath the organism at the edges (Figure 4.6b).

The stresses measured in these experiments appear significantly larger than previously measured traction forces with a maximum of ∼400Pa as compared to the minimum ∼2000 Pa measured here [20–23]. A significant portion of this discrepancy is due to the scales over which these measurements were taken. TFM studies focused on *Physarum* microplasmodia, where the entire organism was less than ∼500 µm in diameter. These microplasmodia appear tubular and lack larger vein-like structures. Here, larger *Physarum* organisms that possessed vein-like structures were studied (See supplemental section S4 for details on slime mold size measurement). While organisms of roughly the same size as the microplasmodia observed in Rieu et al. were examined here, our samples were extracted from *Physarum* macroplasmodia of much larger size. Stockem and Brix extensively described the morphology and structures of both macro and microplasmodia [39, 43–45]. We speculate that the larger organisms studied here may exhibit higher stresses than those observed by Zhang et al., Rieu et al., and Lewis et al. due to larger, more organized cytoskeletal structures found in macroplasmodia [20, 22, 23, 39]. These larger structures may produce stronger adhesion and migration stresses than those observed in microplasmodia.

Furthermore, measured stresses were observed to scale with the size of the plasmodium. Larger plasmodium sections such as a vein or plasmodium > 100 µm in diameter were observed to induce fluoresce in higher threshold films such as NCDA. In contrast, smaller sections of the plasmodium < 100 µm and the exploring edge of the slime mold could not induce the blue to red transition Figure 4.7. The "size" of the slime mold was defined by the width of the spreading plasmodium through a given area (See supplemental section S4 for details). Normal stress induced transitions were not considered to be significant contributors to the observed fluorescence of the PDA films. PDA films are an order of magnitude more sensitive to shear stress than normal stress (Figures 4.2, 4.4).

In addition to migration induced fluorescence, evidence of slime mold migration stems from the observation of "puncta" or dark holes carved out from the film by the slime mold. As the slime

mold advances into a region, these puncta indicia were present throughout the plasmodium and leading edge of the slime mold. The puncta were highly circular and distinguishable from any cracks or defects in the PDA Films, which typically follow polymer domain boundaries (Figure 4.8). We speculate that this is a potentially unrecognized mechanism by which the slime mold samples or senses the local environment. By using films with a high transformation shear stress, the puncta could be readily identified without the added complications of migration induced fluorescence. This can be seen in Figures 4.6c and 4.7, where inside, and just outside the slime mold, the film is covered in puncta, indicating the plasmodium had migrated over that region. In the higher stress threshold NCDA film, figure 4.6c, the film is littered with puncta, but there is minimal fluorescence from the migrating slime mold. Figure 4.8 shows the difference between cracks in the PDA film and puncta.

Larger slime mold plasmodium with veins and a size greater than 250 µm were observed to produce larger puncta in the film than smaller spreading plasmodium lacking veins, Figure 4.9. Fluorescence around the edges of the puncta indicated the film was ripped and detached by the slime mold, as similar ripping induced fluorescence can be seen during SFA experiments when the two disks are rapidly separated.

Based on these experiments, PDA Langmuir films offer a potential new avenue to non-invasively examine migration and related forces of cells and microorganisms. PDA films could potentially be used with mammalian cells and track the movement of fibroblasts and related epithelial cells during a wound healing assay or other biological processes. The carboxylic DA head group is readily functionalizable and could be modified to enhance cell adhesion, detect the presence of biomolecules on the surface of cells, and offer additional avenues to tailor stress sensitivity.

4.5. Comparison of PDA films to other techniques

TABLE 4.1. Comparison of PDA thin-flims to other well-established techniques for measuring cellular forces. Table adapted from Polacheck and Chen [46].

Technique	Stress range	Number of cells	Spatial resolution[a]	Substrate and stiffness	Special requirements	Strengths	Major limitations	References
Collagen Gel	N/A	1×10^4 to 1×10^6	N/A	Young's modulus: 0.01-0.1 kPa	None	Ease of Implementation	Qualitative, cannot determine stress from single cells	[46, 47]
Traction Force Microscopy	0.05-0.6 kPa	1 to 1000	2 µm	Collagen, PEG, PDMS or PA Young's modulus: 1.2-1000 kPa	Hydrogel, PDMS synthesis & functionalization, particle tracking algorithms	Standard laboratory equipment and fluorescent microscopy	2-D, synthetic substrate	[46, 48–54]
Micro-pillars	0.06-8 kPa	1-10	1 µm	Collagen or PDMS, pillar stiffness 1.9-1556 nN µm^{-1}	microfabrication, PDMS functionalization	Ease of implementation and computation	Fabrication, Forces are independent for posts	[46, 55–59]
Polydiacetylenes (PDA)	∼2-30 kPa	1-1000s[b]	>µm[c]	Glass[d]	PDA films	Inexpensive, passive, precalibratred, permanent fluorescence, binary stress threshold	2-D, binary transition, cytotoxicity not evaluated, others substrates not evaluated	This Work, [1, 10, 12, 14, 60]

[a] The minimum distance between which two point forces can be resolved.

[b,c,d] See text for details.

PDA thin films may potentially act as more general cell migration sensors. Compared to other techniques for measuring cell migration, PDAs offer several potential advantages. Polacheck and Chen extensively reviewed a number of commonly used cell migration techniques, which have been summarized in Table 4.1 [46]. PDA based cell migration sensors potentially can image thousands of cells, as PDA films can be uniformly deposited over 10s of cm^2, with imaging limited only by the

field of view of the microscope (Table 4.1, note b). The stress range and sensitivity of PDAs may be further enhanced by depositing PDAs onto more compliant, elastic materials (Table 4.1, note d).

PDA films may offer high spatial resolution of exerted forces. Carpick et al. and Juhasz et al. examined mechanochromism of PDA Langmuir films at the nanometer scale. They observed that mechanochromism induced by an AFM tip is viewable with wide-field fluorescence microscopy. Hence, forces exerted on the sub-micrometer scale may be readily observed due to the localized fluorescence of the red phase PDA(Table 4.1, note c).

The primary advantages of PDA films lie in that the precursor diacetylenes are inexpensive, and the fluorescence left by mechanical stress is permanent and generally irreversible. Requiring only a standard fluorescent microscope, this permanent, non-photobleaching fluorescence potentially allows for passive monitoring of cell migration without the continuous use of a fluorescent microscope. PDA films are not without challenges. Other more compliant substrates need to be evaluated, the cytotoxicity and compatibility of PDAs with other cells has not been thoroughly examined, and the range of stress sensitivities could be improved and refined through head-group functionalization, and deposition onto more elastic substrates.

4.6. Conclusions

2D mechanical stress sensors with high sensitivity can be easily made from PDA Langmuir films. The binary readout of the films blue-to-red / non-fluorescent to fluorescent transformation provides a simple readout of mechanical stress in real time or to record stress events for later examination. PDA films are sensitive to both normal and lateral stress induced transitions, with significantly higher sensitivity to lateral stress. Importantly the mechanical stress threshold can be readily tuned by modifying film formation parameters. Increasing the monomer alkyl tail length or incorporation of divalent salts into the film can dramatically increase the critical stress required to induce the blue to red transition. Low transition threshold PDA films can be exploited to examine the locomotion and migration of single cells and micro-organisms as demonstrated using the model organism *Physarum polycephalum*, or slime mold. Furthermore, the forces exerted by *Physarum* during locomotion were assessed quantitatively and previously unreported behavior was observed. PDA thin-film sensors

are a straightforward method for examining the stresses involved in cell migration and movement in other systems of interest.

4.7. Acknowledgments

The authors thank Kevin Yates for initial assistance with slime mold cultures, and Zhongrui Liu for assistance with preparing SFA experiments.

This work was partially supported by NIH R01 HL159993-01 and NIH T32 HL086350.

4.8. Supporting Information

Supporting Information is available in the Appendix of this document, or online at https://onlinelibrary.wiley.com/doi/10.1002/admi.202201808

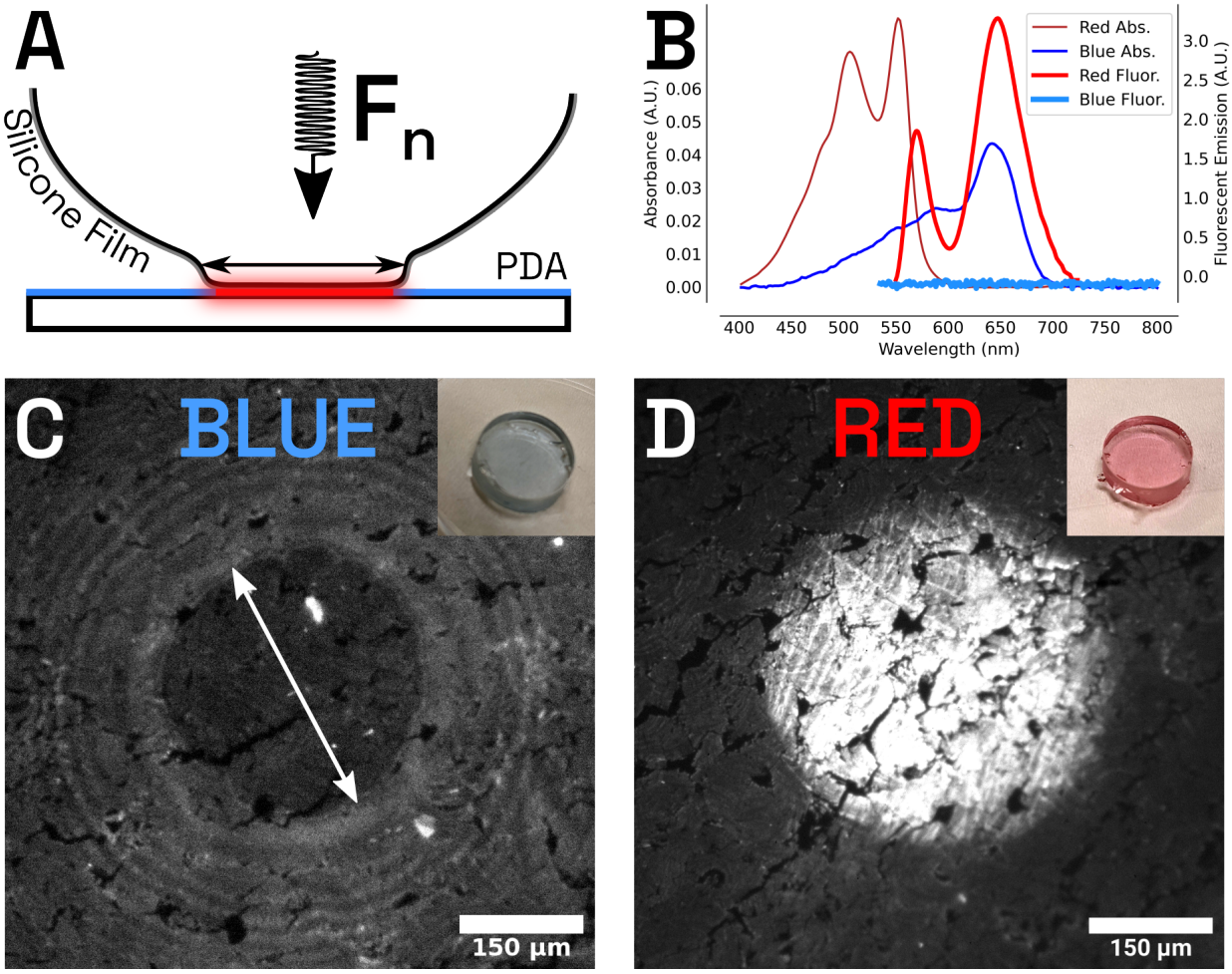

FIGURE 4.1. (A) Schematic of normal stress experiments: films are loaded with well-defined normal forces and the contact area and fluorescent response is measured. The black arrow denotes the contact area diameter. (B) Absorbance and emission spectra of PDA (PCDA) formed on a pure water subphase. (C) Fluorescent micrograph of TCDA (C23) film with edges and pinholes beginning to transform, inset: blue phase of a planar 1 cm SFA disk before loading. The White arrow denotes the contact area diameter. (D) Micrograph of fully transformed TCDA (C23) film from normal stress, inset: red phase of a planar 1 cm SFA disk after macro-scale stress loading.

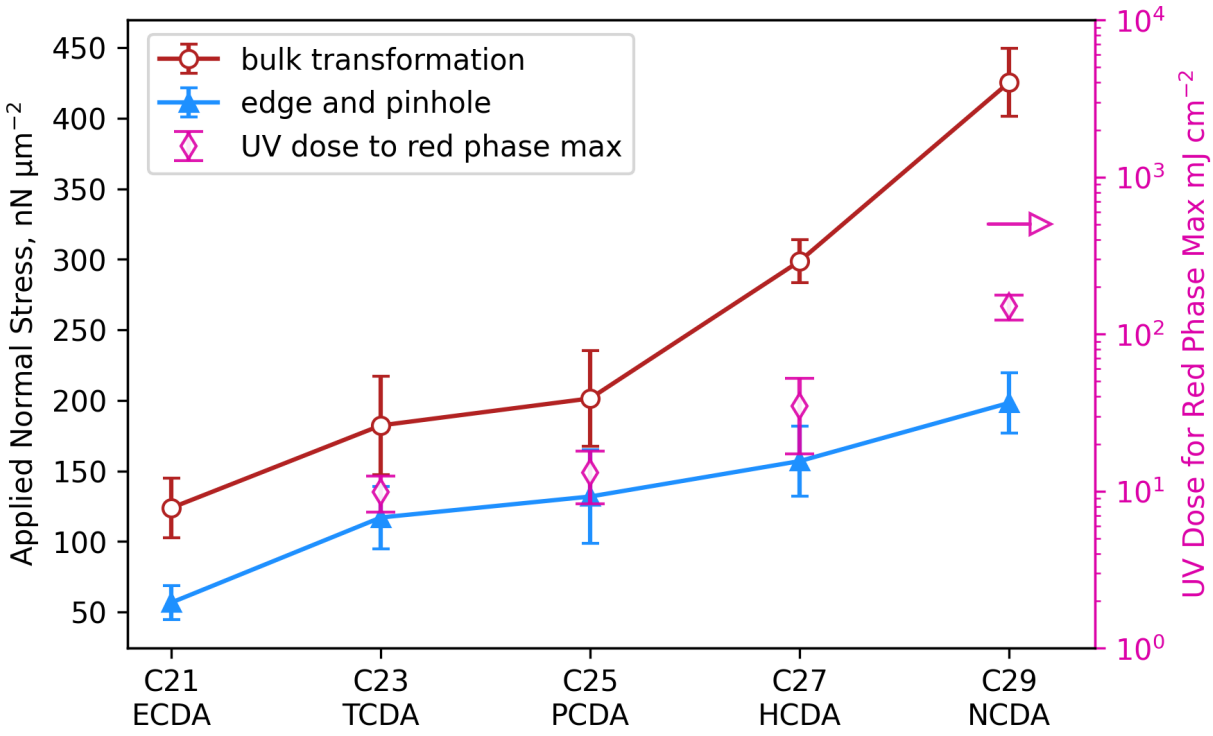

FIGURE 4.2. Critical normal stress required to induce the blue to red transition for PDA films formed from different monomers. UV dose to induce the blue to red transition and produce fully red phase films at the air-water in a Langmuir trough is added for comparison (right axis) [24].

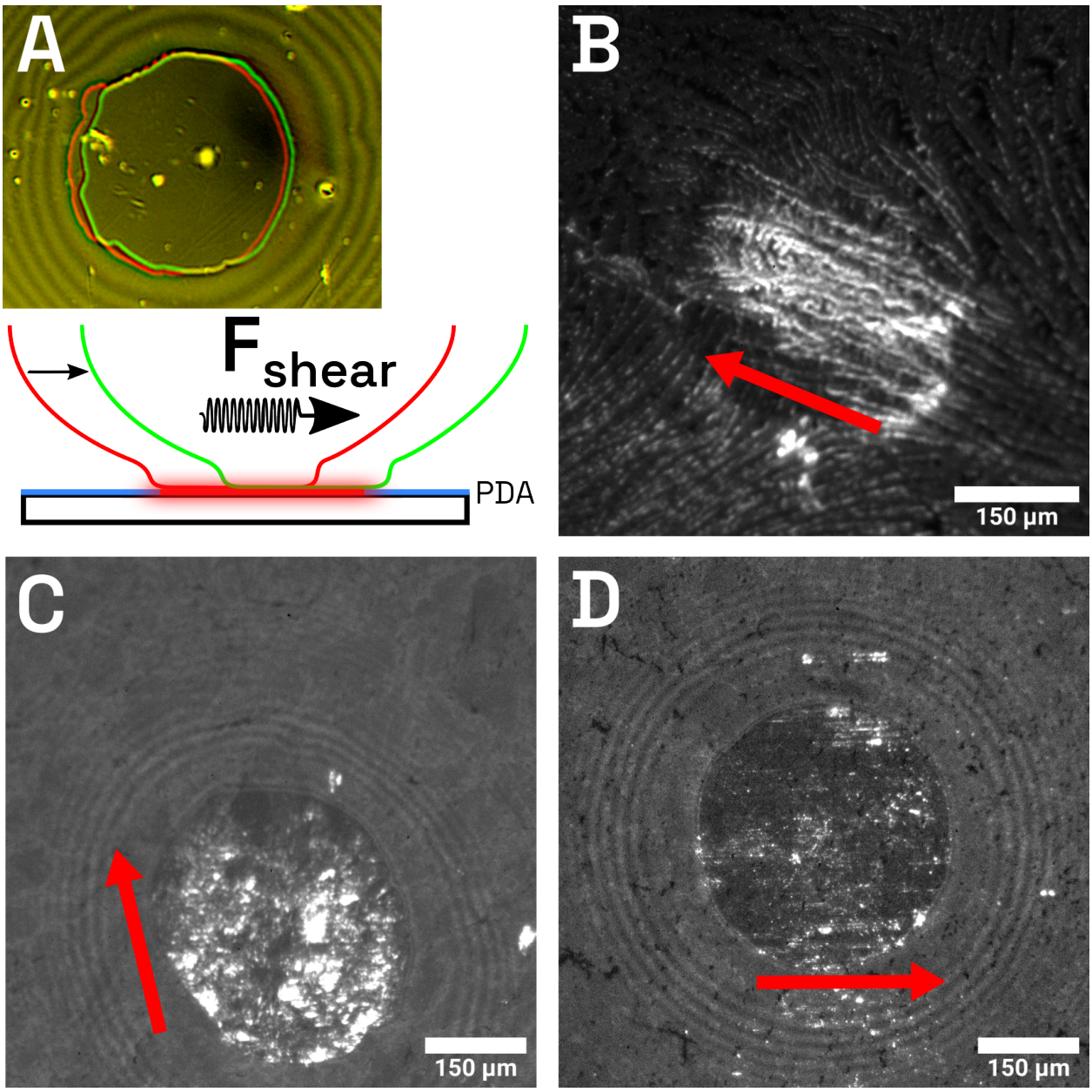

FIGURE 4.3. (A) Schematic of shear stress experiments: a film in contact with a silicone surface is sheared, and the shear force and contact area are measured. Shearing produces a measurable shift in contact area. The red line indicates the initial location of the contact area and the green line indicates the location of the contact area after shearing. Shear induced transitions in films with increasing stress threshold: (B) TCDA/C23, (C) PCDA/C25, (D) NCDA/C29. The red arrow indicates shearing direction.

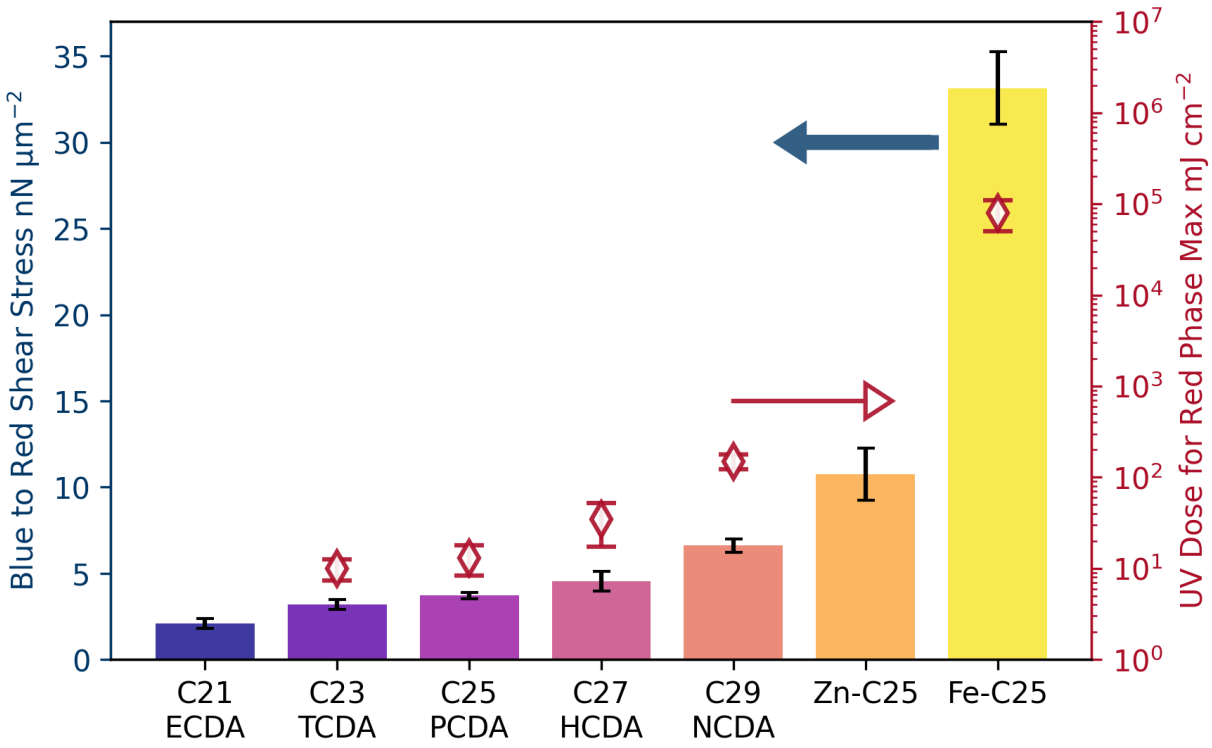

FIGURE 4.4. Critical shear stress required to induce transitions in various PDA films. UV dose to induce the blue to red transition at the air-water interface is added for comparison (right axis), from [24]

.

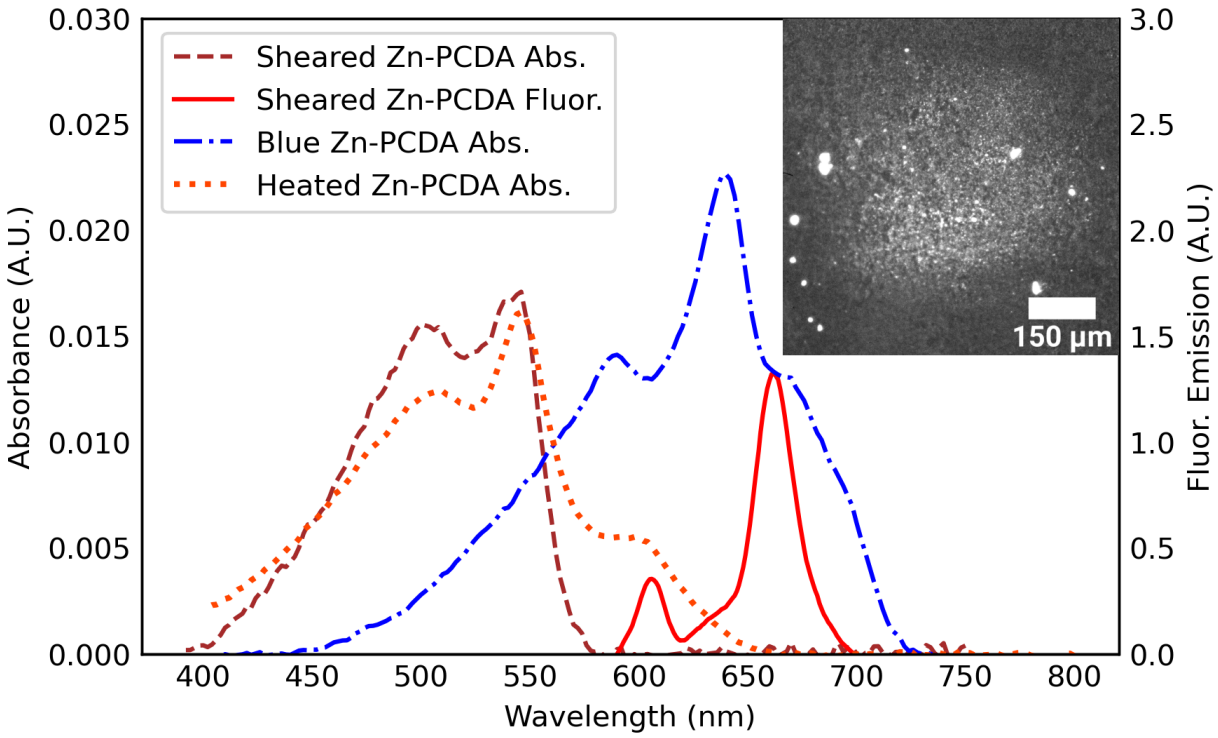

FIGURE 4.5. Absorbance and fluorescent emission spectra of Zn-modified PCDA. Before shearing the film appears visibly blue (Blue Zn-PCDA Abs). Upon heating, the film undergoes appears visibly red, but lacks significant fluorescence (Heated Zn-PCDA Abs). Shearing blue phase Zn-PCDA films induces the blue to red transition and fluorescence (Sheared Zn-PCDA Abs/Fluor). **inset:** Fluorescent micrograph of Zn-PDA film after shearing, scale bar is 150 µm.

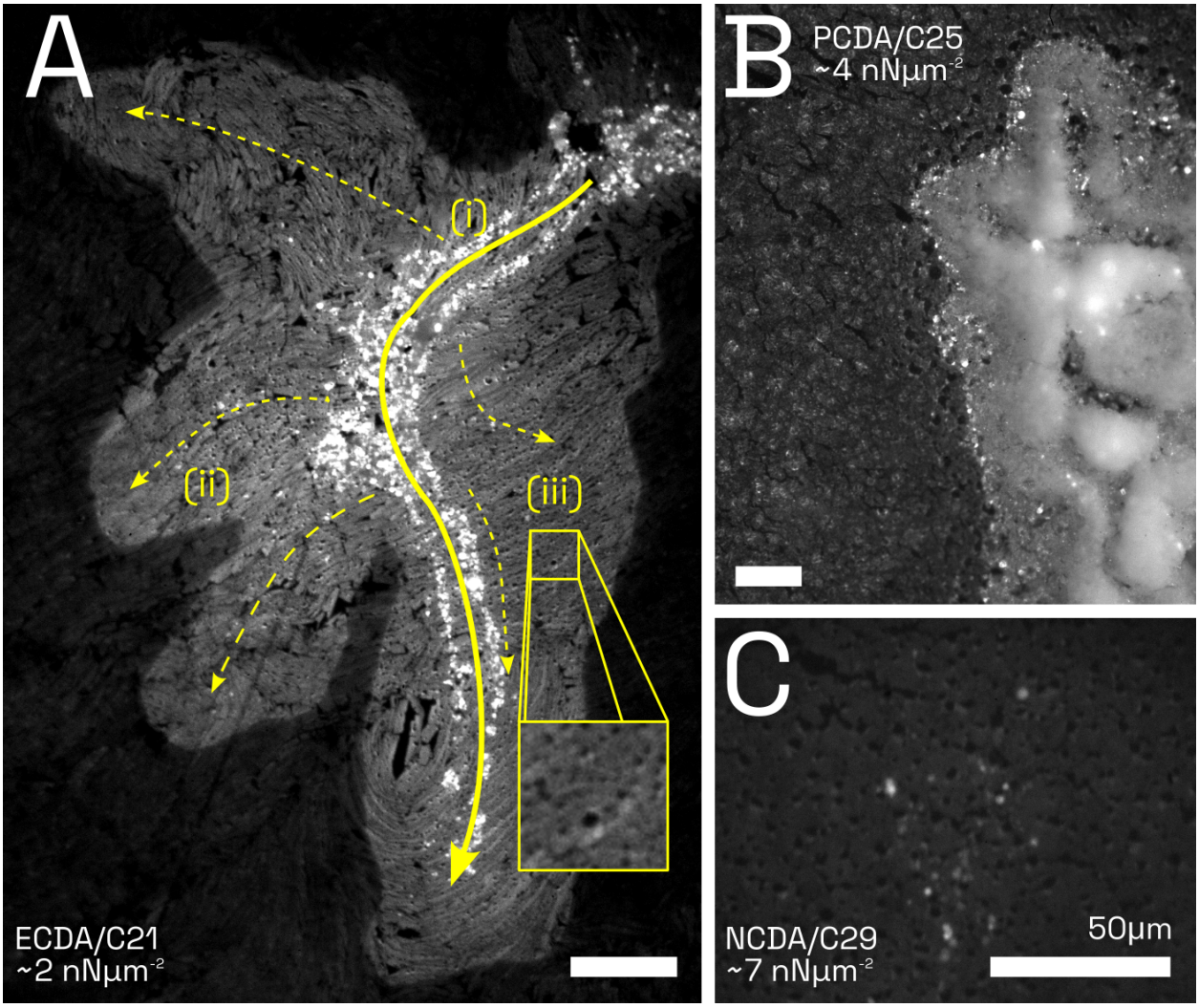

FIGURE 4.6. Fluorescence induced by migration of *Physarum polycephalum* on PDA. Blue to red shear stress (from SFA experiments) is reported for each film system. (A) A variation of fluorescence intensity occurs on a low stress threshold ECDA film. (i) Solid line indicates the primary path of slime mold migration with a high density of fluorescence. (ii) Secondary "exploratory" paths as indicated by more diffuse fluorescence and dashed arrows. (iii) inset highlighting puncta (small dark circular holes) within the slime mold migration region where the PDA film has been removed by the slime mold. (B) Slime mold actively migrating on medium threshold PCDA, puncta and fluorescence can be seen within the slime mold and in the immediate adjacent area. (C) On high threshold NCDA, post migration fluorescence is very low and only localized around puncta and holes. Scale bars are 50μm.

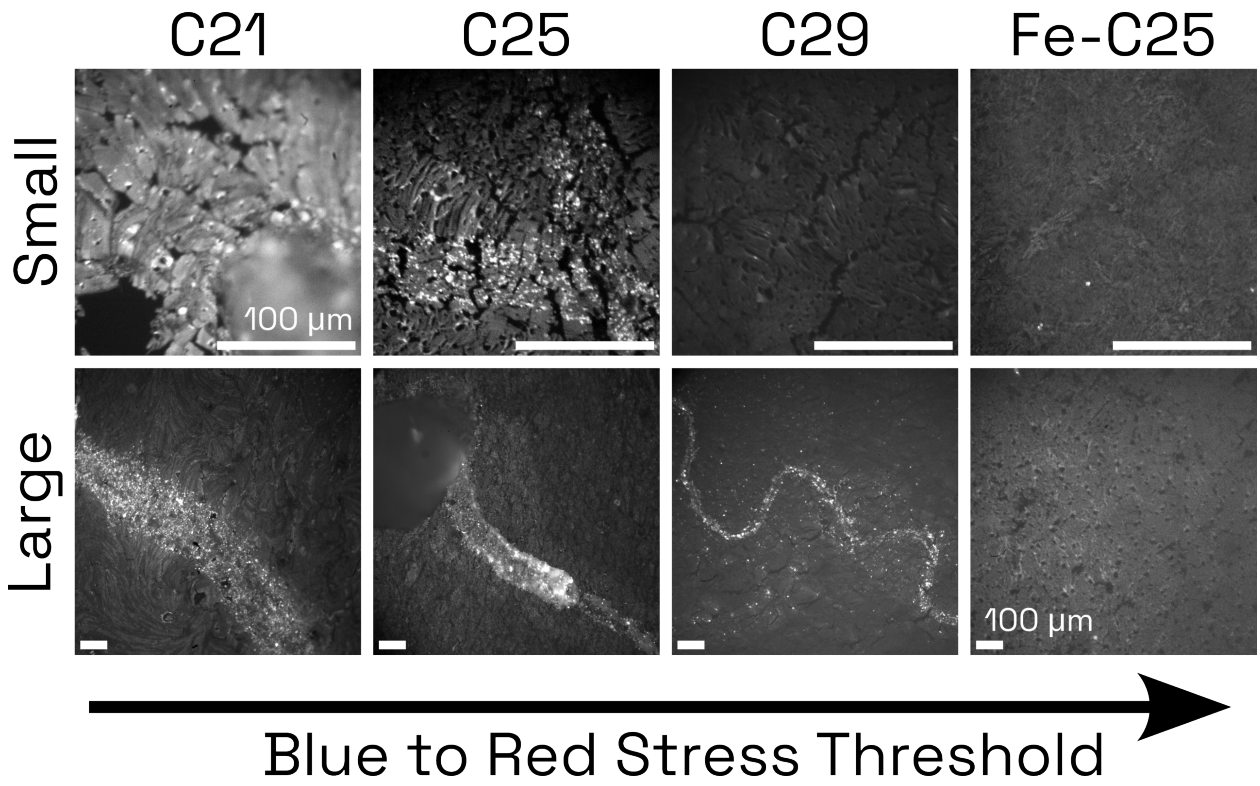

FIGURE 4.7. Relation of slime mold size and film fluorescence on PDA films of increasing blue to red stress threshold. **Top:** Small slime molds ($< 100\mu m$) readily transform C21/ECDA (2.1 ± 0.5 nN µm^{-2}), C25/PCDA (3.7 ± 0.2 nN µm^{-2}), but do not transform C29/NCDA (6.7 ± 0.5 nN µm^{-2}) (bright regions), or Fe-C25 (33 ± 2 nN µm^{-2}). No significant puncta are present on Fe-C25. **Bottom:** Fluorescence from larger slime molds $> 100\mu m$ can be seen in all films except Fe-C25, where only puncta due to removal of the film by the slime mold can be seen.

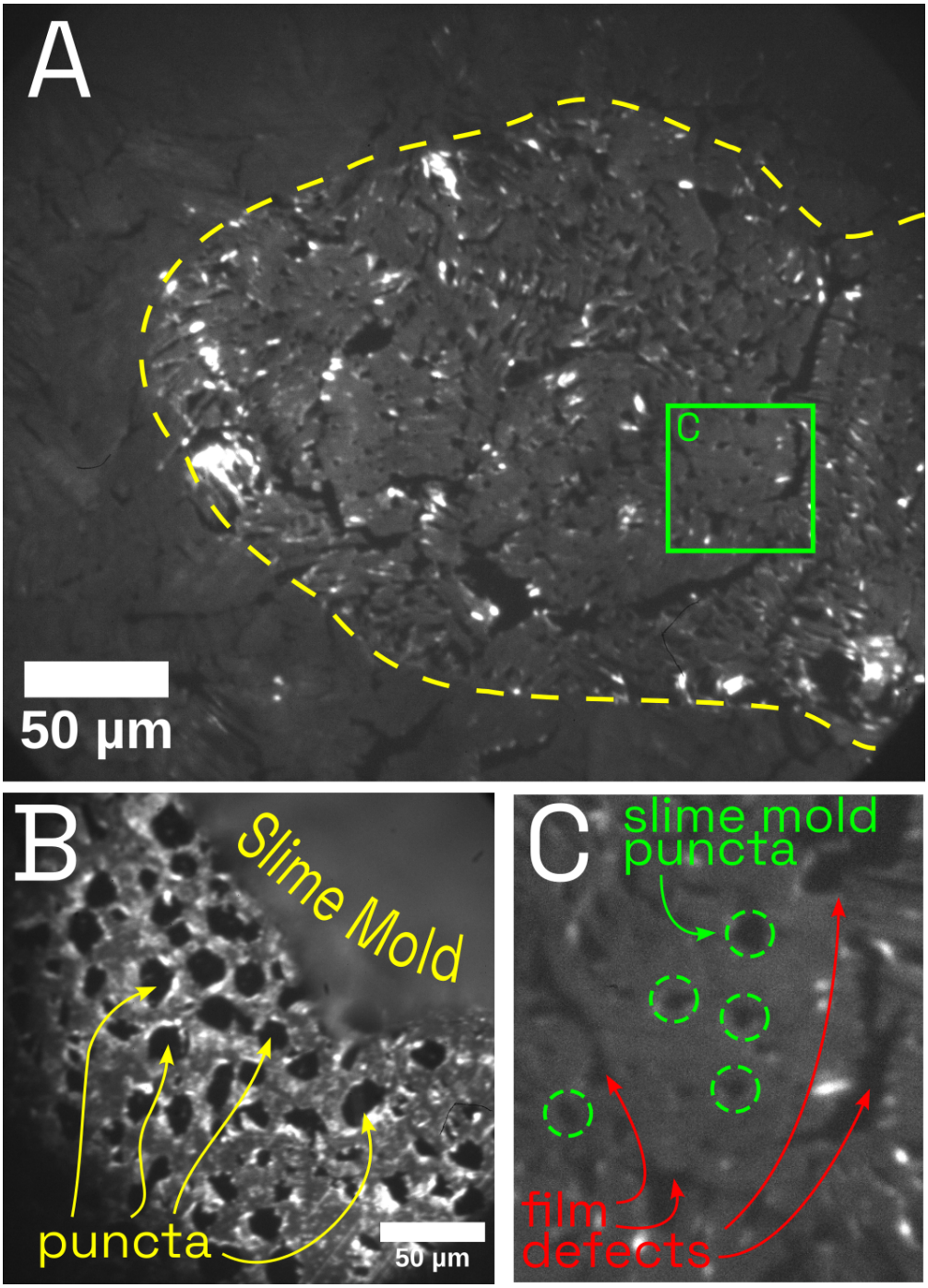

FIGURE 4.8. Comparison of slime mold induced puncta and inherent cracks and defects within a PDA film. (A) PDA film cracks tend to be large and jagged, whereas slime mold puncta are relatively circular, and distributed everywhere within the area that a slime mold migrated. The dashed yellow line shows the extent of slime mold migration. (B) Puncta surrounding a migrating slime mold appear relatively circular, often with a fluorescent halo that we hypothesize was caused by ripping during puncta formation. (C) Zoomed inset comparing select puncta (green circles) to film defects (red arrows).

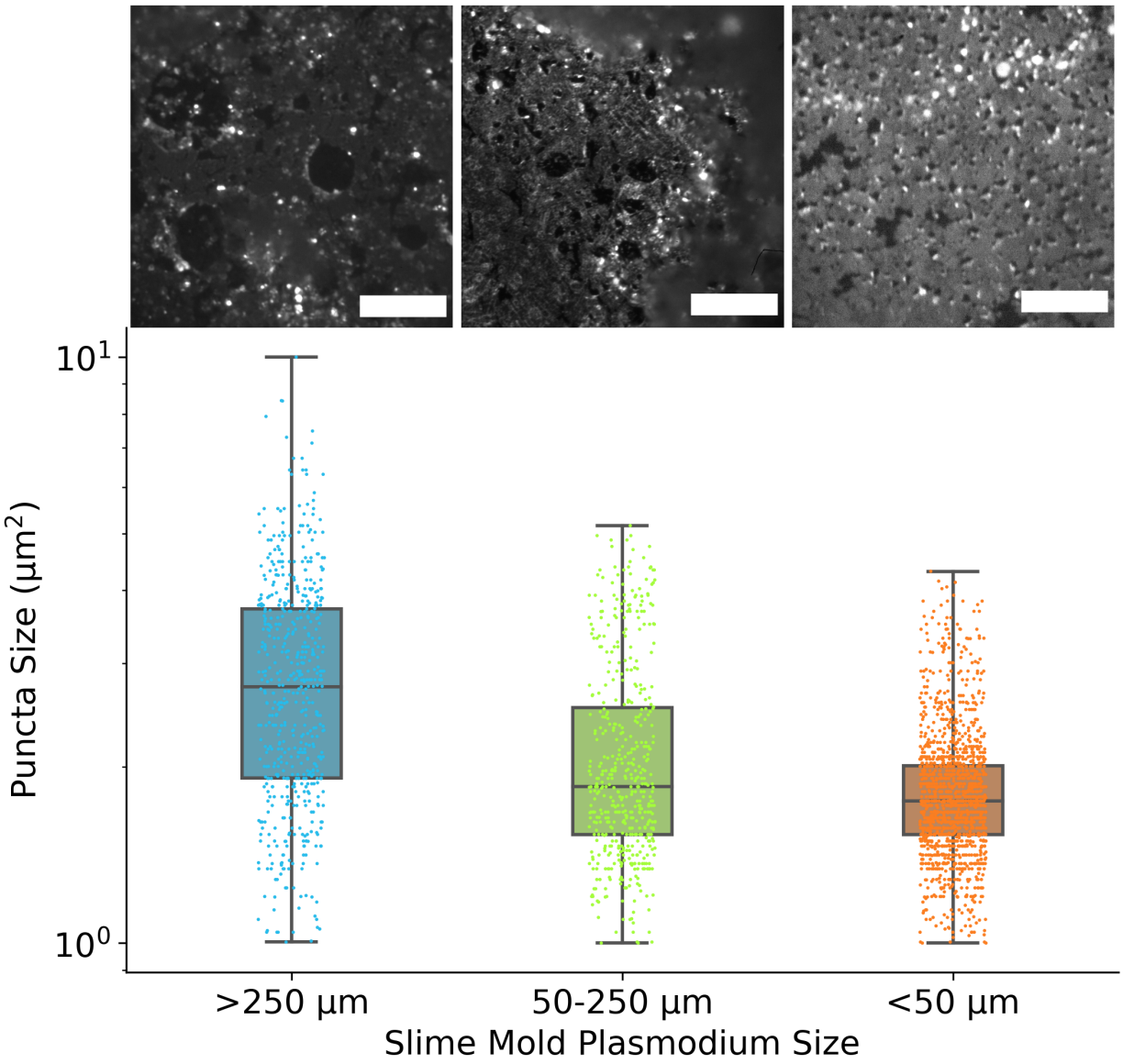

FIGURE 4.9. Relation of slime mold size to measured punctate areas. Above each slime mold size category is an exemplar image of corresponding puncta. Scale bar is 50μm.

References

[1] Bratati Das, Seiko Jo, Jianlu Zheng, Jiali Chen, and Kaori Sugihara. Recent Progress in Polydiacetylene Mechanochromism. *Nanoscale*, 14(5):1670–1678, 2022. doi: 10.1039/D1NR07129G.

[2] Gerhard Wegner. Topochemische Reaktionen von Monomeren mit konjugierten Dreifachbindungen / Tochemical Reactions of Monomers with conjugated triple Bonds. *Zeitschrift für Naturforschung B*, 24(7):824–832, 2014. ISSN 1865-7117. doi: 10.1515/znb-1969-0708.

[3] T. Barisien, L. Legrand, G. Weiser, J. Deschamps, M. Balog, B. Boury, S. G. Dutremez, and M. Schott. Exciton spectroscopy of red polydiacetylene chains in single crystals. *Chemical Physics Letters*, 444(4):309–313, August 2007. ISSN 0009-2614. doi: 10.1016/j.cplett.2007.07.031.

[4] Michel Schott. The Colors of Polydiacetylenes: A Commentary. *The Journal of Physical Chemistry B*, 110(32):15864–15868, August 2006. ISSN 1520-6106. doi: 10.1021/jp0638437.

[5] Yevgeniy Lifshitz, Yuval Golan, Oleg Konovalov, and Amir Berman. Structural Transitions in Polydiacetylene Langmuir Films. *Langmuir*, 25(8):4469–4477, April 2009. ISSN 0743-7463. doi: 10.1021/la8029038.

[6] Qing Li, Yi-Xuan Wang, and Yulan Chen. Unraveling Ultrasonic Stress Response of Nanovesicles by the Mechanochromism of Self-Assembled Polydiacetylene. *ACS Macro Lett.*, 11(1):103–109, January 2022. doi: 10.1021/acsmacrolett.1c00715.

[7] Chanita Khanantong, Nipaphat Charoenthai, Tinnakorn Phuangkaew, Filip Kielar, Nisanart Traiphol, and Rakchart Traiphol. Phase transition, structure and color-transition behaviors of monocarboxylic diacetylene and polydiacetylene assemblies: The opposite effects of alkyl chain length. *Colloids and Surfaces A: Physicochemical and Engineering Aspects*, 553:337–348, September 2018. ISSN 0927-7757. doi: 10.1016/j.colsurfa.2018.05.081.

[8] Yeol Kyo Choi, Sang Yup Lee, and Dong June Ahn. Hyperconjugation-induced chromism in linear responsive polymers. *Journal of Materials Chemistry C*, 7(42):13130–13138, October 2019. ISSN 2050-7534. doi: 10.1039/C9TC03204E.

[9] Roberto Diego Ortuso. *Characterisation of Polydiacetylene for the Detection of Forces in Membranes*. PhD thesis, University of Geneva, 2019.

[10] R. W. Carpick, D. Y. Sasaki, and A. R. Burns. First Observation of Mechanochromism at the Nanometer Scale. *Langmuir*, 16(3):1270–1278, February 2000. ISSN 0743-7463. doi: 10.1021/la990706a.

[11] R.W. Carpick, D.Y. Sasaki, and A.R. Burns. Large friction anisotropy of a polydiacetylene monolayer. *Tribology Letters*, 7(2):79–85, September 1999. ISSN 1573-2711. doi: 10.1023/A:1019113218650.

[12] Robert W. Carpick, Darryl Y. Sasaki, Matthew S. Marcus, M. A. Eriksson, and Alan R. Burns. Polydiacetylene films: A review of recent investigations into chromogenic transitions and nanomechanical properties. *Journal of Physics: Condensed Matter*, 16(23):R679–R697, May 2004. ISSN 0953-8984. doi: 10.1088/0953-8984/16/23/R01.

[13] S. R. Sheth and D. E. Leckband. Direct Force Measurements of Polymerization-Dependent Changes in the Properties of Diacetylene Films. *Langmuir*, 13(21):5652–5662, October 1997. ISSN 0743-7463. doi: 10.1021/la962107z.

[14] Levente Juhasz, Roberto D. Ortuso, and Kaori Sugihara. Quantitative and Anisotropic Mechanochromism of Polydiacetylene at Nanoscale. *Nano Lett.*, 21(1):543–549, January 2021. ISSN 1530-6984. doi: 10.1021/acs.nanolett.0c04027.

[15] Huw Colin-York and Marco Fritzsche. The future of traction force microscopy. *Current Opinion in Biomedical Engineering*, 5:1–5, March 2018. ISSN 24684511. doi: 10.1016/j.cobme.2017.10.002.

[16] Toshiyuki Nakagaki, Hiroyasu Yamada, and Ágota Tóth. Maze-solving by an amoeboid organism. *Nature*, 407(6803):470–470, September 2000. ISSN 1476-4687. doi: 10.1038/35035159.

[17] Christina Oettmeier, Klaudia Brix, and Hans-Günther Döbereiner. Physarum polycephalum—a new take on a classic model system. *Journal of Physics D: Applied Physics*, 50(41):413001, September 2017. ISSN 0022-3727. doi: 10.1088/1361-6463/aa8699.

[18] Christina Oettmeier and Hans-Günther Döbereiner. A lumped parameter model of endoplasm flow in Physarum polycephalum explains migration and polarization-induced asymmetry during the onset of locomotion. *PLOS ONE*, 14(4):e0215622, April 2019. ISSN 1932-6203. doi: 10.1371/journal.pone.0215622.

[19] Christina Oettmeier, Toshiyuki Nakagaki, and Hans-Günther Döbereiner. Slime mold on the rise: The physics of Physarum polycephalum. *Journal of Physics D: Applied Physics*, 53(31):310201, May 2020. ISSN 0022-3727. doi: 10.1088/1361-6463/ab866c.

[20] Shun Zhang, Robert D. Guy, Juan C. Lasheras, and Juan C. del Álamo. Self-organized mechano-chemical dynamics in amoeboid locomotion ofPhysarumfragments. *Journal of Physics D: Applied Physics*, 50(20):204004, April 2017. ISSN 0022-3727. doi: 10.1088/1361-6463/aa68be.

[21] Shun Zhang, Juan C. Lasheras, and Juan C. del Álamo. Symmetry breaking transition towards directional locomotion inPhysarummicroplasmodia. *Journal of Physics D: Applied Physics*, 52 (49):494004, September 2019. ISSN 0022-3727. doi: 10.1088/1361-6463/ab3ec8.

[22] Jean-Paul Rieu, Hélène Delanoë-Ayari, Seiji Takagi, Yoshimi Tanaka, and Toshiyuki Nakagaki. Periodic traction in migrating large amoeba of Physarum polycephalum. 12(106):20150099. doi: 10.1098/rsif.2015.0099. URL https://royalsocietypublishing.org/doi/full/10.1098/rsif.2015.0099.

[23] Owen L. Lewis, Shun Zhang, Robert D. Guy, and Juan C. del Álamo. Coordination of contractility, adhesion and flow in migrating Physarum amoebae. *Journal of The Royal Society Interface*, 12(106):20141359, May 2015. doi: 10.1098/rsif.2014.1359.

[24] Tanner J Finney, Sanjai J Parikh, Amir Berman, Darryl Y Sasaki, and Tonya L Kuhl. Characterizing and Tuning the Properties of Polydiacetylene Films for Sensing Applications. *Langmuir*, page 12, November 2021. doi: 10.1021/acs.langmuir.1c02004.

[25] S. N. Staritsyn, V. V. Mamashin, V. V. Zakharychev, I. V. Yaminsky, E. V. Dubrovin, A. M. Lomonosov, V. A. Tverdislov, and S. A. Yakovenko. Mixed monolayers of amphiphile-modified nucleic bases and diynoic acids. I. Phase states at air-water interface and in Langmuir-Blodgett films. *Biophysics*, 49(4):635–645, 2004.

[26] J. Israelachvili, Y. Min, M. Akbulut, A. Alig, G. Carver, W. Greene, K. Kristiansen, E. Meyer, N. Pesika, K. Rosenberg, and H. Zeng. Recent advances in the surface forces apparatus (SFA) technique. *Reports on Progress in Physics*, 73(3):036601, January 2010. ISSN 0034-4885. doi: 10.1088/0034-4885/73/3/036601.

[27] Henry Pinkard, Nico Stuurman, Ivan E. Ivanov, Nicholas M. Anthony, Wei Ouyang, Bin Li, Bin Yang, Mark A. Tsuchida, Bryant Chhun, Grace Zhang, Ryan Mei, Michael Anderson, Douglas P. Shepherd, Ian Hunt-Isaak, Raymond L. Dunn, Wiebke Jahr, Saul Kato, Loïc A. Royer, Jay R. Thiagarajah, Kevin W. Eliceiri, Emma Lundberg, Shalin B. Mehta, and Laura Waller. Pycro-Manager: Open-source software for customized and reproducible microscope control. *Nature*

Methods, 18(3):226–228, March 2021. ISSN 1548-7105. doi: 10.1038/s41592-021-01087-6.

[28] Arthur D. Edelstein, Mark A. Tsuchida, Nenad Amodaj, Henry Pinkard, Ronald D. Vale, and Nico Stuurman. Advanced methods of microscope control using μManager software. *Journal of Biological Methods*, 1(2):e10, November 2014. ISSN 2326-9901. doi: 10.14440/jbm.2014.36.

[29] Johannes Schindelin, Ignacio Arganda-Carreras, Erwin Frise, Verena Kaynig, Mark Longair, Tobias Pietzsch, Stephan Preibisch, Curtis Rueden, Stephan Saalfeld, Benjamin Schmid, Jean-Yves Tinevez, Daniel James White, Volker Hartenstein, Kevin Eliceiri, Pavel Tomancak, and Albert Cardona. Fiji: An open-source platform for biological-image analysis. *Nature Methods*, 9(7):676–682, July 2012. ISSN 1548-7105. doi: 10.1038/nmeth.2019.

[30] Revathi Ananthakrishnan and Allen Ehrlicher. The Forces Behind Cell Movement. *International Journal of Biological Sciences*, 3(5):303–317, June 2007. ISSN 1449-2288.

[31] Gustavo Luengo, Franz-Josef Schmitt, Robert Hill, and Jacob Israelachvili. Thin Film Rheology and Tribology of Confined Polymer Melts: Contrasts with Bulk Properties. *Macromolecules*, 30(8):2482–2494, April 1997. ISSN 0024-9297. doi: 10.1021/ma9519122.

[32] C. Gourier, M. Alba, A. Braslau, J. Daillant, M. Goldmann, C. M. Knobler, F. Rieutord, and G. Zalczer. Structure and Elastic Properties of 10-12 Pentacosadiyonic Acid Langmuir Films. *Langmuir*, 17(21):6496–6505, October 2001. ISSN 0743-7463. doi: 10.1021/la001799v.

[33] Lionel Salem. Attractive Forces between Long Saturated Chains at Short Distances. *The Journal of Chemical Physics*, 37(9):2100–2113, November 1962. ISSN 0021-9606. doi: 10.1063/1.1733431.

[34] José A. Martins. Toward a Physical Definition of Entanglements. *Journal of Macromolecular Science, Part B*, 50(4):769–794, February 2011. ISSN 0022-2348. doi: 10.1080/00222341003785151.

[35] Xin Huang, Siguang Jiang, and Minghua Liu. Metal Ion Modulated Organization and Function of the Langmuir-Blodgett Films of Amphiphilic Diacetylene: Photopolymerization, Thermochromism, and Supramolecular Chirality. *The Journal of Physical Chemistry B*, 109(1): 114–119, January 2005. ISSN 1520-6106. doi: 10.1021/jp046500m.

[36] Yevgeniy Lifshitz, Alexander Upcher, Anatoly Kovalev, Dmitry Wainstein, Alexander Rashkovsky, Leila Zeiri, Yuval Golan, and Amir Berman. Zinc modified polydiacetylene Langmuir films. *Soft Matter*, 7(19):9069–9077, September 2011. ISSN 1744-6848. doi: 10.1039/C1SM05904A.

[37] Alexander Upcher, Yevgeniy Lifshitz, Leila Zeiri, Yuval Golan, and Amir Berman. Effect of metal cations on polydiacetylene Langmuir films. *Langmuir: the ACS journal of surfaces and colloids*, 28(9):4248–4258, March 2012. ISSN 1520-5827. doi: 10.1021/la204735t.

[38] Si Wu, Libin Pan, Youju Huang, Ni Yang, and Qijin Zhang. Co-assemblies of polydiacetylenes and metal ions for solvent sensing. *Soft Matter*, 14(33):6929–6937, 2018. doi: 10.1039/C8SM01282B.

[39] Wilhelm Stockem and Klaudia Brix. Analysis of Microfilament Organization and Contractile Activities in Physarum. In Kwang W. Jeon and Jonathan Jarvik, editors, *International Review of Cytology*, volume 149, pages 145–215. Academic Press, January 1994. doi: 10.1016/S0074-7696(08)62088-4.

[40] Toshiyuki Nakagaki, Shoji Umemura, Yasutaka Kakiuchi, and Tetsuo Ueda. Action Spectrum for Sporulation and Photoavoidance in the Plasmodium of Physarum polycephalum, as Modified Differentially by Temperature and Starvation. *Photochemistry and Photobiology*, 64(5):859–862, 1996. ISSN 1751-1097. doi: 10.1111/j.1751-1097.1996.tb01847.x.

[41] Masakatsu Hato, Tetsuo Ueda, Kenzo Kurihara, and Yonosuke Kobatake. Phototaxis in True Slime Mold Physarum polycephalum. *Cell Structure and Function*, 1(3):269–278, 1976. doi: 10.1247/csf.1.269.

[42] Fernando Patino-Ramirez, Chloé Arson, and Audrey Dussutour. Substrate and cell fusion influence on slime mold network dynamics. *Scientific Reports*, 11(1):1498, January 2021. ISSN 2045-2322. doi: 10.1038/s41598-020-80320-2.

[43] Klaudia Brix and Wilhelm Stockem. Functional analysis of actin fibrils in Physarum polycephalum. *Cell and Tissue Research*, 257(1):115–122, July 1989. ISSN 1432-0878. doi: 10.1007/BF00221640.

[44] Klaudia Brix, J. Kukulies, and W. Stockem. Studies on microplasmodia ofPhysarum polycephalum. *Protoplasma*, 137(2):156–167, June 1987. ISSN 1615-6102. doi: 10.1007/BF01281151.

[45] Christiane Ohl, Klaudia Brix, and Wilhelm Stockem. Studies on microplasmodia of Physarum polycephalum. *Cell and Tissue Research*, 264(2):283–291, May 1991. ISSN 1432-0878. doi: 10.1007/BF00313965.

[46] William J. Polacheck and Christopher S. Chen. Measuring cell-generated forces: A guide to the available tools. *Nature Methods*, 13(5):415–423, May 2016. ISSN 1548-7105. doi: 10.1038/nmeth.3834.

[47] E Bell, B Ivarsson, and C Merrill. Production of a tissue-like structure by contraction of collagen lattices by human fibroblasts of different proliferative potential in vitro. *Proceedings of the National Academy of Sciences*, 76(3):1274–1278, March 1979. doi: 10.1073/pnas.76.3.1274.

[48] J Lee, M Leonard, T Oliver, A Ishihara, and K Jacobson. Traction forces generated by locomoting keratocytes. *Journal of Cell Biology*, 127(6):1957–1964, December 1994. ISSN 0021-9525. doi: 10.1083/jcb.127.6.1957.

[49] Stacey A. Maskarinec, Christian Franck, David A. Tirrell, and Guruswami Ravichandran. Quantifying cellular traction forces in three dimensions. *Proceedings of the National Academy of Sciences*, 106(52):22108–22113, December 2009. doi: 10.1073/pnas.0904565106.

[50] Nathalie Q. Balaban, Ulrich S. Schwarz, Daniel Riveline, Polina Goichberg, Gila Tzur, Ilana Sabanay, Diana Mahalu, Sam Safran, Alexander Bershadsky, Lia Addadi, and Benjamin Geiger. Force and focal adhesion assembly: A close relationship studied using elastic micropatterned substrates. *Nature Cell Biology*, 3(5):466–472, May 2001. ISSN 1476-4679. doi: 10.1038/35074532.

[51] Christian Franck, Stacey A. Maskarinec, David A. Tirrell, and Guruswami Ravichandran. Three-Dimensional Traction Force Microscopy: A New Tool for Quantifying Cell-Matrix Interactions. *PLOS ONE*, 6(3):e17833, March 2011. ISSN 1932-6203. doi: 10.1371/journal.pone.0017833.

[52] James P. Butler, Iva Marija Tolić-Nørrelykke, Ben Fabry, and Jeffrey J. Fredberg. Traction fields, moments, and strain energy that cells exert on their surroundings. *American Journal of Physiology-Cell Physiology*, 282(3):C595–C605, March 2002. ISSN 0363-6143. doi: 10.1152/ajpcell.00270.2001.

[53] Ning Wang, Iva Marija Tolić-Nørrelykke, Jianxin Chen, Srboljub M. Mijailovich, James P. Butler, Jeffrey J. Fredberg, and Dimitrije Stamenović. Cell prestress. I. Stiffness and prestress are closely associated in adherent contractile cells. *American Journal of Physiology-Cell Physiology*, 282(3):C606–C616, March 2002. ISSN 0363-6143. doi: 10.1152/ajpcell.00269.2001.

[54] Robert J. Pelham and Yu-li Wang. Cell locomotion and focal adhesions are regulated by substrate flexibility. *Proceedings of the National Academy of Sciences*, 94(25):13661–13665, December 1997. doi: 10.1073/pnas.94.25.13661.

[55] John L. Tan, Joe Tien, Dana M. Pirone, Darren S. Gray, Kiran Bhadriraju, and Christopher S. Chen. Cells lying on a bed of microneedles: An approach to isolate mechanical force. *Proceedings of the National Academy of Sciences*, 100(4):1484–1489, February 2003. doi: 10.1073/pnas.0235407100.

[56] Jianping Fu, Yang-Kao Wang, Michael T. Yang, Ravi A. Desai, Xiang Yu, Zhijun Liu, and Christopher S. Chen. Mechanical regulation of cell function with geometrically modulated elastomeric substrates. *Nature Methods*, 7(9):733–736, September 2010. ISSN 1548-7105. doi: 10.1038/nmeth.1487.

[57] Léa Trichet, Jimmy Le Digabel, Rhoda J. Hawkins, Sri Ram Krishna Vedula, Mukund Gupta, Claire Ribrault, Pascal Hersen, Raphaël Voituriez, and Benoît Ladoux. Evidence of a large-scale mechanosensing mechanism for cellular adaptation to substrate stiffness. *Proceedings of the National Academy of Sciences*, 109(18):6933–6938, May 2012. doi: 10.1073/pnas.1117810109.

[58] Olivia du Roure, Alexandre Saez, Axel Buguin, Robert H. Austin, Philippe Chavrier, Pascal Siberzan, and Benoit Ladoux. Force mapping in epithelial cell migration. *Proceedings of the National Academy of Sciences*, 102(7):2390–2395, February 2005. doi: 10.1073/pnas.0408482102.

[59] Saba Ghassemi, Giovanni Meacci, Shuaimin Liu, Alexander A. Gondarenko, Anurag Mathur, Pere Roca-Cusachs, Michael P. Sheetz, and James Hone. Cells test substrate rigidity by local contractions on submicrometer pillars. *Proceedings of the National Academy of Sciences*, 109 (14):5328–5333, April 2012. doi: 10.1073/pnas.1119886109.

[60] Darryl Y. Sasaki, Robert W. Carpick, and Alan R. Burns. High Molecular Orientation in Mono- and Trilayer Polydiacetylene Films Imaged by Atomic Force Microscopy. *Journal of Colloid and Interface Science*, 229(2):490–496, September 2000. ISSN 0021-9797. doi: 10.1006/jcis.2000.7043.

CHAPTER 5

Structure of Blue and Red Phase Polydiacetylene Langmuir Films

Purpose, Scope and Future Directions

A version of this chapter will be submitted for publication, very likely some differences will exist between the current state and the published version.

This chapter details our work in building structural models of the blue and red phase using grazing incidence x-ray diffraction, atomic force microscopy and x-ray reflectivity. Developing new structural models is essential to the further development of PDAs as sensors. Highly effective PDA sensors require a strong understanding of the structural underpinnings of the blue to red transition. As certain aspects of the transition remain elusive, we embarked upon a molecular scale study of these polymers to develop new models of their behavior. These models were then evaluated using density functional theory to demonstrate their feasibility. We observed that the blue phase is very likely planar with the side chains aligned along a single direction. The red phase is non-planar, and in either a twisted or kinked geometry. Boronic acid functionalized PDAs (BA-PCDA) were also studied. BA-PCDA was exhibited highly reversible blue to red transitions and exhibiting remarkable similarity to the monomer structure with a much wider spacing between adjacent monomers in the polymer. This description of the blue and red phase structures will aid in the design of new PDA sensors (through functionalization or tuning the alkyl chain length), as DAs that promote "twisting" of the backbone will likely make it easier to undergo the blue to red transition. Whereas those that have a wide molecular spacing potentially favor the blue phase more strongly and could be developed as more general reversible PDA sensors.

There are several improvements that could be made through future GIXD measurements. First, the trilayer structure significantly complicates analysis of the GIXD and XRR results. A uniform monolayer would provide the best information. Ethanolamine functionalized PCDA (Et-PDA)

was synthesized, but it was not ready in appreciable quantities or quality prior to our allocated beamtime. Ethanolamine functionalized PCDA is known to form uniform, stable polymerizable monolayers. BA-PCDA (a boronic acid functionalized diacetylene) was also synthesized for related, ongoing, yet-to-be-published work. It was suspected that BA-PCDA might form a monolayer based on previous literature and its pressure-area isotherm. However, the study here found that the film's morphology is much more varied than a uniform monolayer. Rather the film is structurally heterogeneous, and decorated with an extensive network of multilayer buildup.

Yamada et al. developed a modified Langmuir trough to fabricate giant single domain monolayers from PCDA. This, combined with diacetylenes such as Et-PCDA that naturally form a stable monolayer may enable the development of large, extremely uniform, single-domain films. It is unclear if PDAs domains are entirely in crystalline registry as the Scherrer lengths observed here are much smaller than the domain size. Hence, even a single domain monolayer spanning the entire Langmuir trough may lack positional registry beyond a few nanometers. However, a single domain polymer monolayer would enable unambiguous determination of the polymer structure using GIXD, (or Grazing Incidence Wide Angle X-ray Scattering (GIWAXS)), and X-ray Reflectivity (XRR).

Abstract

Polydiacetylenes (PDAs) have attracted significant interest due to their chromatic transitions and potential use as stimuli responsive sensors. Key to developing them as sensors, is to understand the changes in the structure responsible for the chromatic transitions. Here, synchrotron grazing incidence X-ray diffraction (GIXD), X-ray Reflectivity (XRR), Atomic Force Microscopy (AFM) and DFT calculations were used to develop structural models of the blue and red phases of PDA Langmuir films. Monomer films were found to have significant multilayer registry, which is subsequently lost after polymerization. The blue phase polymer was found structurally similar to the monomer: uniformly tilted as a consequence of topochemical polymerization. The red phase was found to be significantly less tilted, with a non-planar conformation of the polymer backbone. Modeling of the red phase GIXD patterns suggest two potential conformations, a kinked geometry and a twisted geometry. AFM and XRR measures reveal that the PDA Langmuir films are highly heterogeneous, with many regions of extensively multilayer buildup.

5.1. Introduction

The remarkable chromatic transitions of polydiacetylenes (PDAs) have been extensively studied. Despite decades of interest and widespread investigations into their use as sensors, the underlying mechanism of the blue to red transition remains elusive. In particular the structures of the blue and red phase remain under-explored. The first PDAs synthesized were symmetric molecules with tosyl side chains [1–3]. Tieke et al. first synthesized PDAs derived from diacetylene fatty acids, which are amenable to the production of Langmuir films [4–7]. Colorless as monomers, exposure to UV light induces polymerization and produces blue phase PDA which is non-fluorescent, Figure 5.1. This process, coined topochemical polymerization by Wegner, has strict geometrical and packing requirements for the polymerization to occur [8]. Application of external stimuli, whether in the form of light [9], heat [10], specific molecules [11, 12] or mechanical stress [13, 14] induces a colorimetric transition from the non-fluorescent blue phase to the fluorescent red phase.

Initial investigation suggested that the blue to red transition may arise from isomerization, that is, a change from an alternating double, triple bond structure to a repeating double bond structure. However, crystallographic [15], C13 NMR [16, 17] and theoretical studies [18] have ruled out the butatrienic structure as a realistic depiction of this transition. Rather, the backbone of the blue phase is thought to be linear, with all side chains aligned in the same plane [19–22]. The red phase is then non-planar, either through twisting, folding, or kinking of the polymer backbone. The structure and preferred phase of the polymer backbone strongly depends on the side chains.

5.1.1. Review of Existing PDA Structural Data. The governing feature of PDAs is the specific spacing requirements which must be met for polymerization to occur. Schematically this polymerization is shown in Figure 5.1. In general the diacetylene moiety from two adjacent molecules must be located within ~ 4 Å of each other, with the spacing between neighboring molecules being less than 4.9-5.2 Å [15, 23–25]. As the DA assembly undergoes polymerization, there is rotation around the center of each diacetylene center to produce the polymer chain. As no diffusion, or phase transition is required, this polymerization process can produce large defect free single crystals.

The structure of PDA Langmuir films has been characterized with a number of techniques including x-ray diffraction, electron diffraction and atomic force microscopy. These techniques have enabled

direct observation of the structure of the film as it polymerizes and undergoes the blue to red transition. Using electron diffraction (ED) and small angle x-ray scattering (SAXS) on Cd-PDA multilayers, Tieke and Lieser measured a unit cell with parameters of a = 4.86 Å, b = 7.4 Å, with "a" defined as the spacing along the polymer backbone. SAXS measurements suggested the polymer layers are tilted as much as 50° to 60° from normal. Similarly, Kuriyama et al. measured unit cell parameters of a = 4.9 Å and b = 8.4 Å, with $\gamma = 88°$ for the blue phase, and a = 4.9 Å, b = 8.2 Å, and $\gamma = 90°$ for the red phase. They suggest that the shift in packing between the blue and red phase is likely due to the transition from a planar orientation of a zig-zag, or otherwise non-planar conformation of the polymer backbone [27, 28].

Using ED, Day and Lando studied self-assembled films of NCDA on a Li^+ subphase. They reported an unpolymerized unit cell with a = 4.83 Å along the polymer backbone, and b = 9.2 Å, and polymerized unit cell with parameters a = 4.98 Å and b = 8.11 Å, with the molecules being highly tilted, approximately 57° [29, 30].

X-ray diffraction and reflectivity have likewise been used to probe the structure of PDA Langmuir films. Gourier et al. examined monolayers of PCDA using grazing incidence x-ray diffraction (GIXD) and x-ray reflectivity (XRR). While the chromatic behavior of the PDA film was not commented on by Gourier et al., García-Espejo et al. suggested that the films studied by Gourier et al. were likely red phase, with parameters of a = 5.05 Å, b = 4.81 Å and $\gamma = 122°$ when presented in a distorted hexanogal unit cell. XRR by Gourier et al. revealed that monomer films were highly tilter. However, polymerization of these films was challenged however by the basic subphase necessary to produce stable monolayers of PCDA [31]. Göbel et al. examined "Bronco" (dimethyl-bis-(2-hexacosa-10,12-diinoyl)-oxaethyl-ammonium bromide), a two tailed positively charged diacetylene surfactant at different temperatures. At room temperature, they observed that the monolayer was titled approximately 32° from normal. Polymerization via UV-light induces a shift in tilt to 23°. At lower temperatures, they observed that the monomer films undergo a transition to a vertical orientation during polymerization [33].

Lifshitz et al. measured the evolution of the structure of diacetylene films while being polymerized and transformed by the measuring x-rays. They modeled the system as two layers, the carboxyl

terminated chain and the methyl terminated chain, joined by the polymer backbone. Their indexing and modeling scheme assigned the monomer and blue phase to be in a hexagonal, or centered rectangular structure. With the monomer having unit cell parameters a = 5.27 Å, b = 9.13 Å, γ = 90°. Polymerization to the blue phase shifts the unit cell to a = 4.9 Å, b = 9.73 Å, γ = 85°. Their modeling approach suggested that the methyl terminated tail was highly tilted, 40°, with the carboxyl terminated structure being vertical in the monomer phase and slightly tilted (18°) in the blue phase. The red phase then exhibited a shift to an oblique unit cell, a = 4.9 Å, b = 7.82 Å, c = 84°, and a completely vertical alignment of the carboxyl and methyl terminated chains. Subsequent GIXD studies in which PDA mixed with either dyes or other surfactants have based their analysis on this model [32, 35]. Using XRD on PDA multilayers, Fischetti et al. measured a tilt of 35° and 0° for the blue and red phase respectively [36]. Similarly, Shufang et al. examined multilayers of PCDA on a Tb^{3+} and Cd^{2+} subphases using XRD [37].

Atomic force microscopy (AFM) has also been used to probe the in-plane and out-of-plane structure of PDA Langmuir films [38–43].Carpick et al. measured blue and red phase PCDA trilayers using atomic force microscopy. They measured the blue phase to have a height of 7.4 ± 0.8 nm and the red phase to have a height of 9.0 ± 0.9 nm. From AFM they inferred that the blue phase was significantly more tilted than the red phase, ∼39°, as compared to ∼20° [38, 39]. Likewise, Lio et al. using high resolution AFM measured the spacing between monomers along the polymer backbone to be 4.8±Å. They further observed an increase in film thickness of approximately 15% from the blue to red phase. Vithana et al. examined the unit cell parameters of polymerized and unpolymerized multilayers of PCDA using scanning probe microscopy [41]. Lattice parameters of monomer films were observed to be location dependent and varied based on where in the film imaging was carried out. Polymer multilayers were indexed to have a = 4.68 Å and b = 5.57 Å with the angle between "a" and "b" equal to 102°.

Presented here is a systematic characterization of PDA Langmuir films using Grazing Incidence X-ray Diffraction (GIXD) with complementary X-ray Reflectivity (XRR), Atomic Force Microscopy (AFM) measurements and DFT calculations. Unpolymerized monomer films were examined first to establish the original packing and structure of the film. Blue Phase PDAs were observed to

exhibit a decrease in packing as compared to the monomer. As blue phase PDA is an intermediate state, the diffraction patterns include both monomer and red phase reflections. Hence, Zn modified PDA films were used to probe the structure of the blue phase without confounding influence of the residual monomer or formation of the red phase. The red phase was observed to exhibit a non-planar geometry. Several potential non-planar structures for red phase structures were identified and their spectra was evaluated using DFT calculations. Boronic acid functionalized DAs have been noted for their strong thermochromic reversibility [44–47]. Boronic acid PDAs exhibit strong hydrogen bonding leading to a polymer that generally retains the structure of the unpolymerized DA. Structural characterization of reversible PDAs may lead to improvements in the design of reversible PDA sensors.

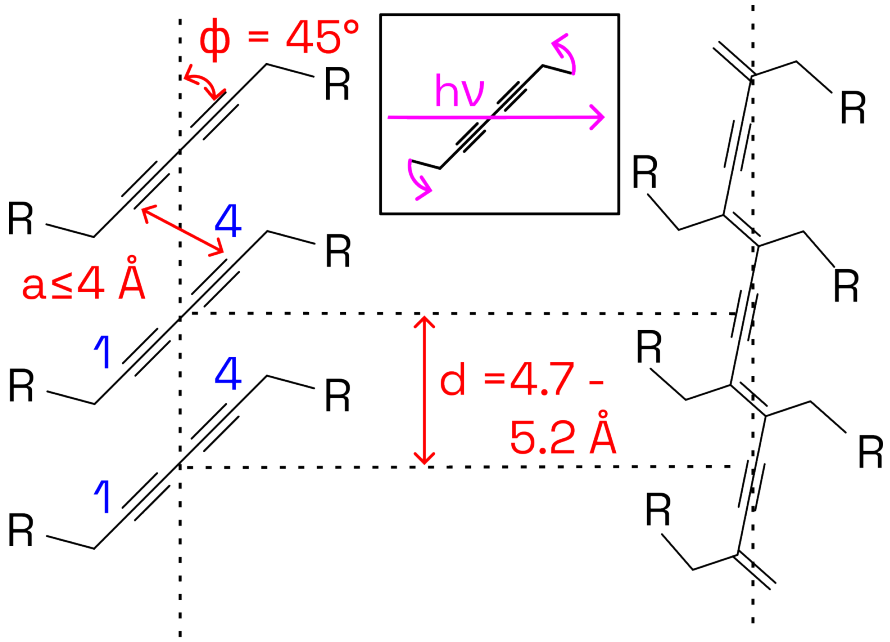

FIGURE 5.1. Spacing and packing requirements for topochemical polymerization of diacetylenes in the solid phase. The "1" carbon (noted in blue) must be less than 4 Å from the adjacent "4" carbon on another chain. The photo-initiated polymerization process necessitates a rotation in the monomer triple bond moiety to form a linear PDA chain. Figure is adapted from Wegner, Menzel et al. [3, 15, 24, 48].

5.2. Experimental Methods

5.2.1. Materials. 10,12-pentacosadiynoic acid (PCDA), 10,12-tricosadiynoic acid (TCDA), and 10,12-nonacosadiynoic acid (NCDA) were from TCI America and GFS Chemicals and purified

prior to use (See next sections). Anhydrous zinc chloride ($ZnCl_2$) was from Honeywell Fluka and was ACS grade. Chloroform (ethanol stabilized, 99.8%) was from Sigma Aldrich. Deionized, 18.2 MΩ·cm water (Barnstead NANOpure) was used for all Langmuir trough experiments carried out at UC Davis. A MilliQ DI system was used at APS.

1-Ethyl-3-(3-dimethylaminopropyl)carbodiimide HCl (EDC) was obtained from Millipore Sigma and stored under an Ar blanket at -4 °C. 6-Chloro Hydroxybenzotriazole (6-Cl HOBt) was obtained from Aapptec. Triethylamine (TEA) was obtained from Fisher Scientific. 4-Aminophenyl boronic acid HCl was obtained from Boron Molecular.

5.2.2. Synthesis of Boronic Acid Functionalized PCDA (BA-PCDA). BA-PCDA, (4-(pentacosa-10,12-diynamido)phenylboronic acid) was synthesized using an EDC-HOBt coupling reaction. To a 5 mL round bottom flask with tiny stir bar, 100 mg (0.267 mmol, 1 eq) of 10,12-pentacosadiynoic acid (PCDA) was added. PCDA was purified with silica gel chromatography to remove excess polymer content using chloroform (Rf = 0.23) and then rotovapped to dryness and stored at -20 °C. 49.8 mg of 6-Cl HOBt (1.1 eq, 0.29 mmol) and 56.3 mg (1.1 eq, 0.29 mmol) of EDC were added to the vial. The powders were then dissolved in a small amount of N,N-dimethyalformamide (DMF), approximately 400 µL. 108 mg of triethylamine (TEA) (4 eq, 1.067 mmol) was then added to the solution. The reaction was carried out at room temperature in the dark and stirred for 24 hours. After which, 1 mL of water was added. The solution was then vacuum filtered using a small Büchner funnel lined with Whatman No 1 filter paper. The filter paper was rinsed with water and ethyl acetate 3 times each to wash away unreacted PCDA, EDC and Cl-HOBt and DMF. The filter paper was removed and dried under vacuum overnight in a dark desiccator. NMR (see Figure B.12) in DMSO-d6 showed a pure compound and was used without further purification. NMR was taken using a Bruker 400 MHz NMR spectrometer with Topspin 3.2 running ICONNMR. BA-PCDA was stored in the dark in a -20°C freezer. BA-PCDA is not appreciably soluble in most organic solvents (chloroform, ethyl acetate etc.) or water. For Langmuir film deposition a spreading solution of 90%:10% chloroform:methanol was used.

5.2.3. Langmuir Film Preparation. Diacetylene monomers were dissolved in a solution of either chloroform or benzene at a concentration of 0.4 $\mathrm{mg\,mL^{-1}}$. The solution was then deposited

onto the air-water interface using a glass syringe. A Nima 611D (600 cm^2) trough was used to deposit films for atomic force microscopy and spectrophotometry measurements. For X-ray diffraction and reflectivity, a purpose built in-situ Nima Langmuir trough was utilized. Our techniques for preparing relatively uniform PDA Langmuir films has been described previously [9]. A factor in preparing uniform Langmuir films of diacetylenes is ensuring that the deposited solution contains minimal polymer content. Commercially available DAs contain significant polymer content, which must be removed. The most effective approach is a passing the DAs through a silica gel column using chloroform as a mobile phase.

5.2.4. Grazing Incidence Diffraction (GIXD). Grazing Incidence X-ray Diffraction (GIXD) experiments were carried out at NSF's ChemMatCARS Beamline 15-ID-C at the Advanced Photon Source (APS) at Argonne National Laboratory in Lemont, IL. An in-line Langmuir trough at beamline 15-ID-C was used to fabricate the PDA Langmuir films. The trough was in a helium purged enclosure with X-ray transparent Kapton windows. A Dectris PILATUS 100 Detector was used to capture diffraction patterns, and samples were illuminated with a 10 keV X-ray beam. The reflectometer setup at beamline 15-ID-C has been described in detail elsewhere [49, 50].

5.2.4.1. *Analysis of GIXD results.* The resulting diffraction patterns were indexed and structures solved using techniques described by Watkins et al., Leveiller et al. and several others [51–58]. The analysis scheme is described in detail in the supplemental information section B.1, example code and all raw data generated will be available after publication of this chapter. In brief, two two-dimensional scattering patterns are integrated along the z direction and the in-plane, two-dimensional crystal structure is derived from the integrated q_{xy} Bragg peaks. Molecular tilts and vertical structure is obtained from Bragg rods in q_z.

5.2.4.2. *Theoretical Calculations.* The 8 repeat unit long reconstructed structures (methodology detailed in supplemental section B.12) were then optimized using b3lyp DFT method in Gaussian16. Red Phase PDAs were optimized using the semi-empircal PM6 method in Gaussin16. UV-vis spectra from the structures were then calculated using TD-SCF b3lyp with the svp basis set with 100 singlet states.

5.2.5. X-ray Reflectivity. X-ray Reflectivity (XRR) measurements were carried out at Beamline 15-ID-C using the same setup as the GIXD measurements. The roughness and heterogeneity of the PDA films prevented an in-depth and rigorous analysis of X-ray reflectivity profiles. A limited amount of information about the vertical electron density profile was obtained through stochastic fitting methods provided by the Stochfit package [59]. A model independent fit of the X-ray reflectivity was obtained using Stochfit and then a box-model fit of the electron density was carried out using a least squares regression. More details on this methodology is described in supplemental section B.2.

5.2.6. Atomic Force Microscopy. Langmuir films of PDAs were deposited using an angled Langmuir-Blodgett technique onto cleaned glass coverslips, or freshly cleaved mica as described previously [9, 14]. The deposited films were imaged using Tap300Al-G and Tap190Al-G tips from Budget Sensors in a NanoSurf CoreAFM in dynamic force (tapping) mode. The resulting scans were analyzed using Gwyddion [60].

5.2.7. Other Characterization Techniques. PDA Langmuir-Blodgett Films were imaged using a Nikon E600 upright microscope with an Andor Zyla 5.5 sCMOS or Photometrics Kinetix sCMOS camera and Texas Red filter cube. Microscopy control utilized μmanager and pycromanager [61, 62]. UV-Vis spectra were collected using a Perkin-Elmer Lambda 750, and Fluorescence Emission spectra were captured using a Varian Cary Eclipse spectrofluorometer.

5.3. Results & Discussion

PDA Langmuir films were prepared at the in-situ Langmuir trough at Beamline 15-ID-C at NSF's ChemMatCARS. Films were compressed to 25 $\mathrm{mN\,m^{-1}}$, with unpolymerized films being held at constant pressure during the measurement. The barrier & pressure control were turned off for films after polymerization. The PDA film was exposed to a calibrated and defined dose of UV light, ≈4-6 seconds at 850 $\mu\mathrm{W\,cm^{-2}}$ to produce blue phase PCDA and ≈12 minutes to produce red phase PCDA. While some beam-induced transitions inevitably occur, the stage was translated to an unexposed portion of film several times and independent films were characterized to ensure reproducibility. Figure 5.2 shows the results of indexing the two-dimensional, in-plane diffraction pattern. The monomer and blue phase were indexed to a centered rectangular unit cell, and the

red phase was indexed to an oblique unit cell. Figures 5.3, 5.6 and 5.8 show the out of plane scattering, which correspond to the tilt and inter-layer organization of the film. X-ray reflectivity (XRR) was also carried out at ChemMatCARS, with an example shown in 5.5. However, significant film heterogeneity and roughness, as is evident in the AFM scans, Figure 5.4, prevented in-depth analysis of the film thickness profile. However, using a stochastic, model independent fitting method, an overall electron density profile and thickness was measured [59]. Modeling of the GIXD profiles enabled construction of the polymer structure. Calculated UV-vis spectra from optimized variants of these structures using Gaussian16 [63] are shown in Figure 5.10.

5.3.1. Monomer Diacetylene Films. 2-D (in-plane) indexing yields a centered rectangular unit cell with parameters a = 5.58 and b = 9.67 Å, with an area per molecule of 26.98 $Å^2$. This aligns reasonably well with the area per molecule as measured by a Langmuir-Blodgett trough (approximately 25-26 $Å^2$) [9, 38]. Examination of the full-width half maximum of the Bragg peaks yields in plane Scherrer lengths of approximately 376.26 ± 57 Å, similar to those of phospholipids and other fatty acids [51, 57, 58, 64].

The profile in q_z is more complex. It is likely convolution of Bragg rods from the individual layers and inter-layer registry, leading to smeared, but definable peaks within the Bragg rod profile. This is similar to Miller et al. where well-defined peaks were observed in cadmium arachidate [65–67]. This is complicated however, by the fact that the collapsed state of PCDA is heterogeneous and variable in thickness [68, 69]. This leads to a number of observable peaks that are difficult to reconcile in the simple model presented here. Following technqiues developed by Truger et al., these peaks were fit and indexed to obtain molecular tilts and lengths perpendicular to the air-water interface (supplemental section B.1) [54]. From this model, it can be observed that the individual PCDA layers are somewhat tilted, several degrees off normal. This model does not necessarily include any description of internal tilt that might be necessary for topochemical polymerization. The calculated length c seems to be several Ängstroms short of the full molecule length, and that may be a limitation of this model. A Scherrer length of ≈ 76 Å suggests that the outer layer may be disordered, or the film is highly tilted, shortening the effective length of the molecule, which

is consistent with previous measurements using atomic force microscopy, which suggest that the monolayer and blue phase are shorter than their full extension length [39–41].

While a trilayer structure is typically ascribed to PDA films formed at the air-water interface, further multilayer buildup can be observed in TCDA films, where the crystaline length, L_z is approximately 105 Å, potentially consistent with 4 or 5 layers, depending on molecular tilt. This is further supported by the "splitting" of the Bragg rod profile at higher q_z into more well-defined peaks with smaller full width half maximums, suggesting a thicker, ordered multilayer Figure 5.3, B.5. Otherwise, monomer films made from TCDA are generally similar to those made from PCDA, with similar 2D packing and crystalline lengths. XRR of the PCDA monomer film yields an overall thickness of approximately 68.7 ± 8.4 Å, in reasonable agreement with a tilted trilayer, Figure 5.5 (see section B.3.2). Atomic force microscopy of polymerized films further suggests that PDAs have many regions of extensive multilayer buildup, Figure 5.4 (see also supplemental Figures B.38, B.18).

5.3.1.1. *Boronic Acid Functionalized PCDA.* While the BA-PCDA films studied here were all polymerized and in the blue phase, their behavior was remarkably similar to that of unpolymerized PCDA. BA-PCDA films appear visibly blue (Supplemental section B.4), however the diffraction pattern and resulting indexed structure is strongly reminiscent of monomeric diacetylenes. Indexing of the in-plane q_{xy} structure revealed a centered rectangular unit cell with dimensions of a = 5.63 Å and b = 9.75 Å and an area per molecule of 27.45 Å. Despite the wide spacing between molecules, BA-PCDA appears deep blue, indicating a high degree of polymerization. This suggests that strong hydrogen bonding between neighboring boronic acid headgroups may create a stable network that strongly favors the blue phase. Indeed, similar to our previously reported results on Zn-PCDA, BA-PCDA appears only weakly fluorescent and requires very high temperatures (> 200 °C) to undergo the blue to red transition, Figure B.11 [9]. Unlike unfunctionalized PCDA, BA-PCDA retains the spacing and Bragg rod profile close it its monomer after polymerization. Rather than any change in d-spacing or packing, as seen in other blue and red phase PDAs, Figure 5.2, the observed reflections only become more intense with prolonged UV irradiation and x-ray beam exposure. This suggests that the film is becoming more polymerized, but remaining in this unique structure. With extensive UV irradiation and beam exposure a weak reflection at $q_{xy} = 1.65$ Å^{-1} appears. No wide

scale blue to red transition or even beam damage was observed in BA-PCDA films. This may be from small amounts of unfunctionalized PCDA left-over from the synthesis of BA-PCDA.

Like monomer PCDA, distinct peaks in q_z can be observed in the Bragg rod profile of BA-PCDA. These arise from registry between individual layers. AFM measurements, Figure 5.4D,H, reveal a diverse array of features and multilayers. The model-independent x-ray reflectivity profiles, Figure 5.5, suggest a thickness of 67.7 ± 3.5 Å, relatively consistent with thickness measurements of the AFM film (52.7 ± 2.4 Å), and in relative agreement with the Scherrer length in q_z of 54.27 Å (Table 5.1). The Bragg rod profile (Supplemental Figure B.8) suggests a shorter crystaline length in the z direction and the spacing between peaks suggest a longer molecule. Indexing and refinement yields a unit cell with $c = 31.89$Å. This is relatively close to an empirically optimized BA-PCDA molecule with length of approximately 34 Å. Hence, a bilayer stabilized by a strong hydrogen bonding network may be the most likely underlying structure, albeit one extensively populated with regions of heterogeneous multilayers.

BA-PCDA and other similar diacetylenes with boronic acid headgroups have been investigated previously due to their high degree of thermochromic reversibility, among other interesting properties [44, 46, 47]. The high degree of reversibility observed in the colorimetric transitions of BA-PCDA and the structure observed here may suggest an underlying structural origin for reversibility. Compared to blue phase PCDA formed on pure water, the spacing between adjacent monomers along the polymer backbone is much larger: a = 5.242 Å for blue phase PCDA (table 5.2), a = 5.63 Å for blue phase BA-PCDA. Furthermore, the film appears much less tilted. This creates a widely spaced blue phase polymer that may be unable to permanently undergo the blue to red transition without application of significant external stimuli.

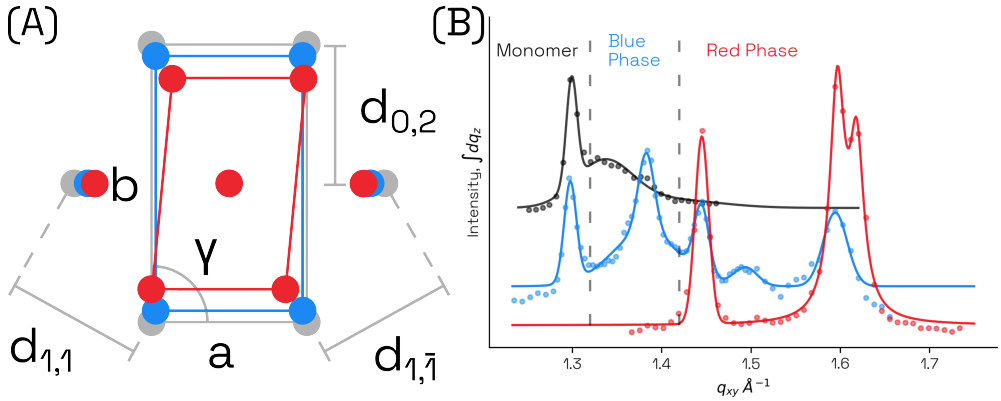

FIGURE 5.2. Construction of centered rectangular 2-D unit cell from observed Bragg peaks for the monomer, blue and red phases of PDA (PCDA). Monomer and Blue phase PDA are indexed to a centered rectangular unit cell with degenerate reflections centered at a single Bragg Peak. The red phase is indexed to an oblique unit cell with three unique reflections as described in the text.

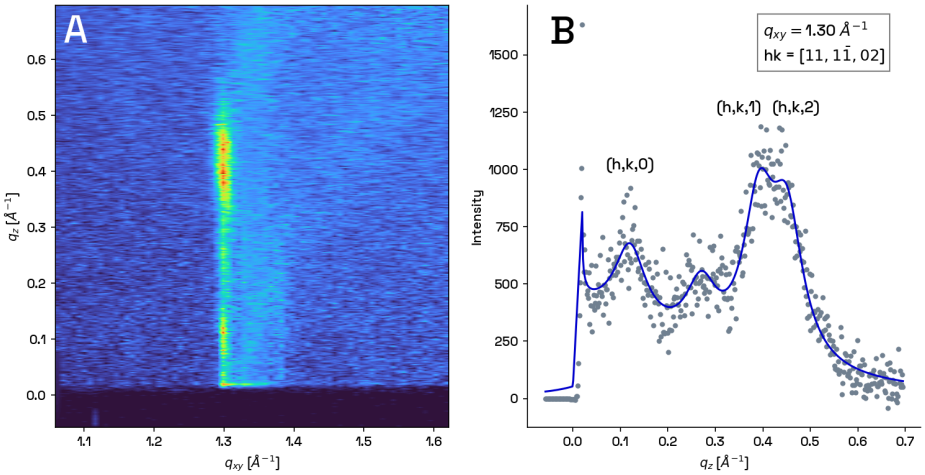

FIGURE 5.3. Reciprocal space map and Bragg rod profile of unpolymerized PCDA. Multiple out-of-plane peaks are observed, which are attributed to multilayer buildup of PCDA.

	$q_{xy}[Å^{-1}]$	a [Å]	b [Å]	c [Å]	γ [°]	α [°]	β [°]	L_{xy} [Å]	L_z [Å]
PCDA	1.299	5.58	9.67	26.35 ± 0.336	90	88.73 ± 0.214	96.75 ± 0.233	376.26 ± 57.107	76.17 ± 8.276
TCDA	1.299	5.59	9.68	24.00 ± 0.152	90	88.52 ± 0.127	97.13 ± 0.07	347.72 ± 16.003	105.19 ± 2.293
BA-PCDA	1.299	5.63	9.75	31.89 ± 0.685	90	88.61 ± 0.361	98.04 ± 0.438	344.74 ± 68.081	54.27 ± 6.6

TABLE 5.1. Summary of GIXD results for monomeric PCDA, TCDA and polymerized BA-PCDA films: Indexed two and three dimensional unit cell parameters and Scherrer lengths in the xy-plane and z direction

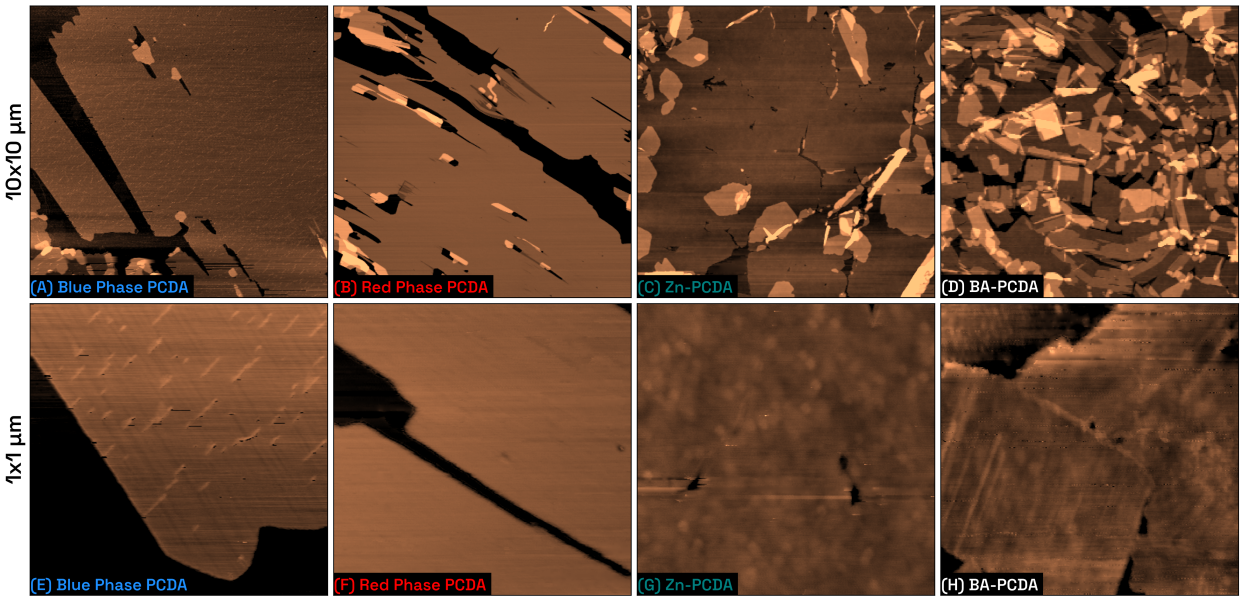

FIGURE 5.4. Atomic Force Microscopy (AFM) topography scans of PDA Langmuir films deposited on mica. (A,E) Blue Phase PCDA, most of the film appears to be a highly tilted trilayer, with multilayer islands and some large cracks along the polymer backbone. Striations from the polymer backbone are visible in the 1 µm scans. The film thickness was measured to be 50 ± 2.2 Å. (B,F) Red Phase PCDA, more cracks and fractures appear, and are parallel to the polymer backbone. A film thickness of 82.8 ± 1.0 Å was measured. Like the blue phase, the polymer strands can be seen in the 1 µm scan. (C,G) Blue Phase Zn-PCDA, the film is observed to be more heterogeneous with many regions of multilayer buildup. Polymer strands are difficult to see in the 1 µm scan. (D,H) Blue Phase BA-PCDA, the film is extremely heterogeneous, with many regions of multilayer buildup. The polymer domains are much smaller, less than 1 µm, but polymer strands are visible within a domain.

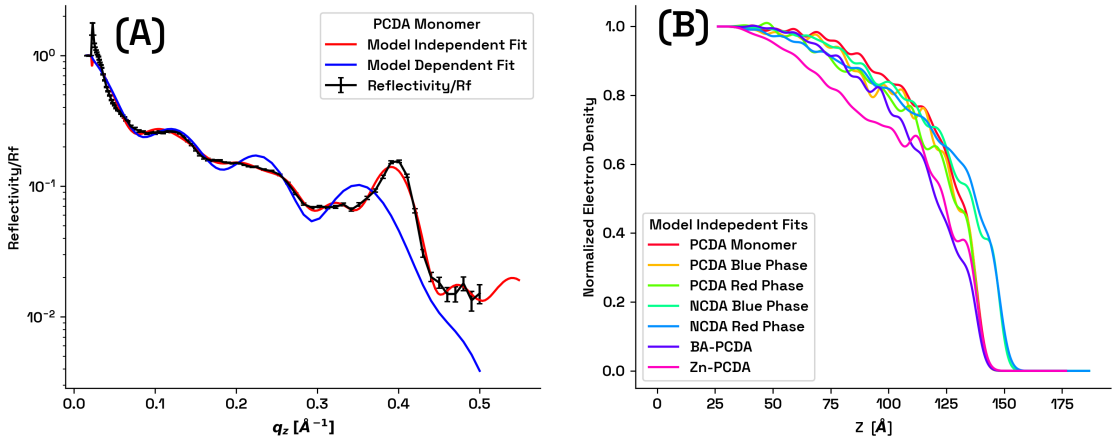

FIGURE 5.5. (A) X-ray Reflectivity (XRR) profile of unpolymerized PCDA at the air-water interface with model independent and model dependent fits of the profile. (B) Comparison of XRR profiles from the range of DAs studied here. As is evident from the AFM scans, the surface is extremely heterogeneous, negating high resolution analysis of the profile.

5.3.2. The Blue Phase. Exposure of the film to UV light (254 nm) induces polymerization to the blue phase. The blue phase for DAs formed on a pure water subphase is generally an intermediate, meta-stable state [68, 70]. Hence blue phase films are inherently "mixtures", composed of both blue and red phase PDA and unpolymerized PCDA monomers.

Indexing of the blue phase of PDA for all configurations yields a centered rectangular unit cell, see Table 5.2. A number of reflections are present in the reciprocal space maps of blue phase PDA, Figures 5.6, and 5.2. However, only one of these was uniquely assignable to the blue phase. This reflection, $q_{xy} \approx 1.38\text{Å}^{-1}$, was used to index the unit cell by assuming the reflections $[11], [1\bar{1}], [02]$ were all degenerate as in the case of a centered rectangular unit cell. Other reflections present in the blue phase are attributable residual unpolymerized (monomer) film and the early stages of the formation of red phase PDA as labeled in Figures 5.2, 5.6.

Lifshitz et al. utilized these weaker reflections to formulate unit cell parameters [34]. Here, blue phase Zn-PCDA was used to guide and simplify the analysis. Zn-PCDA does not readily undergo the blue to red transition, and therefore can be extensively polymerized in the blue phase, and only one reflection at $q_{xy} \approx 1.38\text{Å}^{-1}$ is present (See supplemental Figure B.24). Blue phase PDA

Langmuir films formed on pure water share this reflection. Hence, it was assumed that both are structurally similar, and that reflection was used for indexing pure water blue phase films. The in-plane structure of the blue phase was found to be similar to the monomer structure except with smaller unit cell parameters: a = 5.242 Å and b = 9.0 angstrom for PCDA, see Table 5.2. This shrinking of the unit cell is a consequence of topochemical polymerization [25, 29].

Analysis of the Bragg rod profiles of the blue phase reveal a highly tilted film. Unlike films of monomer diacetylenes, blue phase PDAs appear to lack positional registry between layers. Using polarized light microscopy, PDA films appear to be in complete inter-layer registry as the domains completely rotate plane polarized light [9]. However, the lack of out of plane reflections suggest that they are not in registry at the molecular scale, compare Figures 5.3 and 5.6.

Bragg rod profiles were fit to a points-on-a-line structure (see supplemental section B.1), corresponding to the atoms in the fatty acid tail. Results of this fitting suggests the molecules are uniformly tilted in an intermediate direction, close to the [11] direction. The [11] direction appears to be the direction of polymerization. This analysis was carried out for each diacetylene configuration with the Euler angles necessary to generate the structure reported as ϕ and ψ (see supplemental figure B.4) in Table 5.2. The uniform tilt of the PDA molecules, while retaining the structure of the monomer is in good agreement with previous structural studies [19, 21, 39, 40, 71]. The tilt angles obtained for these Bragg rod profiles are not necessarily unique, as the limited number of unique reflections limits full validation of the tilts obtained here. The full-width half-maximum of the Bragg rods suggests a relatively short Scherrer length, roughly the length of the titled molecule in the z direction, (see Table 5.2). This is further supported by XRR and AFM. XRR analysis, Figure 5.5, Supplemental section B.2, suggests an overall film thickness of 74.7 ± 11.6 Å.

Atomic force microscopy measurements indicate an average height of 50 ± 2.2 Å for most of the film. This suggests a highly tilted trilayer. If it is assumed that a fully stretched out diacetylene monomer is approximately 29 Å long, each layer would be tilted approximately 55°. 1 µm scans reveal the so-called linear strand morphology arising from the polymer backbone. Many ridges perpendicular to the polymer backbone can be seen, Figure 5.4A,E. These ridges are approximately 20 Å taller than the surrounding film (Supplemental Figure B.18). The origin of the ridges is unclear, but they

may be buckled film, or perhaps small regions of a monolayer above the trilayer. Interestingly, as the film is driven into the red phase, these ridges disappear, Figure 5.4F.

AFM topography scans also reveal the origins of the rough and heterogeneous XRR profiles, Figure 5.5. While large regions of the film may be mostly a trilayer, the film is also littered with collapsed bilayers and thicker multilayers stacked on top of the trilayer basal layer, with large holes throughout the film, Figure 5.4A,E (See also supplemental Figures B.18, B.38). Hence, while films appear uniform at the mm and even 100s µm scale (Supplemental Figure B.19), the actual microstructure is extremely varied. This heterogeneity and multilayer buildup limit the depth of the analysis that can be carried out with GIXD and XRR of PDA trilayers.

5.3.2.1. *Zn Modified PDA Films.* PDA films made from PCDA with a 1 mM $ZnCl_2$ subphase were also examined. Films formed from Zn-PCDA were driven into the blue phase via exposure to UV-light. Prolonged exposure did not produce any measurable red phase and the films appeared deep blue. Extended periods of x-ray beam exposure did not appreciably damage Zn-PCDA films. A small amount of Zn-PCDA was driven into the red-phase via repeated exposure to the x-ray beam, however there were no measurable changes in the reflectivity or diffraction patterns (see supplemental figure B.24). Compared to pure PCDA, the in-plane structure is remarkably similar, with minimal differences in unit cell parameters and area per molecule, see Table 5.2, 5.5. The out of plane structure appears somewhat different. The same Bragg road analysis and fitting was carried out and yielded similar molecular tilts. The Zn-PCDA films appeared much more disordered, rather than a vertical Bragg rod, the out of plane structure appears similar to a Scherrer ring, indicating a much less oriented film in the z-direction [72]. Atomic force microscopy scans reveal a highly varied film, Figure 5.4C,G. A film height of 44.8 $\pm$ 3 Å was measured in the most uniform region, suggesting a highly tilted trilayer, similar to blue phase PDA films formed on pure water. However, a wide range of features were also observed, including significant multilayer buildup and large cracks (supplemental Figures B.38, B.28). XRR measurements suggest an extraordinarily rough interface with an average thickness of 80.0 ± 5Å (Supplemental section B.8.2). Hence, this is the origin of the Scherrer-like ring observed in the observed in the GIXD measurements, while the film may appear relatively uniform with widefield microscopy (see supplemental Figure B.29) the actual film is even

more heterogeneous than pure water PDA films, but at length scales below what can be resolved with optical microscopy.

5.3.2.2. *NCDA and TCDA Films.* In Addition to PCDA, films of NCDA (C29) and TCDA (C23) were investigated. In general their structures were similar to PCDA, with nearly identical in-plane parameters and molecular tilts. Although NCDA and TCDA differ from PCDA by 4 and 2 carbons respectively, their out-of-plane crystalline lengths do not vary significantly. Notably, the in-plane Scherrer lengths for NCDA are significantly shorter than for PCDA or TCDA, suggesting a less crystaline film. This appears to correlate with the small domain sizes measured at the macro-scale as compared to PCDA or TCDA [9]. Macro-scale domains of PDAs are often on the order of 100s of µms [9, 30, 39, 73]. Regardless of DA choice, the short Scherrer lengths measured here suggests that PDA films exist in a "hexatic" phase, with short range positional and translational order and longer range orientational order, such that they appear as single domains at the macro scale.

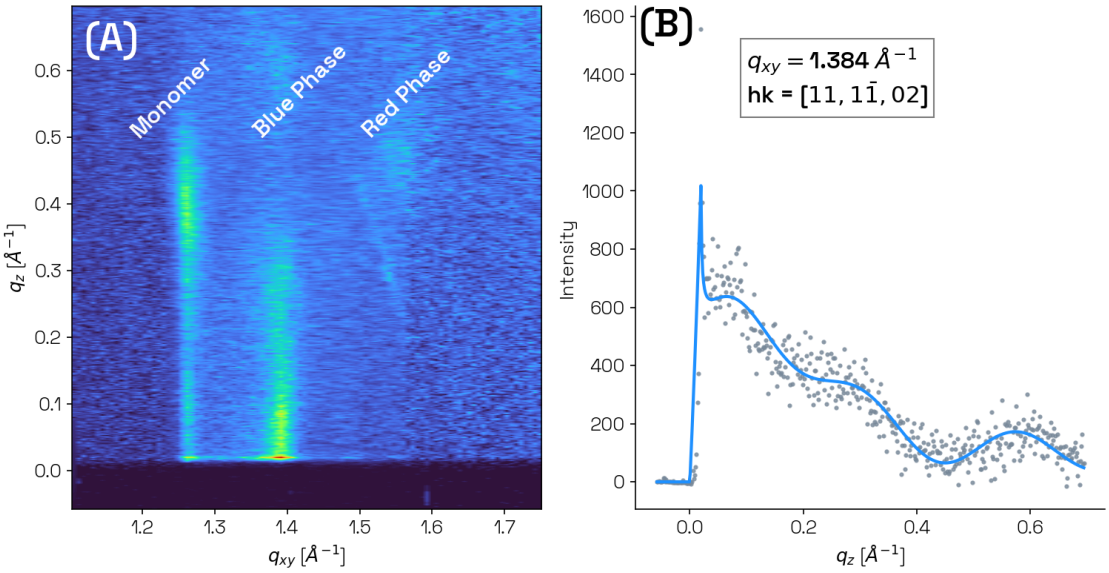

FIGURE 5.6. (A) Reciprocal space map and (B) Bragg rod profile of the blue phase reflections for PCDA. In addition to the blue phase reflection indexed at $q_{xy} \approx 1.38$ Å^{-1}, reflections from remaining un-polymerized film and the beginnings of red phase can be observed. This is due to the meta-stable, intermediate nature of the blue phase in PCDA.

	q_{xy}[Å^{-1}]	a [Å]	b [Å]	γ [°]	ϕ [°]	ψ [°]	L_{xy} [Å]	L_z [Å]
PCDA	1.384	5.242	9.079	90	-28.92 ± 2.08	28.22 ± 3.51	296.20 ± 44.59	19.55 ± 0.79
TCDA	1.384	5.243	9.080	90	-29.75 ± 0.07	30.96 ± 0.05	211.27 ± 40.69	23.62 ± 1.67
NCDA	1.365	5.317	9.209	90	-33.37 ± 0.82	35.01 ± 1.43	125.15 ± 10.67	21.35 ± 4.26
Zn-PCDA	1.38	5.259	9.11	90	-29.60 ± 0.51	30.08 ± 0.50	256.89 ± 32.05	29.14 ± 4.86

TABLE 5.2. Summary of indexed GIXD patterns for blue phase PDA Langmuir films. ψ refers to the tilt of the individual molecules along the x-axis and ϕ refers to the tilt of the molecules along to the y-axis.

5.3.3. The Red Phase. In addition to the notable differences in optical properties, the red phase is structurally different from the blue phase. Films were driven into the red phase via prolonged exposure to UV light at the air-water interface. The splitting of reflections that were degenerate in the blue phase into three unique q_{xy} suggests an oblique unit cell [57, 70]. While this could be indexed to a primitive oblique cell, for continuity between the lattice parameters used to describe the monomer and blue phase, a centered oblique unit cell with reflections $[11], [1\bar{1}], [02]$ was assigned to the non-degenerate q_{xy} values, Figures 5.2,5.7. Table 5.3 summarizes the in-plane lattice parameters for red phase PDAs.

The Bragg rods of the red phase are not well approximated by a set of uniformly tilted molecules like in the blue phase. Rather, attempts at modeling have followed previous investigations, and assumed that the acyl chain and alkyl chain are independently oriented in different directions [34]. Two models seem plausible: A "kinked" model, with the acyl and alkyl side chains tilted uniformly

in different directions, and a "twisted" model, where the side chains are rotated or twisted around the center of the polymer backbone. These are represented schematically in Figure 5.9.

5.3.3.1. *The Kinked Model.* Results from modeling using the kinked model can be found in Table 5.3, represented by the angles ϕ_i and ψ_i, which correspond to the tilt along the y-axis (along the b direction) and ψ_i, the tilt along the x-axis (along the a-direction). The red phase was observed to be significantly less tilted, with the acyl chain, represented by ψ_1 and ϕ_1 being close to vertical, with more tilt in the alkyl chains, ψ_2, ϕ_2. These tilt angles are likely not unique, and several sets of angles were found to fit the Bragg rod profiles reasonably well.

5.3.3.2. *The Twisted Model.* The twisted model builds upon the kinked model, but also assumes that subsequent side chains rotate around the polymer backbone. Like the kinked model, the alkyl chain and acyl chain are allowed to vary in rotation from each other. The profile fit in figure 5.8 assumed uniform ψ tilt of approximately 2°. The acyl and alkyl chains were modeled with an initial tilt of $\phi_{\text{acyl}} \approx 6.2°$ and $\phi_{\text{alkyl}} \approx -4.5°$. Subsequent chains were then rotated around the polymer backbone with $\phi_x \approx -3°$. This particular fit utilized 4 unique tilts of ϕ_x, terminating at $\phi_{\text{acyl}} \approx -1°$ and $\phi_{\text{alykl}} \approx -14°$. Similar to the kinked model, a number of potential rotational systems exist that generally approximate the features found in Figure 5.8, hence these are more suggestions of potential conformations rather than definitive declarations of out of plane tilting and structure.

In either model, the red phase is significantly less tilted than in the blue phase. AFM measurements of the red phase of PCDA, Figure 5.4B,F, reveal a much taller film with an average trilayer height of 79 ± 7 Å, much taller than the blue phase (≈ 50 Å). XRR measurements of red phase NCDA reveal an average thickness 86.3 ± 10.2 Å. This is an increase in the average thickness as compared to blue phase NCDA, 74.86 ± 3.45 Å. The red phase also has significantly more gaps, cracks and holes than in the blue phase. These cracks and gaps occur along the direction of the polymer bacbkone, assigned as [1,1]. This likely arises from the shrinking unit cell as neighboring polymer chains are only weakly bound by van der Waals interactions. Hence, as the film re-arranges and becomes taller, gaps appear in the film. Examination of the Scherrer lengths further support this, as the crystalline length significantly decreases in the $[1,\bar{1}]$ and [0,2] directions, Table 5.4. Interestingly, L_z appears to increase relative to the blue phase, suggesting an increase in registry the z direction along the $[1, 1]$ direction.

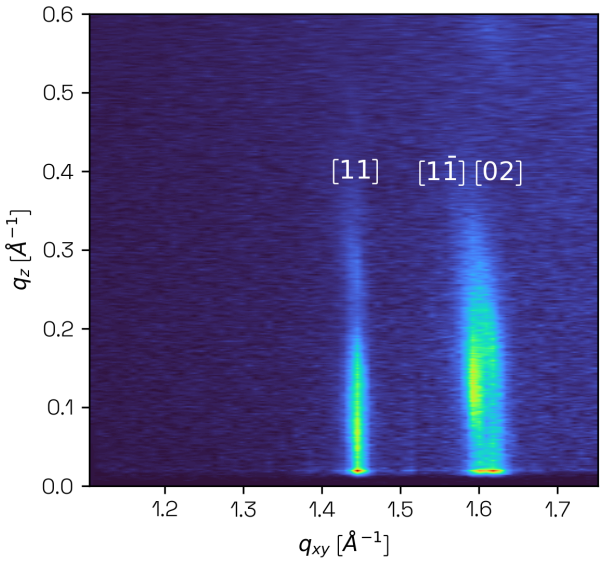

FIGURE 5.7. Reciprocal space map of red phase PCDA, three unique peaks in q_{xy} are visible, indicating an oblique unit cell.

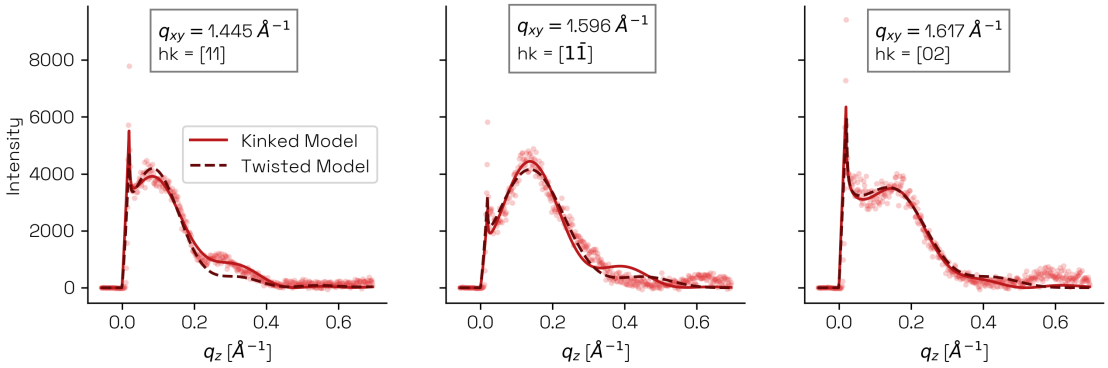

FIGURE 5.8. Bragg rod profile and fit using two different models described in Figure 5.9. The "kinked" model assumes a uniformly bent conformation of the side chains. The "twisted" model assumes the side chains are rotated around the polymer backbone.

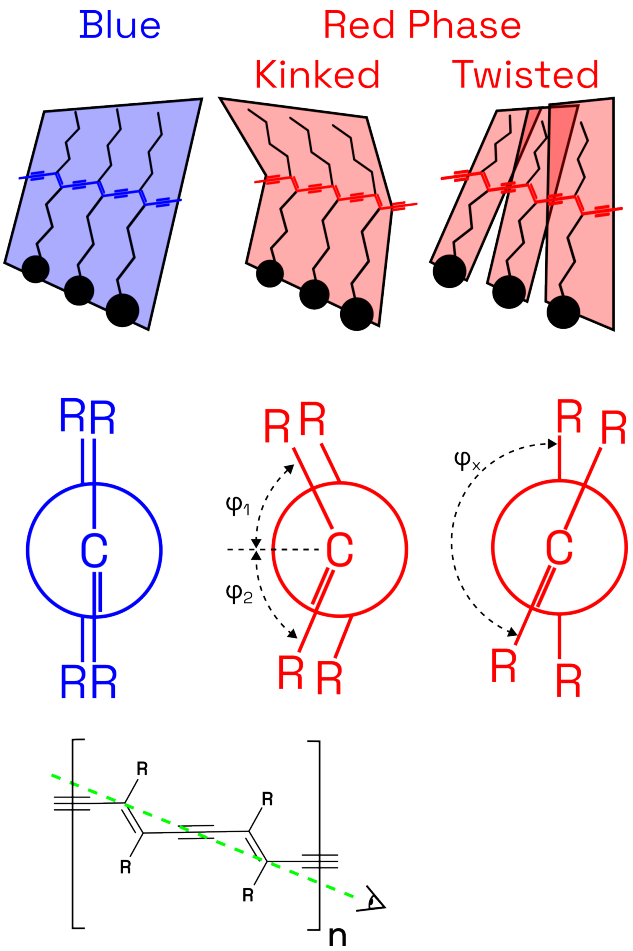

FIGURE 5.9. Comparison of the structural aspects of blue phase and red phase PDA. The blue phase is well modeled by a planar orientation of the alkyl chains and backbone. Two models are proposed for the red phase. The "kinked" model assumes the side chains are uniformly rotated off center. The "twisted" model assumes neighboring side chains are rotated around the polymer backbone with an angle of phi_x between them. These are represented with a Newman projection along the polymer backbone to highlight tilt variation along the polymer backbone.

	a [Å]	b [Å]	γ [°]	ϕ_1 [°]	ϕ_2 [°]	ψ_1 [°]	ψ_2 [°]
TCDA	4.907	7.788	83.763	3.167	-16.162	-3.507	4.432
PCDA	4.905	7.802	83.585± 0.155	1.924± 0.102	−14.537± 0.843	−2.079± 0.909	4.849± 2.178
NCDA	4.902	7.755	83.804± 0.021	1.279± 0.201	−19.549± 3.058	0.005± 0.747	11.169± 5.025

TABLE 5.3. Red Phase two-dimensional unit cell parameters and tilts obtained using the kinked model. ϕ_i corresponds to the tilt around the polymer backbone (in the direction of b), and ψ_i corresponds to the tilt along the polymer backbone, in the direction of a.

	[h,k]	$q_{xy}[Å^{-1}]$	L_{xy} [Å]	L_z [Å]
PCDA	11	1.444	308.573± 71.542	49.574± 8.807
	$1\bar{1}$	1.597	228.25 ± 32.887	37.386± 7.412
	02	1.621	157.979± 38.235	33.236± 7.781
NCDA	11	1.449	297.048± 15.666	44.962± 7.105
	$1\bar{1}$	1.598	268.177± 9.313	28.364± 0.721
	02	1.63	220.513± 21.59	28.066± 0.308
TCDA	11	1.446	273.35	45.609
	$1\bar{1}$	1.595	232.738	30.717
	02	1.623	165.231	20.694

TABLE 5.4. Indexed Reflections, corresponding q_{xy} values and Scherrer Lengths for red phase PDA.

	Monomer	Blue Phase	Red Phase
PCDA	26.98	23.80	19.02
TCDA	27.04	23.80	18.99
NCDA	-	24.48	18.90
BA-PCDA	27.45	-	-
Zn-PCDA	-	23.95	-

TABLE 5.5. Comparison of the Area Per Molecule (APM) in $Å^2$ for monomer, blue and red phase diacetylenes.

5.3.4. Comparison of Blue and Red Phase. GIXD, XRR and AFM measurements all suggest that the blue phase is structurally similar its unpolymerized state, with a planar backbone and tilted side chains. This is in good agreement with previous measurements and calculations. Hence, a picture of the *monomer* $\rightarrow$ *blue phase* transition can be developed. Exposure of packed monomers to UV light produces a blue phase polymer that is constrained by steric interactions, hydrogen bonding and van der Waals attractions from the side chains, namely the head groups and fatty acid tails. The tilted orientation is a consequence of the topochemical requirements, Figure 5.1, where the molecules must be tilted for polymerization to occur. Optimization of the blue phase backbone structure derived from GIXD and DFT calculations show that the derived structure is in reasonable agreement with experimental UV-vis spectra. Figure 5.10 compares the GIXD derived and DFT optimized spectra to experimental spectra.

All proposed mechanisms of the blue to red transition suggest a structural shift in the polymer backbone from a planar state to a non-planar geometry [19]. The structure of the red phase remains

unclear, but the two proposed models here show that either a kinking of the side chains, or twisting of 2-3 ° between neighboring monomers is sufficient to blue-shift the absorbance spectra towards shorter wavelengths, Figure 5.10. This sort of dihedral torsion and subsequent blue shift in the absorbance spectra has been observed in other conjugated organic polymers [74, 75].

Notably different are films formed from Zn-PCDA and BA-PCDA. While structurally similar to blue phase PCDA, Zn-PCDA is unable to undergo the blue to red transition via UV irradiation or x-ray beam exposure and remains in the blue phase. This is likely due to the strong bridging interactions between Zn^{2+} cations and the carboyxlic acid head groups [9, 76–79]. These strong bridging interactions also inhibit the already limited ability of PDAs to form uniform polymer domains, and drastically alter the collapsed multilayered state of the film. Furthermore, the blue and red phases of Zn-PCDA appear structurally similar. AFM measurements reveal no significant height different between them: 44.8 ± 3 Å in the blue phase as compared to 44.5 ± 1.4 in the red phase, Supplemental Figure B.28.

BA-PCDA exhibits reversible thermochromism up to ≈ 200 °C, and is structurally unique. Compared to blue phase PCDA, it has a much larger area per molecule, Table 5.5 and is significantly more heterogeneous, Figure 5.4, with very small domain sizes and features. It also appears to retain inter-layer registry, lacking in the polymerized phases of unfunctionalized PCDA. These are all a likely consequence of a bulkier headgroup with strong hydrogen bonding and potential $\pi - \pi$ stacking interactions. These measured conformal differences between the blue and red phase, and with functionalized films (Zn-PCDA, BA-PCDA) provide evidence for methods to tune the blue to red transition and enable reversibility. The experiments conducted here also show that the morphology of PDA Langmuir films is much more varied than just a trilayer. While many regions may be a true trilayer, the overall morphology is significantly more varied than it is typically presented and difficult to reliably reproduce (Figure B.38). This heterogeneity bedevils in-depth analysis of the molecular structure of the films and hence an understanding of the chromatic transitions. Future work should focus on developing stable, uniform PDA monolayers, similar to ethanolamine-DA synthesized by Sasaki et al. [38, 80]. A future avenue of exploration would be to revisit macro-scale single domain monolayers of PDA as described by Yamada and Shimoyama [73]. Through development of more

uniform "ideal" PDA films, in-depth GIWAXS/GIXD and XRR experiments and modeling could further elucidate the structures of the blue and red phases.

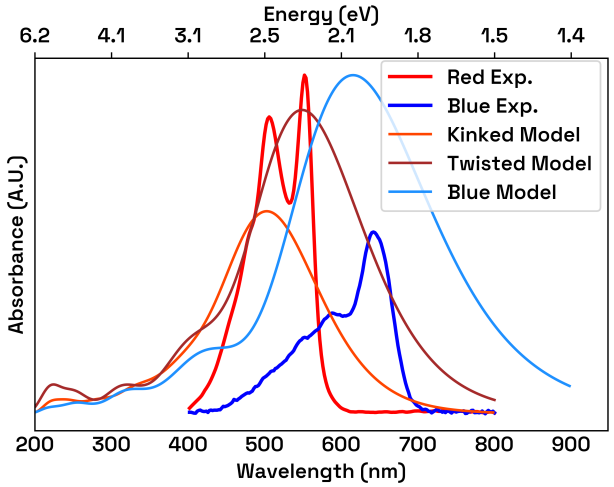

FIGURE 5.10. Comparison of calculated absorption spectra to spectra derived from quantum mechanical calculations. Experimental spectra are from [9, 14].

5.4. Conclusions

Presented here are structures for the blue and red phase of fatty acid PDAs as determined by GIXD and supported by AFM and XRR measurements. The blue phase was observed to have a planar backbone with uniformly tilted side chains. Quantum calculations on the X-ray derived structure yields reasonable agreement with experimental spectra. Two structures for the red phase are also proposed, with calculations showing a significant spectral shift, in agreement with the blue to red transition.

5.5. Acknowledgement

The authors thank Prof. Roland Faller for access to HPC1, Dr. Kevin Yates for thoughtful contributions to the notation, Joaquin Santamaria, Meghna Jha and Matthew Lawrence for assistance with the AFM measurements, Dr. Wei Bu and Dr. Binhua Lin for their expertise and assistance at CHEMMATCARS (Sector 15), and Dr. Erik Watkins for assistance with initial development of the model.

This work was supported by NIH R01 HL159993-01, NIH T32 HL086350, and NIH RXXXXX

NSF's ChemMatCARS, Sector 15 at the Advanced Photon Source (APS), Argonne National Laboratory (ANL) is supported by the Divisions of Chemistry (CHE) and Materials Research (DMR), National Science Foundation, under grant number NSF/CHE- 1834750. This research used resources of the Advanced Photon Source, a U.S. Department of Energy (DOE) Office of Science user facility operated for the DOE Office of Science by Argonne National Laboratory under Contract No. DE-AC02-06CH11357.

References

[1] Gerhard Wegner. Topochemical reactions of monomers with conjugated triple-bonds. IV. Polymerization of bis-(p-toluene sulfonate) of 2.4-hexadiin-1.6-diol. *Die Makromolekulare Chemie*, 145(1):85–94, 1971. ISSN 0025-116X. doi: 10.1002/macp.1971.021450107.

[2] Gerhard Wegner. Topochemische Reaktionen von Monomeren mit konjugierten Dreifachbindungen / Tochemical Reactions of Monomers with conjugated triple Bonds: I. Mitt.: Polymerisation von Derivaten des 2.4-Hexadiin-1.6-diols im kristallinen Zustand. *Zeitschrift für Naturforschung B*, 24(7):824–832, July 1969. ISSN 1865-7117. doi: 10.1515/znb-1969-0708.

[3] G. Wegner. Topochemical polymerization of monomers with conjugated triple bonds. *Die Makromolekulare Chemie*, 154(1):35–48, 1972. ISSN 0025-116X. doi: 10.1002/macp.1972.021540103.

[4] B. Tieke, G. Wegner, D. Naegele, and H. Ringsdorf. Polymerization of Tricosa-10,12-diynoic Acid in Multilayers. *Angewandte Chemie International Edition in English*, 15(12):764–765, 1976. ISSN 1521-3773. doi: 10.1002/anie.197607641.

[5] B. Tieke, H. J. Graf, G. Wegner, B. Naegele, H. Ringsdorf, A. Banerjie, D. Day, and J. B. Lando. Polymerization of mono- and multilayer forming diacetylenes. *Colloid and Polymer Science*, 255(6):521–531, June 1977. ISSN 0303-402X, 1435-1536. doi: 10.1007/BF01549738.

[6] B. Tieke, G. Lieser, and G. Wegner. Polymerization of diacetylenes in multilayers. *Journal of Polymer Science: Polymer Chemistry Edition*, 17(6):1631–1644, 1979. ISSN 1542-9369. doi: 10.1002/pol.1979.170170607.

[7] Bernd Tieke. Polymerization of butadiene and butadiyne (diacetylene) derivatives in layer structures. In Henri Benoit, Hans-Joachim Cantow, Gino Dall'Asta, Karel Dušek, John D.

Ferry, Hiroshi Fujita, Manfred Gordon, Gisela Henrici-Olivé, Günter Heublin, Hartwig Höcker, Hans-Henning Kausch, Joseph P. Kennedy, Anthony Ledwith, Seizo Okamura, Salvador Olivé, Charles G. Overberger, Helmut Ringsdorf, Takeo Saegusa, Günther Victor Schulz, William P. Slichter, and John K. Stille, editors, *Analysis/Reactions/Morphology*, volume 71, pages 79–151. Springer Berlin Heidelberg, Berlin, Heidelberg, 1985. ISBN 978-3-540-15482-2 978-3-540-39435-8. doi: 10.1007/3-540-15482-5_8.

[8] Hans-Joachim Cantow, Hans-Joachim Cantow, Gino Dall'Asta, Karel Dušsek, John D. Ferry, Hiroshi Fujita, Manfred Gordon, Gisela Henrici-Olivé, G. Heublein, H. Höcker, Joseph P. Kennedy, Werner Kern, Seizo Okamura, Salvador Olivé, Charles G. Overberger, Takeo Saegusa, Günter Victor Schulz, William P. Slichter, and John K. Stille, editors. *Polydiacetylenes*, volume 63 of *Advances in Polymer Science*. Springer, Berlin, Heidelberg, 1984. ISBN 978-3-540-13414-5 978-3-540-38951-4. doi: 10.1007/BFb0017649.

[9] Tanner J Finney, Sanjai J Parikh, Amir Berman, Darryl Y Sasaki, and Tonya L Kuhl. Characterizing and Tuning the Properties of Polydiacetylene Films for Sensing Applications. *Langmuir*, page 12, November 2021. doi: 10.1021/acs.langmuir.1c02004.

[10] R. W. Carpick, T. M. Mayer, D. Y. Sasaki, and A. R. Burns. Spectroscopic Ellipsometry and Fluorescence Study of Thermochromism in an Ultrathin Poly(diacetylene) Film: Reversibility and Transition Kinetics. *Langmuir*, 16(10):4639–4647, May 2000. ISSN 0743-7463, 1520-5827. doi: 10.1021/la991580k.

[11] Deborah H. Charych, Jon O. Nagy, Wayne Spevak, and Mark D. Bednarski. Direct Colorimetric Detection of a Receptor-Ligand Interaction by a Polymerized Bilayer Assembly. *Science*, 261 (5121):585–588, July 1993. doi: 10.1126/science.8342021.

[12] Johann Nuck and Kaori Sugihara. Mechanism of Polydiacetylene Blue-to-Red Transformation Induced by Antimicrobial Peptides. *Macromolecules*, 53(15):6469–6475, August 2020. ISSN 0024-9297. doi: 10.1021/acs.macromol.0c00718.

[13] Bratati Das, Seiko Jo, Jianlu Zheng, Jiali Chen, and Kaori Sugihara. Recent Progress in Polydiacetylene Mechanochromism. *Nanoscale*, 14(5):1670–1678, 2022. doi: 10.1039/D1NR07129G.

[14] Tanner J. Finney, Skye L. Frank, Michael R. Bull, Robert D. Guy, and Tonya L. Kuhl. Tracking Mechanical Stress and Cell Migration with Inexpensive Polymer Thin-Film Sensors.

Advanced Materials Interfaces, n/a(n/a):2201808, November 2022. ISSN 2196-7350. doi: 10.1002/admi.202201808.

[15] H. Bässler. Photopolymerization of diacetylenes. In Hans-Joachim Cantow, editor, *Polydiacetylenes*, Advances in Polymer Science, pages 1–48, Berlin, Heidelberg, 1984. Springer. ISBN 978-3-540-38951-4. doi: 10.1007/BFb0017650.

[16] Hajime Tanaka, M. A. Gomez, A. E. Tonelli, and M. Thakur. Thermochromic phase transition of a polydiacetylene, poly(ETCD), studied by high-resolution solid-state carbon-13 NMR. *Macromolecules*, 22(3):1208–1215, March 1989. ISSN 0024-9297, 1520-5835. doi: 10.1021/ma00193a036.

[17] G. M. Carter, Y. J. Chen, M. F. Rubner, D. J. Sandman, M. K. Thakur, and S. K. Tripathy. Chapter III-3 - Degenerate Third-Order Nonlinear Optical Susceptibility of Polydiacetylenes. In D. S. Chemla and J. Zyss, editors, *Nonlinear Optical Properties of Organic Molecules and Crystals*, pages 85–120. Academic Press, January 1987. ISBN 978-0-12-170612-8. doi: 10.1016/B978-0-12-170612-8.50005-5.

[18] Hideki Katagiri, Yukihiro Shimoi, and Shuji Abe. A density functional study of backbone structures of polydiacetylene: Destabilization of butatriene structure. *Chemical Physics*, 306 (1):191–200, November 2004. ISSN 0301-0104. doi: 10.1016/j.chemphys.2004.07.033.

[19] Michel Schott. The Colors of Polydiacetylenes: A Commentary. *The Journal of Physical Chemistry B*, 110(32):15864–15868, August 2006. ISSN 1520-6106. doi: 10.1021/jp0638437.

[20] Qun Huo, K. C. Russell, and Roger M. Leblanc. Chromatic Studies of a Polymerizable Diacetylene Hydrogen Bonding Self-Assembly: A "Self-Folding" Process To Explain the Chromatic Changes of Polydiacetylenes. *Langmuir*, 15(11):3972–3980, May 1999. ISSN 0743-7463, 1520-5827. doi: 10.1021/la990025f.

[21] Jean-Sébastien Filhol, Jérôme Deschamps, Sylvain G. Dutremez, Bruno Boury, Thierry Barisien, Laurent Legrand, and Michel Schott. Polymorphs and Colors of Polydiacetylenes: A First Principles Study. *Journal of the American Chemical Society*, 131(20):6976–6988, May 2009. ISSN 0002-7863. doi: 10.1021/ja803768u.

[22] A. Al Choueiry, T. Barisien, J. Holcman, L. Legrand, M. Schott, G. Weiser, M. Balog, J. Deschamps, S. G. Dutremez, and J.-S. Filhol. Twisted polydiacetylene quantum wire:

Influence of conformation on excitons in polymeric quasi-one-dimensional systems. *Physical Review B*, 81(12):125208, March 2010. doi: 10.1103/PhysRevB.81.125208.

[23] Hans Sixl. Spectroscopy of the intermediate states of the solid state polymerization reaction in diacetylene crystals. In Hans-Joachim Cantow, editor, *Polydiacetylenes*, Advances in Polymer Science, pages 49–90, Berlin, Heidelberg, 1984. Springer. ISBN 978-3-540-38951-4. doi: 10.1007/BFb0017651.

[24] H. Menzel, S. Horstmann, M. D. Mowery, M. Cai, and C. E. Evans. Diacetylene polymerization in self-assembled monolayers: Influence of the odd/even nature of the methylene spacer. *Polymer*, 41(22):8113–8119, October 2000. ISSN 0032-3861. doi: 10.1016/S0032-3861(00)00148-8.

[25] David Bloor. Topochemical Polymerization: Diynes. In *Comprehensive Polymer Science and Supplements*, pages 233–249. Elsevier, 1989. ISBN 978-0-08-096701-1. doi: 10.1016/B978-0-08-096701-1.00156-7.

[26] Bernd Tieke and Günter Lieser. Influences of the structure of long-chain diynoic acids on their polymerization properties in Langmuir—Blodgett multilayers. *Journal of Colloid and Interface Science*, 88(2):471–486, August 1982. ISSN 0021-9797. doi: 10.1016/0021-9797(82)90276-4.

[27] Keisuke Kuriyama, Hirotsugu Kikuchi, and Tisato Kajiyama. Chromatic Phase of Polydiacetylene Langmuir-Blodgett Film. *Langmuir*, 14(5):1130–1138, March 1998. ISSN 0743-7463. doi: 10.1021/la970831r.

[28] Keisuke Kuriyama, Hirotsugu Kikuchi, and Tisato Kajiyama. Chromatic Phase and Molecular Packings of Polydiacetylene Langmuir-Blodgett Films. *Chemistry Letters*, 24(12):1071–1072, December 1995. ISSN 0366-7022. doi: 10.1246/cl.1995.1071.

[29] David Day and J. B. Lando. Structure Determination of a Poly(diacetylene) Monolayer. *Macromolecules*, 13(6):1483–1487, November 1980. ISSN 0024-9297. doi: 10.1021/ma60078a024.

[30] David Day and J. B. Lando. Morphology of Crystalline Diacetylene Monolayers Polymerized at the Gas-Water Interface. *Macromolecules*, 13(6):1478–1483, November 1980. ISSN 0024-9297, 1520-5835. doi: 10.1021/ma60078a023.

[31] C. Gourier, M. Alba, A. Braslau, J. Daillant, M. Goldmann, C. M. Knobler, F. Rieutord, and G. Zalczer. Structure and Elastic Properties of 10-12 Pentacosadiyonic Acid Langmuir Films. *Langmuir*, 17(21):6496–6505, October 2001. ISSN 0743-7463. doi: 10.1021/la001799v.

[32] Gonzalo García-Espejo, Marta Pérez-Morales, Michel Goldmann, María T. Martín-Romero, Juan J. Giner-Casares, and Luis Camacho. Organization and structure of mixed Langmuir films composed of polydiacetylene and hemicyanine. *Journal of Colloid and Interface Science*, 508:583–590, December 2017. ISSN 0021-9797. doi: 10.1016/j.jcis.2017.08.069.

[33] H. D Göbel, K Kjaer, J Als-Nielsen, and H Möhwald. Reorientation of aliphatic tails during the photopolymerization of a diacetylenic lipid. *Thin Solid Films*, 179(1):41–52, November 1989. ISSN 0040-6090. doi: 10.1016/0040-6090(89)90163-6.

[34] Yevgeniy Lifshitz, Yuval Golan, Oleg Konovalov, and Amir Berman. Structural Transitions in Polydiacetylene Langmuir Films. *Langmuir*, 25(8):4469–4477, April 2009. ISSN 0743-7463. doi: 10.1021/la8029038.

[35] Alfred Yeboah, David Sowah-Kuma, Wei Bu, and Matthew F. Paige. Single-Molecule Fluorescence Spectroscopy of Phase-Separated 10,12-Pentacosadynoic Acid Films. *The Journal of Physical Chemistry B*, 125(15):3953–3962, April 2021. ISSN 1520-6106. doi: 10.1021/acs.jpcb.1c00951.

[36] Robert F. Fischetti, Mark Filipkowski, Anthony F. Garito, and J. Kent Blasie. Profile structures of ultrathin periodic and nonperiodic multilayer films containing a disubstituted diacetylene by high-resolution x-ray diffraction. *Physical Review B*, 37(9):4714–4726, March 1988. doi: 10.1103/PhysRevB.37.4714.

[37] Yu Shufang, Zhou Huilin, and He Pingsheng. X-ray diffraction analysis of 10,12-pentacosadiynoic acid Langmuir-Blodgett films during polymerization. *Journal of Materials Science*, 34(13): 3149–3154, July 1999. ISSN 1573-4803. doi: 10.1023/A:1004617520047.

[38] Darryl Y. Sasaki, Robert W. Carpick, and Alan R. Burns. High Molecular Orientation in Mono- and Trilayer Polydiacetylene Films Imaged by Atomic Force Microscopy. *Journal of Colloid and Interface Science*, 229(2):490–496, September 2000. ISSN 0021-9797. doi: 10.1006/jcis.2000.7043.

[39] R. W. Carpick, D. Y. Sasaki, and A. R. Burns. First Observation of Mechanochromism at the Nanometer Scale. *Langmuir*, 16(3):1270–1278, February 2000. ISSN 0743-7463. doi: 10.1021/la990706a.

[40] Anna Lio, Anke Reichert, Dong June Ahn, Jon O. Nagy, Miquel Salmeron, and Deborah H. Charych. Molecular Imaging of Thermochromic Carbohydrate-Modified Polydiacetylene Thin

Films. *Langmuir*, 13(24):6524–6532, November 1997. ISSN 0743-7463. doi: 10.1021/la970406y.

[41] Hemasiri Vithana, David Johnson, Raymond Shih, and J. Adin Mann. Characterization of 12-8-diacetylene Langmuir-Blodgett films by scanning-force microscopy. *Physical Review E*, 51 (1):454–461, January 1995. ISSN 1063-651X, 1095-3787. doi: 10.1103/PhysRevE.51.454.

[42] O. Marti, H. O. Ribi, B. Drake, T. R. Albrecht, C. F. Quate, and P. K. Hansma. Atomic Force Microscopy of an Organic Monolayer. *Science, New Series*, 239(4835):50–52, 1988.

[43] Barbara M. Goettgens, Ralf W. Tillmann, Manfred Radmacher, and Hermann E. Gaub. Molecular order in polymerizable Langmuir-Blodgett films probed by microfluorescence and scanning force microscopy. *Langmuir*, 8(7):1768–1774, July 1992. ISSN 0743-7463, 1520-5827. doi: 10.1021/la00043a014.

[44] Masazo Niwa, Syunsuke Shibahara, and Nobuyuki Higashi. Diacetylenic monolayers containing a boronic acid moiety form a chemically and thermally stable poly(diacetylene) film on water. *Journal of Materials Chemistry*, 10(12):2647–2651, 2000. doi: 10.1039/B004371K.

[45] Masazo Niwa, Takashi Sawada, and Nobuyuki Higashi. Surface Monolayers of Polymeric Amphiphiles Carrying a Copolymer Segment Composed of Phenylboronic Acid and Amine. Interaction with Saccharides at the Air-Water Interface. *Langmuir*, 14(14):3916–3920, July 1998. ISSN 0743-7463. doi: 10.1021/la971261y.

[46] Songyi Lee, Kyung Mi Lee, Minji Lee, and Juyoung Yoon. Polydiacetylenes Bearing Boronic Acid Groups as Colorimetric and Fluorescence Sensors for Cationic Surfactants. *ACS Applied Materials & Interfaces*, 5(11):4521–4526, June 2013. ISSN 1944-8244. doi: 10.1021/am3030245.

[47] Shiwei Gu, Chang Guo, Hui Wang, Guangjun Tian, Suying Xu, and Leyu Wang. A Versatile Strategy for Surface Functionalization of Hydrophobic Nanoparticle by Boronic Acid Modified Polymerizable Diacetylene Derivatives. *Frontiers in Chemistry*, 7, 2019. ISSN 2296-2646.

[48] Volker Enkelmann. Structural aspects of the topochemical polymerization of diacetylenes. In Hans-Joachim Cantow, editor, *Polydiacetylenes*, Advances in Polymer Science, pages 91–136, Berlin, Heidelberg, 1984. Springer. ISBN 978-3-540-38951-4. doi: 10.1007/BFb0017652.

[49] Peter S. Pershan and Mark Schlossman. *Liquid Surfaces and Interfaces: Synchrotron X-ray Methods*. Cambridge University Press, Cambridge, 2012. ISBN 978-0-521-81401-0. doi: 10.1017/CBO9781139045872.

[50] Brown, Fox, Maslen, O'Keefe, and Willis. Chapter 6.1. Intensity of diffracted intensities. In *International Tables for Crystallography*, volume C, pages 554–595. International Union of Crystallography, two thousand, sixth edition, July 2019. ISBN 978-1-119-46870-7.

[51] E. B. Watkins, C. E. Miller, J. Majewski, and T. L. Kuhl. Membrane texture induced by specific protein binding and receptor clustering: Active roles for lipids in cellular function. *Proceedings of the National Academy of Sciences*, 108(17):6975–6980, April 2011. doi: 10.1073/pnas.1014579108.

[52] Franck Leveiller, Didier Jacquemain, Leslie Leiserowitz, Kristian Kjaer, and Jens Als-Nielsen. Toward a determination at near atomic resolution of two-dimensional crystal structures of amphiphilic molecules on the water surface: A study based on grazing incidence synchrotron x-ray diffraction and lattice energy calculations. *The Journal of Physical Chemistry*, 96(25): 10380–10389, December 1992. ISSN 0022-3654. doi: 10.1021/j100204a051.

[53] Kristian Kjaer. Some simple ideas on X-ray reflection and grazing-incidence diffraction from thin surfactant films. *Physica B: Condensed Matter*, 198(1-3):100–109, April 1994. ISSN 09214526. doi: 10.1016/0921-4526(94)90137-6.

[54] Magdalena Truger, Otello M. Roscioni, Christian Röthel, Dominik Kriegner, Clemens Simbrunner, Rizwan Ahmed, Eric D. Głowacki, Josef Simbrunner, Ingo Salzmann, Anna Maria Coclite, Andrew O. F. Jones, and Roland Resel. Surface-Induced Phase of Tyrian Purple (6,6′-Dibromoindigo): Thin Film Formation and Stability. *Crystal Growth & Design*, 16(7): 3647–3655, July 2016. ISSN 1528-7483, 1528-7505. doi: 10.1021/acs.cgd.6b00104.

[55] Josef Simbrunner, Ingo Salzmann, and Roland Resel. Indexing of grazing-incidence X-ray diffraction patterns. *Crystallography Reviews*, 0(0):1–19, March 2023. ISSN 0889-311X. doi: 10.1080/0889311X.2023.2187051.

[56] Josef Simbrunner, Clemens Simbrunner, Benedikt Schrode, Christian Röthel, Natalia Bedoya-Martinez, Ingo Salzmann, and Roland Resel. Indexing of grazing-incidence X-ray diffraction patterns: The case of fibre-textured thin films. *Acta Crystallographica Section A Foundations and Advances*, 74(4):373–387, July 2018. ISSN 2053-2733. doi: 10.1107/S2053273318006629.

[57] Torben R. Jensen and Kristian Kjaer. Structural Properties and Interactions of Thin Films at the Air-Liquid Interface Explored by Synchrotron X-Ray Scattering. In *Studies in Interface*

Science, volume 11, pages 205–254. Elsevier, 2001. ISBN 978-0-444-50948-2. doi: 10.1016/S1383-7303(01)80028-4.

[58] Ivan Kuzmenko, Hanna Rapaport, Kristian Kjaer, Jens Als-Nielsen, Isabelle Weissbuch, Meir Lahav, and Leslie Leiserowitz. Design and Characterization of Crystalline Thin Film Architectures at the Air-Liquid Interface: Simplicity to Complexity. *Chemical Reviews*, 101(6): 1659–1696, June 2001. ISSN 0009-2665. doi: 10.1021/cr990038y.

[59] S. M. Danauskas, D. Li, M. Meron, B. Lin, and K. Y. C. Lee. Stochastic fitting of specular X-ray reflectivity data using StochFit. *Journal of Applied Crystallography*, 41(6):1187–1193, December 2008. ISSN 0021-8898. doi: 10.1107/S0021889808032445.

[60] David Nečas and Petr Klapetek. Gwyddion: An open-source software for SPM data analysis. *Open Physics*, 10(1):181–188, February 2012. ISSN 2391-5471. doi: 10.2478/s11534-011-0096-2.

[61] Arthur D. Edelstein, Mark A. Tsuchida, Nenad Amodaj, Henry Pinkard, Ronald D. Vale, and Nico Stuurman. Advanced methods of microscope control using μManager software. *Journal of Biological Methods*, 1(2):e10, November 2014. ISSN 2326-9901. doi: 10.14440/jbm.2014.36.

[62] Henry Pinkard, Nico Stuurman, Ivan E. Ivanov, Nicholas M. Anthony, Wei Ouyang, Bin Li, Bin Yang, Mark A. Tsuchida, Bryant Chhun, Grace Zhang, Ryan Mei, Michael Anderson, Douglas P. Shepherd, Ian Hunt-Isaak, Raymond L. Dunn, Wiebke Jahr, Saul Kato, Loïc A. Royer, Jay R. Thiagarajah, Kevin W. Eliceiri, Emma Lundberg, Shalin B. Mehta, and Laura Waller. Pycro-Manager: Open-source software for customized and reproducible microscope control. *Nature Methods*, 18(3):226–228, March 2021. ISSN 1548-7105. doi: 10.1038/s41592-021-01087-6.

[63] M. J. Frisch, G. W. Trucks, H. B. Schlegel, G. E. Scuseria, M. A. Robb, J. R. Cheeseman, G. Scalmani, V. Barone, G. A. Petersson, H. Nakatsuji, X. Li, M. Caricato, A. V. Marenich, J. Bloino, B. G. Janesko, R. Gomperts, B. Mennucci, H. P. Hratchian, J. V. Ortiz, A. F. Izmaylov, J. L. Sonnenberg, D. Williams-Young, F. Ding, F. Lipparini, F. Egidi, J. Goings, B. Peng, A. Petrone, T. Henderson, D. Ranasinghe, V. G. Zakrzewski, J. Gao, N. Rega, G. Zheng, W. Liang, M. Hada, M. Ehara, K. Toyota, R. Fukuda, J. Hasegawa, M. Ishida, T. Nakajima, Y. Honda, O. Kitao, H. Nakai, T. Vreven, K. Throssell, J. A. Montgomery, Jr., J. E. Peralta, F. Ogliaro, M. J. Bearpark, J. J. Heyd, E. N. Brothers, K. N. Kudin, V. N. Staroverov, T. A. Keith, R. Kobayashi, J. Normand, K. Raghavachari, A. P. Rendell, J. C.

Burant, S. S. Iyengar, J. Tomasi, M. Cossi, J. M. Millam, M. Klene, C. Adamo, R. Cammi, J. W. Ochterski, R. L. Martin, K. Morokuma, O. Farkas, J. B. Foresman, and D. J. Fox. Gaussian16 Revision C.01, 2016.

[64] C. E. Miller, J. Majewski, E. B. Watkins, and T. L. Kuhl. Part I: An X-Ray Scattering Study of Cholera Toxin Penetration and Induced Phase Transformations in Lipid Membranes. *Biophysical Journal*, 95(2):629–640, July 2008. ISSN 0006-3495. doi: 10.1529/biophysj.107.120725.

[65] Chad E. Miller, Jaroslaw Majewski, Thomas Gog, and Tonya L. Kuhl. Grazing incidence diffraction of cadmium arachidate multilayers at the solid-liquid interface. *Zeitschrift für Kristallographie - Crystalline Materials*, 220(12):987–992, December 2005. ISSN 2196-7105. doi: 10.1524/zkri.2005.220.12.987.

[66] P. Tippmann-Krayer, R. M. Kenn, and H. Möhwald. Thickness and temperature dependent structure of Cd arachidate Langmuir-Blodgett films. *Thin Solid Films*, 210–211:577–582, April 1992. ISSN 0040-6090. doi: 10.1016/0040-6090(92)90346-D.

[67] Satish Vitta, T. H. Metzger, and S. S. Major. Structural assembly of Cd-arachidate molecules in multilayers. *The Journal of Chemical Physics*, 111(24):11088–11094, December 1999. ISSN 0021-9606, 1089-7690. doi: 10.1063/1.480467.

[68] Robert W. Carpick, Darryl Y. Sasaki, Matthew S. Marcus, M. A. Eriksson, and Alan R. Burns. Polydiacetylene films: A review of recent investigations into chromogenic transitions and nanomechanical properties. *Journal of Physics: Condensed Matter*, 16(23):R679–R697, May 2004. ISSN 0953-8984. doi: 10.1088/0953-8984/16/23/R01.

[69] R. Volinsky, F. Gaboriaud, A. Berman, and R. Jelinek. Morphology and Organization of Phospholipid/Diacetylene Langmuir Films Studied by Brewster Angle Microscopy and Fluorescence Microscopy. *The Journal of Physical Chemistry B*, 106(36):9231–9236, September 2002. ISSN 1520-6106. doi: 10.1021/jp020393j.

[70] Yevgeniy Lifshitz, Alexander Upcher, Olga Shusterman, Baruch Horovitz, Amir Berman, and Yuval Golan. Phase transition kinetics in Langmuir and spin-coated polydiacetylene films. *Phys. Chem. Chem. Phys.*, 12(3):713–722, 2010. ISSN 1463-9076, 1463-9084. doi: 10.1039/B915527A.

[71] Yeol Kyo Choi, Sang Yup Lee, and Dong June Ahn. Hyperconjugation-induced chromism in linear responsive polymers. *Journal of Materials Chemistry C*, 7(42):13130–13138, October

2019. ISSN 2050-7534. doi: 10.1039/C9TC03204E.

[72] Jonathan Rivnay, Stefan C. B. Mannsfeld, Chad E. Miller, Alberto Salleo, and Michael F. Toney. Quantitative Determination of Organic Semiconductor Microstructure from the Molecular to Device Scale. *Chemical Reviews*, 112(10):5488–5519, October 2012. ISSN 0009-2665. doi: 10.1021/cr3001109.

[73] Susumu Yamada and Yuhei Shimoyama. Molecular Orientation and Growth Direction of Polydiacetylene Single-Crystal Monolayer at Air-Water Interface. *Japanese Journal of Applied Physics*, 35(Part 1, No. 8):4480–4485, August 1996. ISSN 0021-4922, 1347-4065. doi: 10.1143/JJAP.35.4480.

[74] Samira Agbolaghi and Sahar Zenoozi. A comprehensive review on poly(3-alkylthiophene)-based crystalline structures, protocols and electronic applications. *Organic Electronics*, 51:362–403, December 2017. ISSN 1566-1199. doi: 10.1016/j.orgel.2017.09.038.

[75] Varuni Dantanarayana, Jack Fuzell, Dingqi Nai, Ian E. Jacobs, He Yan, Roland Faller, Delmar Larsen, and Adam J. Moule. Put Your Backbone into It: Excited-State Structural Relaxation of PffBT4T-2DT Conducting Polymer in Solution. *The Journal of Physical Chemistry C*, 122 (12):7020–7026, March 2018. ISSN 1932-7447. doi: 10.1021/acs.jpcc.8b01356.

[76] Xin Huang, Siguang Jiang, and Minghua Liu. Metal Ion Modulated Organization and Function of the Langmuir-Blodgett Films of Amphiphilic Diacetylene: Photopolymerization, Thermochromism, and Supramolecular Chirality. *The Journal of Physical Chemistry B*, 109(1): 114–119, January 2005. ISSN 1520-6106. doi: 10.1021/jp046500m.

[77] Si Wu, Libin Pan, Youju Huang, Ni Yang, and Qijin Zhang. Co-assemblies of polydiacetylenes and metal ions for solvent sensing. *Soft Matter*, 14(33):6929–6937, 2018. doi: 10.1039/C8SM01282B.

[78] Yevgeniy Lifshitz, Alexander Upcher, Anatoly Kovalev, Dmitry Wainstein, Alexander Rashkovsky, Leila Zeiri, Yuval Golan, and Amir Berman. Zinc modified polydiacetylene Langmuir films. *Soft Matter*, 7(19):9069–9077, September 2011. ISSN 1744-6848. doi: 10.1039/C1SM05904A.

[79] Alexander Upcher, Yevgeniy Lifshitz, Leila Zeiri, Yuval Golan, and Amir Berman. Effect of metal cations on polydiacetylene Langmuir films. *Langmuir: the ACS journal of surfaces and*

colloids, 28(9):4248–4258, March 2012. ISSN 1520-5827. doi: 10.1021/la204735t.

[80] Troy E. Wilson, Wayne Spevak, Deborah H. Charych, and Mark D. Bednarski. Enzymic Modification and X-ray Photoelectron Spectroscopy Analysis of a Functionalized Polydiacetylene Thin Film. *Langmuir*, 10(5):1512–1516, May 1994. ISSN 0743-7463, 1520-5827. doi: 10.1021/la00017a031.

APPENDIX A

Supporting Information for Chapter 4

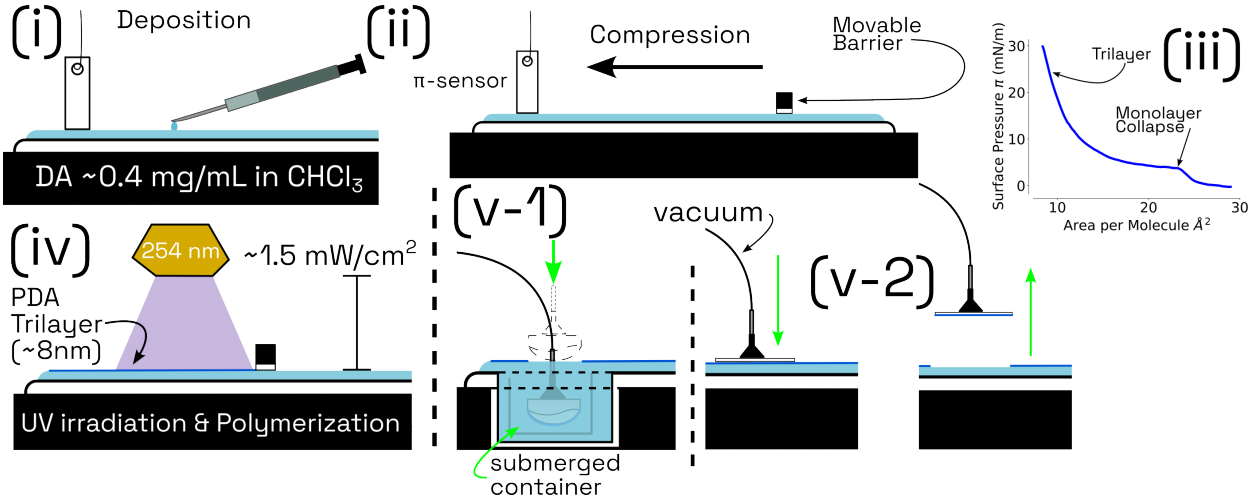

FIGURE A.1. Schematic of PDA Langmuir film assembly, see below for details.

The Langmuir trough was cleaned beforehand with chloroform and filled with 18.2 MΩ cm DI water from a Barnstead Nanopure. If salts were added, the subphase was continuously stirred with a tiny stir bar and integrated magnetic stirrer.

(i) Monomer diacetylenes (DAs) dissolved in chloroform (0.4 mg mL^{-1}) were deposited dropwise onto the surface of a Nima 611D Langmuir trough.

(ii) After allowing for solvent evaporation ($\sim$ 15 minutes), the film was compressed at a rate of 20 cm^2/min to a target pressure of approximately 20-23 mN m^{-1} depending on the diacetylene. The Wilhemly plate is noted as "π-sensor".

(iii) Pressure-Area (π-A) of 10,12 Pentacosadiynoic acid (PCDA). PCDA forms an unstable monolayer and readily collapses at low surface pressure ($\sim$ 5 mN m^{-1}). Continued compression yields a stable trilayer at $\sim$ 20 mN m^{-1}.

(iv) After formation of a stable trilayer, the barrier was stopped and the film was exposed to UV light, inducing polymerization. To prevent deposition stress induced mechanochromism, the film was lightly polymerized to $\sim$ 20% of the optimal dose to produce maximally blue phase PDA. The UV light used in these experiments was regularly calibrated and had an intensity of 1500 $\pm$ 230 $\mu W/cm^2$. Mechanical stress from deposition onto a solid support

(such as a glass coverslip or SFA disk) can induce mechanochromism. Therefore, the film should be only lightly polymerized before deposition. After deposition, the film was further exposed to UV light to finish polymerizing and produce optimally blue phase PDA.

(v-1) **Deposition option 1:** traditional Langmuir-Schaefer where the substrate is transferred through the interface with a horizontal orientation. This technique was used for SFA disks. The SFA disk was immobilized using a vacuum line and then mounted to the trough dipper, and dipped at a rate of 0.7 mm / min. After the surface of the disk was through the air-water interface, the disk was released into a submerged container for retrieval.

(v-2) Deposition option 2: "Lazy" Langmuir-Schaefer. Polymerized DA films are extremely stiff and solid, hence gently pressing a clean glass coverslip to the interface and then leaving it at the air water interface for a 10-20 seconds before gently removing leads to acceptable film transfer. The films were then blown dry under a gentle stream of nitrogen.

Traditional Langmuir-Blodgett (vertical substrate, orthogonal to the film) does not yield good PDA film transfer due to the large, stiff polymerized domains. However, Langmuir-Blodgett deposition with the substrate at an angle of $\sim 45^\circ$ yields acceptable film transfer.

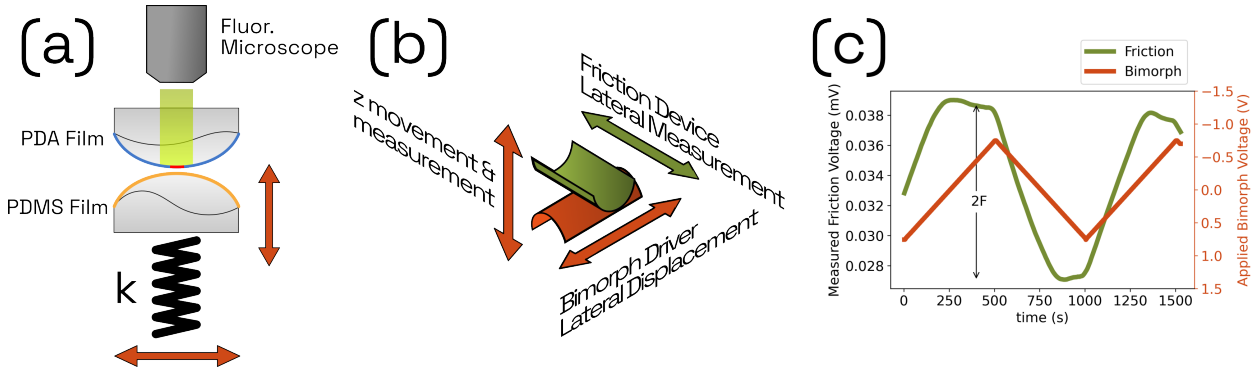

FIGURE A.2. Diagram of SFA experiments, see below for details.

(a) Cross Section of the Surface Forces Apparatus (SFA). The SFA geometry was composed of two cross oriented plano-cylindrical glass lenses often referred to as SFA disks. PDA films were deposited onto the top disk. A 20 µm PDMS film was deposited onto the lower SFA disk. The lower disk was mounted onto a helical spring attached to a motor and encoder for up/down displacement and cantilever springs to measure applied normal force. The SFA was mounted underneath a fluorescent microscope to enable direct measurement of the fluorescence in response to applied normal and lateral forces.

(b) Cross cylinder geometry of the SFA. The lower disk (orange) was mounted to normal force springs and bimorph driver to enable lateral displacement of the lower surface. The bimorph driver was composed of four piezoelectric sheets that apply a uniform displacement in response to an applied voltage from a connected function generator. The top disk (green) was mounted on the friction device, a disk holder with semiconductor strain gauges. These strain gauges provide direct readout of the friction force when calibrated.

(c) Sample of friction force data from an SFA experiment. Applied voltage from an attached function generator drives the bimorph (orange line). The friction response was collected from the semiconductor strain gauges (green line).

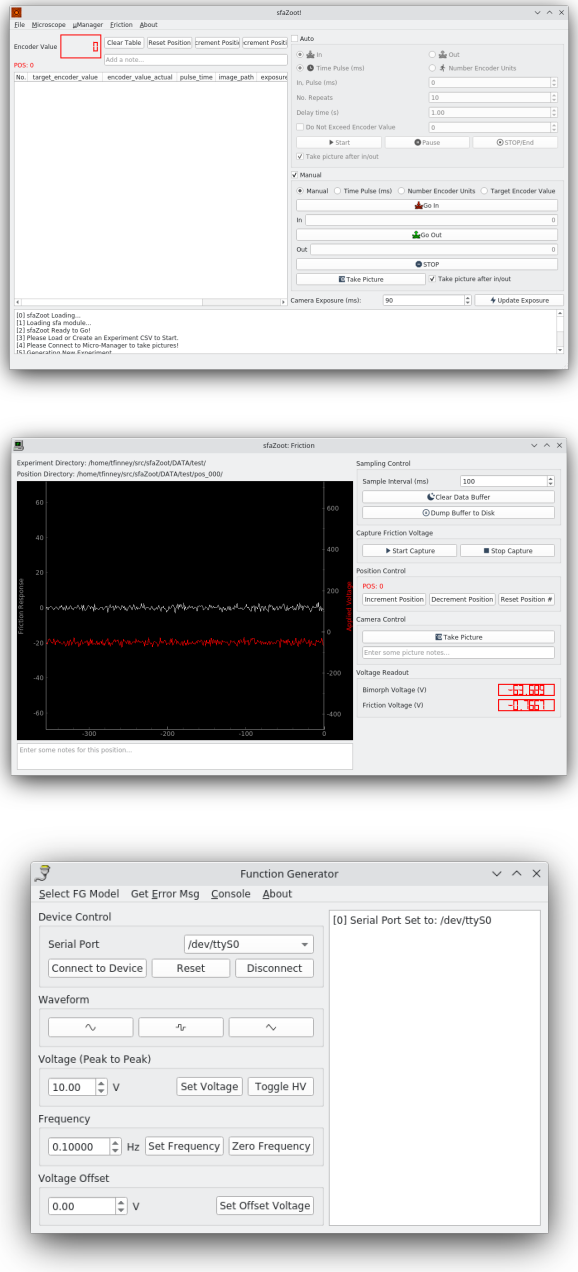

FIGURE A.3. Screenshots of software developed to measure friction force and fluorescent readout. Software was coupled to micro-manager using pycromanager to capture images from the fluorescent microscope. **Top:** Primary control window, enables normal displacement (measurement of normal force) and capture of camera image (contact area). **center:** Friction measurement setup. Function generator for the bimorph and friction device are connected to the computer through a signal conditioning amplifier and voltage sensors, enabling real time measurement of friction force. **Bottom:** Automated control of function generator.

A.2.1. SFA Data Collection & Analysis.

A.2.1.1. *SFA Friction Experiment Overview.*

(1) SFA with PDA and PDMS disks was placed underneath a custom fluorescent microscope.

(2) SFA disks were brought into contact at zero applied load.

(3) The bottom disk was laterally displaced using the bimorph and function generator. A range of displacements was applied, and the fluorescent response was measured. The minimum displacement necessary to induce wide-scale fluorescence was determined.

(4) These experiments were repeated using the friction device attachment to measure the associated friction forces. Due to conflicts between the geometry of the friction device and the fluorescence microscope objectives, simultaneous friction measurement and fluorescent readout was not possible.

(5) These experiments were repeated in triplicate for each different DA.

(6) Friction forces and stresses were calculated by combining measurements of the contact area and the calibrated voltage traces as shown above, Figure A.2.

A.3. Slime Mold Experiments

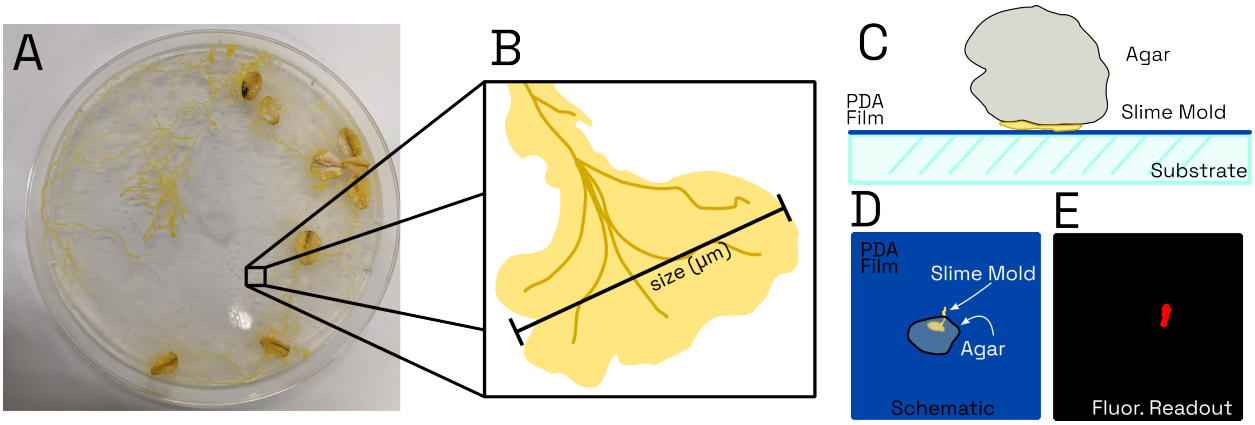

FIGURE A.4. Schematic of experiments with *Physarum polycephalum*.

(A) *Physarum* was cultured in a 2% Agar petri dish with oat flakes.

(B) A small portion of the slime mold was excised using a sharp sterile knife. The size of the slime mold as described in the main manuscript was defined by the width of the spreading plasmodium.

(C) This small portion was placed with the slime mold facing down onto a PDA film coated coverslip.

(D) The slime mold begins to migrate on the PDA film.

(E) This migration may induce fluorescence on the PDA film. Slime molds were imaged with bright field and fluorescent microscopy at regular intervals of 6-12 hours.

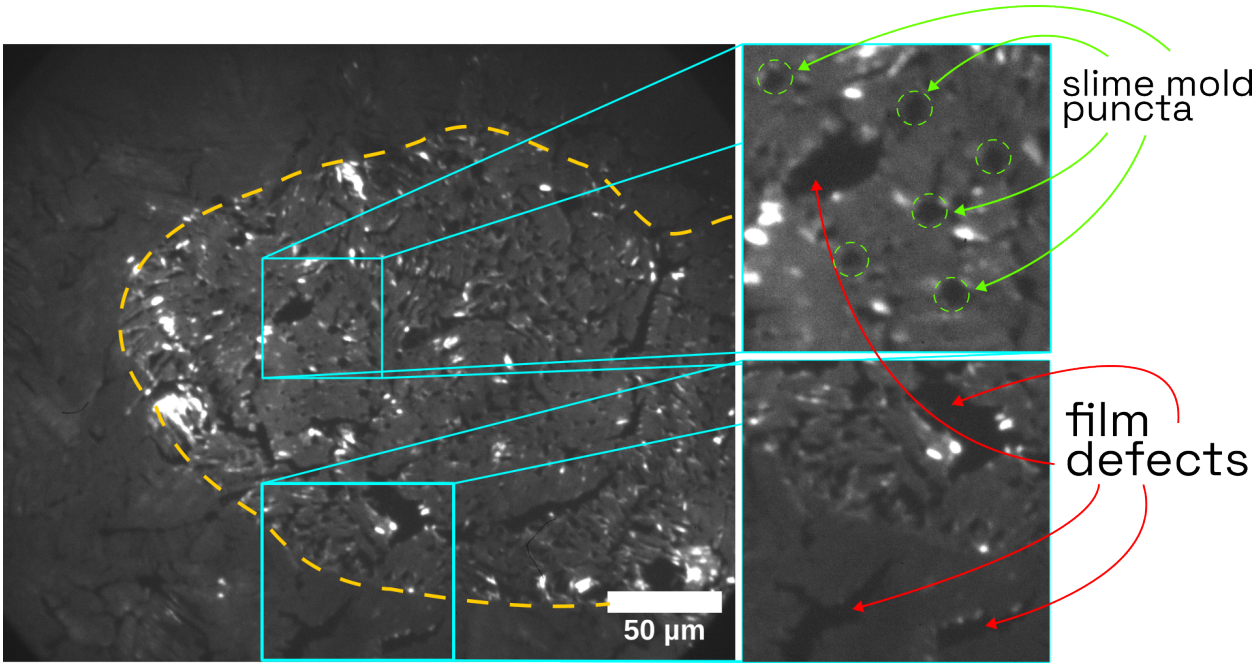

FIGURE A.5. Comparison of slime mold induced puncta and inherent cracks and defects within a PDA Film. PDA film cracks tend to be jagged, square and follow polymer domains. Slime mold puncta are relatively circular and are distributed everywhere within the area which a slime mold migrated. The dashed yellow line shows the extent of the slime mold migration.

A.3.1. Analysis of Slime Mold Puncta.

- Puncta were identified due to their proximity to slime molds and relative circularity compared to film defects in the PDA film.
- Particle counting algorithms in ImageJ and Python were employed to quantify the size distribution.

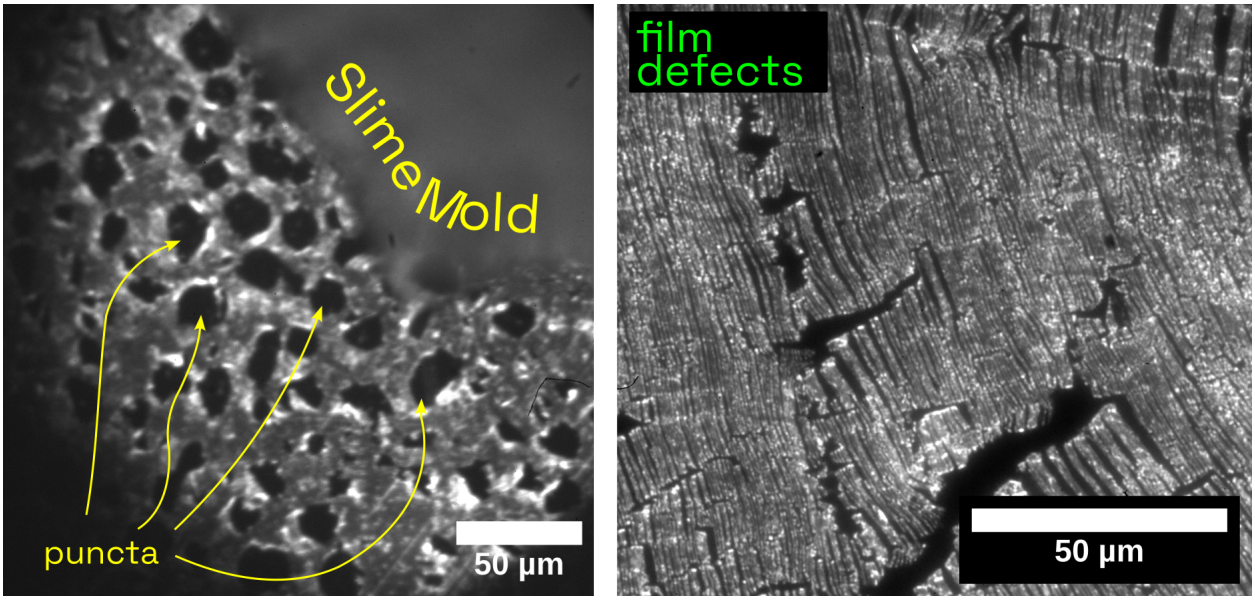

FIGURE A.6. High magnification fluorescent micrographs. **Left:** Slime mold & puncta. Puncta appear relatively circular, often with a fluorescent halo that we hypothesize was caused by ripped during film removal. **Right:** PDA film will lots of deposition defects. These defects follow polymer domain orientation and often appear jagged and linear. Note that most films used in these experiments were largely defect free.

APPENDIX B

Supporting Information for Chapter 5

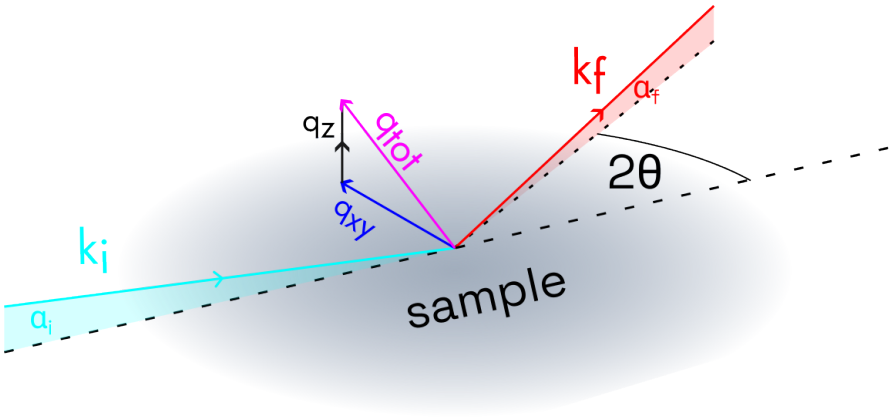

FIGURE B.1. Grazing Incidence Diffraction (GIXD) Geometry

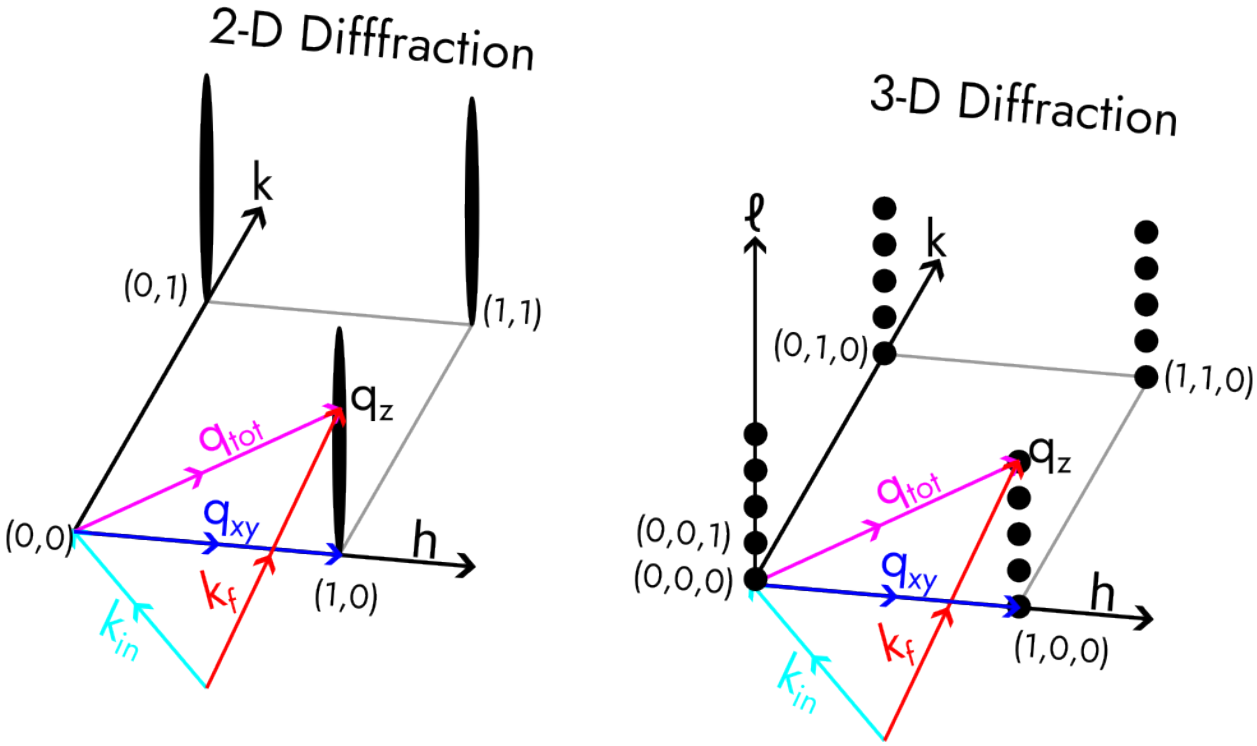

FIGURE B.2. Bragg Rod vs Bragg Peak Geometry, figure adapted from [1] with permission.

B.1.1. Grazing Incidence X-ray Diffraction Geometry. The horizontal, in-plane scattering vector can be represented mathematically as

$$q_{xy} = k\sqrt{\cos^2(\alpha_i) + \cos^2(\alpha_f) - 2\cos(\alpha_i)\cos(\alpha_f)\cos(2\theta_{hor})} \tag{B.1}$$

The vertical, or out-of plane scattering vector is represented mathematically as

$$q_z = k\left(\sin\alpha_i + \sin(\alpha_f)\right) \tag{B.2}$$

More details of the scattering geometry is described by Kjaer [1–3].

B.1.2. Indexing and Analysis of Monomeric Films. Bragg peaks were fit using Gaussian lineshapes. Unpolymerized, monomeric films have one observable reflection, indicating centered rectangular packing (or equivalently hexagonal packing) [2–4]. The sole reflection was indexed to the degenerate indices: [1,1], [1,-1] and [0,2]. Indexing and refinement of the unit cell assumed the general oblique case (equation B.3) and then a minimization routine was implemented using the lmfit library [5]. The resulting two-dimensional unit cell is shown in Figure B.3, where a and b correspond to the in plane unit cell vectors and γ is the angle between them.

$$q_{xy} = \frac{2\pi}{\sin(\gamma)}\left[\frac{h^2}{a^2} + \frac{k^2}{b^2} - 2\frac{hk}{ab}\cos(\gamma)\right]^{1/2} \tag{B.3}$$

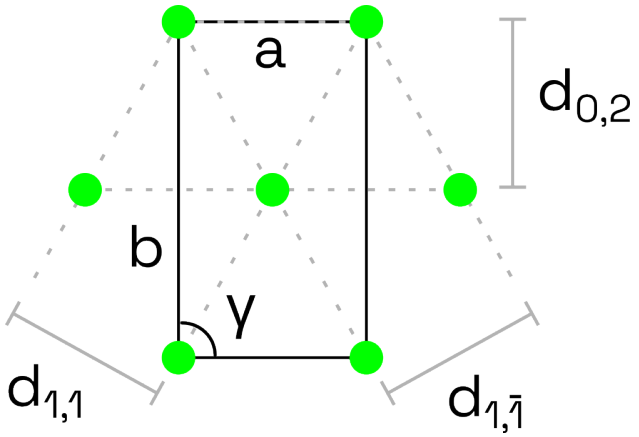

FIGURE B.3. centered rectangular unit cell

The out-of-plane structure is more complicated. Analysis via a traditional Bragg rod approach did not yield reasonable results. Rather the Bragg Rod suggest an ordered multilayer. Peaks in q_z were fit using Lorentzian lineshapes and following Truger et al., were indexed to a triclinic unit cell via equations B.4 - B.8. Values for ℓ were chosen to produce a value for c closest to the molecular length of the diacetylene (approximately 30 Å). This refinement further lead to tilt angles α and β [6–8].

$$\begin{pmatrix} q_{xy,0}^2 \\ q_{xy,1}^2 \\ q_{xy,2}^2 \end{pmatrix} = \begin{pmatrix} h_0^2 & k_0^2 & -2h_0k_0 \\ h_1^2 & k_1^2 & -2h_1k_1 \\ h_2^2 & k_2^2 & -2h_2k_2 \end{pmatrix} \times \begin{pmatrix} \left[\frac{2\pi}{a\sin\gamma}\right] \\ \left[\frac{2\pi}{b\sin\gamma}\right] \\ \left[\frac{2\pi}{a\sin\gamma}\frac{2\pi}{b\sin\gamma}\cos\gamma\right] \end{pmatrix} \tag{B.4}$$

$$\begin{pmatrix} q_{z,0} \\ q_{z,1} \\ q_{z,2} \end{pmatrix} = \begin{pmatrix} -h_0 & -k_0 & l_0 \\ -h_1 & -k_1 & l_1 \\ -h_2 & -k_2 & l_2 \end{pmatrix} \times \begin{pmatrix} \frac{2\pi}{a\sin(\gamma)}\delta \\ \frac{2\pi}{b\sin(\gamma)}\mu \\ \frac{2\pi}{c\sin(\gamma)}\epsilon \end{pmatrix} \tag{B.5}$$

$$\mu = \frac{\cos\alpha - \cos\beta\cos\gamma}{\sin\gamma\sin\epsilon} \tag{B.6}$$

$$\delta = \frac{\cos\beta - \cos\alpha\cos\gamma}{\sin\gamma\sin\epsilon} \tag{B.7}$$

$$\sin\epsilon = \frac{\sqrt{1 - \cos\alpha^2 - \cos\beta^2 - \cos^2\gamma + 2\cos\alpha\cos\beta\cos\gamma}}{\sin\gamma} \tag{B.8}$$

B.1.3. Analysis of PDA Polymer films.

B.1.3.1. *Indexing and Assignment of Bragg Peaks.* Following Jensen and Kjaer, the two-dimensional lattice was indexed using equation B.3, the general equation for an oblique two dimensional lattice, and the following steps [4].

(1) The reciprocal space map was integrated along q_z yielding Intensity, I vs q_{xy}.

(2) Each major peak was fit using a Gaussian Lineshape.

(3) We assumed that the lattice is a centered rectangular lattice, and therefore the primary Bragg peaks arise from the planes: $[h, k] = \{[1, 1], [1, -1], [0, 2]\}$. In the case of red phase, the same reflections are assumed and a distorted centered rectangular / centered oblique lattice is used.

(4) Reflections were assigned to the peaks via the following process:

   (a) reasonable guesses were made for a, b, γ

   (b) Permutations of q_{xy} were computed and Equation B.3 was evaluated.

   (c) The error is minimized using a sum of squared differences using `lmfit.Minimize` with the `BFGS` algorithm.

   (d) the permutation with lowest χ^2 was selected. Equation B.4 was used to validate and check for reasonbleness.

This approach yields physically reasonbaly solutions for the packing and unit cell dimensions: a, b, γ. In many cases, all reflections are degenerate, yielding a unit cell with $\gamma = 90°$. Red Phase PDA is oblique as the reflections split into three unique q_{xy}

B.1.3.2. *Analysis of Bragg Rod Profiles.* Red and Blue Phase PDA appear to lack significant inter-layer registry / order as evidenced by the relatively short coherence length in the z-direction, see Tables in main text. Hence, only tilt information can be derived from the Bragg rods, and the system can be modeled as a single layer [2, 9]. Further complicating the analysis however is (1) the presence of a polymer backbone imposing additional restrictions on the structure of the polymer films, (2) some interlayer registry that is difficult to parse out due to smearing between the various peaks. Analysis using a typical structure and form factor derived from an assumed sinc and Bessel

function profile did not yield promising results [1, 10] Rather a "points-on-a-line" approach was used to determine the molecular tilts.

Following Watkins et al., Leveiller et al., and Kuzmenko et al., we assume that the structure can be represented by a series of points corresponding to the atomic centers of each atom in the fatty acid tails multiplied by the atomic form factor of carbon [10–12]. The spacing between points was assigned to initially be 1.249 Å, with a scaling factor to allow for minor variations. The scaling factor was bounded to ±0.1 The structure factor for a given atom j at indexed reflection hk can then be represented as

$$F_j = f_j e^{iq_{hk}(ax_j + by_j)} e^{iq_z z_j} \tag{B.9}$$

The structure factor is then summed for all atoms in the unit cell

$$F_{hk}(q_z) = \sum_j F_j \tag{B.10}$$

f_j : Atomic form factor as defined by equation B.13
q_{hk} : in-plane reciprocal space scattering vector, q_{xy} indexed to a given hk reflection
a,b : in-plane unit cell parameters
x,y,z : coordinates of each atom in the unit cell
q_z : out-of-plane scattering vector

The atomic form factor [13, 14] for atom j is given by:

$$q_{tot} = \sqrt{q_{xy,j}^2 + q_{z,j}^2} \tag{B.11}$$

$$f_j = f(q_{tot}) \tag{B.12}$$

$$f(q_{tot}) = \sum_{i=1}^{4} a_i \exp\left(-b_i \left(\frac{q_{tot}}{4\pi}\right)^2\right) + c \tag{B.13}$$

Where a_i, b_i, c are found in the International Tables [13, 14]:

The Intensity profile along q_z is then calculated using a simplified structure factor and Refinement as described by Leveiller et al. [11].

For a given hk pair:

(B.14) $$I_{hk}(q_z) = K\frac{f_L f_P f_\sigma}{A_c^2} V|F_{hk}(q_z)|^2 f_{DW}(q_z)$$

Where

$$\begin{aligned} \mathrm{K} &= \text{Scaling factor to scale intensity to measured data} \\ f_L &\propto \tfrac{1}{\sin(2\theta)}, \text{ a correction for the Lorentz factor} \\ f_P &\propto \cos^2(2\theta), \text{ a correction for beam polarization} \\ f_\sigma &= \tfrac{1}{\sin(2\theta)}, \text{ a correction for the cross-beam area} \\ A_c &= ab\sin\gamma, \text{ the unit cell area} \end{aligned}$$

V : Corresponds to the Vineyard-Yoneda peak, a consequence of the grazing incidence geometry [15–17]. Analytically defined as

(B.15) $$r_c = \frac{q_z}{q_c/2}$$

(B.16) $$V(r_c) = \begin{cases} 0 & r_c < 0 \\ 2r_c & 0 < r_c \leq 1 \\ \frac{2r_c}{x+(r_c^2-1)^{1/2}} & r_c > 1 \end{cases}$$

f_{DW} : corresponds to the Debye-Waller factor which corrects for the thermal motion of the individual atoms, capillary waves and dampens higher q_z reflections [10, 11].

(B.17) $$f_{DW} = e^{\left[-q_{hk}^2 xy_{MSD} - q_z^2 z_{MSD}\right]}$$

Where xy_{MSD} and z_{MSD} are the mean square displacement of the x, y, z coordinates of the atoms in the unit cell.

Degenerate reflections (those indexed to same q_{xy}) are summed e.g. $I_{tot} = \sum I_{hk}$. Reflections with unique q_{xy} are co-refined simultaneously e.g. the overall intensity is a three member array $I_{tot} = [I_{11}, I_{1\bar{1}}, I_{02}]$ using the `lmfit` library [5].

To calculate molecular tilt, with the points on a line approach, the `scipy.Rotation` library was utilized. Molecular tilts presented here in the form of their Euler angles derived from tilting and solving.

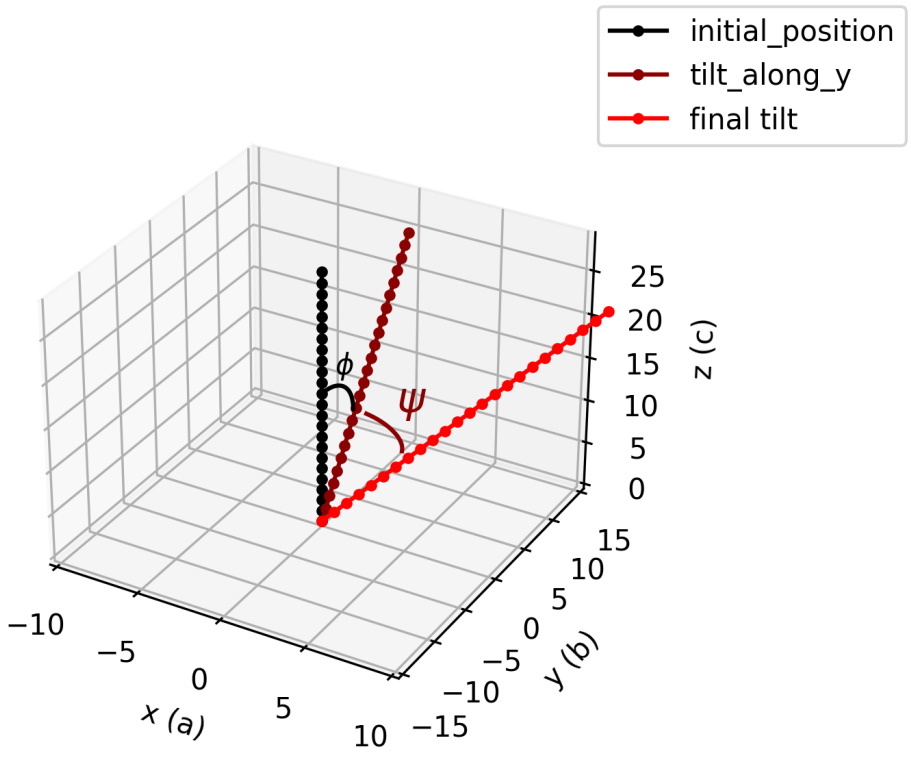

FIGURE B.4. Depiction of tilt angles used in the points on a line approach for a single molecule

B.1.4. Crystalite Size. As diacetylene films are assumed to be randomly oriented crystals or powders at the air-water interface, the crystaline length in the xy and z directions can be analyzed using the Scherrer equation [4].

$$L_{xy} = 0.9\frac{2\pi}{\Delta q_{xy}} \tag{B.18}$$

$$L_z = 0.9\frac{2\pi}{\Delta q_z} \tag{B.19}$$

$$A_0 = \frac{ab\sin(\gamma)}{n_{chains}} \tag{B.20}$$

Where Δq is the full width half maximum of the Bragg peak or rod respectively, see Jensen and Kjaer for details [2, 4].

B.2. X-Ray Reflectivity

The heterogeneity and roughness of the PDA films prevented a thorugh and in-depth analysis of the film thickness using X-ray Reflectivity (XRR). Limited insight was determined by using a stochastic, model independent fitting routine described in the program StochFit [18].

B.2.1. Description of Analysis.

(1) Reflectivity profiles collected at beamline 15-ID-C were stitched together using LSS Reader (https://github.com/chemmatcars/LSS_Reader, https://chemmatcars.uchicago.edu/facilities/software/).

(2) Stochfit was run on OpenSUSE Tumbleweed desktop with i5-6660. Newer AMD Ryzen processors didn't seem to work, and the authors weren't in the mood to recomplie C# code.

(3) Each profile was fit assuming an initial thickness of approximately 90 Å, an initial film scattering length density of approximately water, 9.38 $\times 10^{-6}$Å^{-1} and 40 boxes for the model independent fit.

(4) Once a reasonable fit of the reflectivity was achieved using the model independent method, least squares fitting of the model independent electron density profile was performed. A three box model was then fitted to the profile.

(5) This process was repeated for each reflectivity profile collected, and average values were assembked for each system.

B.3. Monomeric Diacetylene Films

Monomer DA Langmuir films were indexed and analyzed following the methodology developed in section B.1.2.

B.3.1. GIXD of TCDA Monomeric Films.

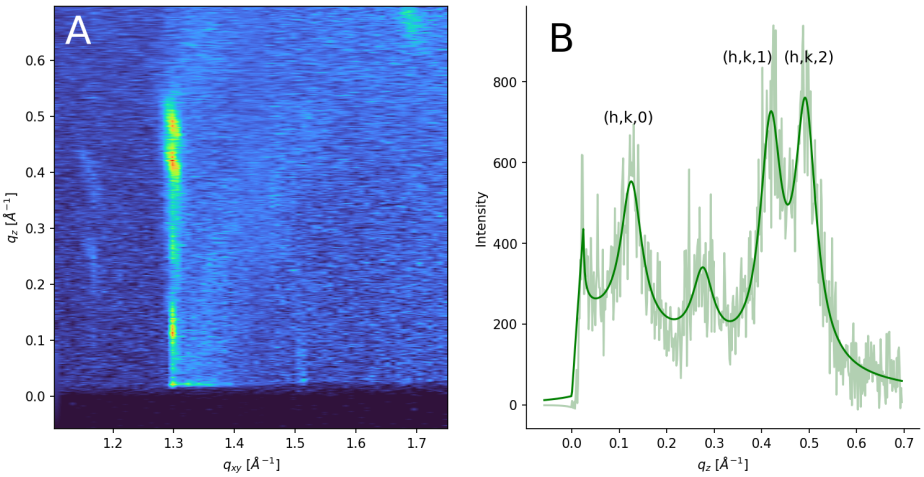

FIGURE B.5. Bragg rod profile of unpolymerized TCDA

B.3.2. XRR of PCDA Monomer Films. The total thickness from fitting was 68.7 ± 8.4 Å

	Thickness [Å]	$\rho_e/\rho_{\text{water}}$	Roughness [Å]
Layer 1	17.4 ± 1.31	0.621 ± 0.035	4.14 ± 0.369
Layer 2	22.8 ± 5.82	0.793 ± 0.0038	-
Layer 3	24.5 ± 5.56	0.913 ± 0.0149	-

TABLE B.1. Summary of calculated electron density profile using StochFit for PCDA monomer at the air-water interface.

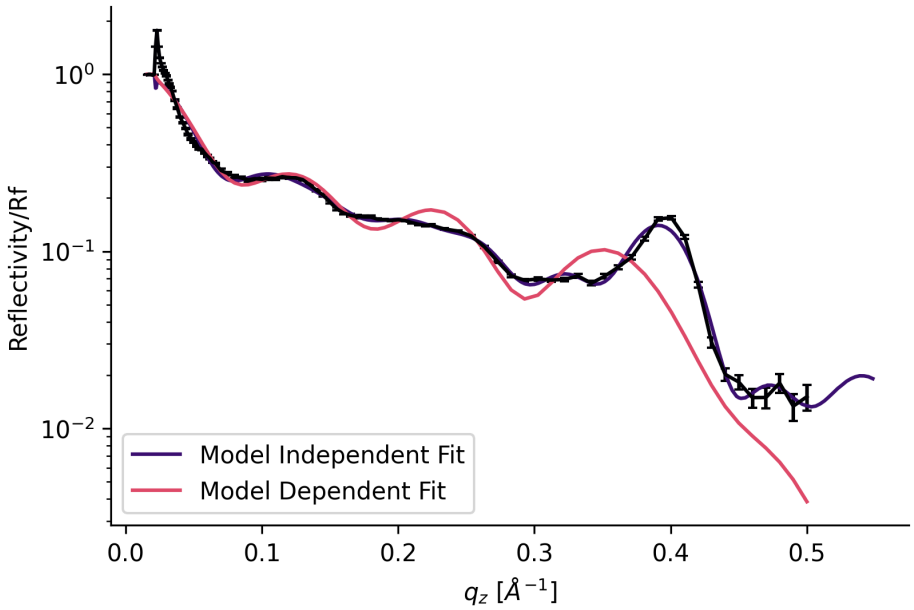

FIGURE B.6. Reflectivity Profile of a Monmeric PCDA Langmuir Film along with model depdendent and model independent fits from Stochfit.

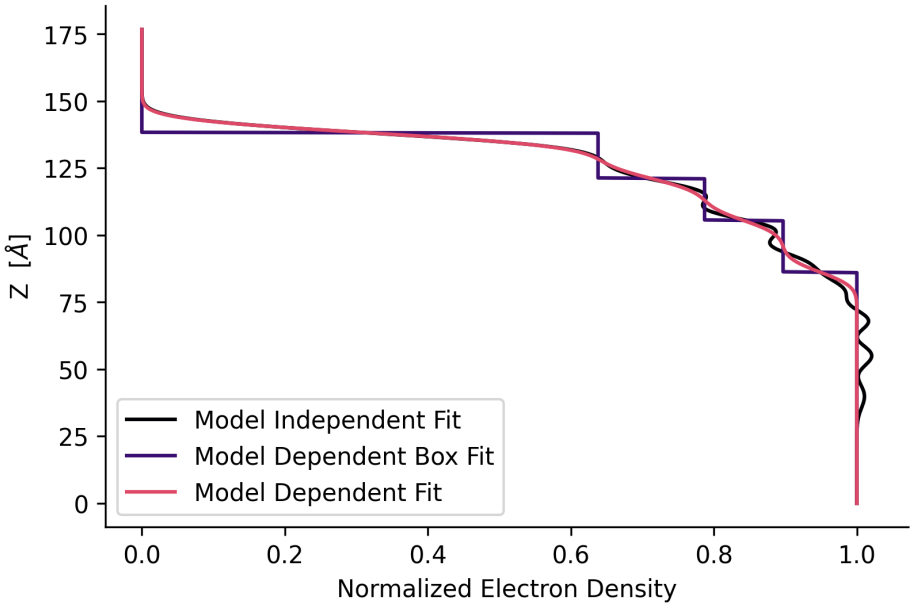

FIGURE B.7. Electron Density Profile generated from model independent fitting for PCDA Monomer, fit to a three box model.

B.4. BA-PCDA Films

B.4.1. Grazing Incidence X-ray Diffraction of BA-PCDA.

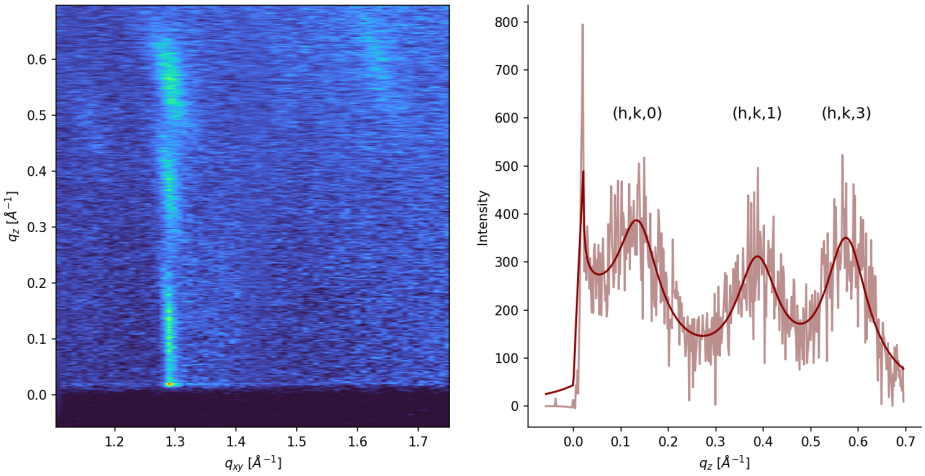

FIGURE B.8. Bragg rod profile of polymerized blue phase boronic acid functionalized PCDA (BA-PCDA)

B.4.2. X-Ray Reflectivity. The total film thickness was measured to be 67.7 ± 3.5 Å

Thickness [Å]	$\rho_e/\rho_{\text{water}}$	Roughness [Å]
19.4 ± 1.2	0.445 ± 0.0191	6.68 ± 0.876
23.4 ± 3.15	0.752 ± 0.0261	6.68 ± 0.876
24.9 ± 1.04	0.891 ± 0.0188	6.68 ± 0.876

TABLE B.2. Stochfit Derived electron density profile for Blue Phase BA-PCDA.

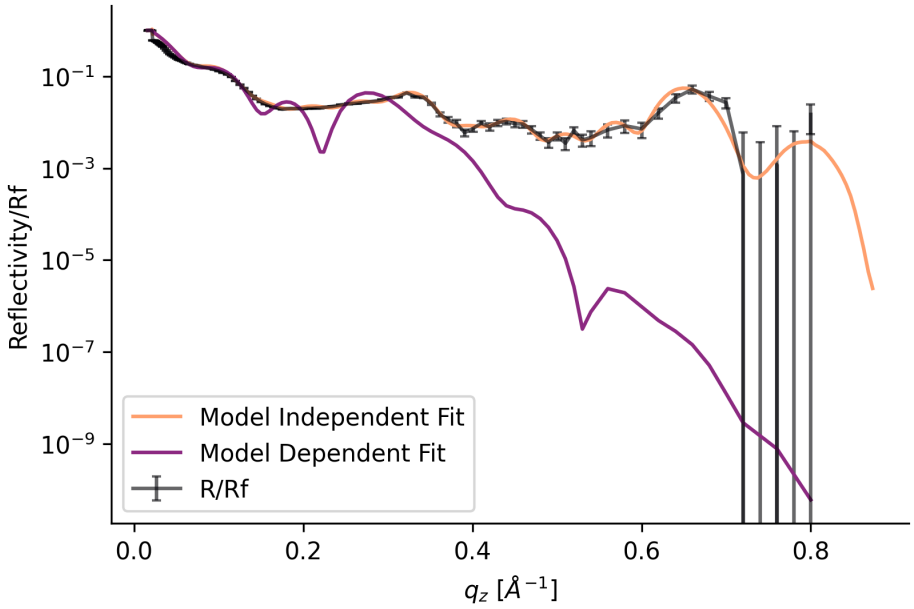

FIGURE B.9. Reflectivity Profile of a BA-PCDA Langmuir Film along with model depdendent and model independent fits from Stochfit.

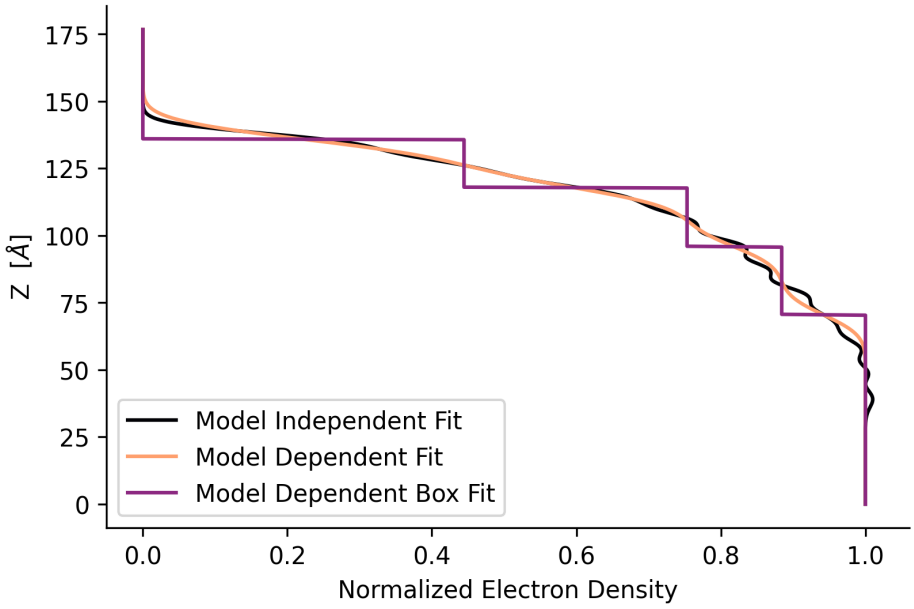

FIGURE B.10. Electron Density Profile generated from model independent fitting for BA-PCDA, fit to a three box model.

B.4.3. UV-Vis & Fluorescent Spectra.

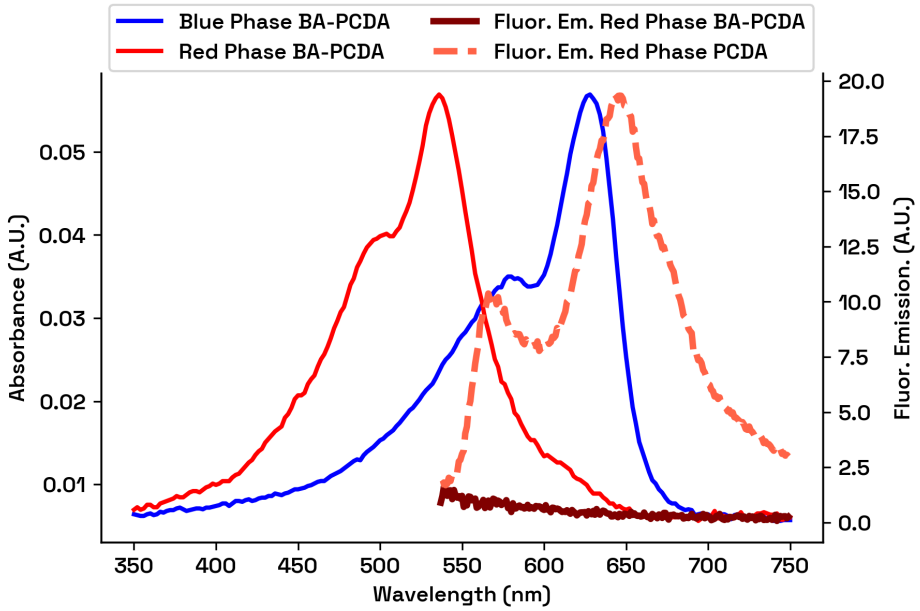

FIGURE B.11. UV-Vis and Fluorescent Emission spectra of BA-PCDA in the blue and red phase. Red Phase was obtained after prolonged heating at temperatures > 200 °C. The red phase was observed to be only weakly fluorescent.

B.4.4. NMR Spectra.

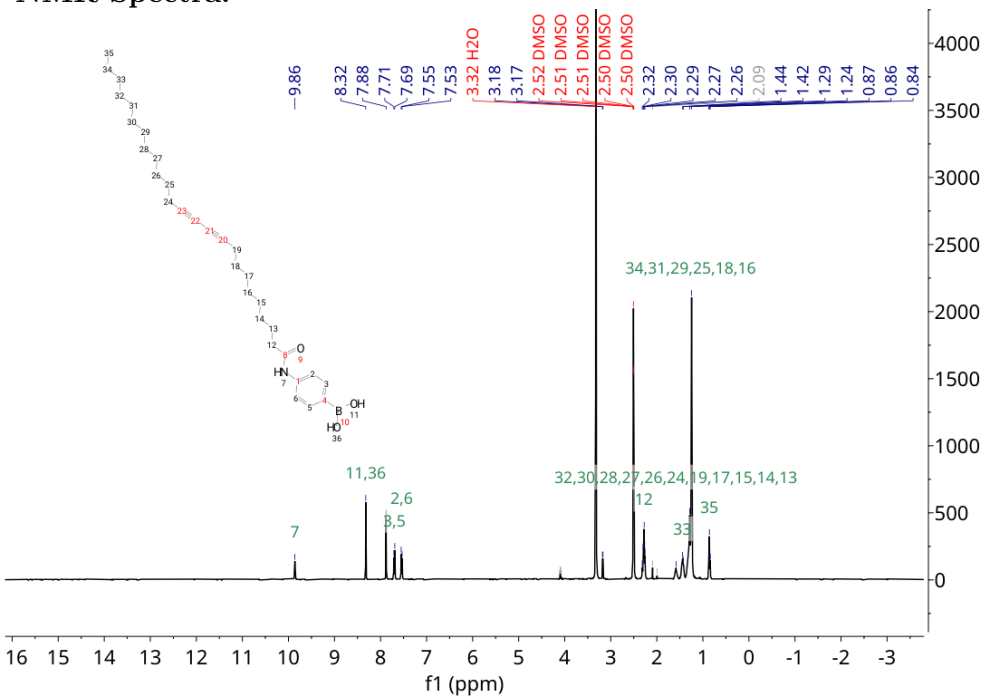

FIGURE B.12. Proton NMR Spectra of BA-PCDA in DMSO-d6 taken on Bruker 400 MHz

B.4.5. Structure.

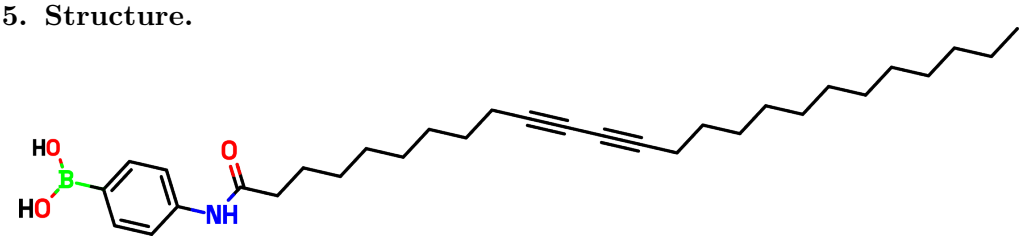

FIGURE B.13. Structure of 4-(pentacosa-10,12-diynamido)phenylboronic acid (BA-PCDA)

B.4.6. Fluorescent Microscopy Images of BA-PCDA Langmuir Films.

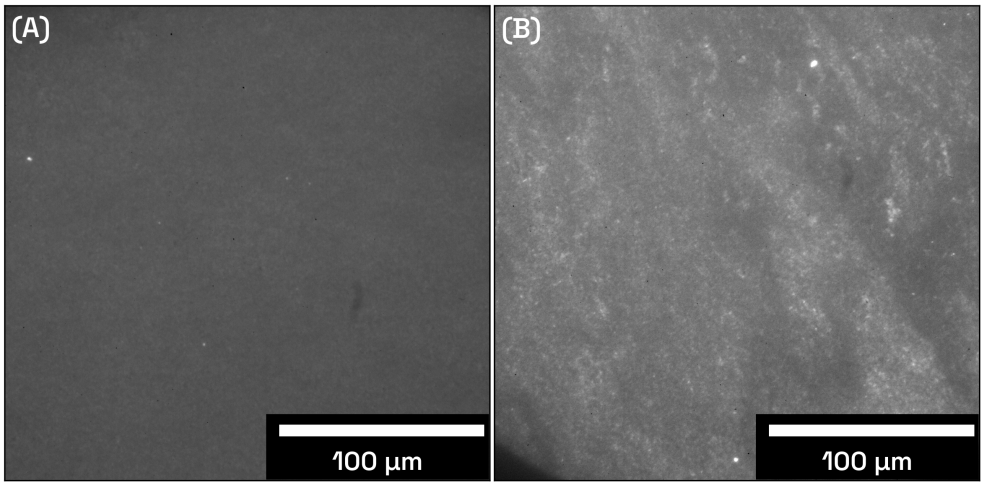

FIGURE B.14. Fluorescent Micrographs of polymerized 4-(pentacosa-10,12-diynamido)phenylboronic acid (BA-PCDA) in the Blue and Red Phase. (A) Blue Phase BA-PCDA Langmuir Film (B) Red Phase BA-PCDA Langmuir Film.

B.4.7. Atomic Force Microscopy of BA-PCDA.

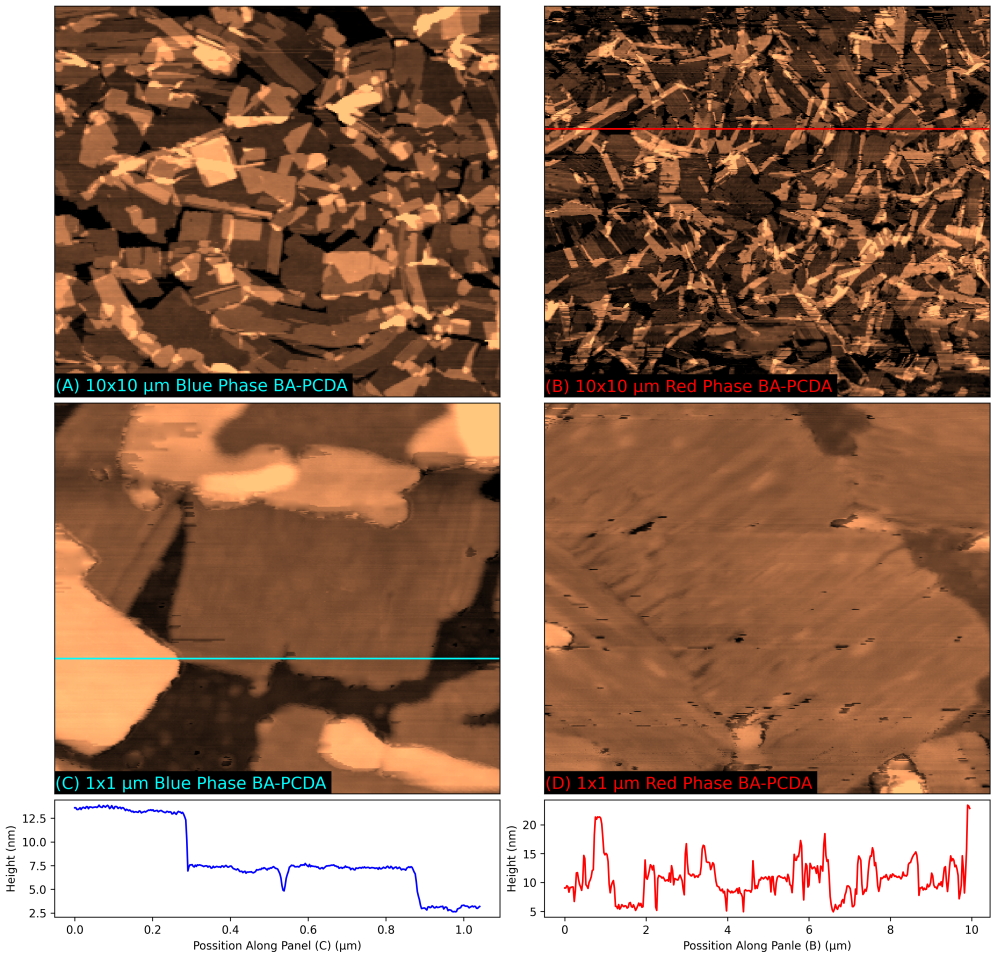

FIGURE B.15. AFM scans of polymerized 4-(pentacosa-10,12-diynamido)phenylboronic acid (BA-PCDA) in the Blue and Red Phase. The thinnest part of the film was measured to be ≈ 50 Å in the blue and red phases.

B.5. Blue Phase PCDA

B.5.1. XRR. A total thickness was measured to be: 74.7 ± 11.6 Å

Thickness [Å]	$\rho_e/\rho_{\text{water}}$	Roughness [Å]
18.6 ± 2.91	0.559 ± 0.088	5.22 ± 1.74
30.2 ± 3.18	0.782 ± 0.0811	-
25.9 ± 10.8	0.91 ± 0.0474	-

TABLE B.3. Stochfit Derived thickness for Blue Phase PCDA

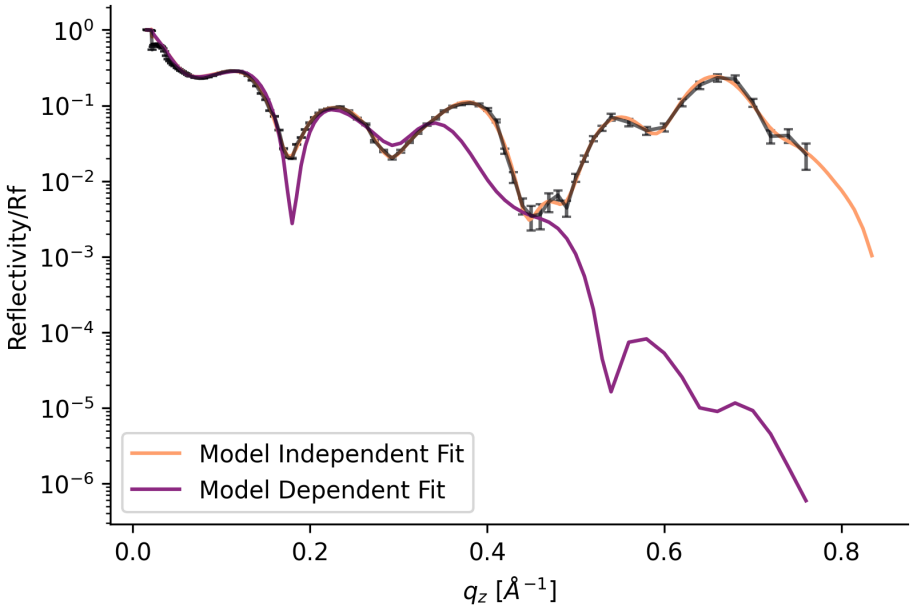

FIGURE B.16. Reflectivity Profile of a Blue phase PCDA Langmuir Film along with model depdendent and model independent fits from Stochfit.

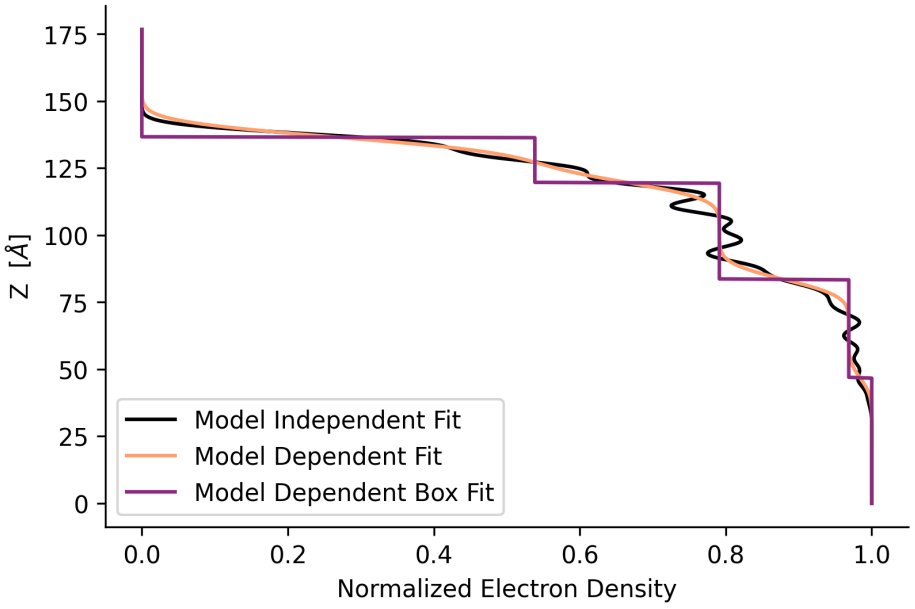

FIGURE B.17. Electron Density Profile generated from model independent fitting for Blue phase PCDA, fit to a three box model.

B.5.2. Atomic Force Microscopy.

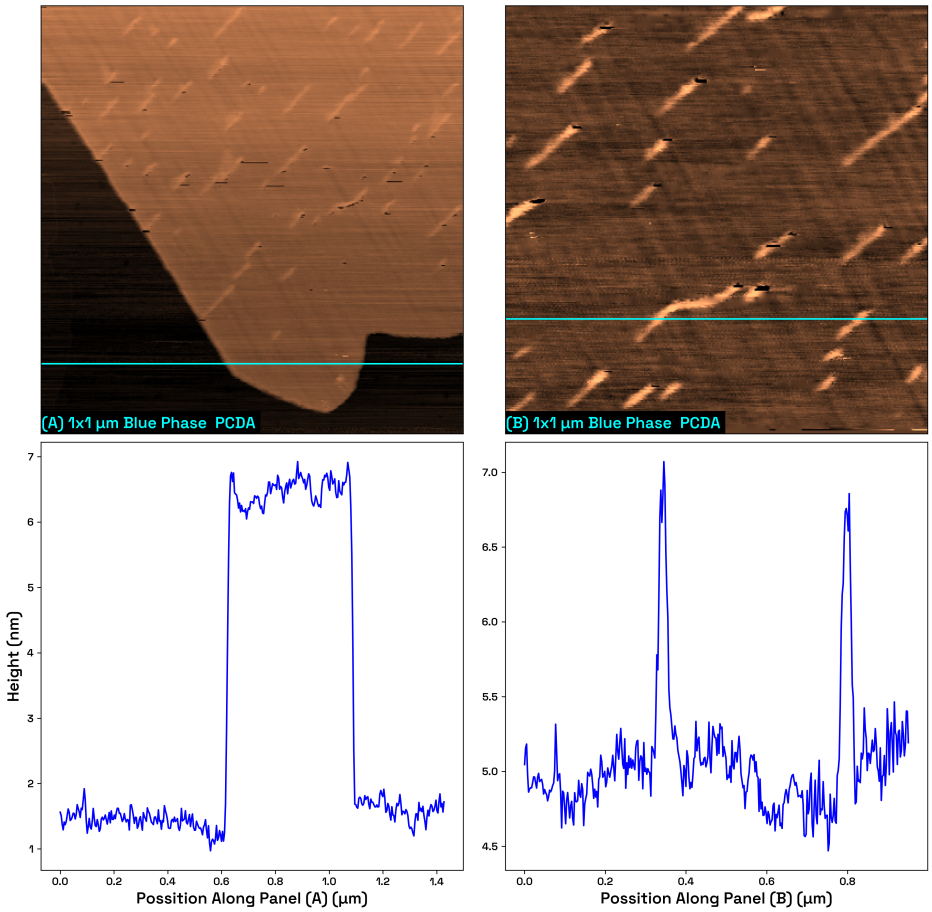

FIGURE B.18. Atomic Force Microscopy scans of Blue Phase PDA showing the polymer backbone and interesting perpendicular ridges. The height contrast between the ridges and the film is approximately 2 nm.

B.5.3. Fluorescence Microscopy.

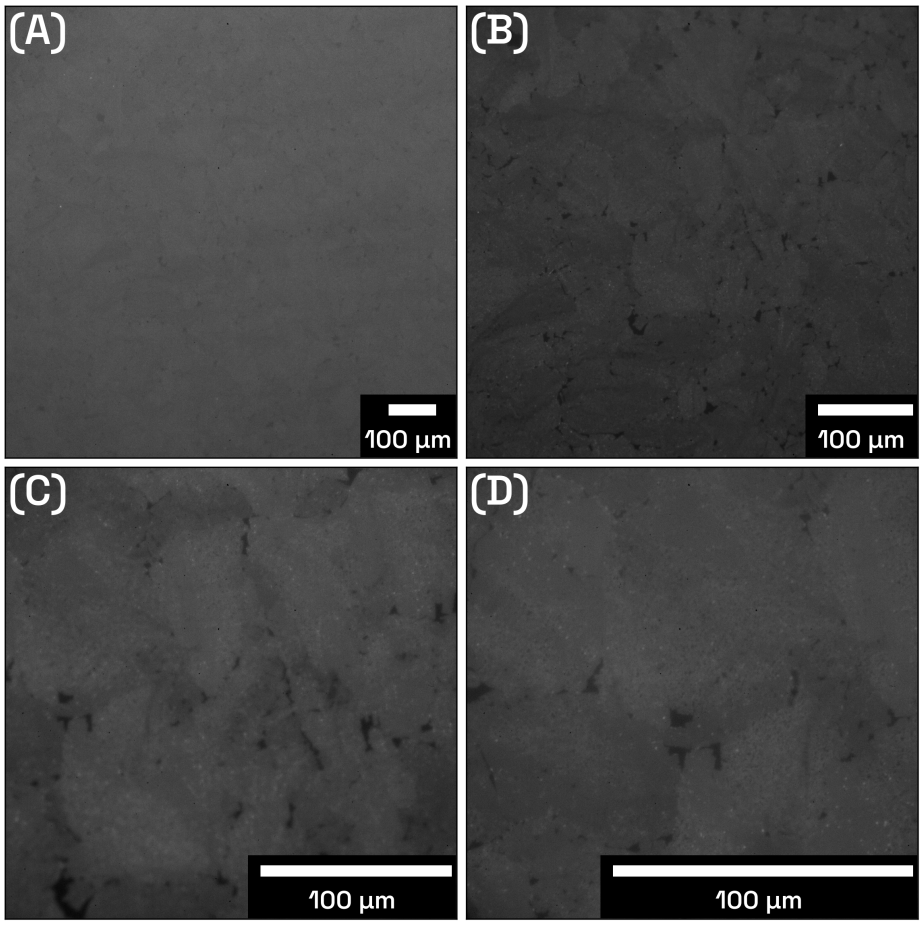

FIGURE B.19. Fluorescent micrographs of blue phase PCDA deposited on mica at increasing magnification. Polymer domains are readily visible at higher magninfication (C,D). Small regions of red phase are present within the domains

B.6. Blue Phase TCDA

B.6.1. GIXD Reciprocal Space Map of TCDA in the Blue Phase.

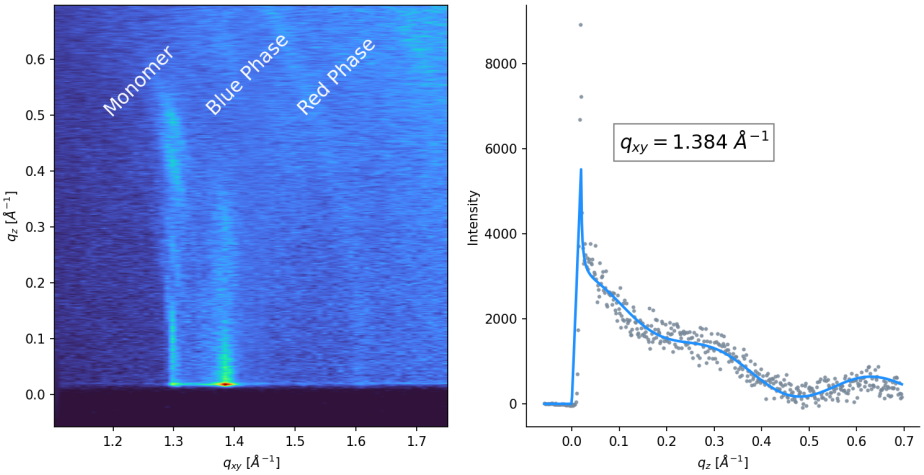

FIGURE B.20. Bragg rod profile of Blue Phase TCDA

B.7. Blue Phase NCDA

B.7.1. GIXD space map of NCDA in the blue phase.

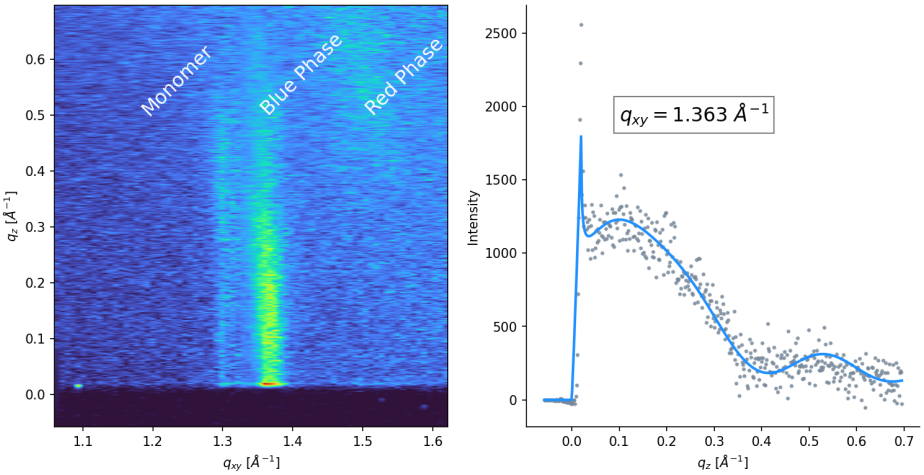

FIGURE B.21. Bragg rod profile of Blue Phase NCDA

B.7.2. XRR. A total film thickness of 74.86 ± 3.45 Å was measured.

Thickness [Å]	$\rho_e/\rho_{\text{water}}$	Roughness [Å]
21.9 ± 0.965	0.538 ± 0.00445	5.68 ± 0.467
27.2 ± 2.97	0.786 ± 0.00124	5.68 ± 0.467
25.8 ± 1.46	0.868 ± 0.0577	5.68 ± 0.467

TABLE B.4. Stochfit Derived thickness for Blue Phase NCDA.

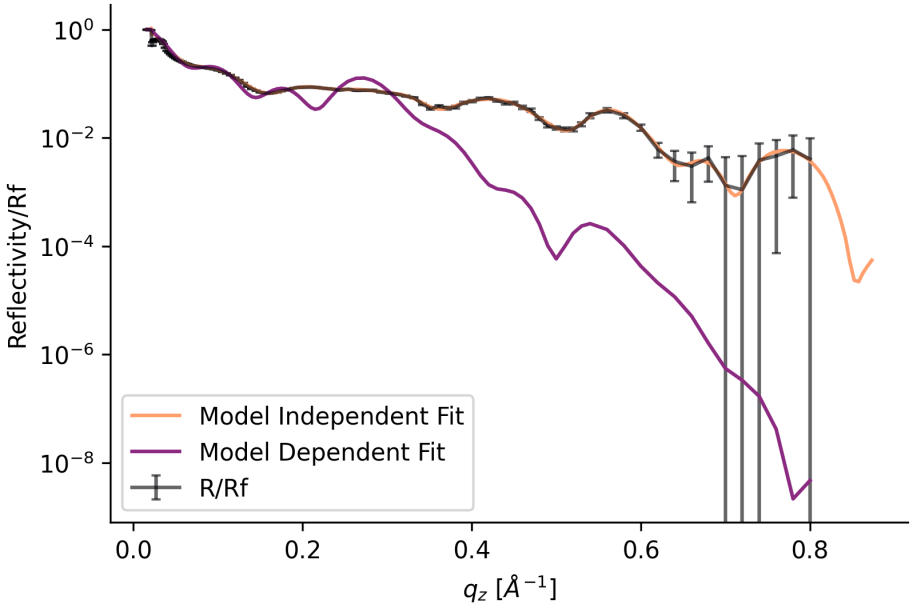

FIGURE B.22. Reflectivity Profile of a NCDA Langmuir Film along with model dependent and model independent fits from Stochfit.

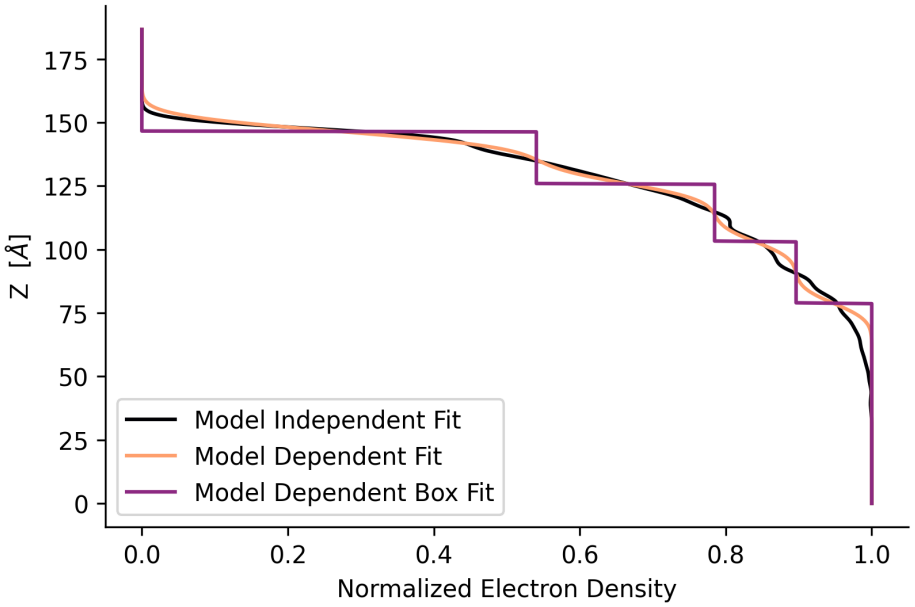

FIGURE B.23. Electron Density Profile generated from model independent fitting for NCDA, fit to a three box model.

B.8. Blue Phase Zn-PCDA

B.8.1. GIXD.

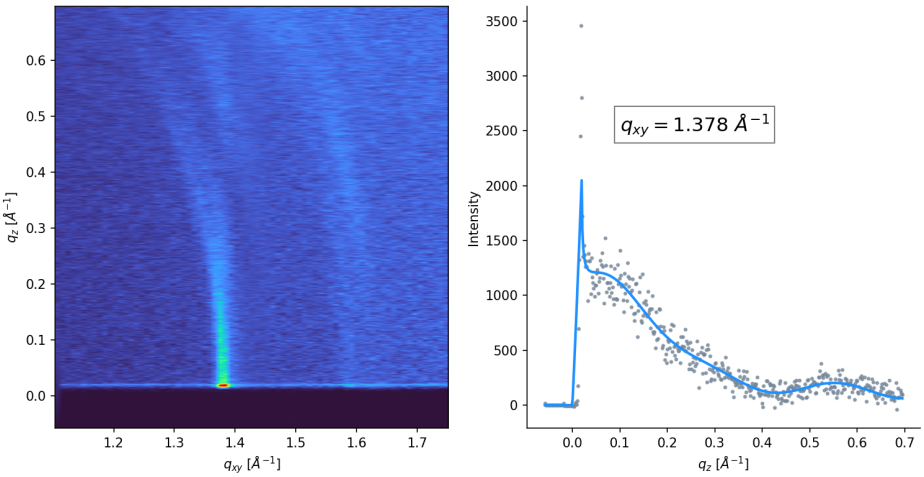

FIGURE B.24. Bragg rod profile of Blue Phase Zn-PCDA

B.8.2. X-Ray Reflectivity. A total thickness of 80 ± 5 Å was measured.

Thickness [Å]	$\rho_e/\rho_{\text{water}}$	Roughness [Å]
22.4 ± 2.8	0.423 ± 0.0115	8.77 ± 2.31
30.8 ± 4.24	0.64 ± 0.0427	-
26.8 ± 0.389	0.848 ± 0.0105	-

TABLE B.5. Stochfit Derived thickness for Zn Modifed PCDA in the Blue Phase.

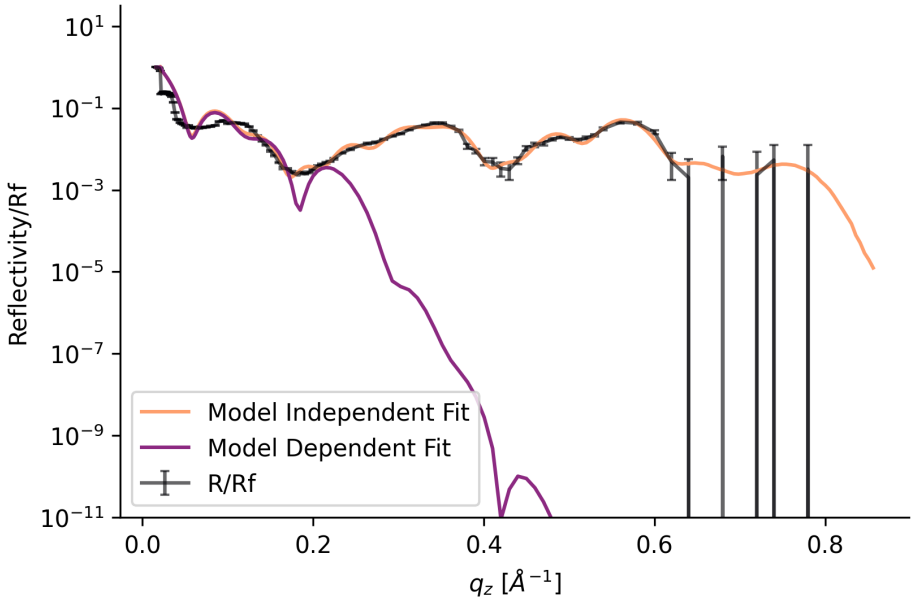

FIGURE B.25. Reflectivity Profile of a Blue Phase Zn-PCDA Langmuir Film along with model dependent and model independent fits from Stochfit.

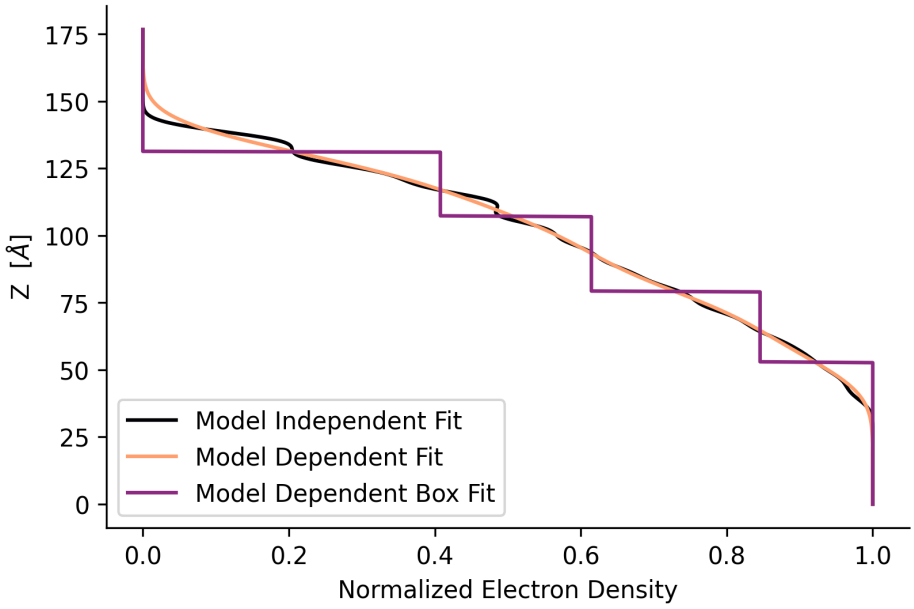

FIGURE B.26. Electron Density Profile generated from model independent fitting for red Phase Blue Phase Zn-PCDA, fit to a three box model.

B.8.3. UV-Vis & Fluorescent Spectra.

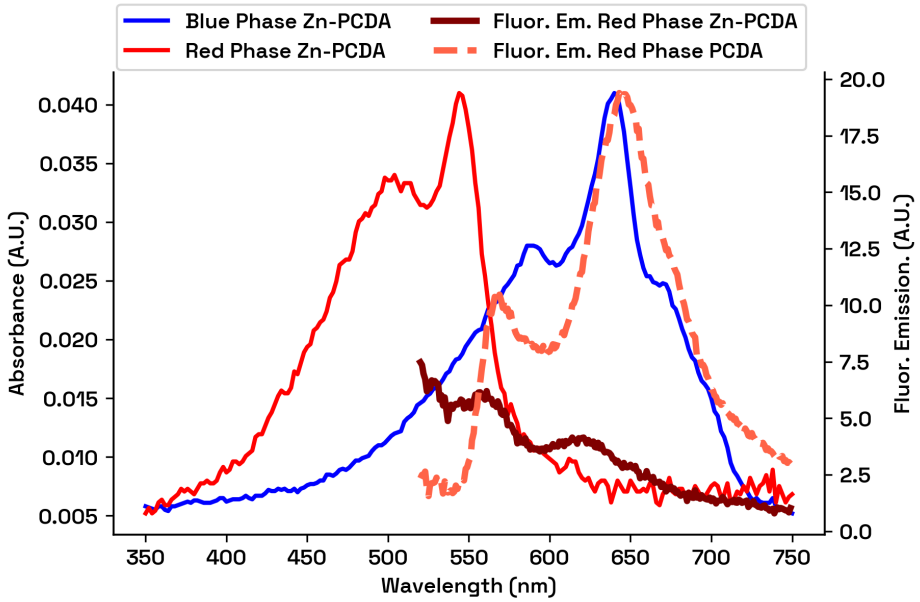

FIGURE B.27. UV-Vis and Fluorescent Emission Spectra from Zn-PCDA in the Blue and Red Phase. The Fluorescent emission is significantly weaker than in the case of films formed on a pure water subphase.

B.8.4. Atomic Force Microscopy.

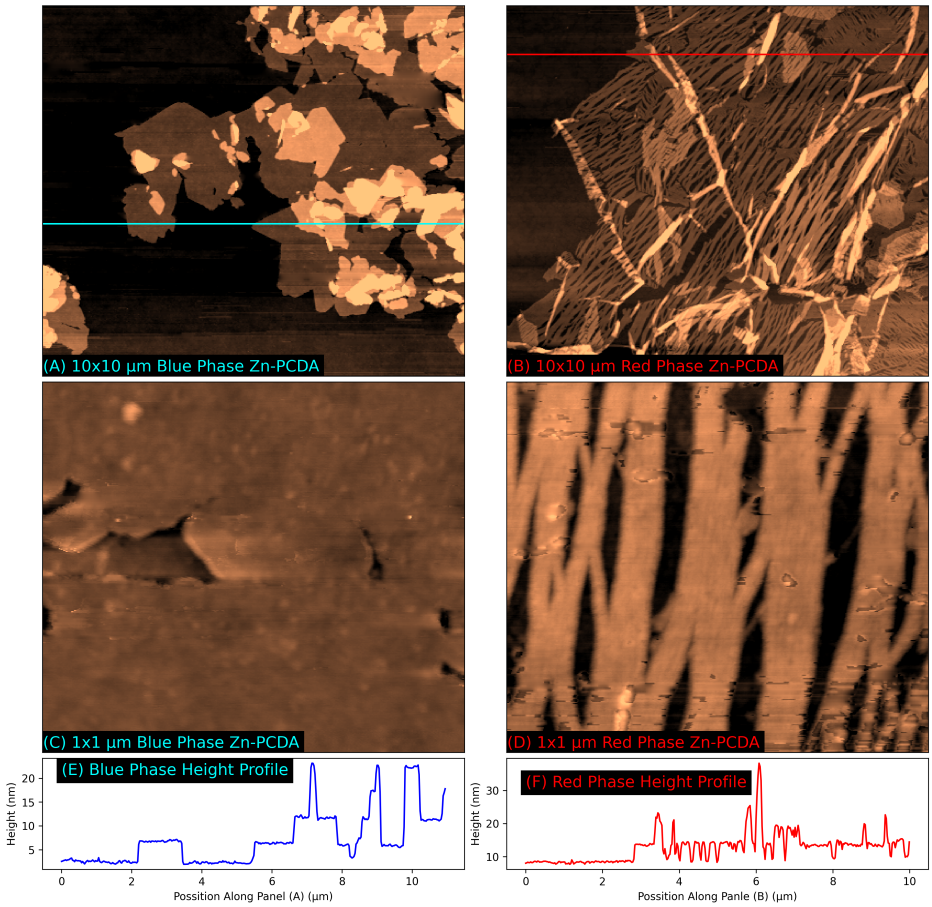

FIGURE B.28. Atomic Force Microscopy scans of Blue Phase and Red Phase Zn-PCDA Langmuir films. Red Phase Zn-PCDA was transformed via heating to T > 200 °C. The thinnest film was measured to be 4.48 ± 0.3 in the blue phase and 4.45 ± 0.14 in the red phase. Polymer strands are not visible in the blue phase (C), but are readily visible in the red phase (D). The film appears significantly more cracked in the red phase, which may be a consequence of heating the films.

B.8.5. Fluorescence Microscopy.

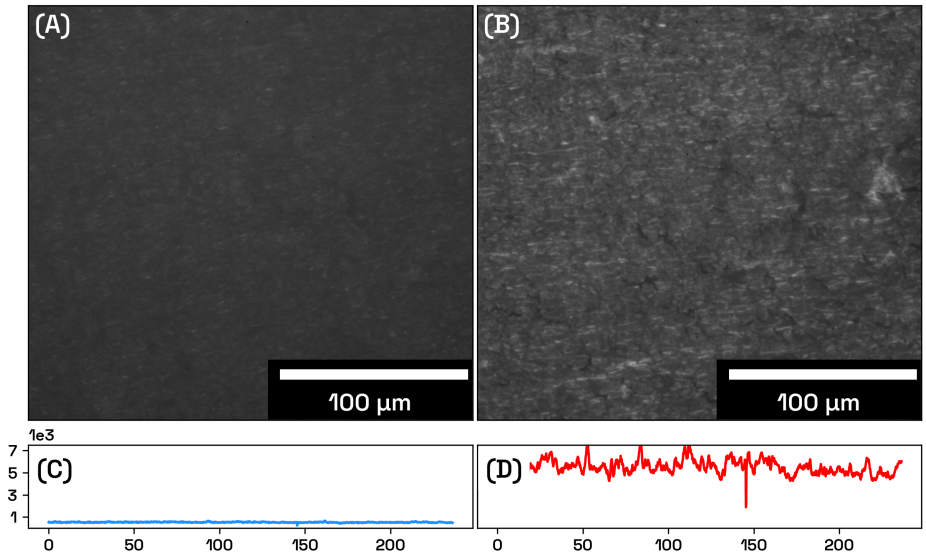

FIGURE B.29. Fluorescent micrographs of Zn-PCDA Langmuir films in the (A) Blue and (B) Red Phase. The red phase can be seen to be somewhat more fluorescent as indicated by fluorescent line profiles in (C) Blue Phase and (D) Red Phase.

B.9. Red Phase PCDA

B.9.1. XRR. A total thickness of approximately 70 Å was measured.

Thickness [Å]	$\rho_e/\rho_{\text{water}}$	Roughness [Å]
20.1	0.573	5.09
21.3	0.767	5.09
29.0	0.884	5.09

TABLE B.6. Stochfit Derived thickness for Red Phase PCDA (unlike other systems, only one reflectivity profile was measured for red phase PCDA.).

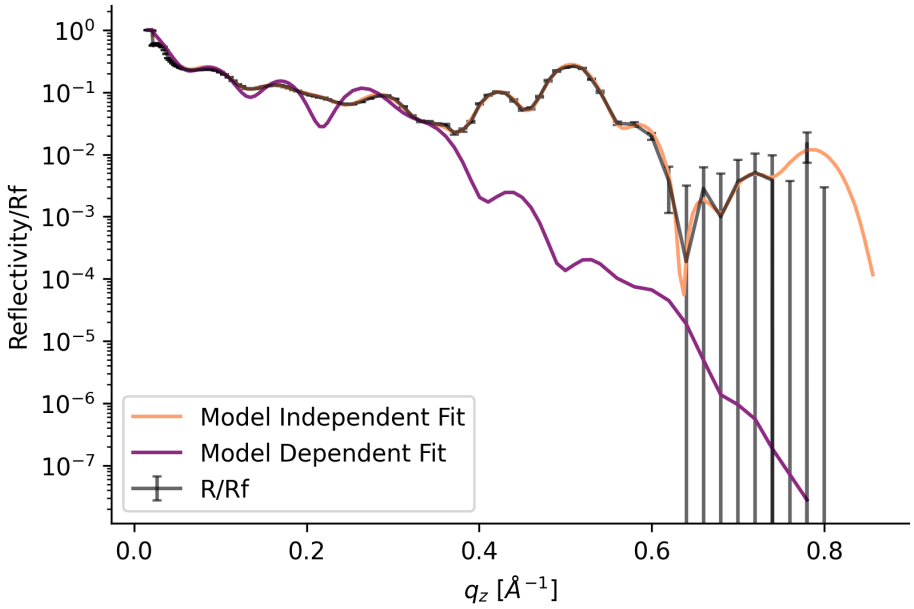

FIGURE B.30. Reflectivity Profile of a Red Phase PCDA Langmuir Film along with model dependent and model independent fits from Stochfit.

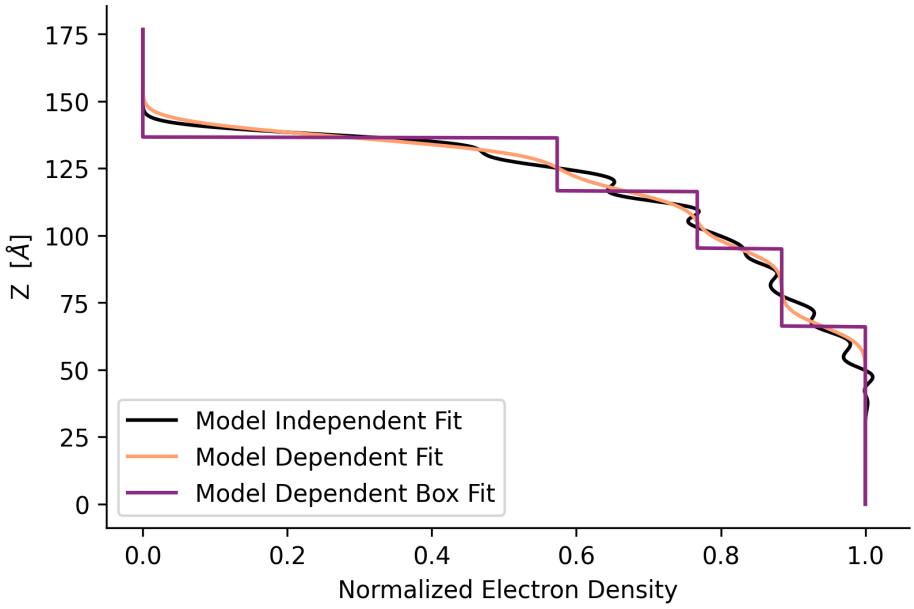

FIGURE B.31. Electron Density Profile generated from model independent fitting for red Phase PCDA, fit to a three box model.

B.9.2. Atomic Force Microscopy.

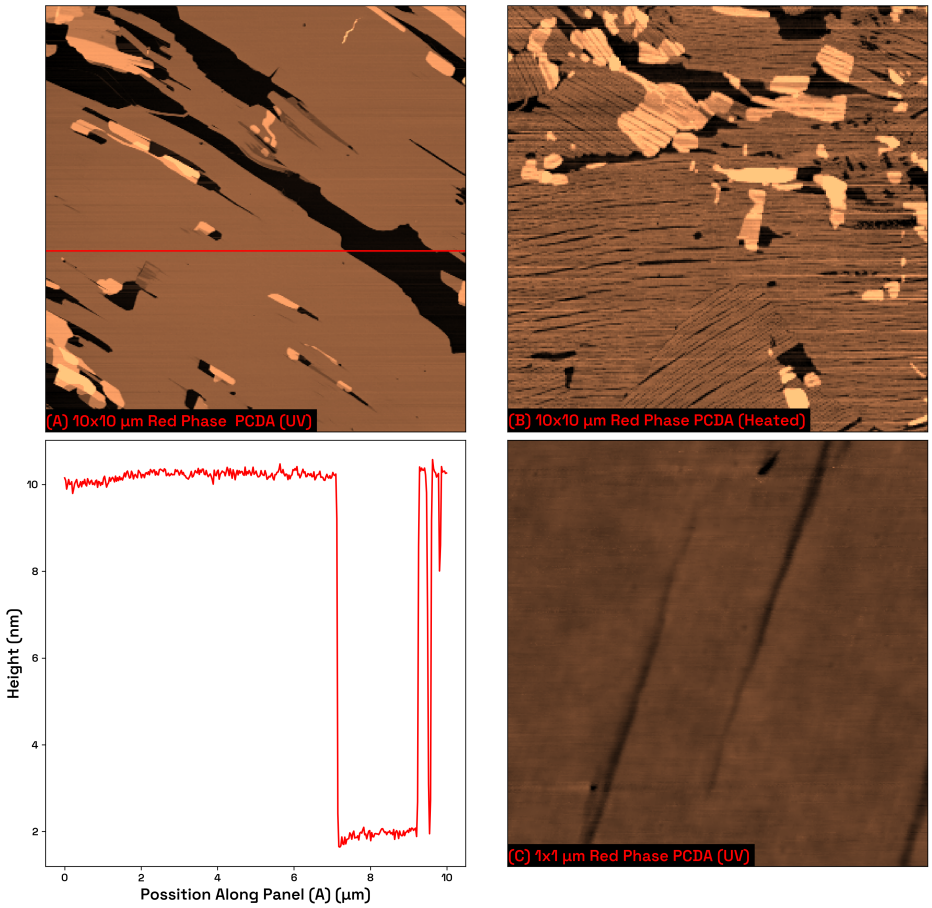

FIGURE B.32. Atomic Force Microscopy scans of Red Phase PCDA Langmuir films. (A) Red Phase PCDA transformed via prolonged UV light exposure at the air-water interface prior to deposition. (B) Thermally transformed Red Phase after deposition. Temperature induced transitions appear to induce significantly more cracks, parallel to the polymer backbone, than UV induced polymerization. (C) Cracks are parallel to the polymer backbone in this UV transformed red phase film. Notably absent in the red phase are the ridges seen in the blue phase.

B.9.3. Fluorescence Microscopy.

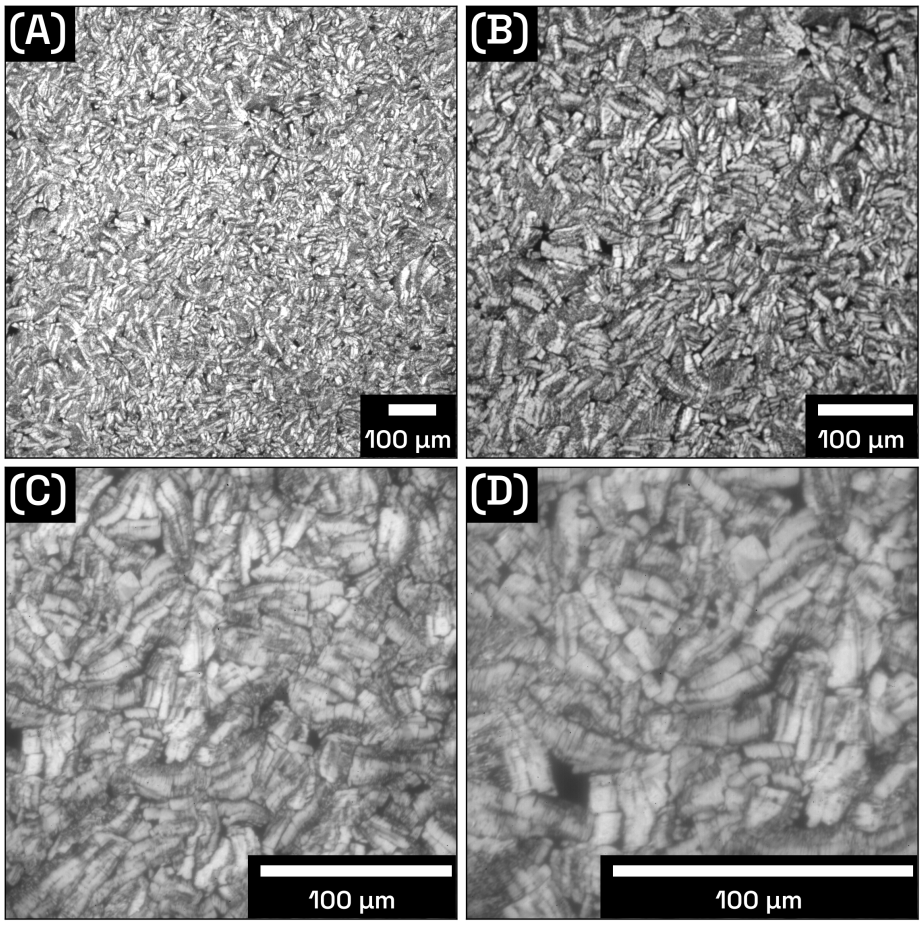

FIGURE B.33. Fluorescent Micrographs of red phase PCDA Langmuir films.

B.10. Red Phase NCDA

B.10.1. GIXD.

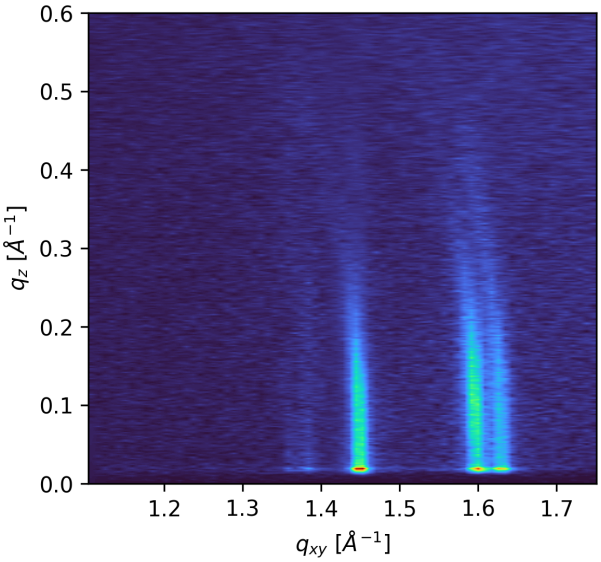

FIGURE B.34. GIXD Reciprocal Space Map of Red Phase NCDA

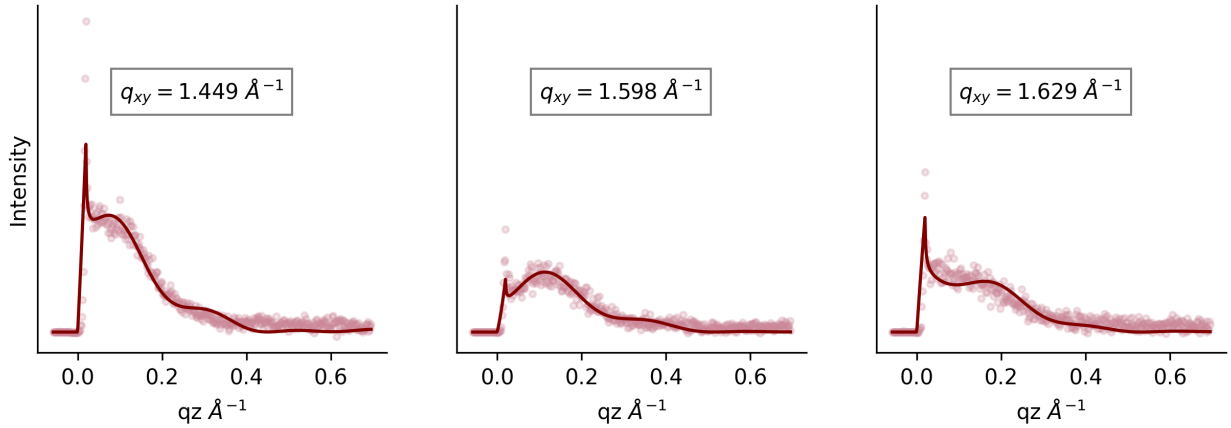

FIGURE B.35. Bragg Rod fit of NCDA to the Kinked Model

Thickness [Å]	$\rho_e/\rho_{\text{water}}$	Roughness [Å]
18.5 ± 8.2	0.65 ± 0.0329	5.29 ± 1.62
31.2 ± 4.65	0.838 ± 0.0494	-
36.6 ± 3.98	0.928 ± 0.0163	-

TABLE B.7. Stochfit Derived thickness for Red Phase NCDA

B.10.2. XRR. For Red Phase NCDA, a total thickness of 86.3 ± 10.2 Å was calculated.

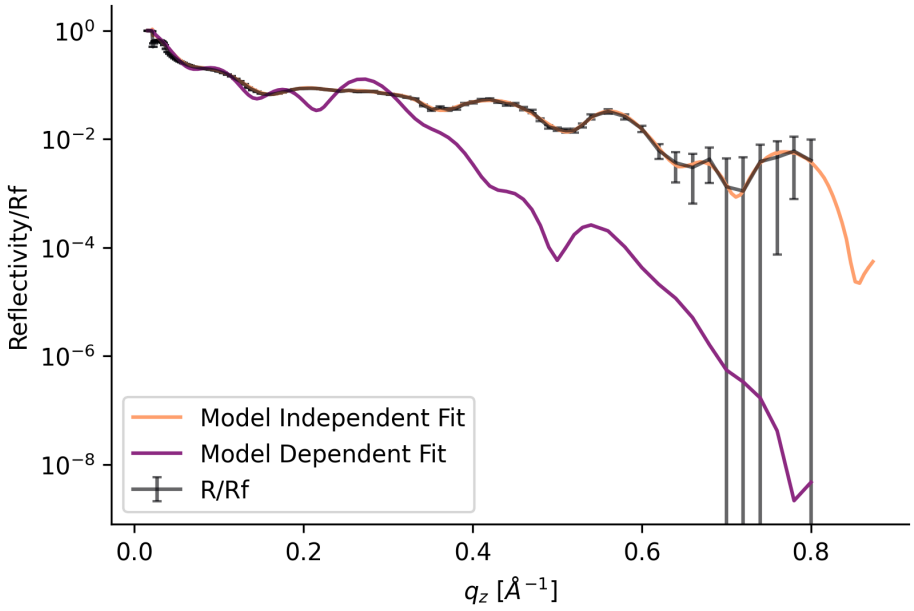

FIGURE B.36. Reflectivity Profile of a NCDA Langmuir Film along with model dependent and model independent fits from Stochfit.

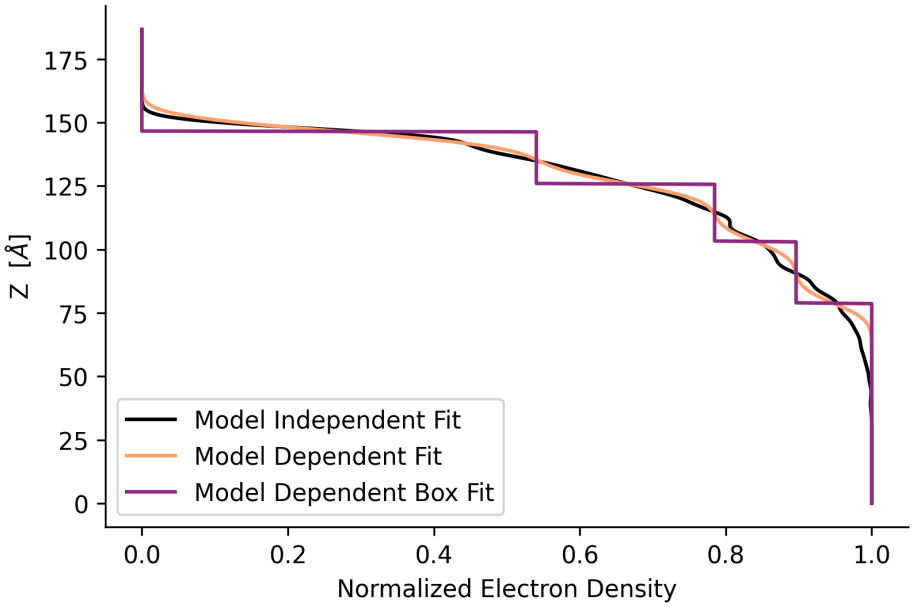

FIGURE B.37. Electron Density Profile generated from model independent fitting for NCDA, fit to a three box model.

B.11. Larger Atomic Force Microscopy Scans

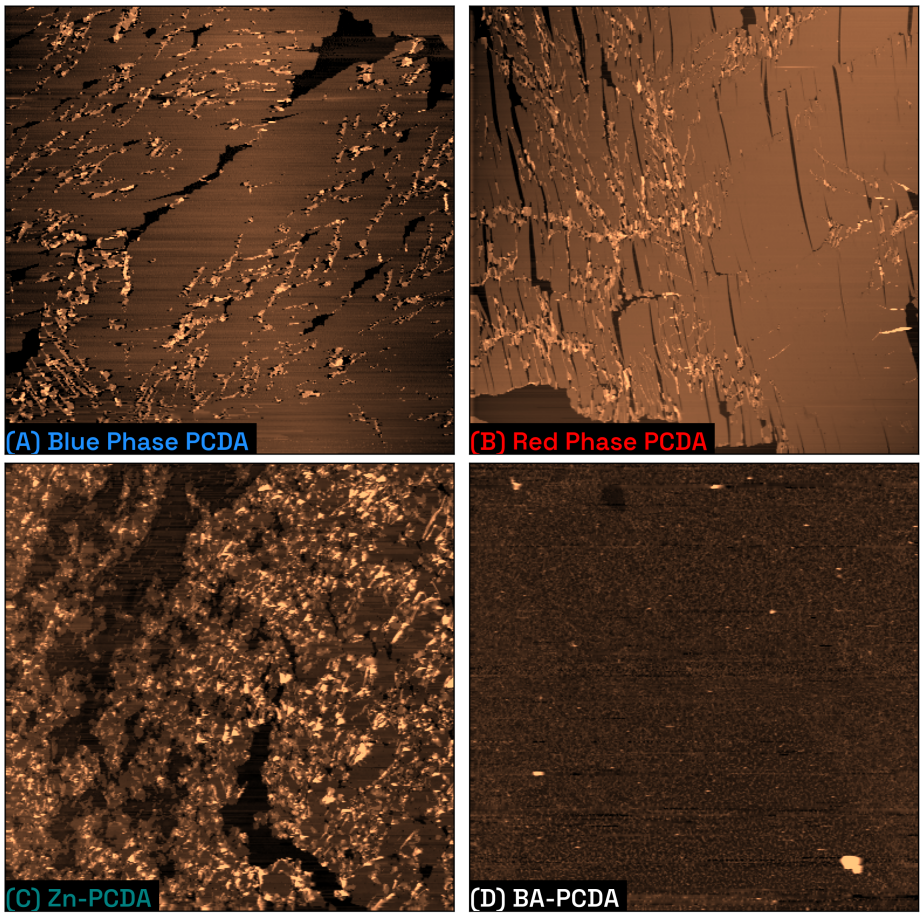

FIGURE B.38. 100x100 µm Atomic force microscopy scans of blue PCDA, red PCDA, Zn-modified (Blue Phase) and BA-PCDA (Red Phase). PCDA films can be seen to have regions of multilayer buildup. (C) Zn-PCDA is very heterogeneous with a wide range of heights. (D) The domains of BA-PCDA are almost too small to be resolved.

B.12. Density Functional Theory Calculations

PDA models were derived from GIXD indexing and fitting to act as starting points for the DFT simulations. The GIXD patterns primarily provide information about the alkyl chains, rather than information directly about the polymer backbone. The points-on-a-line approach assumes that each carbon molecule spaced roughly 1.274 Å apart. After fitting, this was reconstructed as a true alkyl chain with a single bond length of 1.530 Å and an angle of 109.5 °. From in-plane scattering, the two-dimensional unit cell provides information on the spacing between neighboring monomers along the polymer backbone, with the spacing corresponding to "a" in the unit cell. Once spaced properly,

an initial guess based on established bond lengths for PDA was used, with the double bond assumed to be approximately 1.339 Å and the triple bond length approximately 1.2 Å [19]. This enabled generation of three-dimensional structure derived from the GIXD data and bond length heuristics.

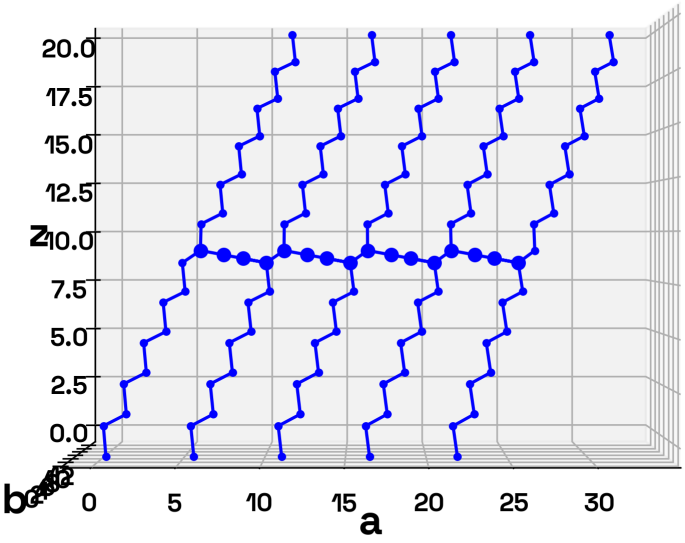

FIGURE B.39. Generation of initial geometry from GIXD analysis

To speed up computation time the side chains were pared down to two carbon atoms with hydrogens on either side of the PDA backbone.

To quickly check the reasonableness of this approach a dimer and 4-mer with extended and short side chains were checked. No significant change in the spectra was observed by altering the side chains, and so the longer molecules were calculated with pared-down side chains.

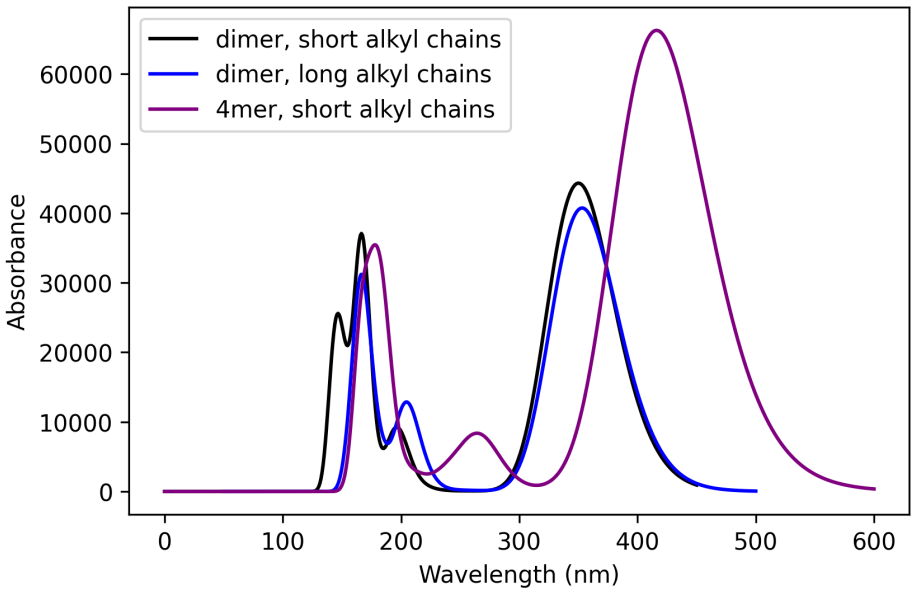

FIGURE B.40. Comparison of shorter chain diacetylene oligomers with varying side chain lengths

For these simulations in Gaussian16, b3lyp and the svp basis set were used. 100 singlet states were calculated with TD-DFT using b3lyp and svp. The red phase conformations were optimized using the semi-emprical PM6 method and then energy calculations were done using TD-DFT using b3lyp and the svp basis set.

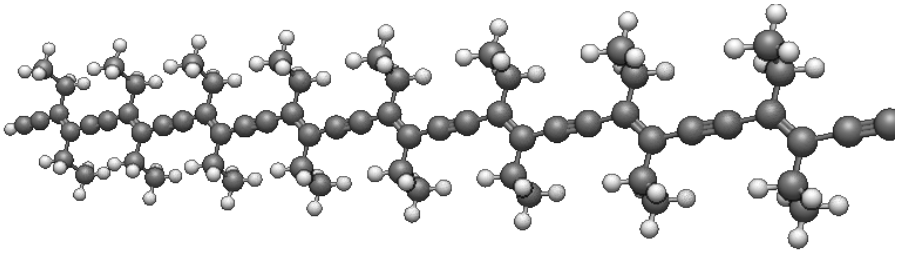

FIGURE B.41. Geometry of optimized blue phase PCDA molecule used for TD-DFT calculations.

For the blue phase, an 8 molecule long chain was optimized and then run through TD-DFT. The optimized geometry had minimal variation from the initial starting point, and produced a reasonable

spectra. For the red phase, an 8 molecule long chain, both the "twisted" and "kinked" models were optimized and then run through TD-DFT with 100 singlet states calculated.

References

[1] Jens Als-Nielsen, Didier Jacquemain, Kristian Kjaer, Franck Leveiller, Meir Lahav, and Leslie Leiserowitz. Principles and applications of grazing incidence X-ray and neutron scattering from ordered molecular monolayers at the air-water interface. *Physics Reports*, 246(5):251–313, October 1994. ISSN 03701573. doi: 10.1016/0370-1573(94)90046-9.

[2] Kristian Kjaer. Some simple ideas on X-ray reflection and grazing-incidence diffraction from thin surfactant films. *Physica B: Condensed Matter*, 198(1-3):100–109, April 1994. ISSN 09214526. doi: 10.1016/0921-4526(94)90137-6.

[3] K. Kjaer, J. Als-Nielsen, C. A. Helm, P. Tippman-Krayer, and H. Moehwald. Synchrotron x-ray diffraction and reflection studies of arachidic acid monolayers at the air-water interface. *The Journal of Physical Chemistry*, 93(8):3200–3206, April 1989. ISSN 0022-3654. doi: 10.1021/j100345a063.

[4] Torben R. Jensen and Kristian Kjaer. Structural Properties and Interactions of Thin Films at the Air-Liquid Interface Explored by Synchrotron X-Ray Scattering. In *Studies in Interface Science*, volume 11, pages 205–254. Elsevier, 2001. ISBN 978-0-444-50948-2. doi: 10.1016/S1383-7303(01)80028-4.

[5] Matt Newville, Renee Otten, Andrew Nelson, Till Stensitzki, Antonino Ingargiola, Dan Allan, Austin Fox, Faustin Carter, Michał, Ray Osborn, Dima Pustakhod, lneuhaus, Sebastian Weigand, Andrey Aristov, Glenn, Christoph Deil, mgunyho, Mark, Allan L. R. Hansen, Gustavo Pasquevich, Leon Foks, Nicholas Zobrist, Oliver Frost, Stuermer, azelcer, Anthony Polloreno, Arun Persaud, Jens Hedegaard Nielsen, Matteo Pompili, and Shane Caldwell. Lmfit 1.2.0. Zenodo, April 2023.

[6] Magdalena Truger, Otello M. Roscioni, Christian Röthel, Dominik Kriegner, Clemens Simbrunner, Rizwan Ahmed, Eric D. Głowacki, Josef Simbrunner, Ingo Salzmann, Anna Maria Coclite, Andrew O. F. Jones, and Roland Resel. Surface-Induced Phase of Tyrian Purple

(6,6′-Dibromoindigo): Thin Film Formation and Stability. *Crystal Growth & Design*, 16(7): 3647–3655, July 2016. ISSN 1528-7483, 1528-7505. doi: 10.1021/acs.cgd.6b00104.

[7] Josef Simbrunner, Ingo Salzmann, and Roland Resel. Indexing of grazing-incidence X-ray diffraction patterns. *Crystallography Reviews*, 0(0):1–19, March 2023. ISSN 0889-311X. doi: 10.1080/0889311X.2023.2187051.

[8] Josef Simbrunner, Clemens Simbrunner, Benedikt Schrode, Christian Röthel, Natalia Bedoya-Martinez, Ingo Salzmann, and Roland Resel. Indexing of grazing-incidence X-ray diffraction patterns: The case of fibre-textured thin films. *Acta Crystallographica Section A Foundations and Advances*, 74(4):373–387, July 2018. ISSN 2053-2733. doi: 10.1107/S2053273318006629.

[9] Yevgeniy Lifshitz, Yuval Golan, Oleg Konovalov, and Amir Berman. Structural Transitions in Polydiacetylene Langmuir Films. *Langmuir*, 25(8):4469–4477, April 2009. ISSN 0743-7463. doi: 10.1021/la8029038.

[10] E. B. Watkins, C. E. Miller, J. Majewski, and T. L. Kuhl. Membrane texture induced by specific protein binding and receptor clustering: Active roles for lipids in cellular function. *Proceedings of the National Academy of Sciences*, 108(17):6975–6980, April 2011. doi: 10.1073/pnas.1014579108.

[11] Franck Leveiller, Didier Jacquemain, Leslie Leiserowitz, Kristian Kjaer, and Jens Als-Nielsen. Toward a determination at near atomic resolution of two-dimensional crystal structures of amphiphilic molecules on the water surface: A study based on grazing incidence synchrotron x-ray diffraction and lattice energy calculations. *The Journal of Physical Chemistry*, 96(25): 10380–10389, December 1992. ISSN 0022-3654. doi: 10.1021/j100204a051.

[12] Ivan Kuzmenko, Hanna Rapaport, Kristian Kjaer, Jens Als-Nielsen, Isabelle Weissbuch, Meir Lahav, and Leslie Leiserowitz. Design and Characterization of Crystalline Thin Film Architectures at the Air-Liquid Interface: Simplicity to Complexity. *Chemical Reviews*, 101(6): 1659–1696, June 2001. ISSN 0009-2665. doi: 10.1021/cr990038y.

[13] nist. X-Ray Form Factor, Attenuation, and Scattering Tables, September 2009.

[14] Brown, Fox, Maslen, O'Keefe, and Willis. Chapter 6.1. Intensity of diffracted intensities. In *International Tables for Crystallography*, volume C, pages 554–595. International Union of Crystallography, two thousand, sixth edition, July 2019. ISBN 978-1-119-46870-7.

[15] George H. Vineyard. Grazing-incidence diffraction and the distorted-wave approximation for the study of surfaces. *Physical Review B*, 26(8):4146–4159, October 1982. doi: 10.1103/PhysRevB.26.4146.

[16] Y. Yoneda. Anomalous Surface Reflection of X Rays. *Physical Review*, 131(5):2010–2013, September 1963. doi: 10.1103/PhysRev.131.2010.

[17] S. K. Sinha, E. B. Sirota, S. Garoff, and H. B. Stanley. X-ray and neutron scattering from rough surfaces. *Physical Review B*, 38(4):2297–2311, August 1988. doi: 10.1103/PhysRevB.38.2297.

[18] S. M. Danauskas, D. Li, M. Meron, B. Lin, and K. Y. C. Lee. Stochastic fitting of specular X-ray reflectivity data using StochFit. *Journal of Applied Crystallography*, 41(6):1187–1193, December 2008. ISSN 0021-8898. doi: 10.1107/S0021889808032445.

[19] M. Schott and G. Wegner. Chapter III-1 - Basic Structural and Electronic Properties of Polydiacetylenes. In D. S. Chemla and J. Zyss, editors, *Nonlinear Optical Properties of Organic Molecules and Crystals*, pages 3–49. Academic Press, January 1987. ISBN 978-0-12-170612-8. doi: 10.1016/B978-0-12-170612-8.50003-1.